# DYNAMICS OF BUBBLE SIZE DISTRIBUTION AND WALL PRESSURE FLUCTUATIONS IN AIRLIFT FERMENTORS

by

CHUNG-HUR LEE

B. S., National Taiwan University, 1979

---

A MASTER'S THESIS

submitted in partial fulfillment of the

requirements for the degree

MASTER OF SCIENCE

Department of Chemical Engineering

KANSAS STATE UNIVERSITY
Manhattan, Kansas

1983

Approved by:

Larry A. Glasgow
Major Professor

LD
2668
.T4
1983
L43
c.2

A11202 578076

# ACKNOWLEDGEMENTS

I am sincerely grateful to my major advisor, Dr. L. A. Glasgow, for his valuable advice, constructive criticism, and continued encouragement during the course of this research. The helpful suggestions and valuable comments from Dr. L. E. Erickson are deeply appreciated. Thanks are also extended to Dr. L. T. Fan for serving on the author's supervisory committee and for reviewing this thesis manuscript. I also wish to express my gratitude to Snehal A. Patel for his help in performing the experiments and discussing the results.

I am extremely fortunate to have had the constant emotional support, unshaken confidence and understanding from my loving wife, Alice. I wish to express my utmost thanks to my beloved parents, Mr. and Mrs. Jing-Far Lee, and the same to my wife's parents, Mr. and Mrs. Shou-Kun Yu, for their continued spiritual and financial support.

I am also grateful to my many friends in the Chemical Engineering Department who have helped me make my graduate career both enjoyable and rewarding.

Finally I wish to acknowledge the financial support of National Science Foundation, Grant CPE-8108799.

TABLE OF CONTENTS


| | | |
|---|---|---|
| CHAPTER I | INTRODUCTION | 1 |
| | REFERENCES | 4 |
| CHAPTER II | TURBULENCE STRUCTURES IN TWO-PHASE FLOW | 5 |
| | 1. Introduction | 5 |
| | 2. Scales of Turbulence | 6 |
| | 3. Turbulence Power Spectrum | 7 |
| | 4. Energy Dissipation Spectrum | 9 |
| | NOMENCLATURE | 10 |
| | REFERENCES | 11 |
| CHAPTER III | BUBBLE BREAK-UP AND COALESCENCE IN FERMENTATION | 13 |
| | 1. Introduction | 13 |
| | 2. Mechanisms of Bubble Break-Up and Coalescence | 14 |
| | 3. Bubble Size Distribution and Size Distribution Dynamics | 19 |
| | 4. Experimental Procedure | 22 |
| | 5. Discussion of Results | 27 |
| | 6. Conclusions | 31 |
| | NOMENCLATURE | 33 |
| | REFERENCES | 36 |
| CHAPTER IV | WALL-PRESSURE FLUCTUATIONS IN TWO-PHASE SYSTEM | 85 |
| | 1. Introduction | 85 |
| | 2. Experimental Procedure | 92 |
| | 3. Discussion of Results | 93 |
| | 4. Conclusions | 99 |
| | NOMENCLATURE | 101 |
| | REFERENCES | 103 |
| CHAPTER V | RECOMMENDATIONS FOR FUTURE WORK | 133 |

APPENDIX ..... 134

# CHAPTER I

## INTRODUCTION

Submerged aerobic cultures of microorganisms are used in a wide range of applications, from food and drug production to waste-water treatment. Of the many essential requirements for cell growth, the most difficult to fulfill are the supply of oxygen and the removal of heat. Because of the low solubility of oxygen in the aqueous phase, one of the most challenging aspects of fermentor design is to continuously dissolve sufficient oxygen in the medium where the microorganisms grow. The rate of oxygen transport from the sparged gas phase to living organisms has frequently been the rate controlling factor in fermentations. The general objectives involved in fermentor design therefore include maximizing the oxygen transfer rate and minimizing the power requirement.

While many fermentor designs have been proposed for increasing the oxygen transfer rate and minimizing the power consumption, one of the most promising designs was found to be the airlift fermentor which was first patented by Lefrancois and coworkers in 1955. The possible advantages of the airlift fermentor over a stirred tank are:

1. possible savings in operating expense because of low power consumption,
2. ease of construction and low cost,
3. simplicity and, therefore, reliability.

Note especially that sterility problems introduced by an impeller shaft are avoided, which become more important as scale increases. Also, improvements might be expected in fermentations which are affected adversely by impeller shear.

Airlift fermentors have been designed, constructed and used for a

variety of experiments and applications. Types of airlift fermentors include the concentric airlift (Hatch 1973, Blenke 1979), rectangular airlift (Gasner 1974), the external recycle airlift (Kanazawa 1975), the split-cylinder airlift (Belfield 1976, Orazem et al. 1979), and multistage airlift columns (Orazem et al. 1979). Recent applications of airlift devices for fermentations, single-cell protein production and waste-water treatment have demonstrated the efficiency of airlift devices for mass transfer. The results of Hatch (1969) show that a potentially large decrease in the power requirement can be achieved with a bench scale airlift fermentor. Snedecor and Wang (1976) have cultured Streptomyces niveus (novobiocin) by batch fermentations in 100 liter and 200 liter airlift fermentors. Their results indicate that novobiocin production in an airlift fermentor is as good or better than results obtained with stirred tank fermentors. They also showed that the airlift fermentor was superior to an aeration tower with respect to oxygen transfer at the same air flow rates and power inputs. Malfait and coworkers (1981) used airlift fermentors for filamentous media in their studies which showed a significant improvement in mass transfer of oxygen to the aqueous phase as compared to mechanically agitated systems. They also showed that savings in energy cost were in excess of 50% for airlift fermentors.

The present investigation seeks to improve the design of airlift devices. A split-cylinder airlift has been constructed with an acrylic cylinder bisected by a vertical baffle. As air is sparged on one side of the baffle, liquid circulation occurs from the upflow zone to the head region and down the other side. The split-cylinder airlift is of simple construction with low power requirements. The reduced wetted area per unit volume increases the liquid velocity which enhances bubble break up and

increases the interfacial area for mass transfer.

Other objectives of this research include advancement of knowledge of vertical two-phase flow, mass transfer, bubble behavior and growth in airlift fermentors and the effect of viscosity upon fermentation processes. These goals were to be attained by:

1). Investigation of turbulence structures in vertical, buoyancy-driven two-phase systems by dynamic pressure fluctuation analysis.

2). Investigation of the mechanics of bubble break up and coalescence with the aid of bubble size distribution measurements in airlift fermentors.

REFERENCES

Belfield, A. R., Jr.," Experimental Studies of Oxygen Transfer in a Split-Cylinder Airlift," M. S. Thesis, University of Maryland (1976)

Blenke, H.," Loop Reactors," Advances in Biochemical Engineering, 13, 121 (1979)

Deshpande, V. A.," Experimental Studies of Gas-Liquid Dispersion in a Split-Cylinder Airlift Fermentor," M. S. Thesis, Kansas State University (1980)

Gasner, L. L.," Development and Application of the Thin Channel Rectangular Airlift Mass Transfer Reactor to Fermentation and Waste-Water Treatment Systems," Biotechnol. and Bioengg., 16, 1179 (1974)

Hatch, R. T.," Mass Transfer Characteristics of an Airlift Fermentor," M. S. Thesis, M. I. T. (1969)

Hatch, R. T.," Experimental and Theoretical Studies of Oxygen Transfer in the Airlift Fermentor," Ph. D. Thesis, M. I. T. (1973)

Kanazawa, M.," The Production of Yeast from n-Paraffins Single-Cell Protein II," (Ed. S. R. Tannenbaum and D. I. C. Wang), M. I. T. Press, Cambridge, Mass., 438 (1975)

Lefrancois, L., C. G. Mariller, and J. V. Mejane," Efectionnements aux procedes de Cultures fongigues et de Fermentations Industrielles," Brevet D'Invention, France # 1.102.200, Delivres le 4 Mai, 1955

Malfait, J. L., D. J. Wilcox, D. G. Mercer, and L. D. Barker," Cultivation of a Filamentous Mold in a Glass Pilot-Scale Airlift Fermentor," Biotechnol. and Bioengg., 23, 863 (1981)

Orazem, M. E., and L. E. Erickson," Oxygen-Transfer Rates and Efficiencies in One and Two-Stage Airlift Towers," Biotechnol. and Bioengg., 21, 69 (1979)

Snedecor, B. and D. I. C. Wang," Oxygen Transfer into a Non-Newtonian Broth Using an Airlift Fermentor," 172nd National Meeting, American Chemical Society, Sept. 1, 1976

# CHAPTER II

# TURBULENCE STRUCTURES IN TWO-PHASE FLOW

## I. Introduction

Efficient dispersion with a view to obtaining large interfacial areas is of great importance for heat and mass transfer processes in gas-liquid systems. In most industrial bioreactors in practical use, gas dispersion is caused mainly by turbulence (Schügerl 1980).

Turbulent flow produces primary eddies which have a wave length (or scale) of magnitude roughly similar to the transverse dimensions of the main flow stream. These large primary eddies are unstable and disintegrate into small eddies by vortex stretching until all of their energy is dissipated by viscous forces. When the Reynolds number of the main flow is high, most of the kinetic energy is contained in the large eddies, but nearly all of the dissipation occurs in the smallest eddies. If the scale of the main flow is large compared with that of the energy dissipating eddies, a wide spectrum of intermediate eddies exist which contain much of but dissipate little of the total energy. In the process the directional nature of the primary eddies is gradually lost.

Kolmogorov (1941) concludes that all eddies which are much smaller than the primary eddies are statistically independent of them, and that the properties of these small eddies are determined solely by the local energy dissipation rate per unit mass of fluid. Thus, at large integral scale Reynolds numbers, the small eddies should have a universal character. First, they are locally isotropic whether the large scale motions are isotropic or not. Second, the motion at very small scales is chiefly governed by viscous forces. In this long series of processes leading to the smallest eddies, the turbulent motion adjusts itself to some definite state. The further down the scale, the less the motion is dependent on the large eddies.

Since in all of the dispersing devices in the operating range of practical importance the gas dispersion takes place in accordance with the mechanism of turbulence, it is to be expected that a relationship exists between the characteristics of the turbulence and the efficiency of the gas dispersion. Turbulent motion cannot be characterized by mean velocity and turbulence intensity alone. Distribution of turbulent energy which is mainly influenced by the presence of turbulent eddies, is also important. In the following sections, the scales of turbulence, turbulence power spectrum, and energy dissipation spectrum are considered; they are believed to be the key quantities for gas dispersion in two-phase systems.

## 2. Scales of Turbulence

Turbulent eddies have a broad energy distribution or spectrum (Hinze 1975). For turbulent flow many length and velocity scales coexist and one can define a Reynolds number based upon any one of these length scales and the corresponding velocity. For the combination of $\eta$ and $v$, the Kolmogorov microscales, the Reynolds number is of order 1, i.e.

$$\frac{\eta v}{\nu} \sim 1 \tag{2.1}$$

turbulence must cease to exist - i.e. $\eta$ and $v$ are the limiting "small scale" components of the turbulent field. The dissipation rate per unit mass $\varepsilon$ of these elements is purely viscous and thus

$$\varepsilon \sim \nu \frac{v^2}{\eta^2} \tag{2.2}$$

Combining both relations leads to the Kolmogorov microscale and velocity expressed in terms of $\nu$ and $\varepsilon$

$$\eta = (\nu^3/\varepsilon)^{1/4}, \quad v = (\nu\, \varepsilon)^{1/4} \tag{2.3}$$

$\varepsilon$ can also be identified with inviscid dynamics using the integral scale $\ell$ and the corresponding velocity U. The amount of kinetic energy per unit mass in the integral scale turbulence is proportional to $U^2$; the rate of transfer of energy is assumed to be proportional to $U/\ell$. The rate of energy supply to the small scale eddies is thus of order $U^2 \cdot U/\ell$. This energy is dissipated at a rate $\varepsilon$, which should be equal to the supply rate. Hence (Taylor 1935)

$$\varepsilon \sim U^3/\ell \tag{2.4}$$

which states that the rate at which turbulence dissipates its energy is determined by the "turnover" time of the most energetic eddies; note that this expression is independent of viscosity.

The "number of degrees of freedom" can be defined by

$$\frac{\ell}{\eta} \sim (U\ell/\nu)^{3/4} = Re^{3/4} \tag{2.5}$$

and is a measure of the range of length scales available to turbulent modes.

## 3. Turbulence Power Spectrum

Turbulence structure can also be described by spectra in which turbulence signals consist of discrete overlapping signals of different frequencies and amplitudes. According to Taylor (1935), a definite eddy size can be associated with each particular frequency. High frequencies represent small eddies and low frequencies represent large eddies, since $\frac{U}{\ell} << \frac{\nu}{\eta}$.

Consider the component $u_1$ of the turbulence velocity fluctuations at a fixed point in the flow field. We assume that this field is quasi-steady, so that it is statistically homogeneous with respect to time. There then

exists a constant average value of $\overline{u_1^2}$, which can be considered to consist of the sum of the contributions of all the frequencies n. Let $E_1(n)\,dn$ be the contribution to $\overline{u_1^2}$ of the frequencies between n and n + dn; the one-dimensional distribution function $E_1(n)$ then has to satisfy the condition

$$\int_0^\infty E_1(n)\,dn = \overline{u_1^2} \tag{2.6}$$

This power spectrum can be calculated from the autocorrelation function, $R_E(\tau)$,

$$E_1(n) = 4\,\overline{u_1^2} \int_0^\infty R_E(\tau)\,\mathrm{Cos}\,(2\pi n\tau)\,d\tau \tag{2.7}$$

or directly from the original signal by Fourier transforming it. The Eulerian time correlation $R_E(\tau)$ is defined as

$$R_E(\tau) = \frac{\overline{u_1(t)u_1(t+\tau)}}{\overline{u_1^2}} \tag{2.8}$$

The wave-number spectrum is similar to the frequency spectrum and is defined by

$$E_1(\kappa_1) = \frac{U_1}{2\pi} E_1(n) \tag{2.9}$$

so that

$$\int_0^\infty E_1(\kappa_1)\,d\kappa_1 = \overline{u_1^2} \tag{2.10}$$

where

$$\kappa_1 = \frac{2\pi n}{U_1}\,, \text{ the wave number}$$

It has been mentioned by Schügerl (1980) that effective gas dispersion is possible only if the fraction of microturbulence is sufficiently large.

The power spectrum of the microturbulence would therefore have to have considerable influence on the turbulent gas dispersion. Figure 2.1 shows a one-dimensional energy spectrum in stirred tanks for various tank dimensions as given by van der Molen and van Maanen (1978). As usual, the energy content of the turbulent eddies was plotted as a function of the wave number $\kappa$. From this diagram one can see the well-known phenomenon that large eddies have high energy content. With increasing wave number the energy content decreases. Considerable energy losses occur when energy is transmitted from large primary eddies to the micro eddies. According to Schügerl (1980), the efficiency of gas dispersion for a bubble column with static spargers is higher than that for stirred tanks, because primary eddies of a considerably smaller size are produced in bubble columns. Therefore, the lower range of wave numbers of the energy spectrum, in which the energy is useless for gas dispersion, is missing in bubble columns.

## 4. Energy Dissipation Spectrum

Eddies of different size have different energy dissipation capabilities. It can be shown that the spectrum of the dissipation, $\Phi(\kappa)$, is given by (Batchelor 1967, Hinze 1975)

$$\Phi(\kappa) = 2\nu\kappa^2 E(\kappa) \tag{2.11}$$

The dissipation rate per unit mass $\varepsilon$ is given by

$$\varepsilon = \int_0^\infty \Phi(\kappa)\, d\kappa = 2\nu \int_0^\infty \kappa^2 E(\kappa)\, d\kappa \tag{2.12}$$

From Equations (2.11) and (2.12) one can recognize that the smallest eddies have the highest energy dissipation rates, whereas their energy content is negligible compared to the large eddies.

NOMENCLATURE

| | | |
|---|---|---|
| $E$ | : | power spectrum |
| $\ell$ | : | integral length scale of the turbulence |
| $n$ | : | frequency associated with turbulent eddy |
| $R_E$ | : | Eulerian correlation function |
| $Re$ | : | Reynolds number |
| $t$ | : | time |
| $u_1$ | : | component of fluctuating velocity in direction 1 |
| $U$ | : | main stream velocity |
| $U_1$ | : | mean velocity in direction 1 |
| $v$ | : | Kolmogorov microscale of velocity |

Greek Letters:

| | | |
|---|---|---|
| $\varepsilon$ | : | energy dissipation rate per unit mass |
| $\eta$ | : | Kolmogorov microscale of length |
| $\kappa$ | : | wave number |
| $\nu$ | : | kinematic viscosity |
| $\tau$ | : | time delay |
| $\Phi$ | : | energy dissipation spectrum |

Subscripts:

| | | |
|---|---|---|
| 1 | : | direction 1 or one-dimensional |

REFERENCES

Batchelor, G. K.," Homogeneous Turbulence," Cambridge University Press, London (1967)

Hinze, J. O.," Turbulence," McGraw-Hill, New York (1975)

Kolmogorov, A. N., Compt. Acad. Sci., USSR 30, 301 (1941)

Schügerl, K.," Neue Bioreaktoren fur aerobe Prozesse," Chem. Ing. Tech., 52, 951 (1980)

Taylor, G. I.," Statistical Theory of Turbulence. Part I-IV," Proc. of the Royal Society, A151, 421 (1935)

van der Molen, K., and H. R. E. van Maanen, Chem. Eng. Sci., 33, 1161 (1978)

**THIS BOOK CONTAINS NUMEROUS PAGES WITH DIAGRAMS THAT ARE CROOKED COMPARED TO THE REST OF THE INFORMATION ON THE PAGE.**

**THIS IS AS RECEIVED FROM CUSTOMER.**

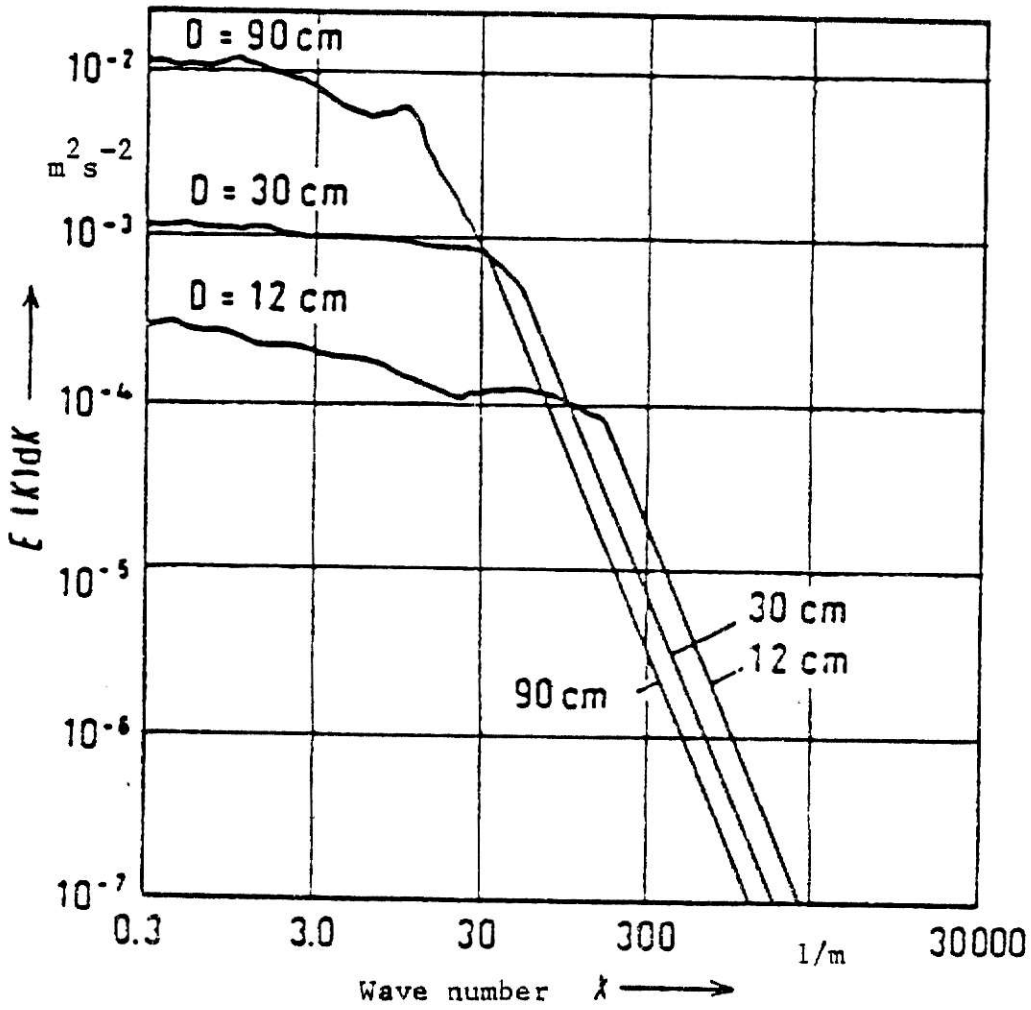



Figure 2.1 One-dimensional energy spectrum in stirred tank with different tank diameters (van der Molen and van Maanen 1978).

THIS BOOK
CONTAINS
NUMEROUS PAGES
WITH THE ORIGINAL
PRINTING BEING
SKEWED
DIFFERENTLY FROM
THE TOP OF THE
PAGE TO THE
BOTTOM.

THIS IS AS RECEIVED
FROM THE
CUSTOMER.

# CHAPTER III

## BUBBLE BREAK-UP AND COALESCENCE IN FERMENTATION

### 1. Introduction

In the pharmaceutical industry, the productivity of fermentations is frequently limited by the transfer of oxygen from the gas phase to the organism in the liquid. Three important factors affect the rate of mass transfer in gas-liquid contactors: the liquid phase mass transfer coefficient $k_L$, the interfacial area a, and the degree of liquid mixing in the system. In systems that are well-mixed, the mass transfer coefficient $k_L$ is not greatly affected by liquid hydrodynamics, changes in the interfacial area generally control the mass transfer rate. Ulbrecht and Ranade (1978) report that $k_La$ can be reduced by a factor of two in viscous solutions and by a factor of ten or more in viscoelastic polymer solutions, primarily due to the decrease in interfacial area.

Two phenomena, bubble break-up and coalescence, control the bubble size distribution and thus the interfacial area. Bubble break-up is controlled by the liquid phase hydrodynamics and is affected by the physical properties of the liquid, the power input to the system and by the sparger design in some cases. There are several types of flow regimes that a bubble may experience in a gas-liquid contactor. These fields can be described as turbulent, laminar or stagnant with respect to the bubble. The mechanism of break-up varies greatly over the range of hydrodynamic conditions. Bhavaraju et al. (1978) have suggested that at low and moderate viscosities bubble break-up is related to liquid-phase turbulence and is independent of conditions in the sparger orifice, but there is no unanimity of opinion with regard to phenomena occurring in the liquid phase. In the investigation of bubble coalescence in a swarm of bubbles rising through a deep pool of liquid, Otake et al. (1977)

found that the liquid viscosity largely determines the extent of bubble coalescence. They also observed that when a following bubble approaches the leading bubble closely enough, it appears to be accelerated and gathered into the back of the leading bubble. The critical distance at which the leading bubble began to exert a noticeable influence on the following one was within about three to four diameters of the leading bubble. The condition for the occurrence of coalescence was determined in terms of overlap between the projected areas of the two bubbles.

The purpose of this chapter is to study the mechanisms involved in bubble break-up and coalescence with the aid of bubble size distribution measurements in an airlift fermentor. The effect of liquid viscosity, electrolyte and power input on coalescence and break-up are also examined.

## 2. Mechanisms of Bubble Break-Up and Coalescence

### Bubble Break-Up

The mechanism of bubble break-up in commercial gas-sparged devices is uncertain. If one formulated a list of plausible causes of bubble size reduction, it might include: viscous shear, impingement, resonant break-up (by critically-sized eddies or vortex-induced oscillation), Rayleigh-Taylor instability, and dynamic pressure deformation.

Clift, Grace, and Weber (1978) have discussed impingement, resonant break-up, and Rayleigh-Taylor instability. The former, of course, is highly dependent upon flow pattern and equipment configuration; obstructions placed in the flow field are requisite. Resonant break-up by vortex-shedding and Rayleigh-Taylor instability are probably not common mechanism for bubble size reduction in air-lift fermentors, although Sevik and Park (1973) have suggested that violent deformation will occur if a bubble encounters an exciting eddy frequency that matches its fundamental mode of vibration.

Hinze (1955) predicted mechanisms for droplet break-up in various flow fields by suggesting that droplet break-up is the result of viscous shear forces and turbulent pressure fluctuations in the vicinity of a droplet. He also pointed out that in dispersions where drops are larger than the Kolmogorov microscale, $\eta$, dynamic pressure forces rather than viscous shear forces control the breakage processes. For a turbulent flow in water with $\varepsilon$ = 1000 $cm^2/sec^3$, $\eta$ = 0.0056 cm; at a dissipation rate of 100 $cm^2/sec^3$, $\eta$ = 0.01 cm. For high viscosity medium such as CMC solution with viscosity equal to 16 cP and $\varepsilon$ = 1000 $cm^2/sec^3$, $\eta$ = 0.045 cm; it seems likely that only the smallest bubbles present in a fermentor could be affected by viscous shear. If we assume that bubble break-up is caused by dynamic pressure forces and opposed by surface tension forces, then at the point of breakage, these forces must balance:

$$\frac{\rho_c \overline{u^2}}{2} = k' \frac{4\sigma}{d_{max}} \qquad (3.1)$$

where $d_{max}$ is the maximum stable bubble diameter in this flow field, and $\overline{u^2}$ is the mean square value of the fluctuating velocity over a distance $d_{max}$. This balance leads to the prediction of a critical Weber number:

$$We_c = \frac{\rho_c \overline{u^2} d_{max}}{2\sigma} \qquad (3.2)$$

Under highly turbulent conditions bubble break-up can be modeled with the statistical theory of turbulence, even though flow fields in process equipment are generally nonisotropic. If the phenomena of interest occur in the equilibrium range of wavenumbers, however, the assumption of local isotropy can be invoked. For this case, the main contribution to the turbulent kinetic energy is made by the fluctuations in the wavenumber region where the Kolmogorov (-5/3) distribution law is valid. In this inertial subrange the

three dimensional wavenumber spectrum $E(\kappa)$ is solely determined by the energy dissipation rate $\varepsilon$ and wavenumber $\kappa$:

$$E(\kappa) = \alpha\varepsilon^{2/3}\,\kappa^{-5/3} \tag{3.3}$$

Since the energy content of this spectrum between wave number $\kappa$ and $\kappa + d\kappa$, is $E(\kappa)d\kappa$, one finds

$$\overline{u^2} = \int_{1/d_{max}}^{\infty} E(\kappa)d\kappa = \int_{1/d_{max}}^{\infty} \alpha\varepsilon^{2/3}\,\kappa^{-5/3}\,d\kappa \tag{3.4}$$

Integrating Eq. (3.4) we obtain

$$\overline{u^2} = C_1\varepsilon^{2/3}\,d_{max}^{2/3} \tag{3.5}$$

where $C_1 = 1.5\alpha$, and is approximately equal to 2.0 according to Batchelor (1951).

If we assume that the viscous shear force is not important, then we obtain from Eq. (3.2)

$$\frac{\rho_c d_{max}}{2\sigma}\,C_1\,(\varepsilon\,d_{max})^{2/3} = \text{const.}$$

or

$$d_{max} = C(\sigma/\rho_c)^{3/5}\,\varepsilon^{-2/5} \tag{3.6}$$

On introducing dimensionless groups into Eq. (3.6) we get

$$\frac{\rho_c\sigma d_{max}}{\mu_c^2} = C\left(\frac{\mu_c^5\,\varepsilon}{\rho_c\sigma^4}\right)^{-2/5} \tag{3.7}$$

This simple result also follows directly from dimensional reasoning once it has become evident that only the quantities $\rho_c$, $\sigma$, and $\varepsilon$ determine the size of the largest bubbles. If we want to apply this result to nonisotropic turbulent flows, we must assume that the turbulence pattern is locally isotropic for wavenumbers comparable to the inverse size of the largest bubbles.

Furthermore, nonisotropic turbulent flows are usually not homogeneous, and so the energy input and dissipation rate are not constant across the flow field; moreover, there is no equilibrium between energy input and dissipation rate at each point. In this case, even if local isotropy is present, the drop size as determined by Eq. (3.6) is still a function of the space coordinates.

For Weber numbers close to the critical value, McBride et al. (1980) have observed several other mechanisms. The first is a "turbulent" mechanism, which results in the explosion of dispersed phase droplets into many smaller droplets of similar size; the second is a "vortex stretching" mechanism, which results in the stretching and break-up of globules into two relatively large daughter drops and many small satellite droplets. The most prevalent is a "turbulent shear" mechanism where a drop is stretched to some great length before it breaks into two drops of approximately equal size. A fourth mechanism occurs less frequently and involves a small drop being stripped from a larger one. According to their experiments, the turbulent shear mechanism of break-up seems to prevail. Drops near the center of the tube are stretched and oscillate. As these oscillations grow a distinct dumbbell shape can be identified. This dumbbell then splits into two daughter drops, one of which is usually slightly larger than the other.

Otake et al. (1977) also observed another type of bubble break-up that does not fall into any of the above categories. They found that a rising bubble, trailing another and displaced horizontally from the leader's centerline, undergoes deformation and rupture at a critical distance of separation. In contrast, when the two bubbles were vertically aligned coalescence usually took place. This photographically-observed breakup phenomenon seems to be related to the vortex street generated by the leading bubble; the vertical compression is a consequence of the trailing bubble's encounters with vortex

structures at the edge of the wake. The leading edge of the deforming bubble experiences concomitant shear stress directed towards the wake interior. This effect, assuming asymmetrical binary breakage, should lead to the larger fragment moving into the center of the wake region with smaller fragment being ejected; the photographic evidence presented by Otake et al. appears to substantiate this hypothesis.

Bubble Coalescence

Bubble coalescence plays a significant role in determining the bubble size distribution and interfacial area in all sorts of gas-liquid contacting devices, and plays a dominant role in gas-liquid separating equipment. In a typical gas-sparged contactor or reactor, coalescence is detrimental because it decreases the surface area of the bubbles; in a separator it is desirable because it increases the size and hence the rise velocity of the bubbles.

Bubble coalescence is usually considered to be a three-step process consisting of:

1. Approach of two bubbles to within a distance of $10^{-4}$ - $10^{-3}$ cm.
2. Further thinning of the liquid layer between the bubbles to $10^{-6}$ - $10^{-3}$ cm.
3. Rupture of the film via an instability mechanism.

The first step of coalescence has been studied by several authors. De Nevers and Wu (1971) performed experiments on air bubbles in glycerine and in water. They studied the interaction and coalescence of bubbles rising-in-line, by using high-speed cinematography. The resulting coalescence behavior has been correlated by a simple " wake capture " model which assumes that each bubble trails a wake, and that the bubble coalescing from below accelerates when it enters the wake of the leading bubble and thus overtakes the leading bubble.

Bhaga (1979) also studied the coalescence of two vertically aligned bub-

bles in highly viscous liquids photographically. He observed that the trailing bubble has relatively little influence on the velocity and the shape of the leading bubble, but the wake of the leading bubble has a significant effect on the velocity and the shape of the trailing bubble. The behavior of the bubble formed by coalescence depends on the viscosity of the liquid as well as the size of the interacting bubbles. Walter et al. (1982) suggested that the thinning process of a liquid film separating two coalescing bubbles consist of two parts. The first stage is a very rapid stretching of the film down to a thickness where forces acting on the film are statically balanced. The second stage of film thinning is the further thinning of the pseudoequilibrium film. The mechanism of this step is the pressure induced drainage of the liquid between the immobile surfaces of the film.

Marucci et al. (1972) investigated the coalescence process in low to medium viscosity Newtonian fluids. They studied bubbles growing side-by-side by using high speed photography. The rupture process was very fast (<1/5000 sec.), and it was concluded that the film drainage process was the rate determining step. Mcbride et al. (1980) have designed a flow system to study angle collisions in turbulent flow fields. Results indicate that wake capture is the most common type of coalescence mechanism for angled approaches. Experimental time constants are of order $10^{-3}$ to $10^{-2}$ seconds, which agree with the results for film rupture times.

3. Bubble Size Distribution and Size Distribution Dynamics

Bubble size distributions in gas-liquid dispersions evolve as a consequence of droplet breakage, coalescence, mass transfer and pressure changes. The dynamic character of breakage and coalescence in emulsification has been recognized by some workers (Valentas et al. 1966, Bajpai et al. 1976) who have attempted a prediction of drop-size distributions by the method of population

balances. However quantitative predictions are precluded by lack of adequate information about droplet breakage and coalescence rates.

Valentas, Bilous and Amundson (1966) considered both breakage and coalescence as occurring at finite rates and predicted drop size distributions which, however, were not compared with experimental observations.

Zeitlin and Tavlarides (1972) have simulated the drop-phenomena in an agitated system by dividing the system into two zones, first the zone of high turbulence where breakage of drops predominates, secondly the zone of circulation where only coalescence takes place. But, no adequate information is available about breakage and coalescence frequencies which appear in their work.

Narsimhan et al. (1979) have proposed a model for transitional breakage probability of droplets in agitated lean liquid-liquid dispersions based on the mechanism of breakage due to deformation by relative velocity fluctuations. An universal dimensionless equilibrium drop size distribution is derived using a population balance equation. But only a qualitative comparison of the derived equilibrium distribution with the experimental observations was made because parameter in this model cannot be evaluated accurately due to lack of information.

Akita and Yoshida (1974) have used photographic techniques to determine interfacial areas in bubble columns; they found that bubble size distribution could be adequately described by the log-normal law:

$$f(d) = \frac{1}{\sqrt{2\pi}\ \ln \sigma_g} \exp\left[-\frac{(\ln d - \ln \bar{d})^2}{2(\ln \sigma_g)^2}\right] \qquad (3.8)$$

where d is the bubble size, $\bar{d}$ is the geometric mean bubble size, and $\sigma_g$ is the geometric standard deviation. The two parameters for this density function, $\bar{d}$ and $\sigma_g$, can be found directly from a plot of data upon logarithmic probability

paper, since:

$\bar{d}$ = geometric mean bubble size = $d_{50\%}$

$\sigma_g$ = geometric standard deviation = $d_{84.13\%}/d_{50\%}$

In the air-lift fermentor under steady state conditions, the total bubble volume $V_{12}$ in a narrow size interval $(d_1, d_2)$ will be spatially variable $(V_{12}(Z))$ due to: breakup, coalescence, mass transfer and pressure effects. By carefully controlling system parameters, the dynamic effects in the model fermentor can be restricted to pressure, breakup and coalescence, thereby permitting application of the conservation equation:

$$\frac{dV_{12}}{dZ} = B\frac{dP}{dZ} + H_{11}(Z) - H_{12}(Z) + G_{22}(Z) - G_{12}(Z) \qquad (3.9)$$

where $H_{11}$: the production of volume within $(d_1, d_2)$ by coalescence of smaller bubbles per unit height.

$H_{12}$: the reduction of volume within $(d_1, d_2)$ by coalescence of bubbles in this interval per unit height.

$G_{22}$: the production of volume within $(d_1, d_2)$ by breakup of larger bubbles per unit height.

$G_{12}$: the reduction of volume within $(d_1, d_2)$ by breakup of bubbles in this interval per unit height.

If we can formulate $H_{11}$, $H_{12}$, $G_{22}$ and $G_{12}$ from theoretical or dimensional arguments, then we may be able to predict the bubble size distribution in the fermentor. Otherwise we need to measure $V_{12}(Z)$, then use this experimental data to fit the proposed forms for $H_{11}$, $H_{12}$, $G_{22}$ and $G_{12}$. For lean systems coalescence is negligible and the terms $H_{11}$ and $H_{12}$ may be omitted.

## 4. Experimental Procedure

A cyclindrical airlift fermentor has been constructed with optically-flat glass panels for bubble size distribution analysis. The fermentor is 136 cm high, 15 cm diameter and air is introduced on the upflow side through 38 1.6 mm holes (see Fig. 3.1). Experiments were conducted for four different systems: air-tap water, air-salt water (0.6% NaCl), air-CMC solution (0.5%) and air-CMC solution (0.8%). Surface tension measurements were made using a Fisher Surface Tensiomat Model 21. The physical properties of these systems are compiled in Table 3.1.

Rheological Behavior

The rheological behavior of Newtonian fluids can be characterized by their viscosity which was measured by the Cannon-Fenske viscometer. For non-Newtonian fluids such as pseudoplastic solutions rheological properties can be characterized by their fluid consistency index K and flow behavior index n. CMC (carboxymethyl cellulose) solutions are pseudoplastic and follow the power law of Ostwald-de Waele:

$$\tau = K\dot{\gamma}^{n} \tag{3.10}$$

where $\tau$ is the shear stress and $\dot{\gamma}$ is the shear rate.

Voigt et al. (1980) have constructed curves to show the dependence of K and n on CMC concentration. The apparent viscosity $\mu_a$ of CMC solution is given by

$$\mu_a = K\dot{\gamma}^{n-1} \tag{3.11}$$

For estimating $\mu_a$, the shear rates in the fermentor with various superficial gas velocities are required. To this end, the relation proposed by Nishikawa et al. (1977) was used. Hence, the apparent viscosity is given by

$$\mu_a = K(50\ V_G)^{n-1} \qquad V_G \geq 4.0 \text{ cm/s} \tag{3.12}$$

or

$$\mu_a = K(100\ V_G)^{n-1/2} \qquad V_G < 4.0 \text{ cm/s} \tag{3.13}$$

where $V_G$ is the superficial gas velocity in the fermentor.

Gas Hold-Up

The mean relative gas hold-up, $E_G$, is defined by

$$E_G = \frac{V - V_L}{V} = \frac{H - H_L}{H} \tag{3.14}$$

where V :the volume of the bubbling layer.

$V_L$:the volume of the bubble-free liquid layer.

H :the height of the bubbling layer.

$H_L$:the height of the bubble-free liquid layer.

The determination of $E_G$ was carried out by measuring H and $H_L$ in the fermentor.

Bubble Size

A direct photographic method for bubble size distribution analysis has been developed in which negatives are scanned and reduced to histographic data by means of a Bausch & Lomb Omnicon system. From the bubble size distribution, the Sauter mean diameter, $d_s$, is calculated by

$$d_s = \frac{\sum_1^N n_i d_i^3}{\sum_1^N n_i d_i^2} \tag{3.15}$$

where $n_i$ is the frequency of the bubbles with the diameter $d_i$. The maximum stable bubble diameter $d_{max}$ was determined from the cumulative bubble size distribution by selecting $d_{max} \simeq D_{95}$ where $D_{95}$ corresponds to 95% cumulative volume.

Specific Interfacial Area

The specific interfacial area with regard to the liquid volume, a, can be calculated by Eq. (3.16):

$$a = \frac{6E_G}{d_s(1 - E_G)} \tag{3.16}$$

assuming the bubbles have a nearly spherical shape.

Power Input

The power input in airlift fermentor can be calculated by applying steady state macroscopic energy balance for the gas phase over the upflow zone as shown in Eq. (3.17):

$$\Delta(1/2V^2) + \Delta\Phi + \int_{P_1}^{P_2} \frac{dP}{\rho_G} + \bar{W} + \bar{F} = 0 \tag{3.17}$$

where $1/2V^2$ : the kinetic energy of gas per unit mass.

$\Phi$ : the potential energy of gas per unit mass.

$\rho_G$ : density of gas.

$P_1$ : pressure at gas sparger.

$P_2$ : pressure at the top of fermentor.

$\bar{W}$ : work done by the unit mass of gas.

$\bar{F}$ : friction loss of gas per unit mass.

If we neglect the friction loss $\bar{F}$, and assume ideal gas behavior, then the power input $\bar{P}$ can be obtained by Eq. (3.18):

$$\bar{P} = -\bar{W} F \rho_G = F\rho_G[\frac{RT}{M_G} \ln (P_1/P_2) - gH - 1/2(V_2^2 - V_1^2)] \tag{3.18}$$

where $\bar{P}$ : power input.

$F$ : volumetric gas flow rate.

$R$ : gas constant.

$T$ : absolute temperature.

$g$ : gravitational acceleration.

$M_G$ : gas molecular weight.

$V_1$ : gas velocity at the inlet of control volume.

$V_2$ : gas velocity at the outlet of control volume.

However, since the second and the third terms together make up only 0.2% of the overall power input, the power input due to gas expansion dominates:

$$\bar{P} = F \rho_G \frac{RT}{M_G} \ln (P_1/P_2) \tag{3.19}$$

The energy dissipation rate per unit mass of liquid, $\varepsilon$, is given by

$$\varepsilon = \frac{\bar{P}}{V_U \rho_c} \tag{3.20}$$

where $V_U$ is the liquid volume in the upflow zone.

Liquid Circulation Velocity

The liquid circulation velocity can be obtained by making a force balance which involves equating the drag force to the buoyancy force on the downflow side bubble which is nearly static. According to Levich (1962) the liquid circulation velocity for air-water system is given by

$$U_L = 2 \sqrt{\frac{g r_B}{0.9}} \tag{3.21}$$

where $r_B$ is the bubble radius.

Critical Weber Number

The critical Weber numbers were calculated by substituting Eq. (3.5) into Eq. (3.2) and letting $C_1 = 2.0$.

Integral Scale Reynolds Number

The integral scale Reynolds number $Re_I$ is defined by Eq. (3.22):

$$Re_I = \frac{\rho_c U_I \ell}{\mu_c} \tag{3.22}$$

where $\ell$ is the integral length scale of the turbulence which is roughly equal to the width of the flow, and $U_I$ is the integral velocity scale which can be obtained by applying Eq. (2.4) if the average energy dissipation rate $\epsilon$ is known.

All the experiments were conducted with bubble-free liquid level about 4 cm below the top of the baffle.

## 5. Discussion of Results

A study of the mechanism of bubble breakup and coalescence in airlift fermentors has been conducted using macrophotography and image analysis to measure bubble size distribution for different systems at various air-flow rates. A typical example of cumulative volume distribution for the air-tap water system is plotted on logarithmic probability paper as shown in Fig. 3.37. If the data on the logarithmic probability paper can be approximated by a straight line, then they are adequately described by the log-normal distribution. This figure indicates that the log-normal distribution is satisfactory except at very large sizes.

The probability density functions shown in Fig. 3.5 to Fig. 3.33 are obtained by numerically differentiating cumulative volume distributions and passing them through a digital triangular filter:

$$f_i = (f_{i-2} + 3f_{i-1} + 5f_i + 3f_{i+1} + f_{i+2})/13 \qquad (3.23)$$

A smoothing filter has an effect equivalent to broadening the width of the bands of the histogram. However, use of the triangular smoothing has the advantage that while discontinuities in the curve are removed, only relatively small dispersion of the data occurs. The basic characteristics of the curve are preserved. Comparisons of the original data with the data after smoothing are shown in Fig. 3.34 to Fig. 3.36.

### Flow Behavior

The liquid hydrodynamic characteristics are shown in Table 3.2. The flow patterns for tap water and salt water show highly turbulent conditions judging from the integral scale Reynolds number of the system. Visually, all systems do appear to be turbulent within the range of flow rates examined although the integral Reynolds number for CMC solutions are much smaller

than those for the tap water and salt water systems. The conditions of liquid turbulence can also be justified by applying the criterion of Bhavaraju et al. (1978) which states that the ratio of the scale of energy containing eddies to the scale of energy dissipating eddies should exceed 200 for the existence of liquid turbulence. As can be seen in Table 3.2, the ratio $\ell/\eta$ is greater than 200 for all of the systems studied.

The integral velocity represents the velocity scale of the largest eddies in the flow field with a length scale roughly equal to the width of the flow R (radius of the column) and is obtained by applying Eq. (2.4). This velocity scale should be approximately equal to the mean liquid velocity in the upflow zone. A comparison of integral velocity with liquid circulation velocity for tap water system is shown in Table 3.3; notice that both velocities are of the same order of magnitude, but the mean liquid velocities are always a little smaller than the integral velocities within the experimental range of air flow rates. One possible source of error results from neglecting the holdup difference between the upflow zone and downflow zone, causing the underestimation of mean liquid velocities on the upflow side.

Dynamics of Bubble Size Distribution

The dynamics of bubble size distribution for tap water system are shown in Fig. 3.5 to Fig. 3.11. As can be seen from Fig. 3.5 to Fig. 3.7, the probability density function in each case gradually shifts towards the small bubble region as the observation moves from the bottom window (#1) to the top window (#4); furthermore, the higher the window position, the more uniform the bubble size distribution. This dynamic behavior can be explained by the continuous breakage of primary bubbles when they leave the sparger and are exposed to the turbulent flow field. The influence of power input on bubble size distribution has been shown in Fig. 3.8 to Fig. 3.11. It is evident from

these figures that the bubble size decreases with increasing air flow rate. The decrease in the critical bubble size (which is the size of the maximum stable bubble diameter in a turbulent flow field) with an increase in dynamic pressure forces as a result of a higher air flow rate causes the bubble size distribution to shift towards the smaller size range. This is because bubbles larger than the critical bubble cannot survive in the turbulent flow field. However, the bubble coalescence frequency also increases with higher air flow rate and thus will tend to offset bubble break-up resulting from the increase in dynamic pressure forces. Fig. 3.8 to Fig. 3.11 show that the bubble size is reduced significantly when the air flow rate is increased from 30 $ft^3/hr$ to 60 $ft^3/hr$, however, the bubble size distribution does not change too much when the air flow rate is further increased to 90 $ft^3/hr$. This is due to the effect of bubble coalescence which can be neglected at low air flow rates (lean dispersions) but will become more important at higher numerical densities (higher gas hold-ups).

The effect of electrolyte on bubble size distribution is shown in Fig. 3.12 to Fig. 3.18 for salt water system which has an ionic strength equal to 0.1 gmoles/liter. A striking difference can be seen by comparing the bubble size distributions of the tap water and salt water systems. The bubble size of salt water system is significantly reduced for each window examined when the air flow rate is increased to 90 $ft^3/hr$. This is probably due to a decreased coalescence rate because of repulsion between individual bubbles as a result of the collection of like charges on their surfaces and a decreased surface tension because of the electrolyte in the solution.

The influence of liquid viscosity on bubble size distribution is shown in Fig. 3.19 to Fig. 3.33; the bubble size reduction can still be observed from window #1 to window #3 for 0.5% CMC solution within the range of air flow rates studied. However, for 0.8% CMC solution the bubble size does not

have a significant change from window #2 to window #4. And the increase of air flow rate no longer contributes to bubble size reduction, moreover, it causes an increase of bubble size apparently because of the increase in bubble coalescence frequency. This can be explained by the shifting balance between bubble break-up and bubble coalescence at higher viscosities. This reasoning can also be justified by comparing the critical bubble size for tap water and CMC solutions as listed in Table 3.4; the higher the viscosity, the larger the maximum stable bubble diameter.

Effect of Energy Input on the Critical Bubble Size

An illustration of the influence of energy input on the critical bubble size has been shown in Fig. 3.2 to Fig. 3.4 for the four systems studied. In Figure 3.2, the critical bubble size is proportional to the -0.38 power of energy input which is very close to the theoretical value -2/5 in Eq. (3.7). If we consider only the low viscosity system as shown in Fig. 3.3, the slope of the regression line is -0.49 which is slightly lower than the theoretical value. But for the high viscosity system the slope is -0.36 as shown in Fig. 3.4 which is larger than that of the low viscosity system, however, it is not too different from the theoretical value. This is probably due to the fact that higher viscosities increase the quantity of energy dissipated by viscous forces and lessen the efficiency of power used in the bubble breakage process.

A comparison of critical Weber numbers for four different systems appears in Table 3.4. For tap water and salt water systems the critical Weber number is about 3~4 and does not change significantly with air flow rate. For CMC solutions the critical Weber number is between 5 and 7 and also does not vary much with air flow rate.

The effect of power input on bubble size can also be justified by comparing the variation of the Sauter mean diameter with superficial gas velocity as shown in Fig. 3.41. The Sauter mean diameter decreases with increasing superficial gas velocity for tap water and salt water systems just as expected. For the 0.5% CMC solution the Sauter mean diameter does not change significantly with superficial gas velocity, but for 0.8% CMC the Sauter mean diameter increases with superficial gas velocity due to the inefficient use of power available for bubble breakage.

Effect of Superficial Gas Velocity On Gas Hold-Up

The influence of superficial gas velocity on gas hold-up is shown in Fig. 3.38. As can be seen from this figure, the gas hold-up for salt water system is higher than that for the tap water system except for the lowest flow rate. This is because small bubbles generated in the salt water system have a longer mean residence time than that of the larger bubbles generated in the tap water system. However, CMC solutions contain large bubbles which have a shorter mean residence time than that of the bubbles generated in the tap water system, so they have a lower gas hold-up as compared to the tap water system.

A comparison of the specific interfacial area for four different systems is shown in Fig.3.42. The addition of an electrolyte has a significant effect on the specific interfacial area as compared to the other three systems with the same power input. This is due to the combined effect of the increase in gas hold-up and the decrease of the Sauter mean diameter with power input.

6. Conclusions

The results of the experiments described in this chapter, lead to the following conclusions:

i) The mechanism of bubble break-up is mainly due to the dynamic pressure

fluctuations in the vicinity of the bubble at positions remote from the sparger for the four systems in the range of air flow rates examined.

ii) The integral velocity scale was found to be approximately equal to the mean liquid velocity for tap water system.

iii) The efficiency of power input for bubble size reduction decreases with increasing liquid viscosity because higher viscosities dissipate more energy.

iv) The addition of an electrolyte may increase the gas hold-up and decrease the mean bubble diameter which results in a higher specific interfacial area.

v) The critical Weber number is about 3~4 for low viscosity systems and is about 5~7 for CMC solutions; $We_c$ is relatively independent of the air flow rate.

vi) The maximum stable bubble diameter is roughly proportional to the -2/5 power of the energy input, and it can be closely predicted using Eq. (3.7).

NOMENCLATURE

| | | |
|---|---|---|
| $a$ | : | interfacial surface area per unit volume of liquid |
| $B$ | : | variation of bubble volume with respect to pressure change |
| $C$, $C_1$ | : | proportionality constant |
| $d$ | : | diameter of bubble |
| $\bar{d}$ | : | geometric mean bubble diameter |
| $d_1$, $d_2$ | : | bubble diameter in interval 1 and 2 respectively |
| $d_{max}$ | : | maximum stable bubble diameter |
| $d_s$ | : | Sauter mean bubble diameter |
| $D_{95}$ | : | bubble diameter lie in the 95 percentile of the density function |
| $E$ | : | three-dimensional wave number spectrum |
| $E_G$ | : | gas hold-up |
| $f$ | : | probability density function of the bubble size |
| $F$ | : | volumetric gas flow rate |
| $\bar{F}$ | : | friction loss of gas per unit mass |
| $g$ | : | acceleration due to gravity |
| $H$ | : | gassed liquid height |
| $H_L$ | : | ungassed liquid height |
| $k'$ | : | proportionality constant |
| $k_L$ | : | liquid phase mass transfer coefficient |
| $K$ | : | fluid consistency index |
| $\ell$ | : | integral length scale of turbulence |
| $M$ | : | molecular weight |
| $n$ | : | flow behavior index |
| $n_i$ | : | frequency of the bubble with size $d_i$ |
| $P$ | : | static pressure |
| $\bar{P}$ | : | power input |
| $P_1$, $P_2$ | : | pressures at gas sparger and top of fermentor respectively |

$r_B$ : bubble radius

R : gas constant

Re : Reynolds number ( $= \frac{U\ell}{\nu}$ )

T : absolute temperature

u : fluctuating velocity

U : main stream velocity

V, $V_L$ : volume of bubbling layer and bubble-free liquid layer respectively

$V_G$ : superficial gas velocity

$V_U$ : liquid volume in the upflow zone

$V_1$, $V_2$ : gas velocity at the inlet and outlet respectively of control volumn

$V_{12}$ : total bubble volume in a size interval ($d_1$, $d_2$)

We : Weber number ( $= \frac{\rho \overline{cu^2} d}{2\sigma}$ )

Z : distance from the sparger in the fermentor

Greek Letters:

$\alpha$ : proportionality constant

$\dot{\gamma}$ : shear rate

$\epsilon$ : energy dissipation rate per unit mass

$\eta$ : Kolmogorov microscale

$\kappa$ : wave number

$\mu$ : viscosity

$\nu$ : kinematic viscosity

$\rho$ : density

$\sigma$ : surface tension

$\sigma_g$ : geometric standard deviation

$\tau$ : shear stress

$\Phi$ : the potential energy of gas per unit mass

Subscripts:

| | | |
|---|---|---|
| a | : | apparent value |
| c | : | continuous phase or critical value |
| G | : | gas phase |
| i | : | bubble size interval |
| I | : | integral scale |
| L | : | liquid phase |
| U | : | upflow zone |

REFERENCES

Akita, K., and F. Yoshida, "Bubble Size, Interfacial Area, and Liquid Phase Mass Transfer Coefficient in Bubble Columns, " Ind. Eng. Chem., Process Des. Develop., 13, 84 (1974)

Bajpai, R. K., D. Ramkrishna, and A. Prokop, "A Coalescence Redispersion Model for Drop-Size Distributions in an Agitated Vessel," Chem. Eng. Sci., 31, 913 (1976)

Batchelor, G. K., "Pressure Fluctuations in Isotropic Turbulence," Proc. Cambridge Phil. Soc., 47, 359 (1951)

Bhaga D., "Bubbles in Viscous Liquids: Shapes, Wakes and Velocities", Ph.D. Dissertation. McGill University, Montreal, Canada (1979)

Bhavaraju, S. M., T. W. F. Russell, and H. W. Blanch, "The Design of Gas Sparged Devices for Viscous Liquid Systems," A.I.Ch.E. J., 24, 454 (1978)

Clift, R., J. R. Grace, and M. E. Weber, "Bubbles, Drops, and Particles," Academic Press, New York (1978)

De Nevers, N., and J. L. Wu, "Bubble Coalescence in Viscous Fluids," A.I.Ch.E. J., 17, 182 (1971)

Hinze, J. O., "Fundamentals of the Hydrodynamic Mechanism of Splitting in Dispersion Processes," A.I.Ch.E. J., 1, 289 (1955)

Levich, V. G., "Physicochemical Hydrodynamics," Prentice-Hall, Inc. Englewood Cliffs, N. J. (1962)

Marucci, G., L. Nicodemo, and D. Acierno, "Cocurrent Gas-Liquid Flow," p. 95, Plenum Press (1972)

McBride, C., J. F. Walter, H. W. Blanch, and T. W. F. Russell, "Bubble Coalescence and Break-Up in Fermentations," Presented at VI Annual Fermentation Symposium, London Cnt. (1980)

Narsimhan, G., J. P. Gupta, and D. Ramkrishna, "A Model for Transitional Breakage Probability of Droplets in Agitated Lean Liquid-Liquid Dispersions," Chem. Eng. Sci., 34, 257 (1979)

Nishikawa, M., H. Kato, and K. Hashimoto, Heat Transfer in Aerated Tower Filled with Non-Newtonian Liquid," Ind. Eng. Chem., Process Des. Dev., 16, 133 (1977)

Otake, T., S. Tone, K. Nakao, and Y. Mitsuhashi, "Coalescence and Breakup of Bubbles in Liquids," Chem. Eng. Sci., 32,377 (1977)

Sevik, M., and S. H. Park, "The Splitting of Drops and Bubbles by Turbulent Fluid Flow," Journal of Fluids Engineering (Trans. of ASME), 53, March (1973)

Ulbrech, J. J., and V. R. Ranade, "Influence of Polymer Additives on the Gas-Liquid Mass Transfer in Stirred Tank," A.I.Ch.E. J., 24, 796 (1978)

Valentas, K. J., and N. R. Amundson, "Breakage and Coalescence in Dispersed Phase Systems," I. & E.C. fundamentals, 5, 533 (1966)

Voigt, J., and K. Schügerl, "Absorption of Oxygen in Countercurrent Multi-stage Bubble Columns-II. Aqueous Solutions with High Viscosity," Chem.Eng. Sci., 35, 1317 (1980)

Walter, J. F., T. Oolman, and H. W. Blanch, "Bubble Breakup and Coalscence in Fermentors," Presented at 1982 Annual A.I.Ch.E. Meeting, Los Angeles (1982)

Zeitlin, M. A., and L. L. Tavlarides, "Fluid-Fluid Interactions and Hydro-dynamics in Agitated Dispersions: A Simulation Model," Can. J. Chem. Eng., 50, 207 (1972)

Table 3.1 Properties of materials used ( at 25°C )

| Materials | $\rho$ , g/cm$^3$ | $\mu$ or $\mu_a$ , cP | $\sigma$ , dyne/cm |
|---|---|---|---|
| Tap Water | 0.989 | 0.89 | 64.8 |
| Salt Water | 0.991 | 0.90 | 55.3 |
| CMC (0.5%) | 0.994 | 6.20 - 6.66 | 68.7 |
| CMC (0.8%) | 0.993 | 13.40 - 15.90 | 65.4 |

Table 3.2 Comparison of hydrodynamic characteristics for four different systems at various air flow rates.

| Systems | Superficial gas velocity $V_G$, cm/s | Power input per unit volume $\bar{P}/V_U$, erg/cm$^3$ s | Ratio* $\ell/\eta$ | Integral Reynolds number $Re_I$ | Integral velocity $U_I$, cm/s |
|---|---|---|---|---|---|
| Tap Water | 2.59 | 2383 | 1827 | 22,000 | 26.4 |
| | 5.18 | 4767 | 2173 | 28,000 | 33.2 |
| | 7.77 | 7150 | 2405 | 32,000 | 38.0 |
| Salt Water | 2.59 | 2388 | 1812 | 22,000 | 26.4 |
| | 5.18 | 4777 | 2154 | 28,000 | 33.2 |
| | 7.77 | 7166 | 2384 | 32,000 | 38.0 |
| CMC (0.5%) | 2.59 | 2395 | 405 | 3,000 | 26.4 |
| | 5.18 | 4791 | 497 | 3,936 | 33.3 |
| | 7.77 | 7187 | 563 | 4,651 | 38.1 |
| CMC (0.8%) | 2.59 | 2394 | 211 | 1,256 | 26.4 |
| | 5.18 | 4788 | 265 | 1,700 | 33.2 |
| | 7.77 | 7190 | 306 | 2,058 | 38.1 |
| | 10.36 | 9587 | 339 | 2,365 | 41.9 |

* This is the ratio of the scale of energy containing eddies to energy dissipating eddies and the integral length scale $\ell$ is equal to the radius of the column (7.62 cm).

Table 3.3 Comparison of integral velocity with liquid circulation velocity for tap water system.

| Superficial gas velocity $V_G$, cm/s | Integral velocity $U_I$, cm/s | Bubble diameter* $d_D$, cm | Circulation velocity estimated by Eq.(3.20) $U_L$, cm/s |
|---|---|---|---|
| 2.59 | 26.4 | 0.15 | 18.0 |
| 5.18 | 33.2 | 0.30 | 26.0 |
| 7.77 | 38.0 | 0.50 | 33.0 |

* The bubble diameter $d_D$ was obtained by visual observation of the bubble size in down flow side.

Table 3.4 Comparison of bubble size and critical Weber number for four different systems at window #4.

| Systems | Superficial gas velocity $V_G$, cm/s | Sauter mean diameter $d_s$, cm | Geometric mean diameter $\bar{d}$, cm | Maximum stable bubble diameter $d_{max}$, cm | Critical Weber number $We_c$ |
|---|---|---|---|---|---|
| Tap Water | 2.59 | 0.50 | 0.66 | 1.35 | 4.53 |
| | 5.18 | 0.38 | 0.49 | 0.82 | 3.14 |
| | 7.77 | 0.36 | 0.49 | 0.81 | 4.03 |
| Salt Water | 2.59 | 0.51 | 0.69 | 1.20 | 5.32 |
| | 5.18 | 0.35 | 0.48 | 0.82 | 3.68 |
| | 7.77 | 0.29 | 0.37 | 0.64 | 3.27 |
| CMC (0.5%) | 2.59 | 0.35 | 0.56 | 1.30 | 4.04 |
| | 5.18 | 0.37 | 0.60 | 1.30 | 6.40 |
| | 7.77 | 0.35 | 0.61 | 1.04 | 5.79 |
| CMC (0.8%) | 2.59 | 0.33 | 0.62 | 1.50 | 5.37 |
| | 5.18 | 0.33 | 0.52 | 1.40 | 7.60 |
| | 7.77 | 0.38 | 0.67 | 1.10 | 6.67 |
| | 10.36 | 0.39 | 0.63 | 0.98 | 6.67 |

Table 3.5 Comparison of bubble size for four different systems at window #1.

| Systems | Superficial gas velocity $V_G$, cm/s | Sauter mean diameter $d_s$, cm | Geometric mean diameter $\bar{d}$, cm |
|---|---|---|---|
| Tap Water | 2.59 | 0.55 | 0.88 |
| | 5.18 | 0.50 | 0.84 |
| | 7.77 | 0.50 | 0.67 |
| Salt Water | 2.59 | 0.56 | 0.96 |
| | 5.18 | 0.48 | 0.71 |
| | 7.77 | 0.34 | 0.44 |
| CMC (0.5%) | 2.59 | 0.53 | 0.88 |
| | 5.18 | 0.79 | 1.20 |
| | 7.77 | 0.86 | 1.23 |
| CMC (0.8%) | 2.59 | 0.54 | 0.90 |
| | 5.18 | 0.97 | 2.00 |
| | 7.77 | 0.50 | 0.74 |
| | 10.36 | 0.91 | 1.50 |

# ILLEGIBLE DOCUMENT

THE FOLLOWING DOCUMENT(S) IS OF POOR LEGIBILITY IN THE ORIGINAL

THIS IS THE BEST COPY AVAILABLE

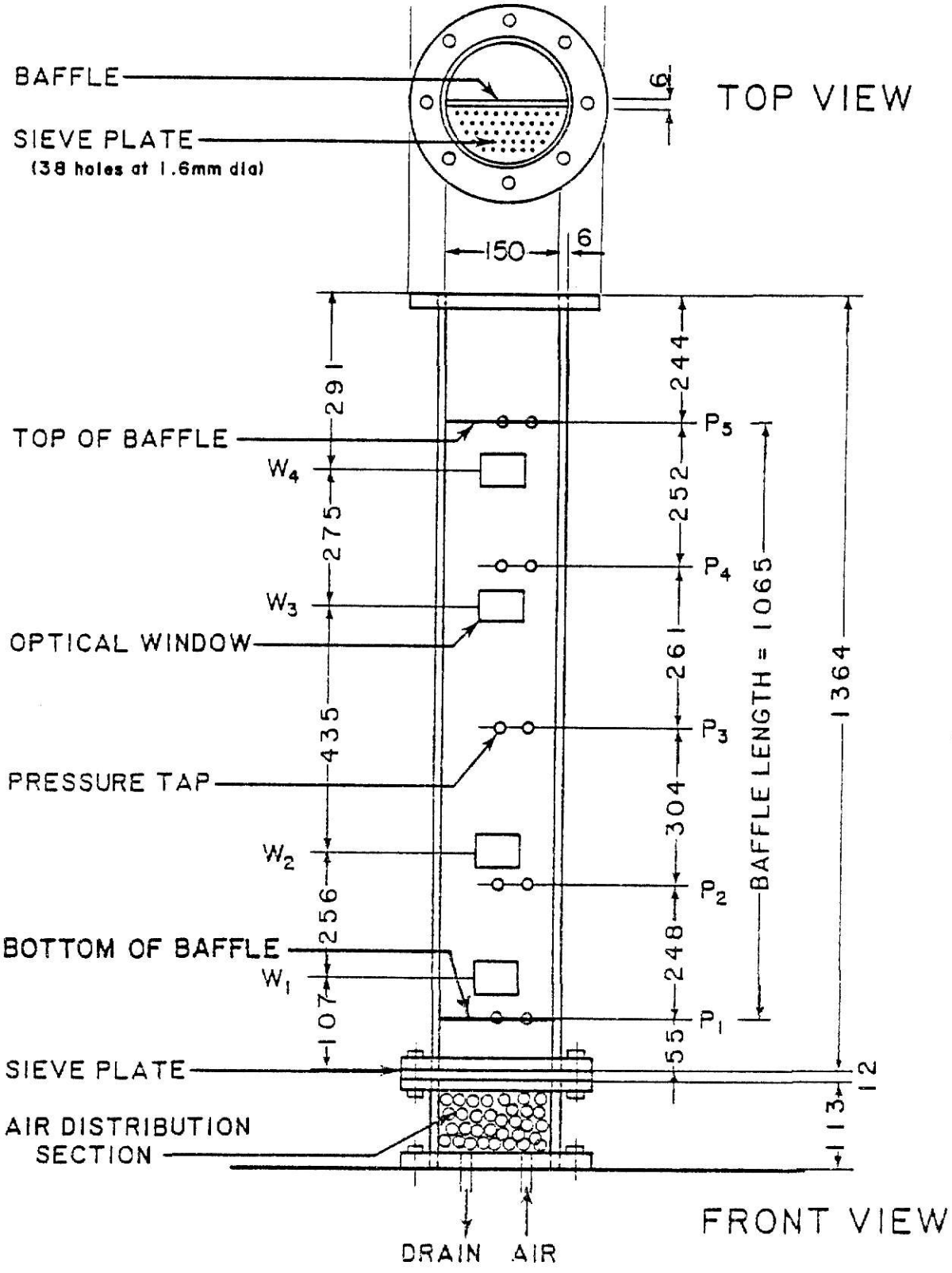



Figure 3.1 Plexi-glass airlift column used in the experiments (all dimensions are in millimeters).

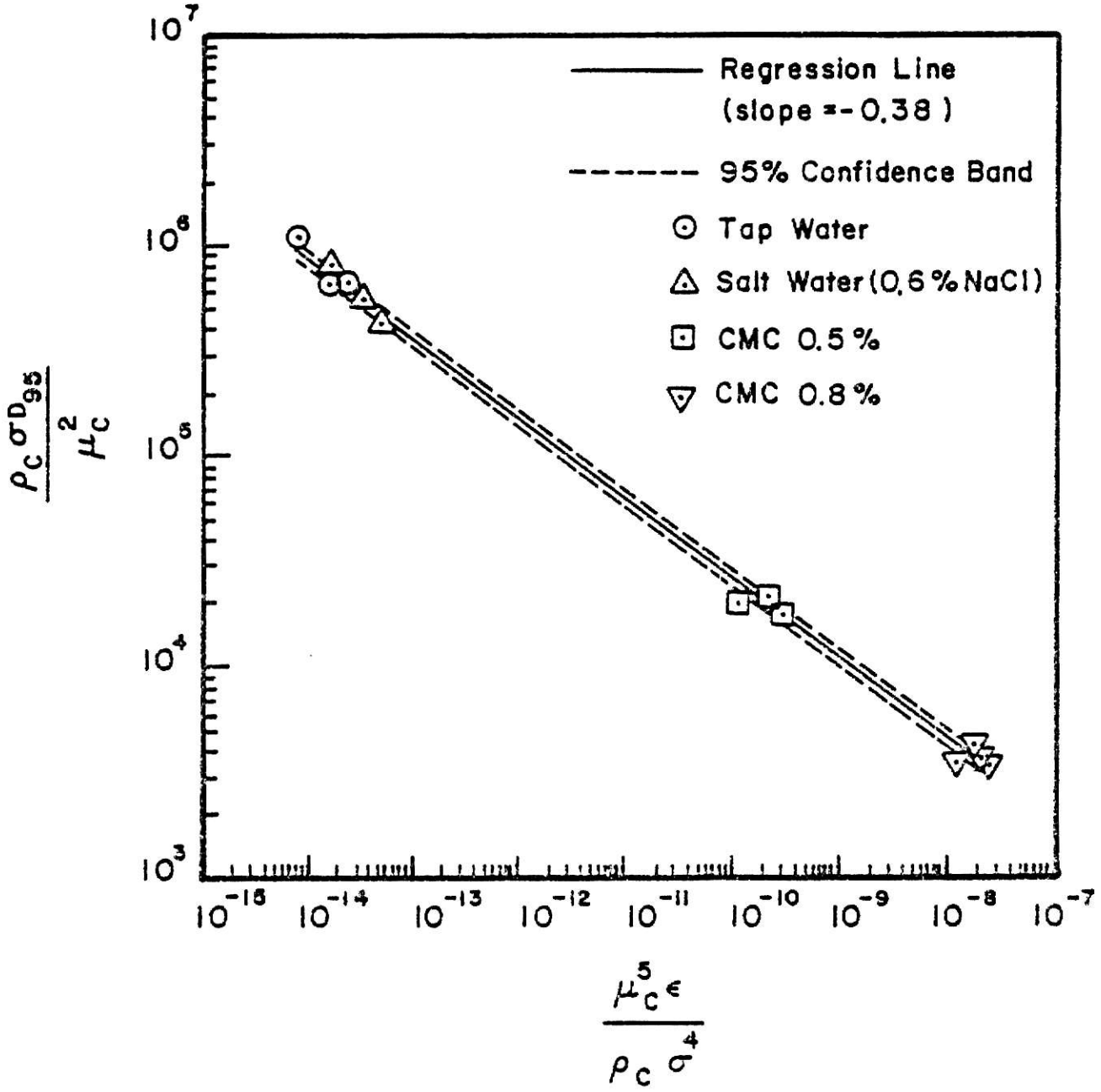



Figure 3.2 Variation of critical bubble size with energy input.

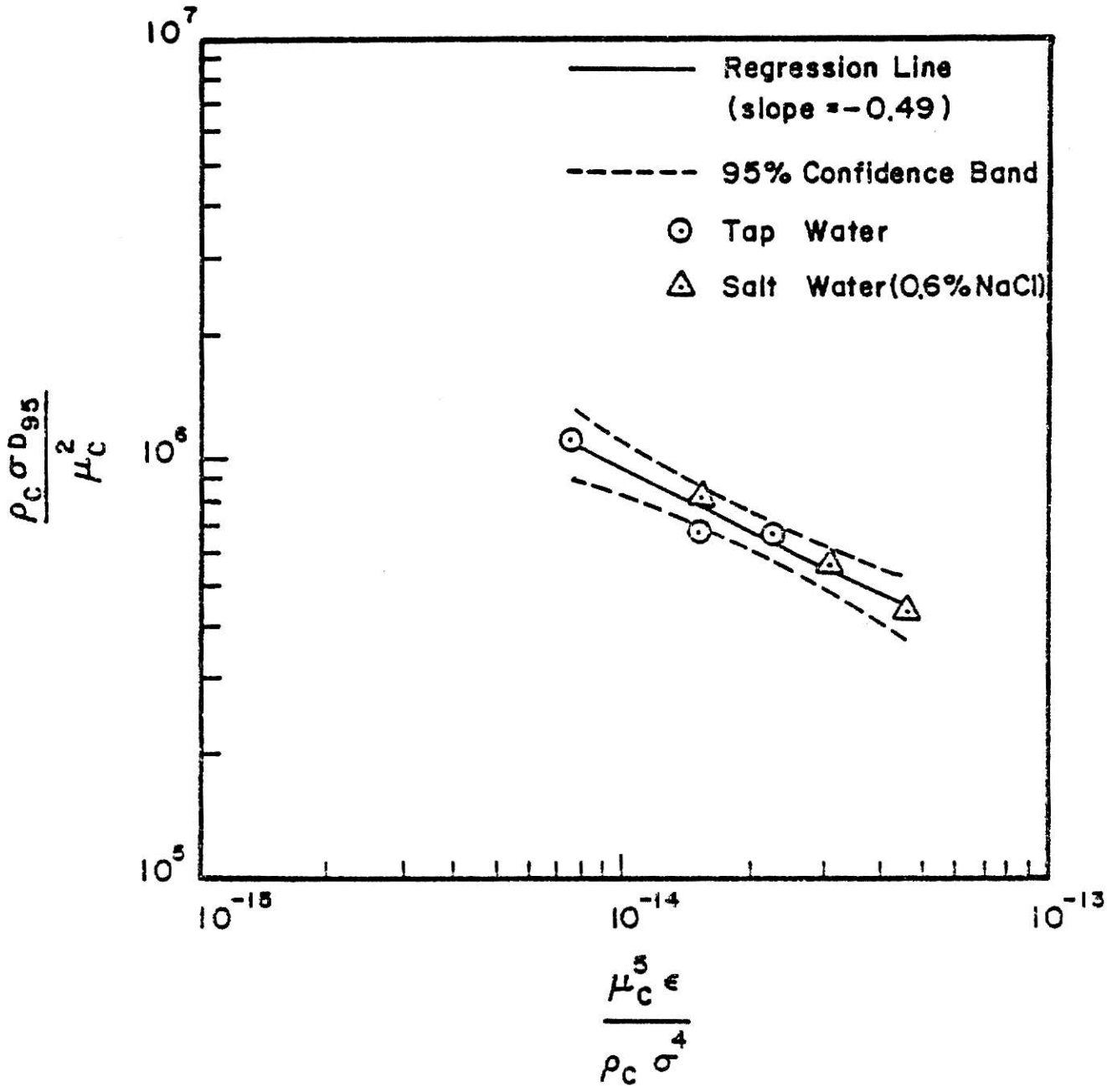



Figure 3.3 Variation of critical bubble size with energy input.

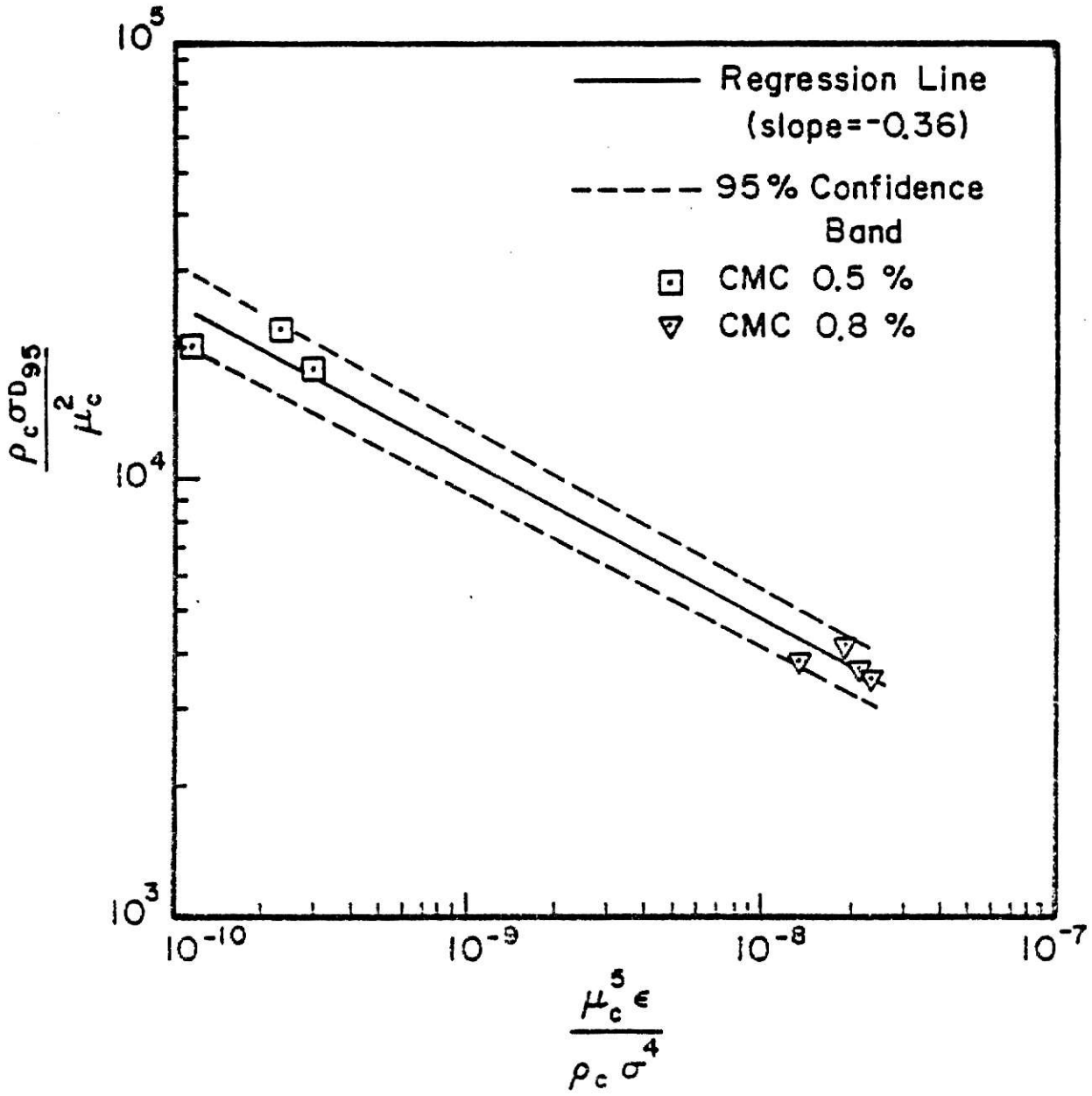



Figure 3.4 Variation of critical bubble size with energy input.

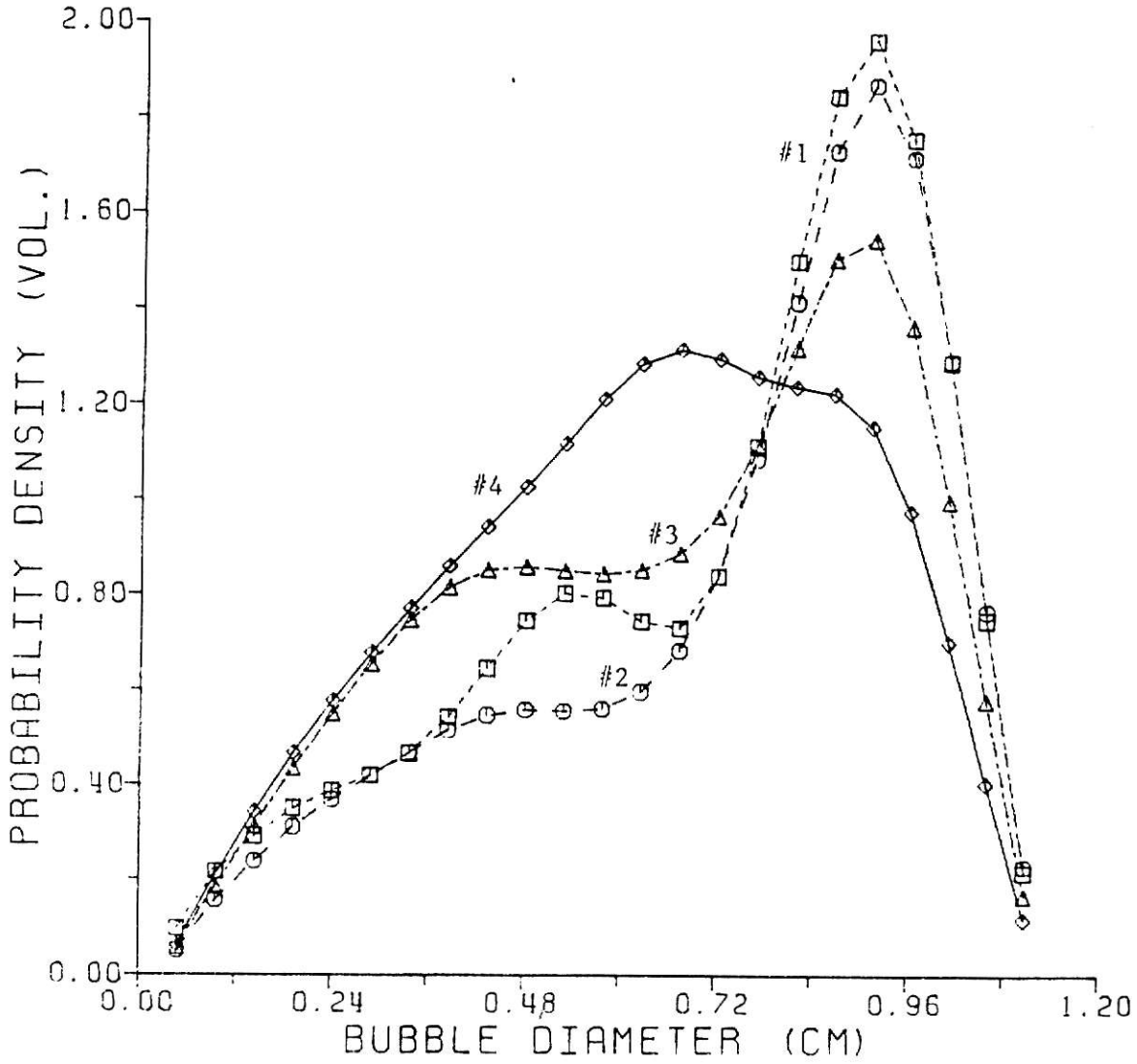



Figure 3.5 Bubble size distribution for air-water system at air flow rate F=30 $ft^3/hr$. (numbers refer to window locations shown in Fig. 3.1)

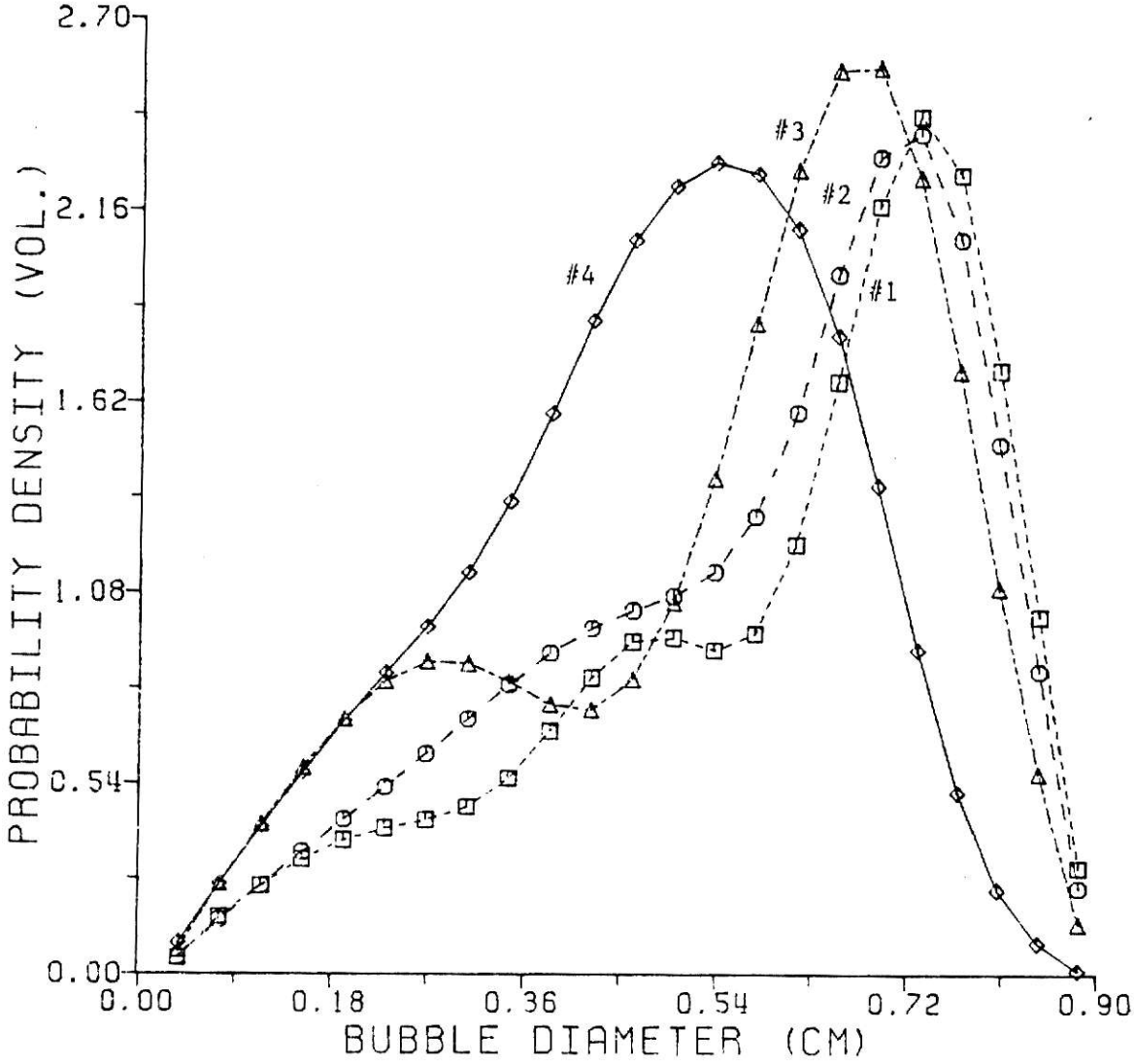



Figure 3.6 Bubble size distribution for air-water system at air flow rate F=60 $ft^3/hr.$ (numbers refer to window locations shown in Fig. 3.1)

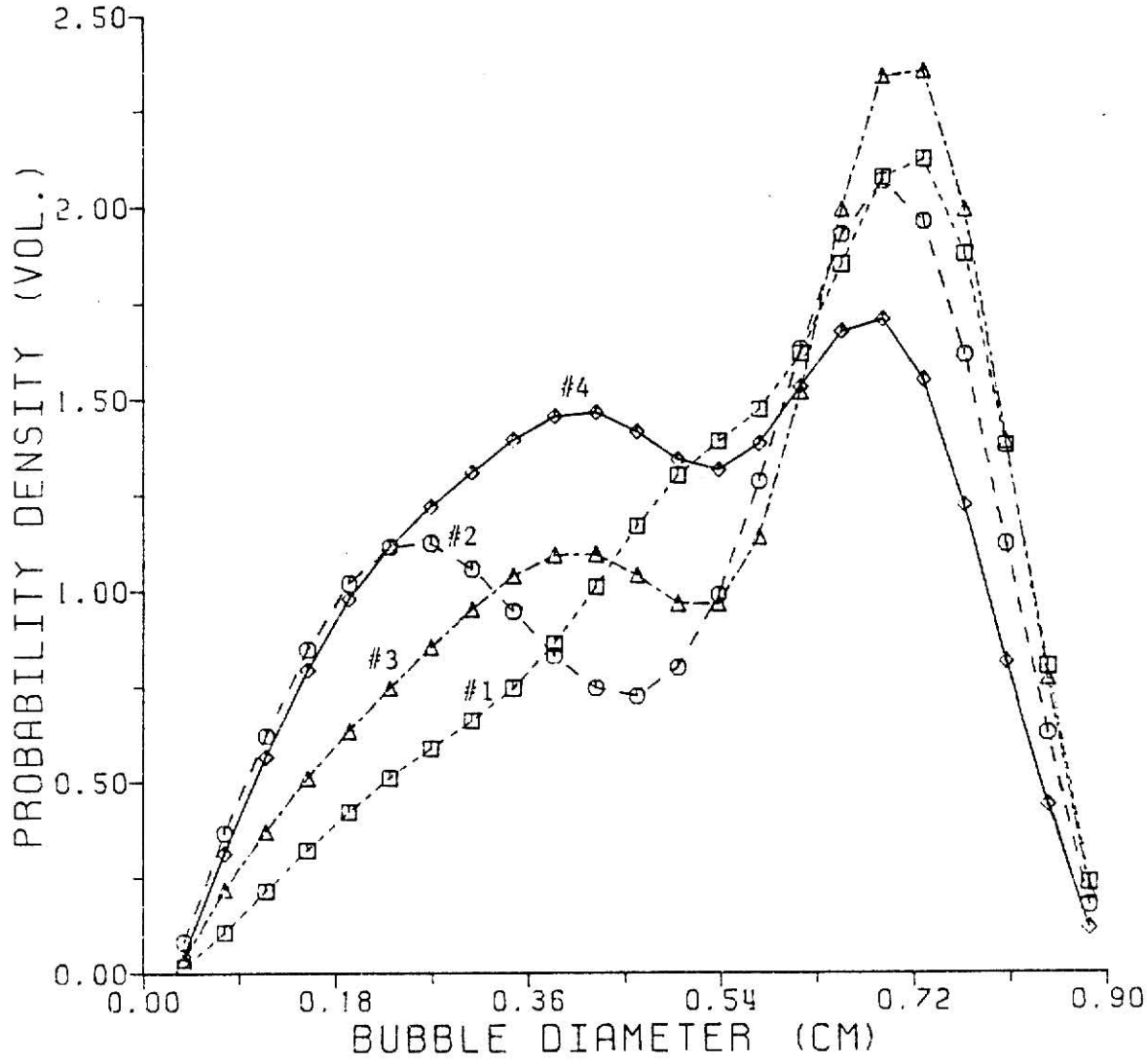



Figure 3.7 Bubble size distribution for air-water system at air flow rate F=90 $ft^3/hr.$ (numbers refer to window locations shown in Fig. 3.1)

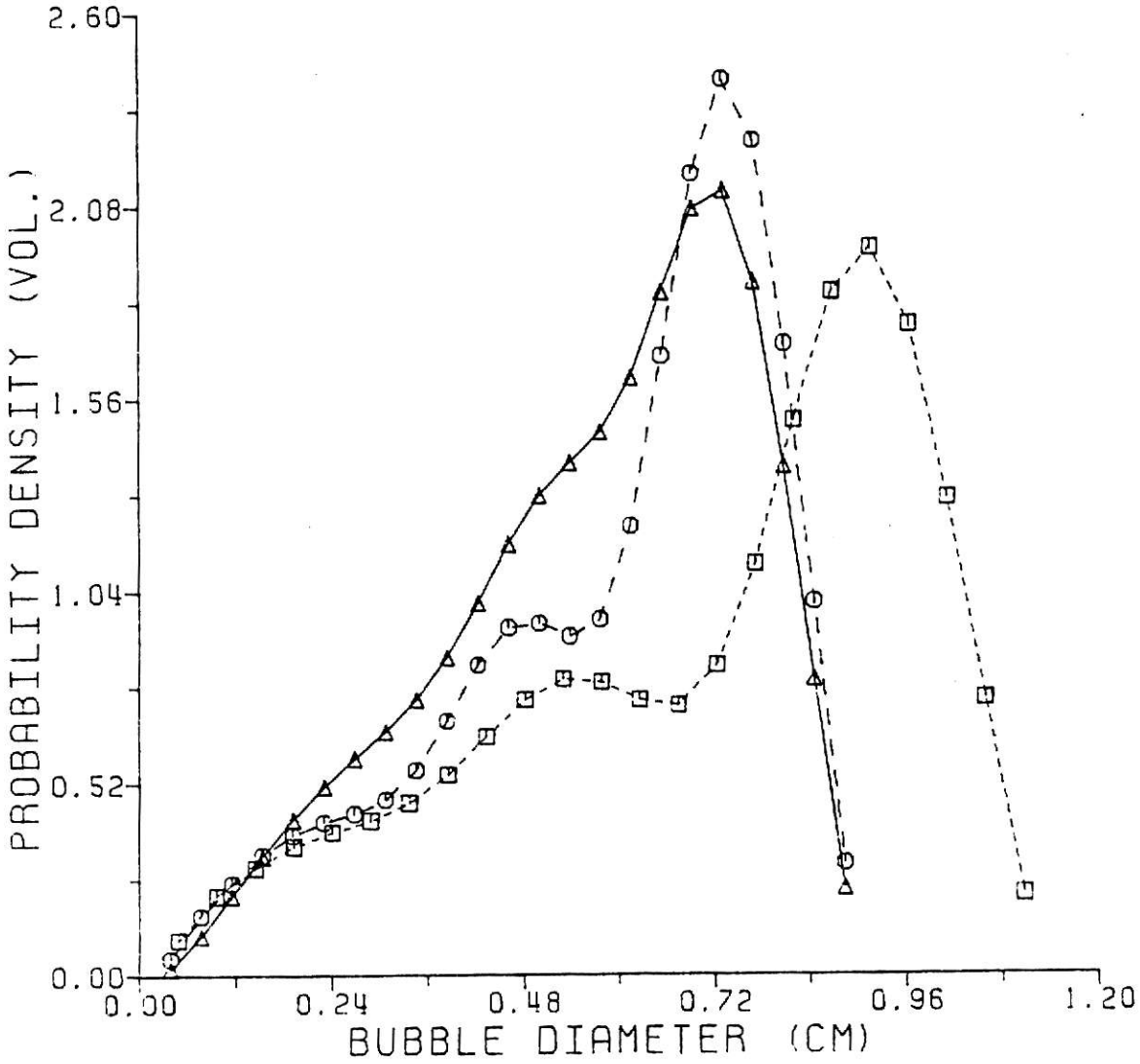



Figure 3.8 Bubble size distribution for air-water system at window #1 for various air flow rates. [□:F = 30 $ft^3/hr$, ○:F = 60 $ft^3/hr$, △:F = 90 $ft^3/hr$]

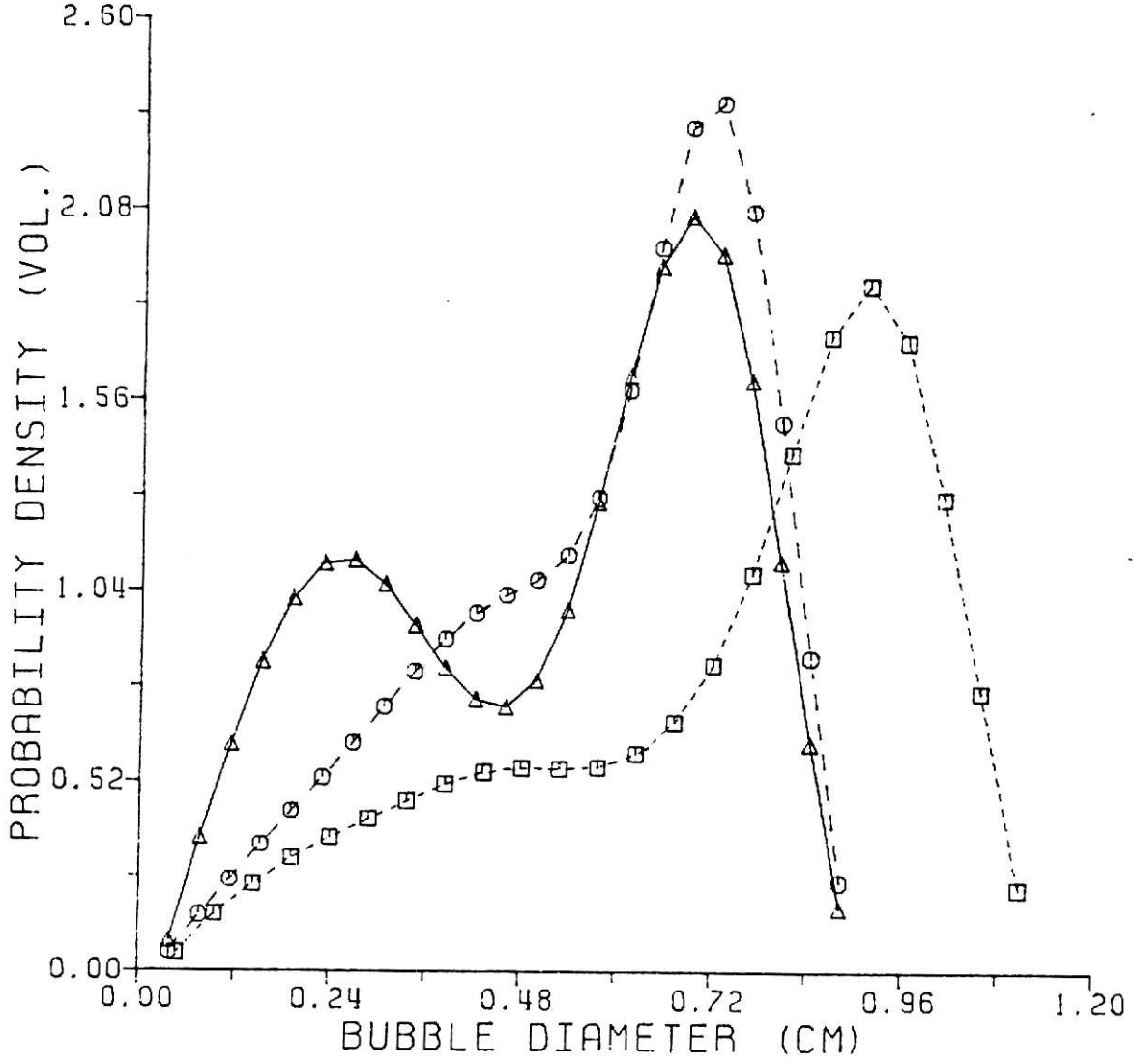



Figure 3.9 Bubble size distribution for air-water system at window #2 for various air flow rates. [□:F = 30 $ft^3/hr$, ○:F = 60 $ft^3/hr$, △:F = 90 $ft^3/hr$]

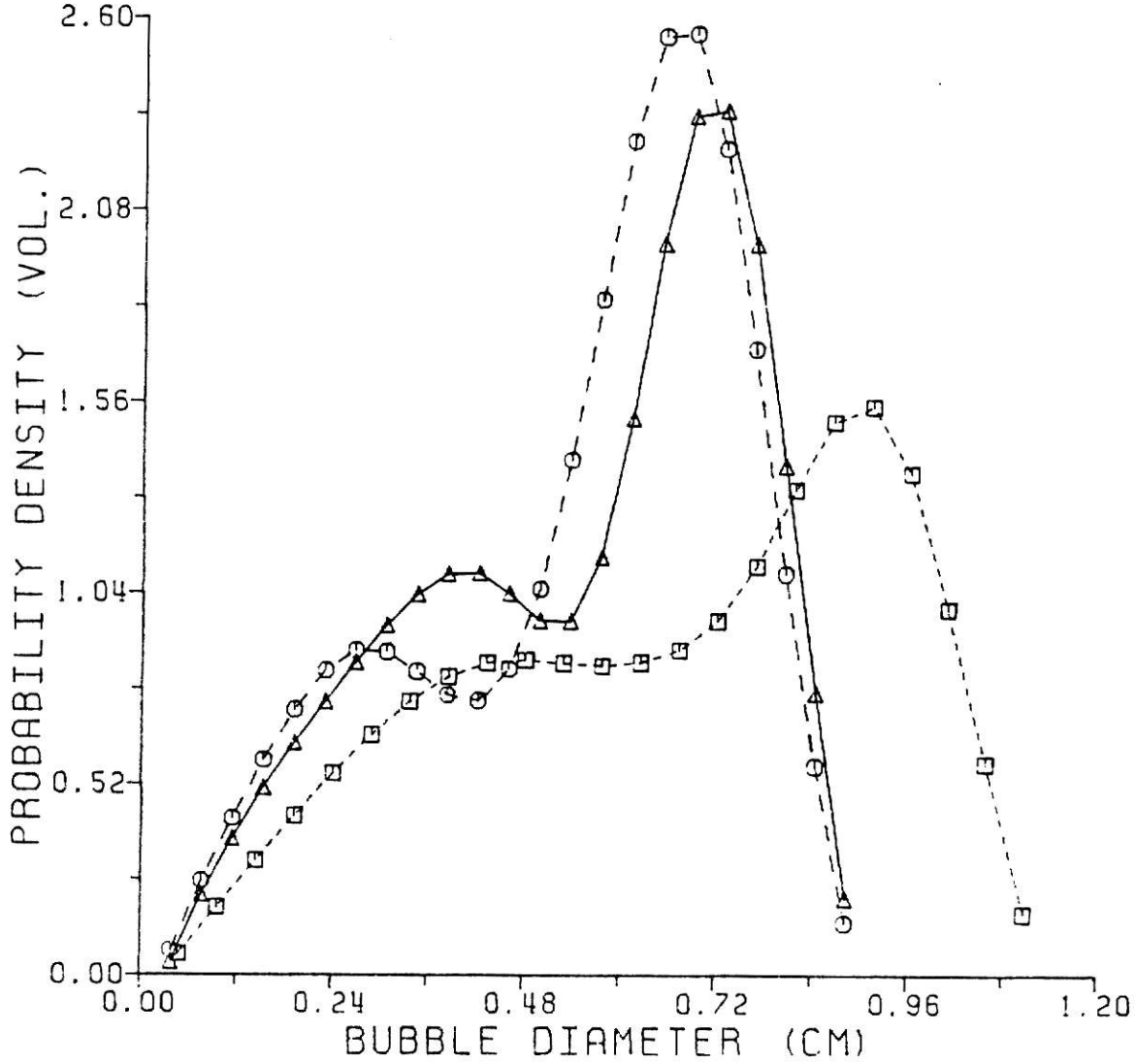



Figure 3.10 Bubble size distribution for air-water system at window #3 for various air flow rates. [□:F = 30 $ft^3/hr$, ○:F = 60 $ft^3/hr$, △:F = 90 $ft^3/hr$]

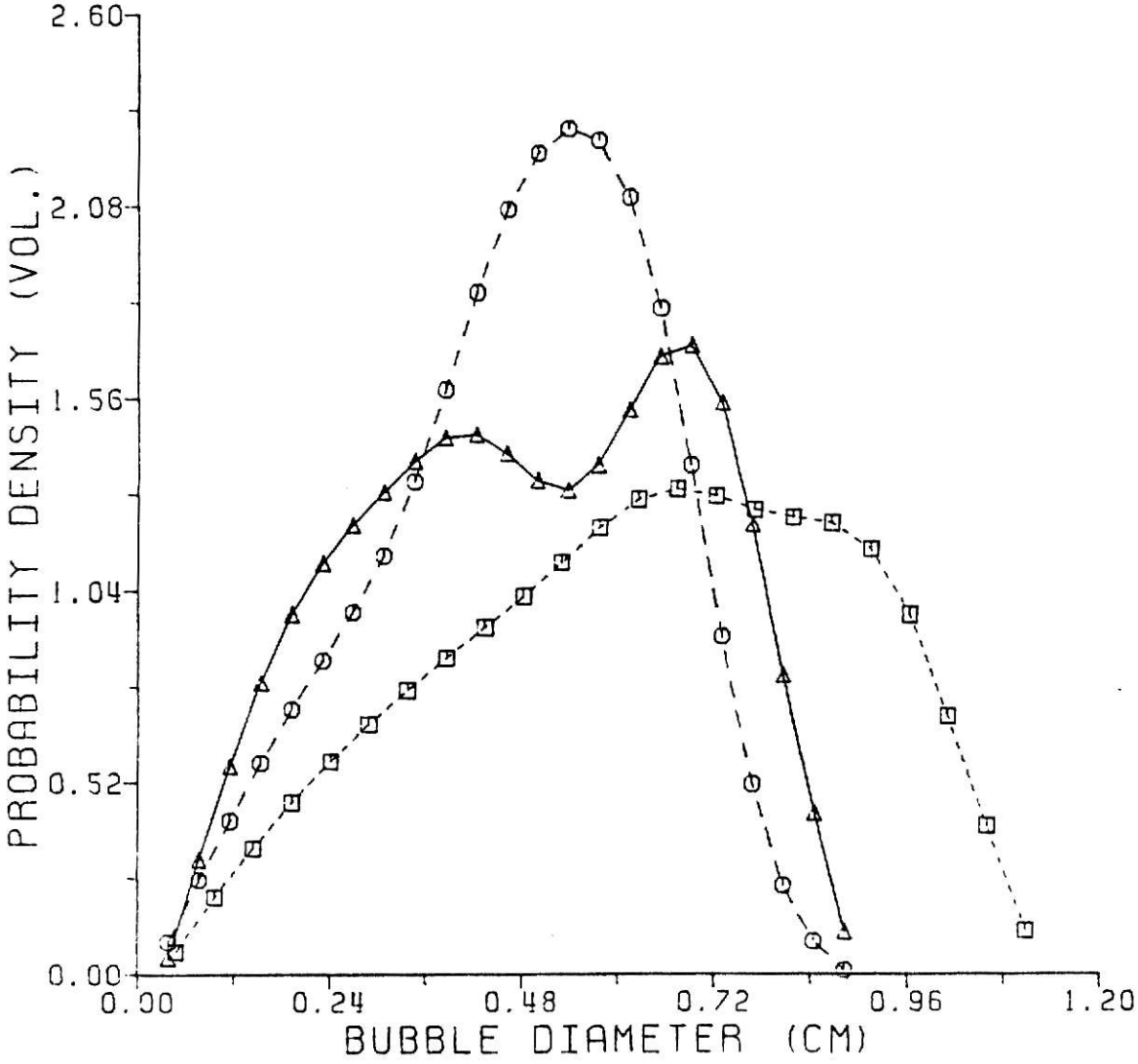



Figure 3.11 Bubble size distribution for air-water system at window #4 for various air flow rates. [□:F = 30 $ft^3$/hr, ○:F = 60 $ft^3$/hr, △:F = 90 $ft^3$/hr]

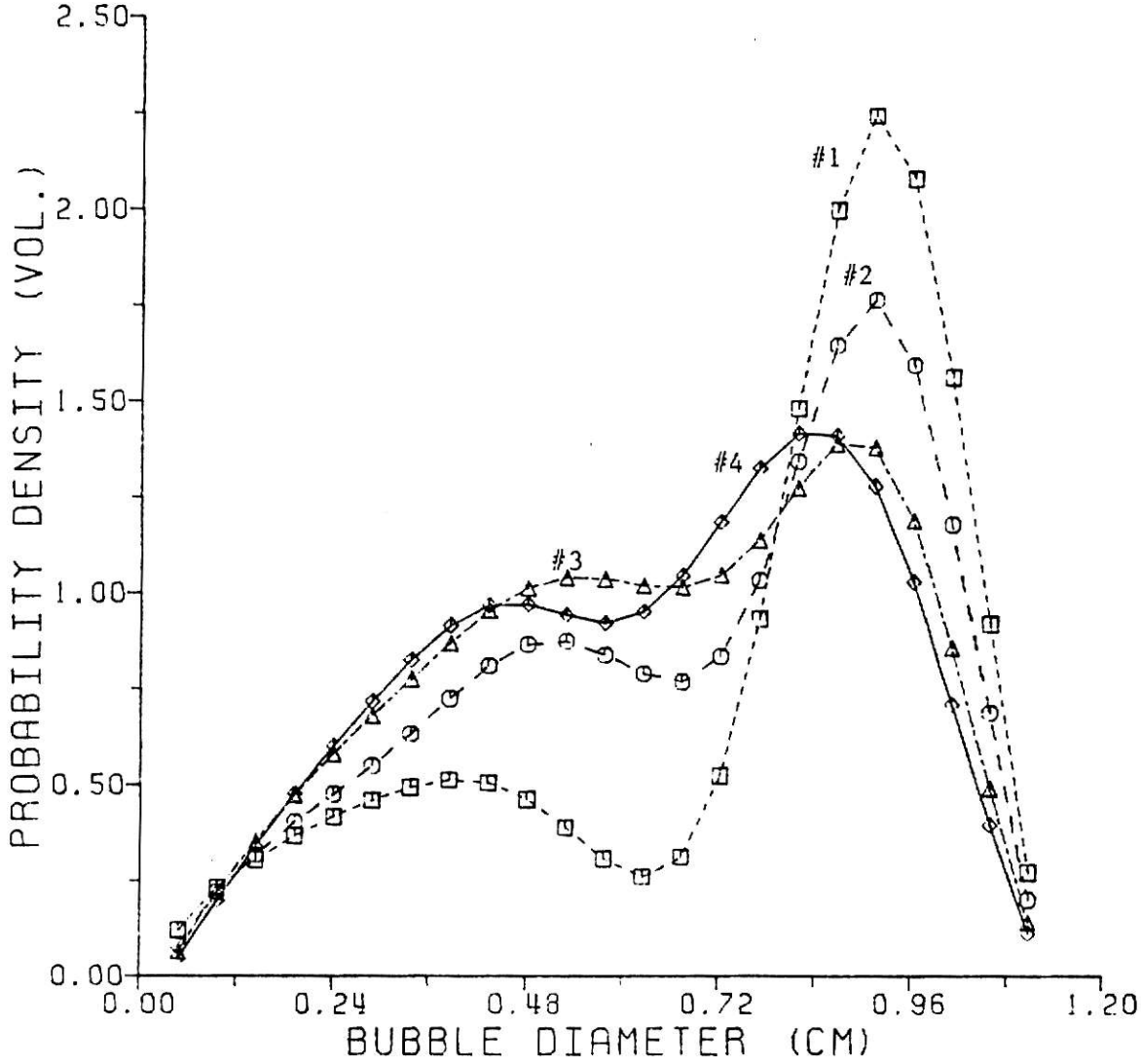



Figure 3.12 Bubble size distribution for air-salt water system at air flow rate F=30 $ft^3/hr$.(numbers refer to window locations shown in Fig. 3.1)

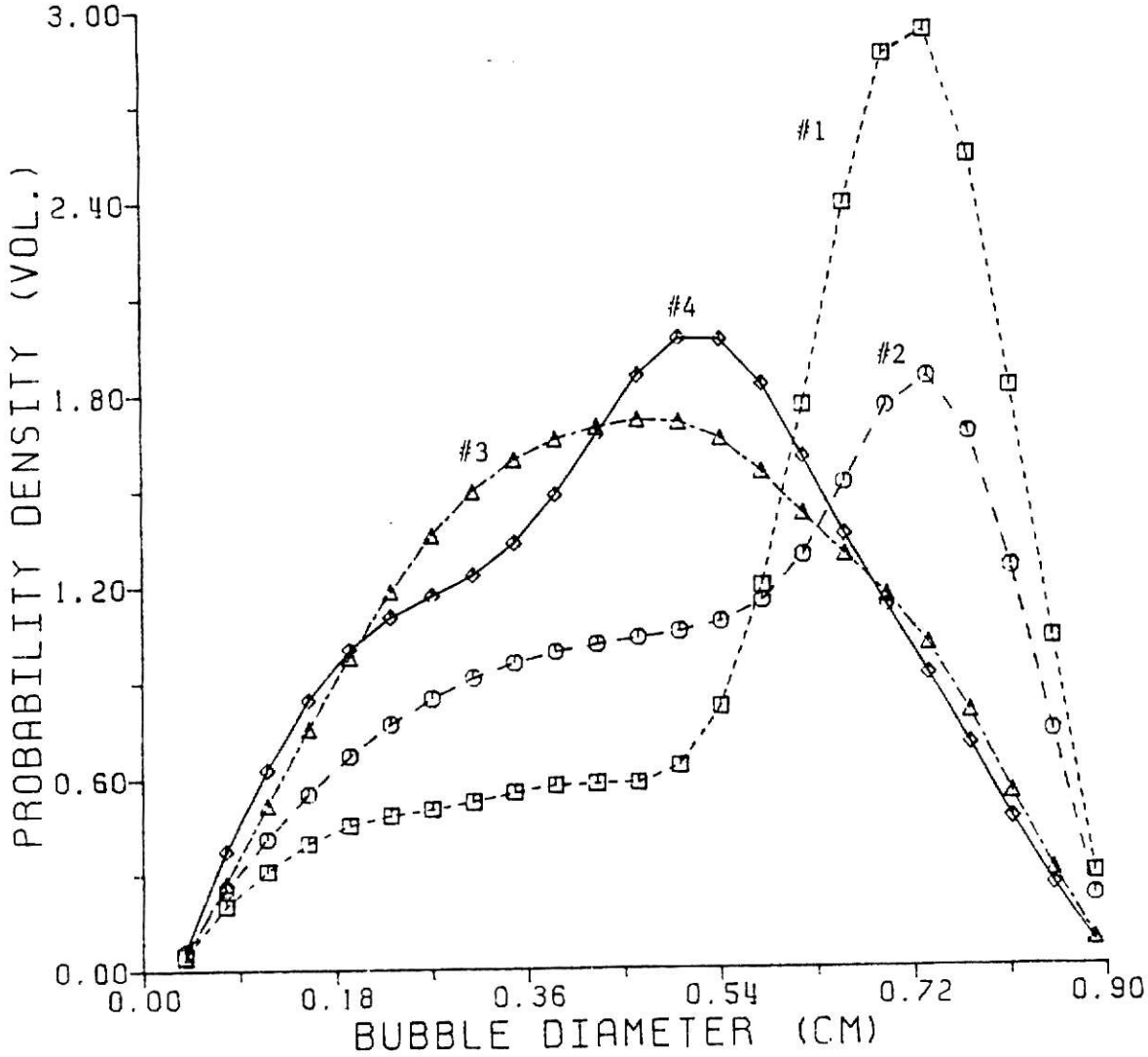



Figure 3.13 Bubble size distribution for air-salt water system at air flow rate F=60 $ft^3/hr.$ (numbers refer to window locations shown in Fig. 3.1)

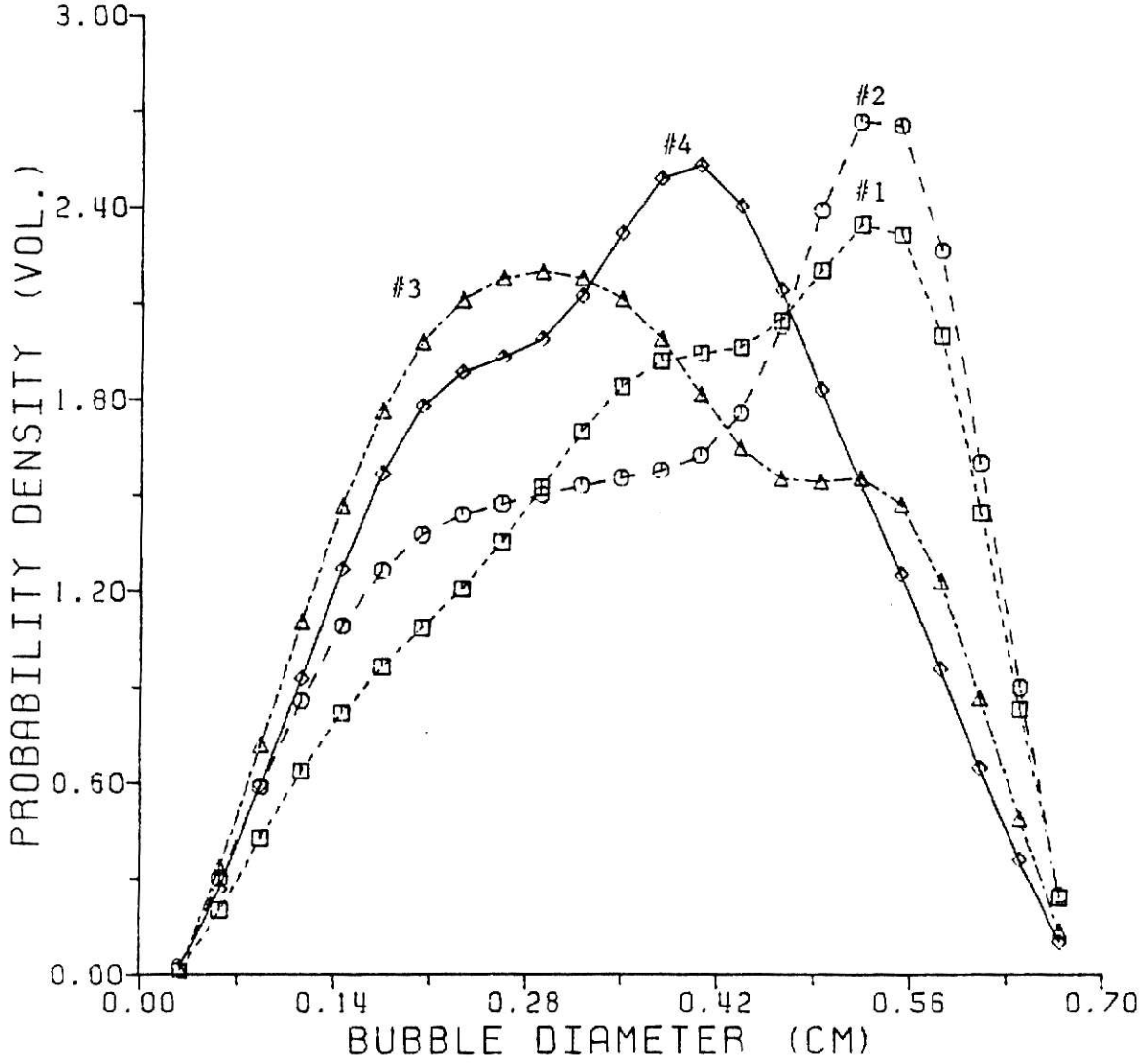



Figure 3.14 Bubble size distribution for air-salt water system at air flow rate F=90 $ft^3/hr$.(numbers refer to window locations shown in Fig. 3.1)

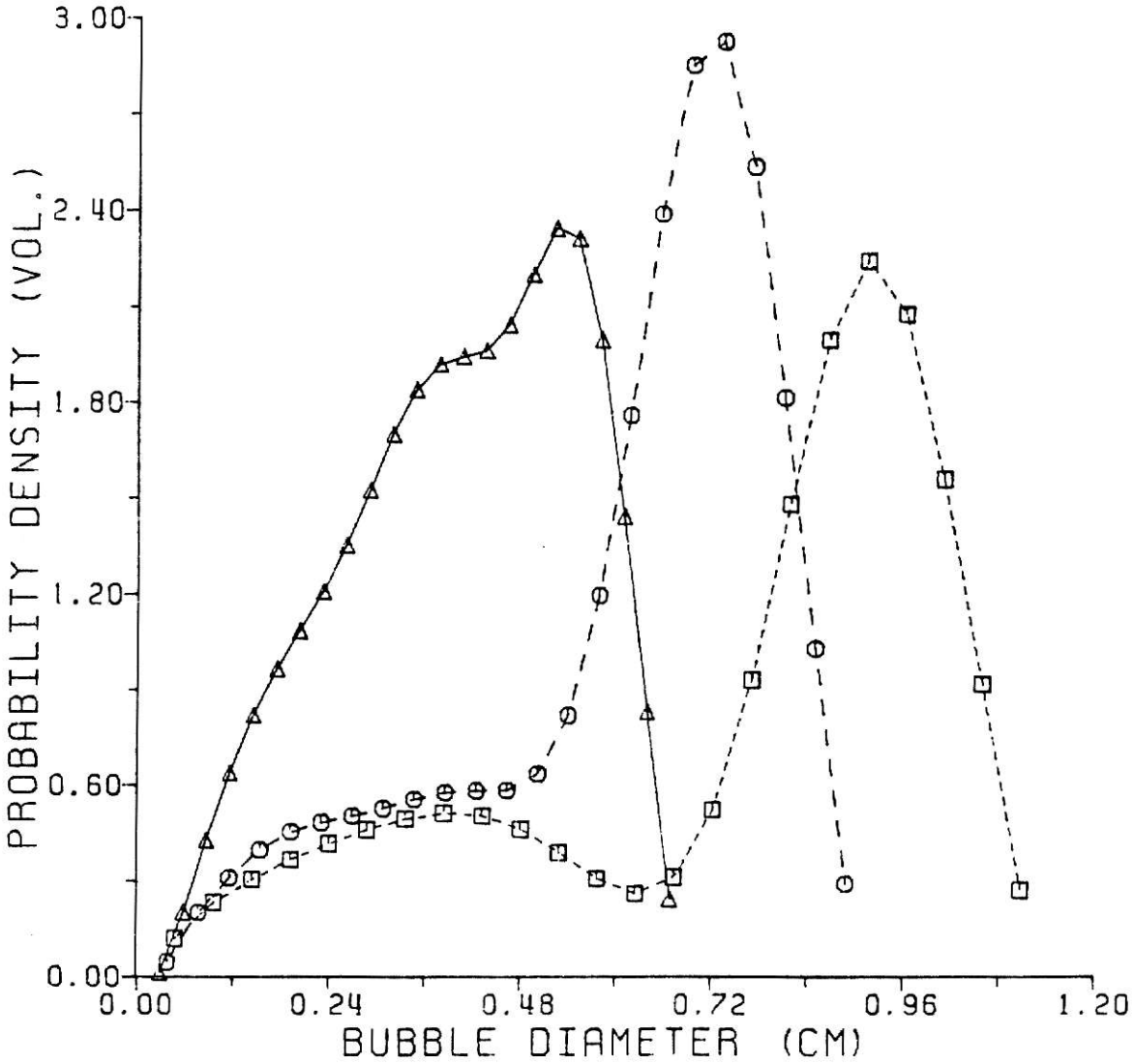



Figure 3.15 Bubble size distribution for air-salt water system at window #1 for various air flow rates. [ □ :F = 30 $ft^3/hr$, ○ :F = 60 $ft^3/hr$, △ :F = 90 $ft^3/hr$ ]

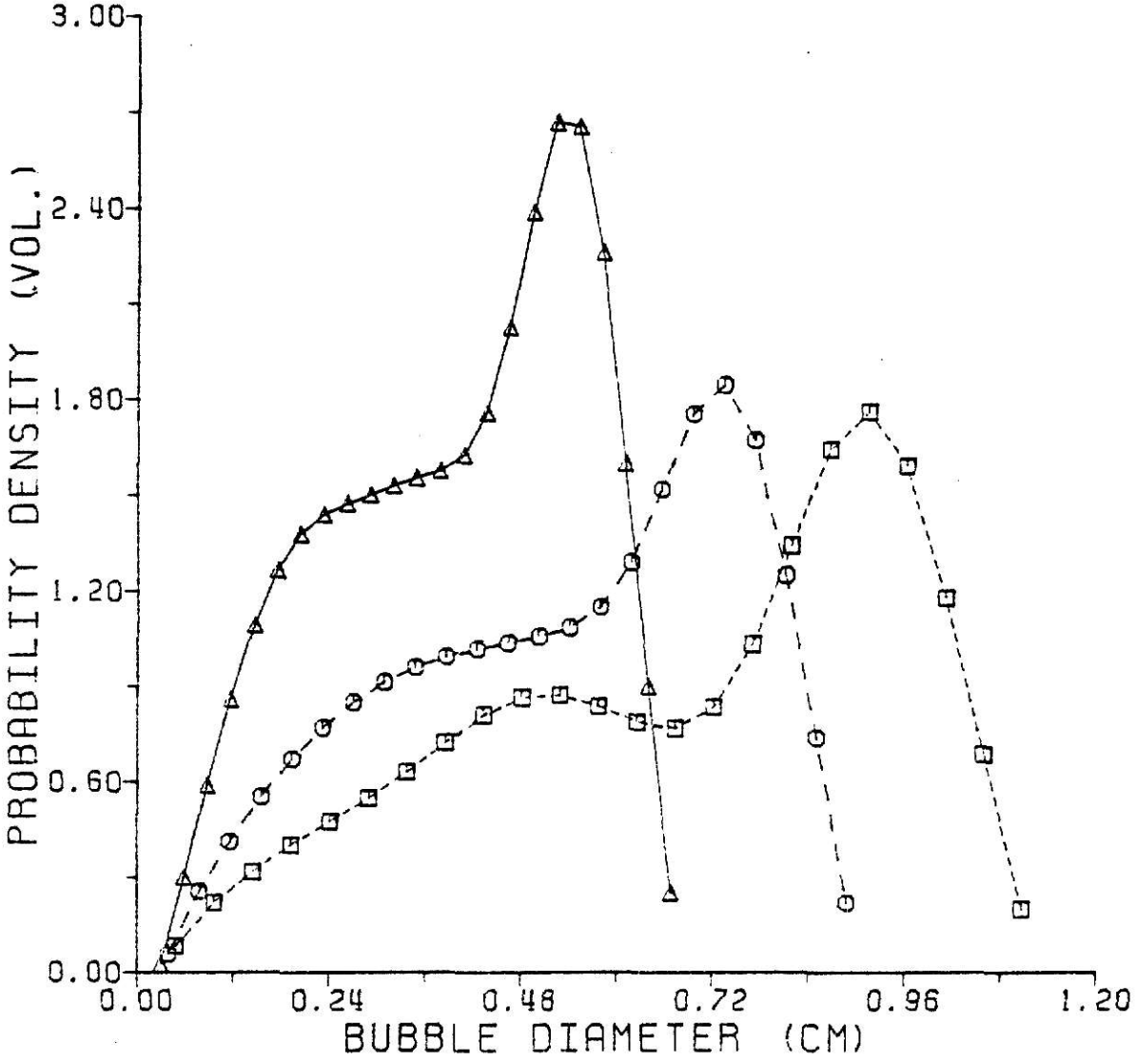



Figure 3.16 Bubble size distribution for air-salt water system at window #2 for various air flow rates. [□:F = 30 $ft^3$/hr, ⏀:F = 60 $ft^3$/hr, △:F = 90 $ft^3$/hr]

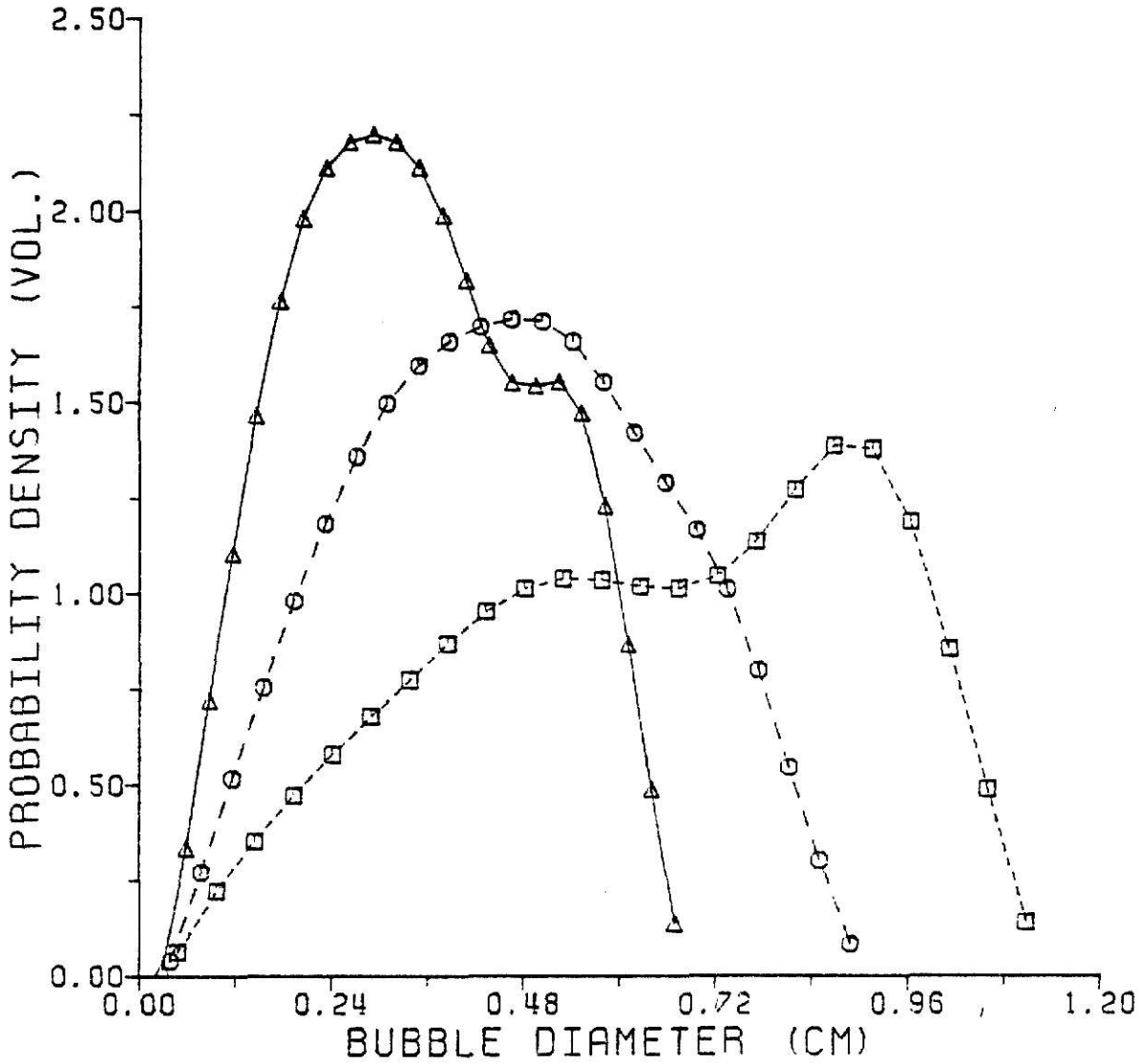



Figure 3.17 Bubble size distribution for air-salt water system at window #3 for various air flow rates. [ □:F = 30 $ft^3/hr$, ○:F = 60 $ft^3/hr$, △:F = 90 $ft^3/hr$ ]

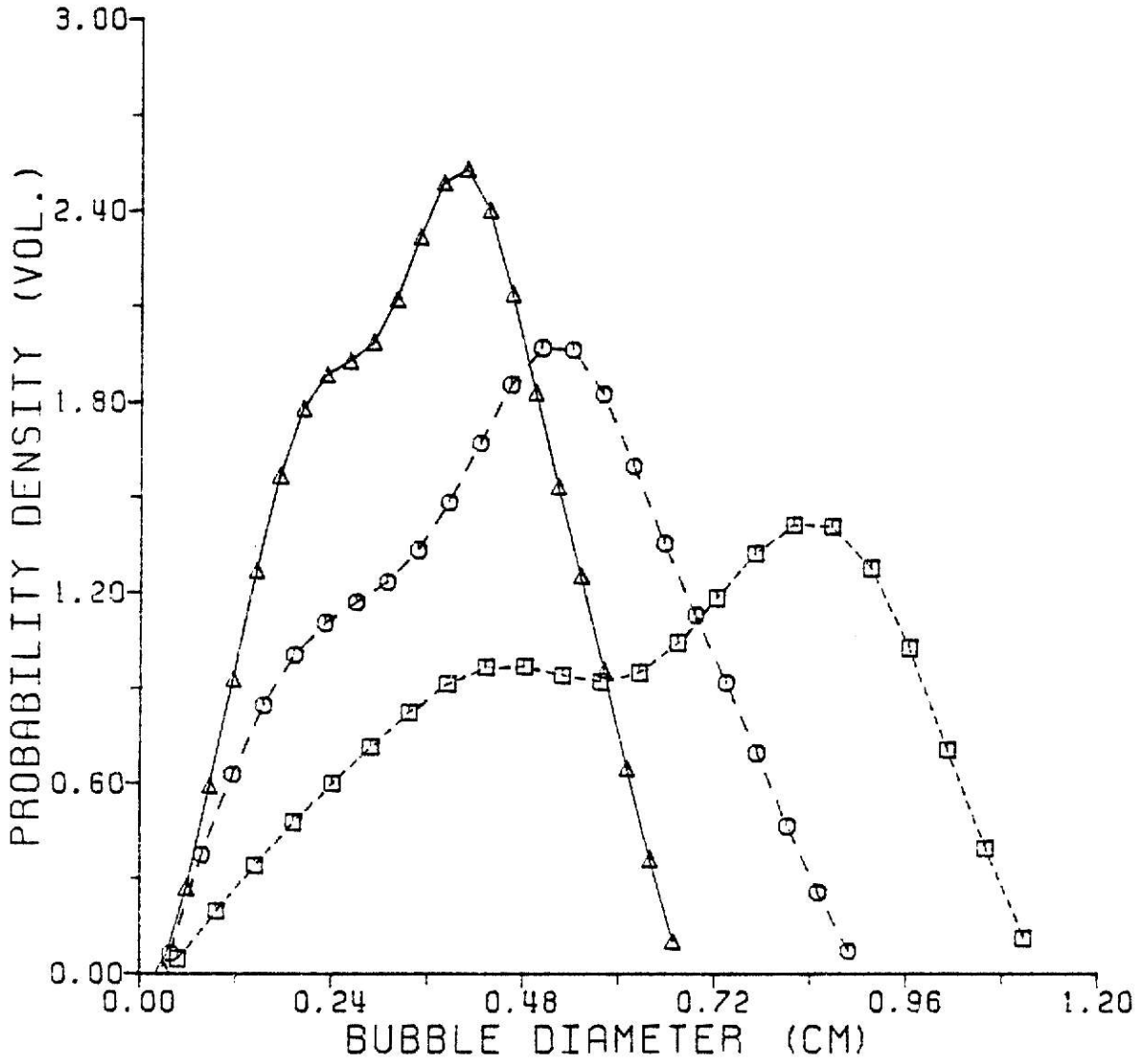



Figure 3.18 Bubble size distribution for air-salt water system at window #4 for various air flow rates. [ □ :F = 30 $ft^3/hr$, ○ :F = 60 $ft^3/hr$, △ :F = 90 $ft^3/hr$ ]

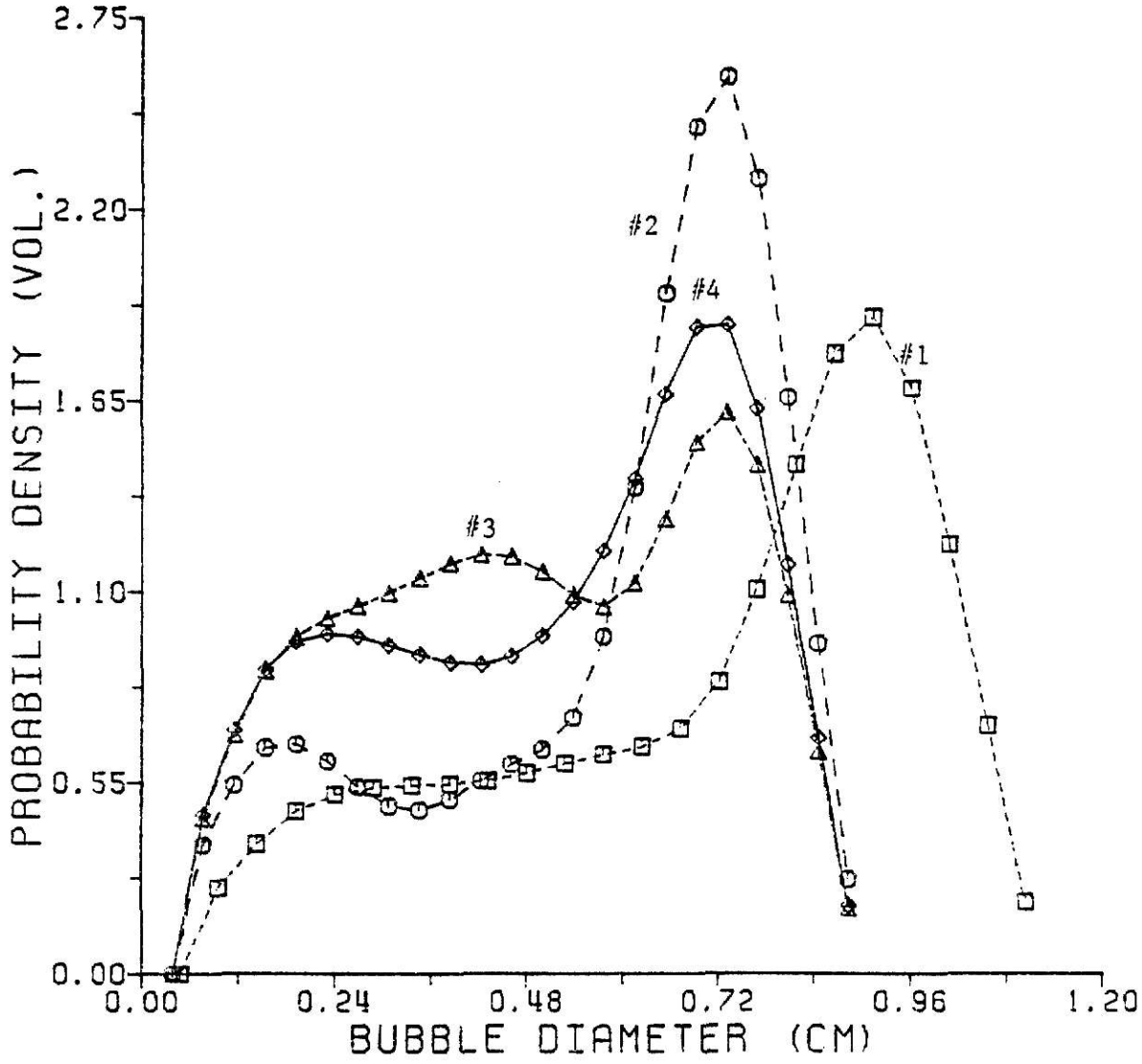



Figure 3.19 Bubble size distribution for air-CMC solution (0.5%) at air flow rate F=30 $ft^3/hr.$ (numbers refer to window locations shown in Fig. 3.1)

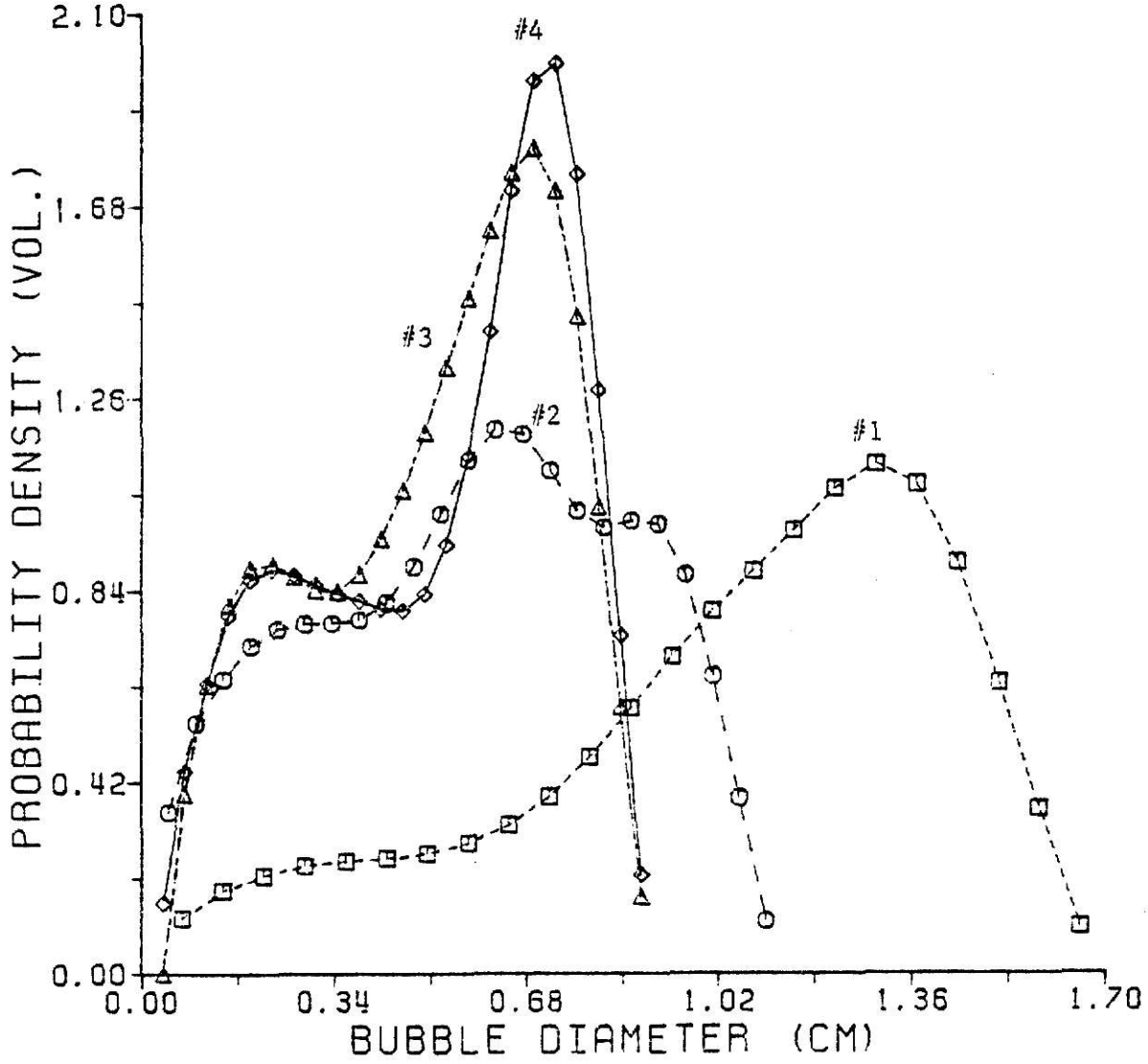



Figure 3.20 Bubble size distribution for air-CMC solution (0.5%) at air flow rate F=60 $ft^3/hr.$ (numbers refer to window locations shown in Fig. 3.1)

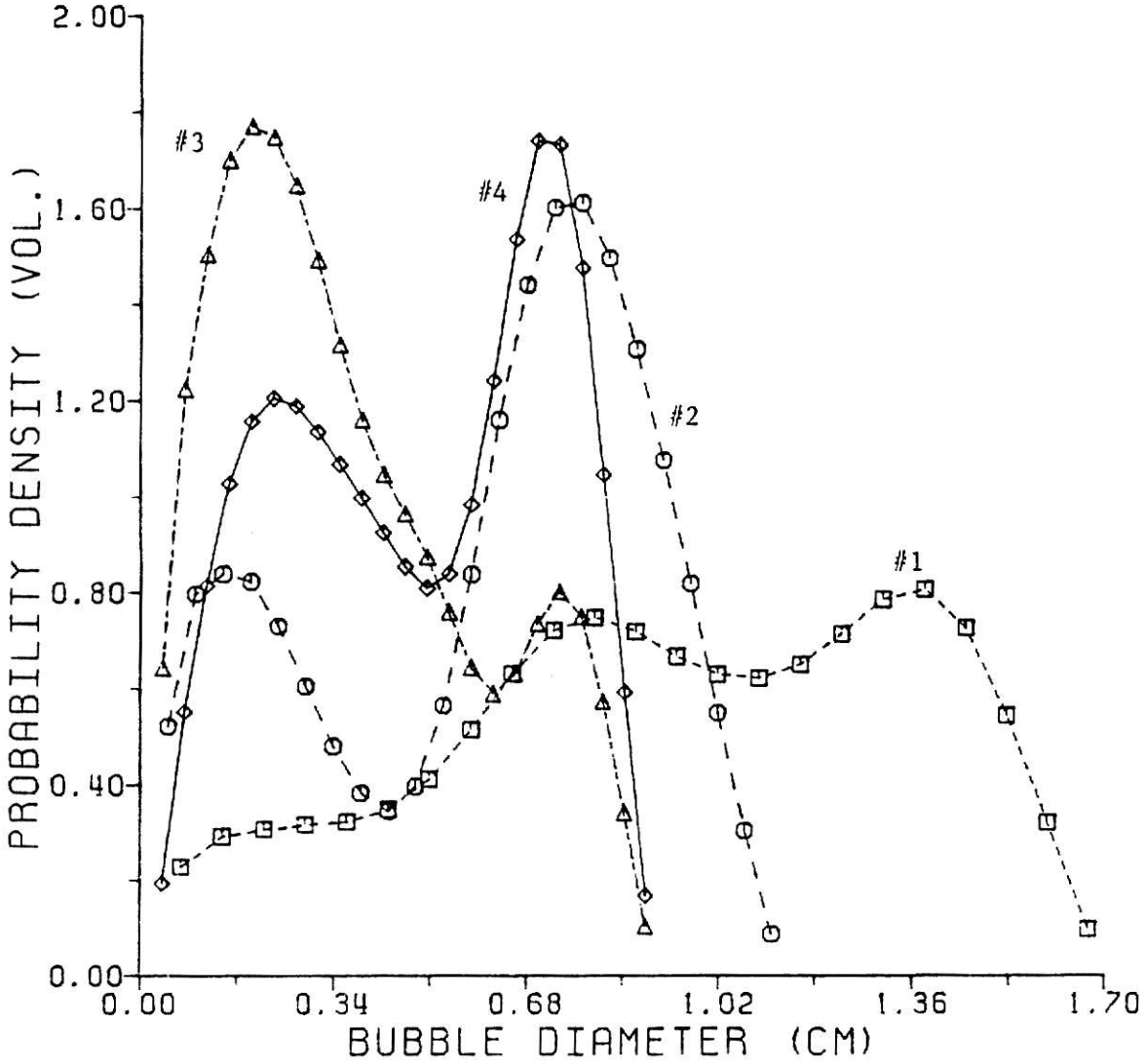



Figure 3.21 Bubble size distribution for air-CMC solution (0.5%) at air flow rate F=90 $ft^3/hr$.(numbers refer to window locations shown in Fig. 3.1)

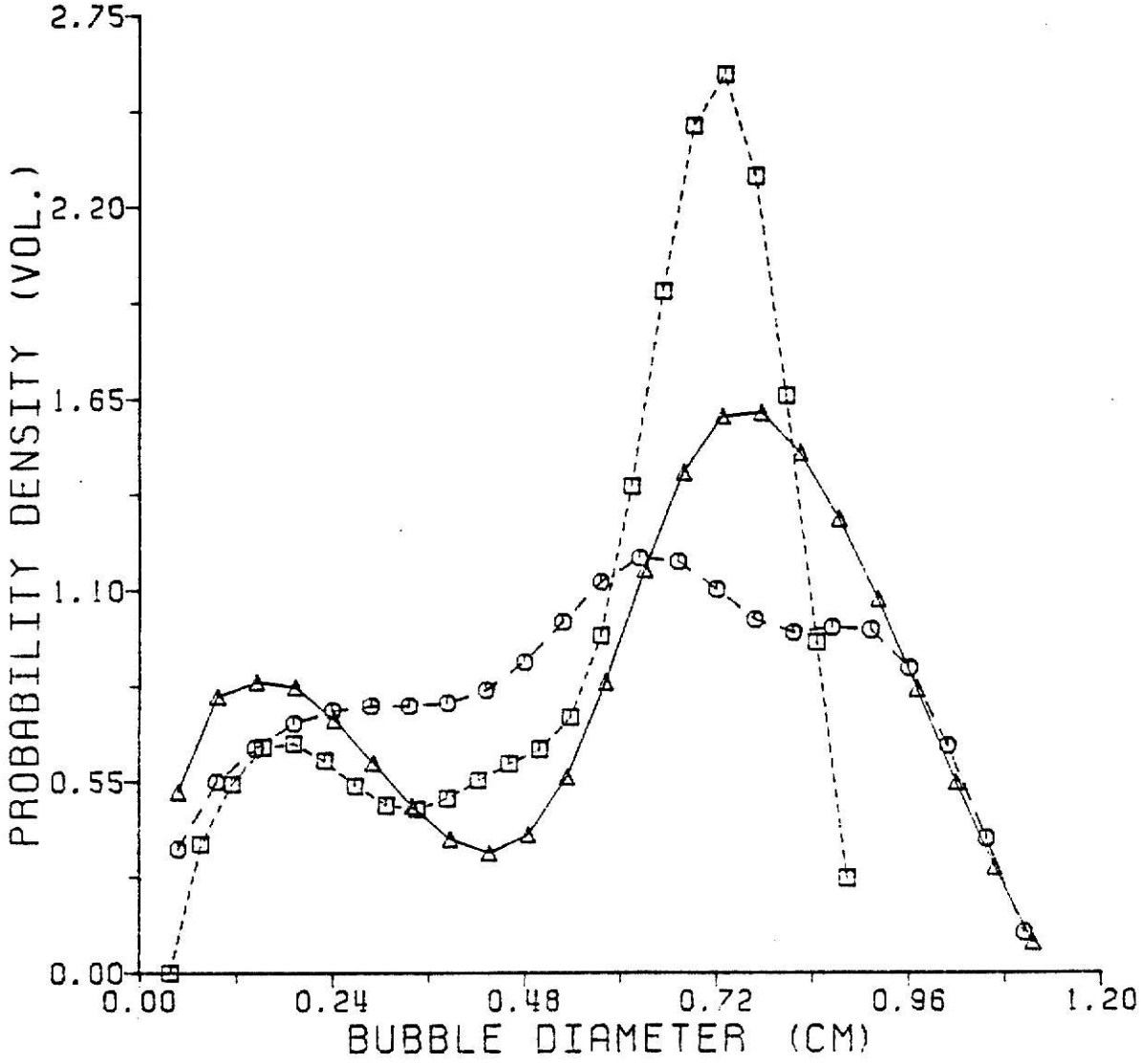



Figure 3.22 Bubble size distribution for air-CMC solution (0.5%) at window #1 for various air flow rates. [ □:F = 30 $ft^3/hr$, ⊙:F = 60 $ft^3/hr$, △:F = 90 $ft^3/hr$ ]

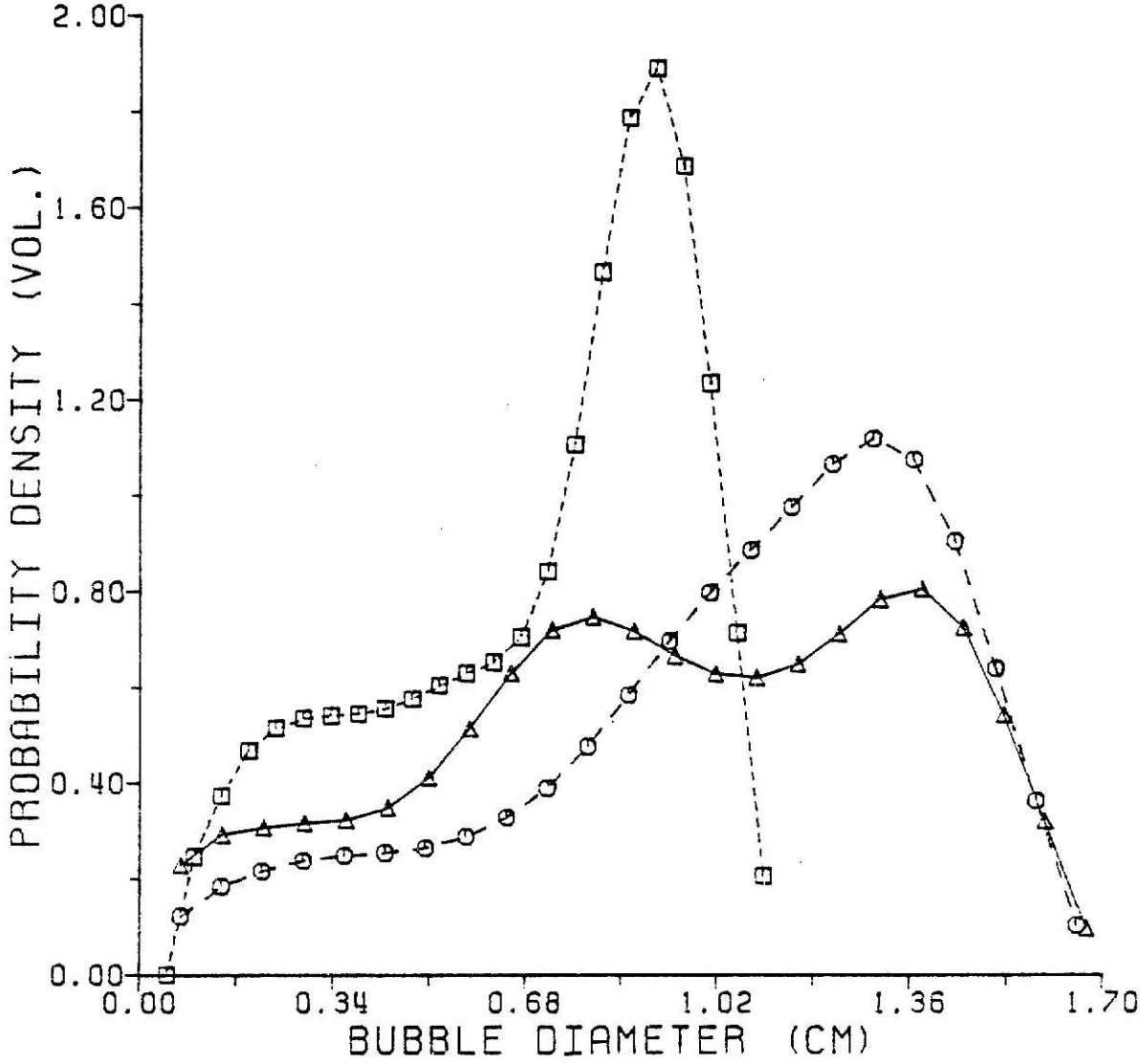



Figure 3.23 Bubble size distribution for air-CMC solution (0.5%) at window #2 for various air flow rates. [□:F = 30 $ft^3/hr$, ○:F = 60 $ft^3/hr$, △:F = 90 $ft^3/hr$]

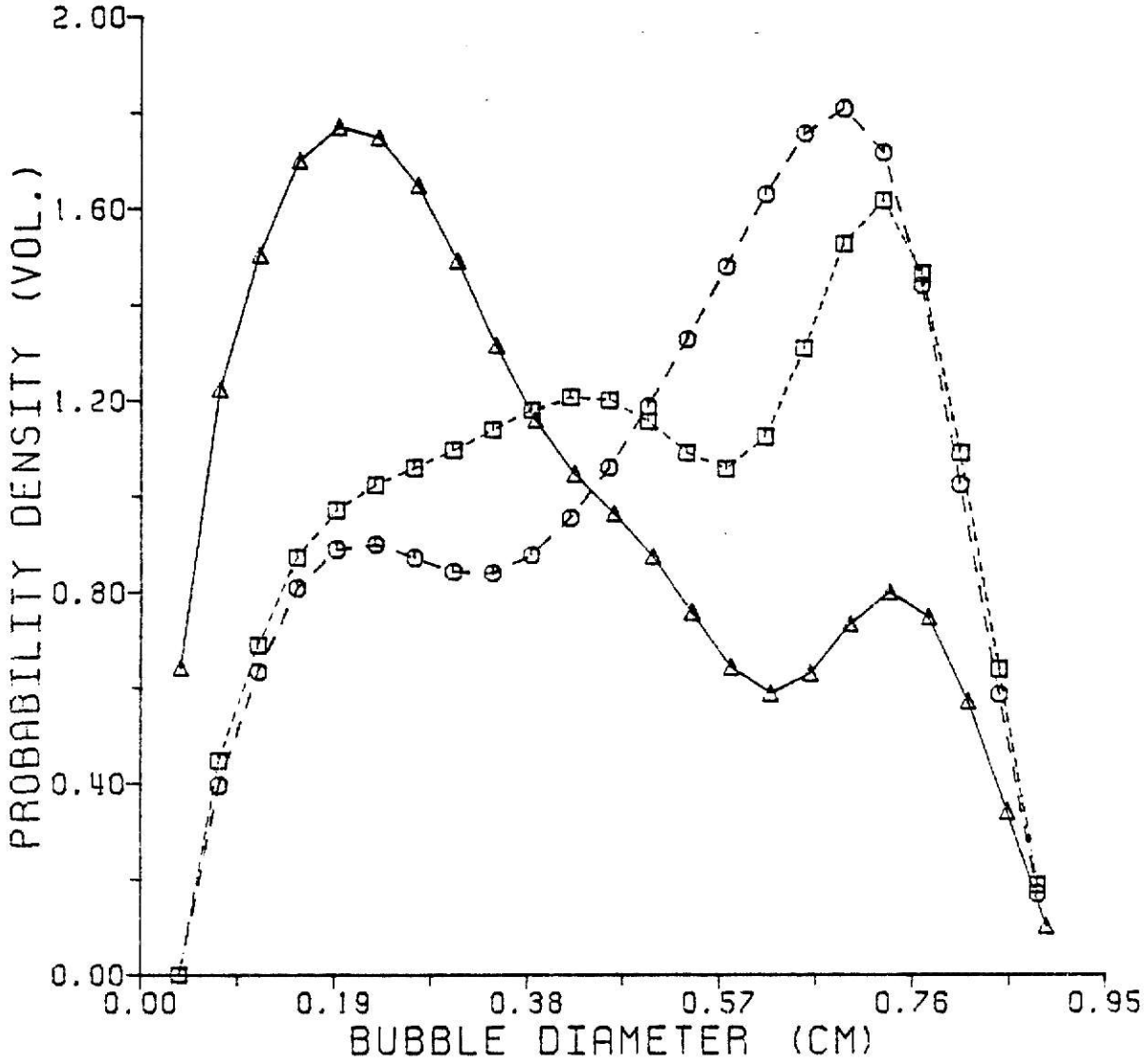



Figure 3.24 Bubble size distribution for air-CMC solution (0.5%) at window #3 for various air flow rates. [ □:F = 30 $ft^3/hr$, ○:F = 60 $ft^3/hr$, △:F = 90 $ft^3/hr$ ]

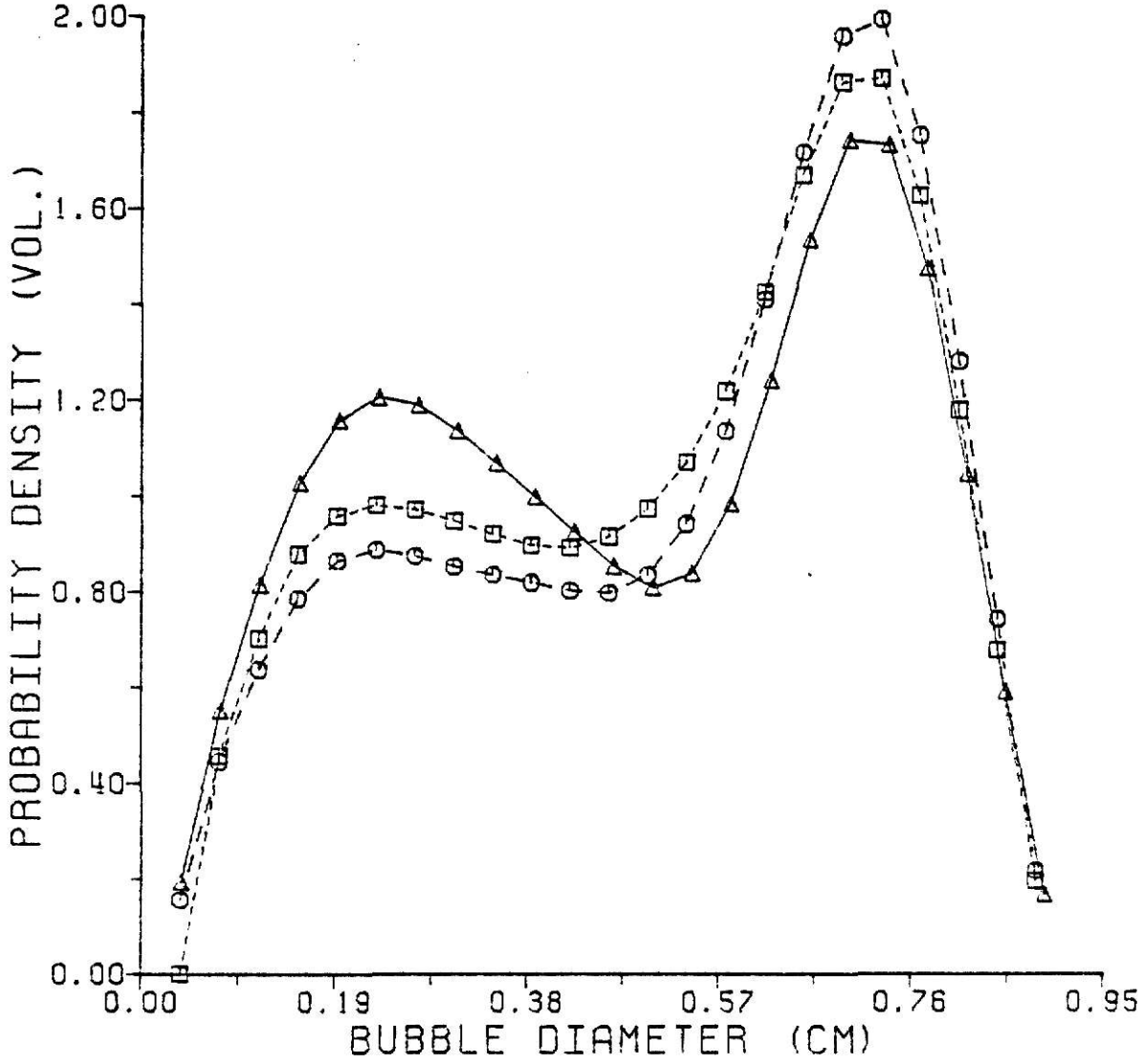



Figure 3.25 Bubble size distribution for air-CMC solution (0.5%) at window #4 for various air flow rates. [□:F = 30 $ft^3/hr$, ○:F = 60 $ft^3/hr$, △:F = 90 $ft^3/hr$ ]

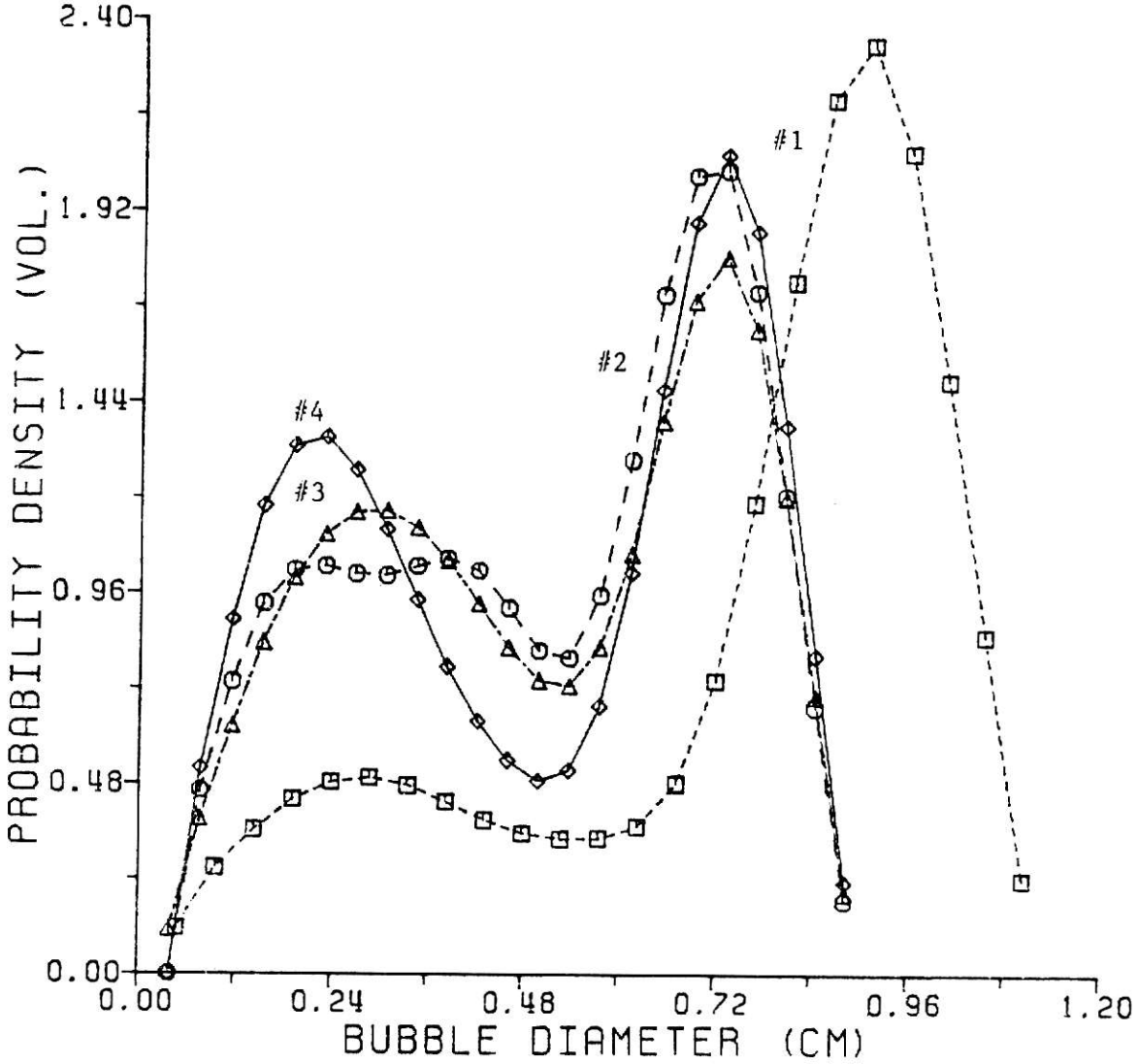



Figure 3.26 Bubble size distribution for air-CMC solution (0.8%) at air flow rate F=30 $ft^3$/hr.(numbers refer to window locations shown in Fig. 3.1)

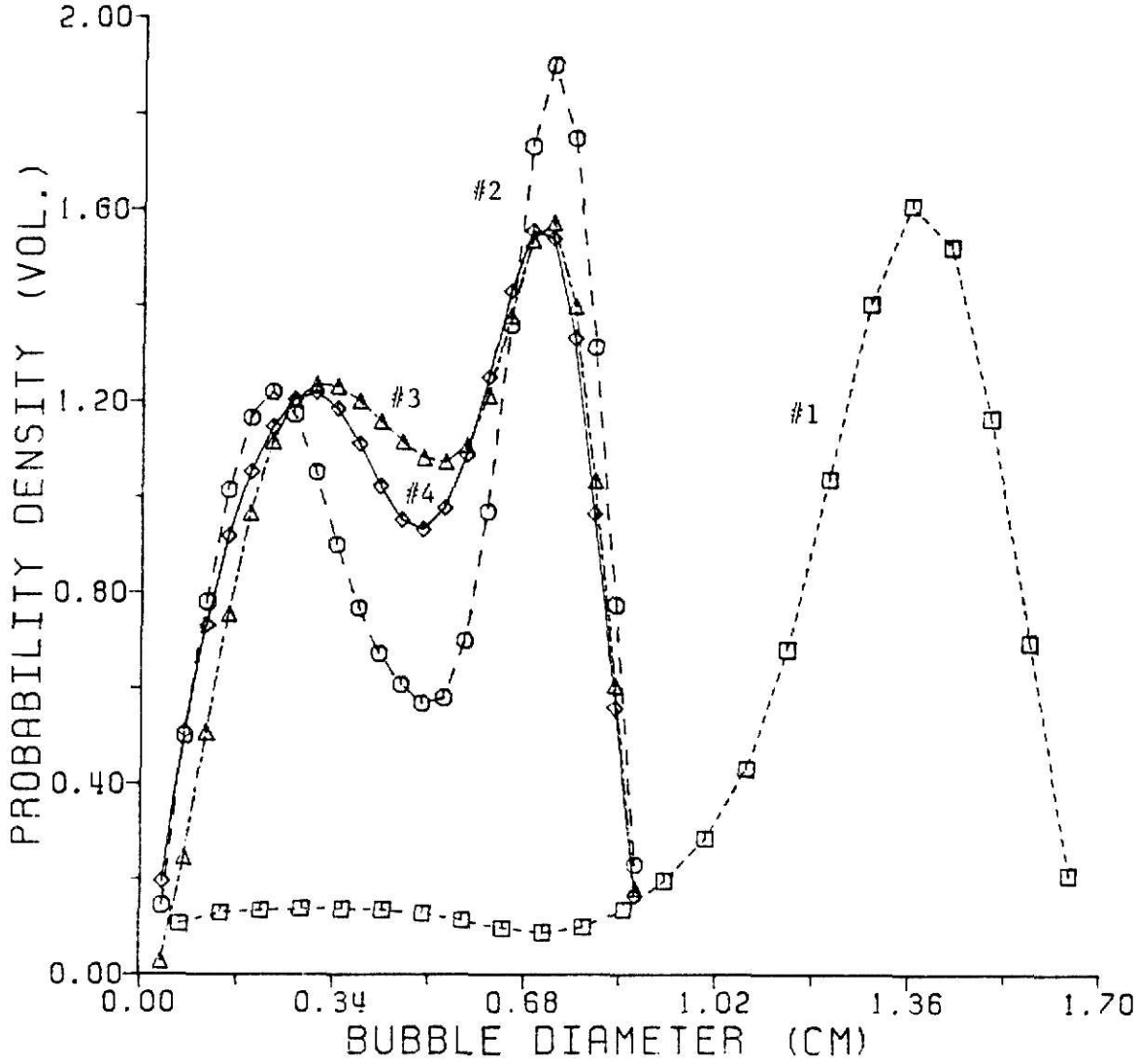



Figure 3.27 Bubble size distribution for air-CMC solution (0.8%) at air flow rate F=60 $ft^3/hr.$ (numbers refer to window locations shown in Fig. 3.1)

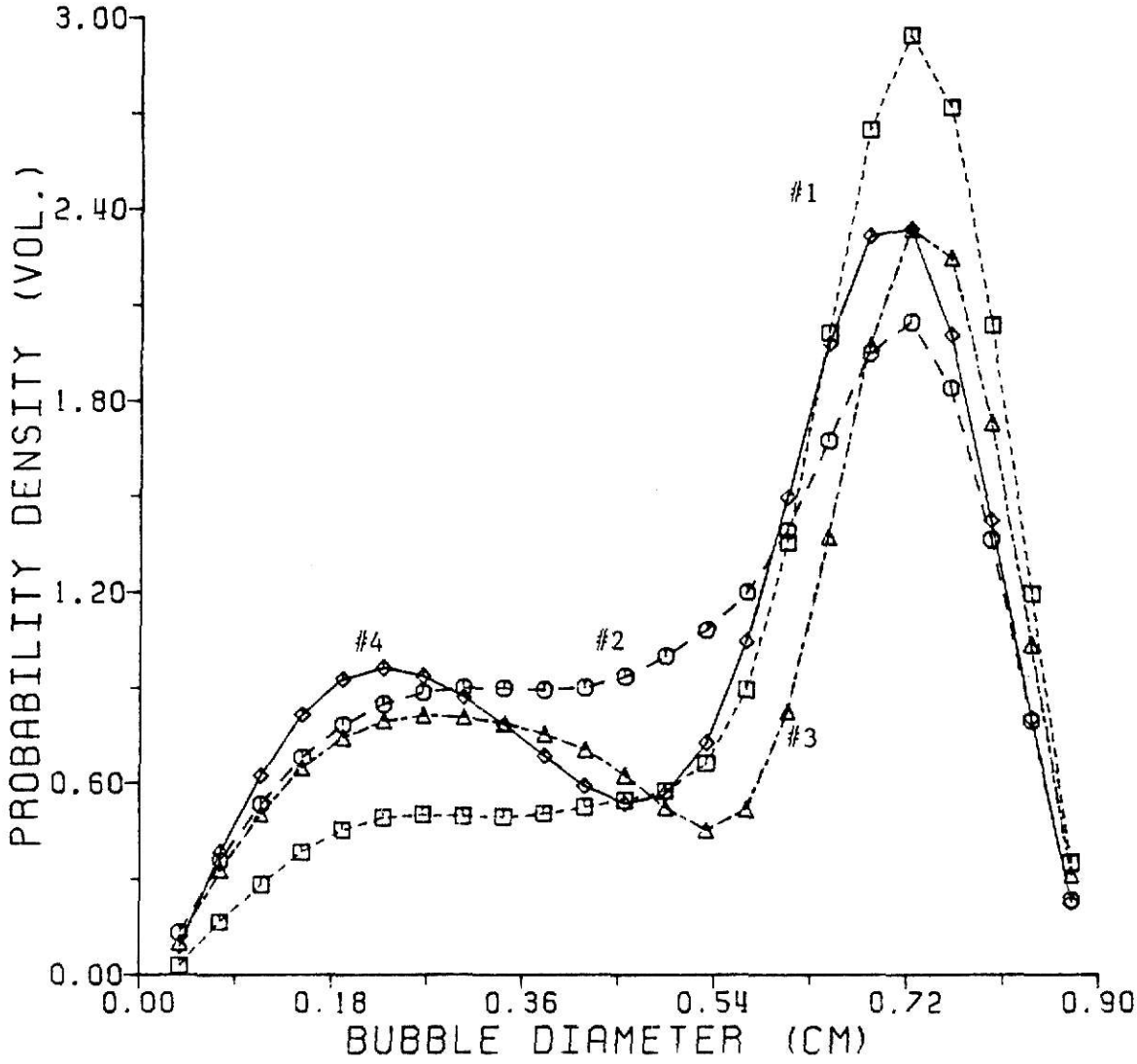



Figure 3.28 Bubble size distribution for air-CMC solution (0.8%) at air flow rate F=90 $ft^3/hr$.(numbers refer to window locations shown in Fig. 3.1)

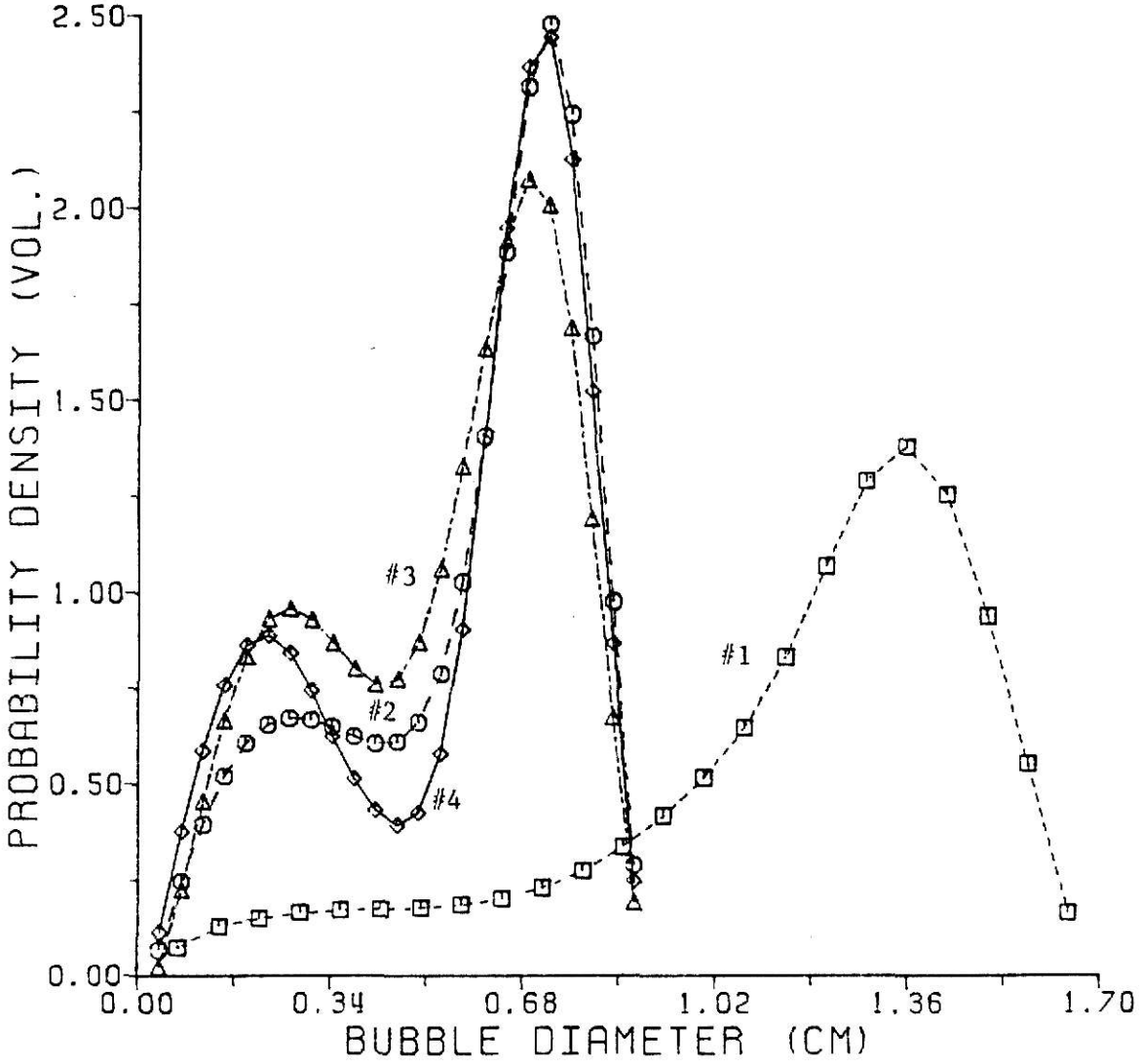



Figure 3.29 Bubble size distribution for air-CMC solution (0.8%) at air flow rate F=120 $ft^3$/hr. (numbers refer to window locations shown in Fig. 3.1)

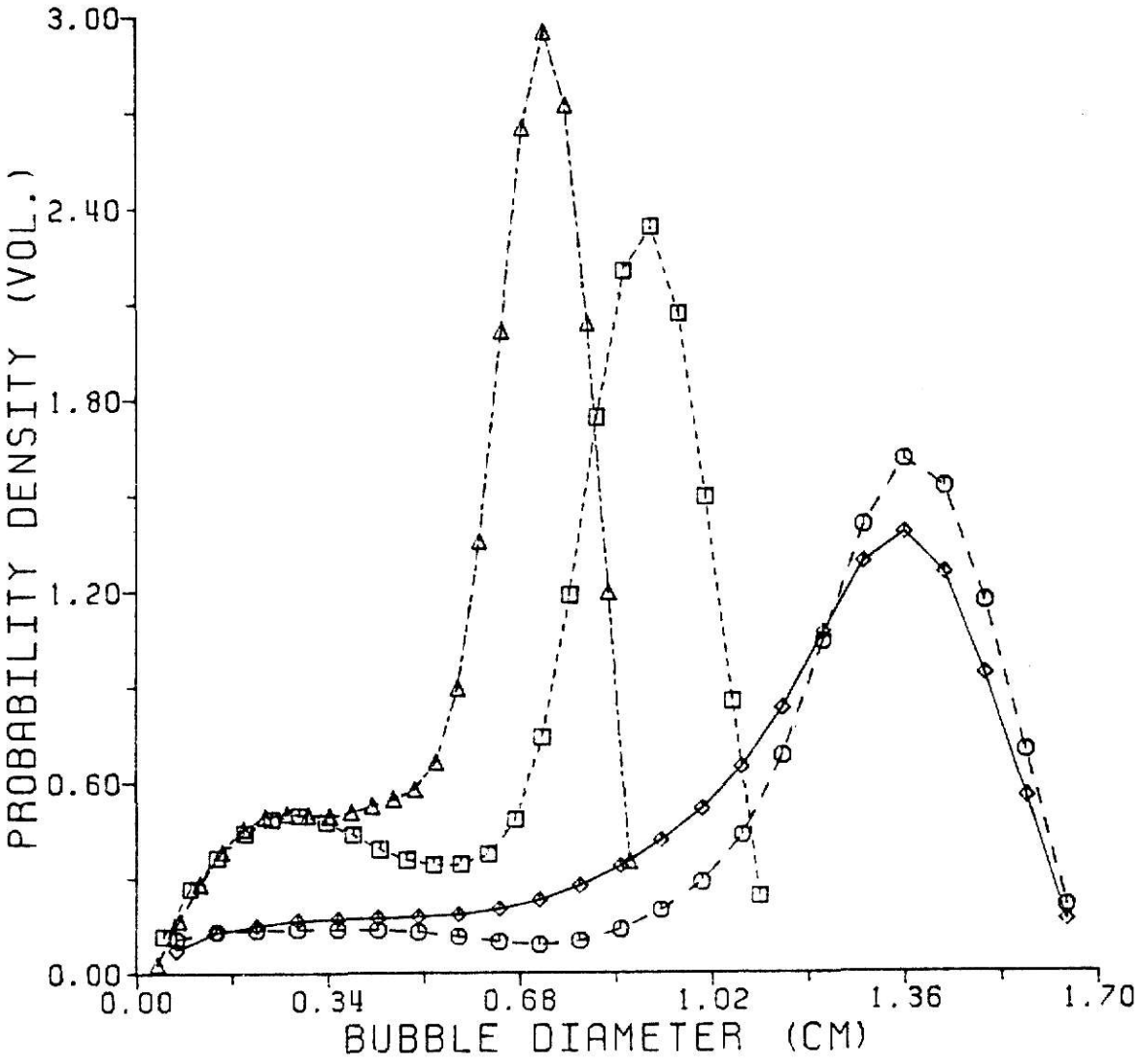



Figure 3.30 Bubble size distribution for air-CMC solution (0.8%) at window #1 for various air flow rates. [ □:F = 30 $ft^3/hr$, ⏀:F = 60 $ft^3/hr$, △:F = 90 $ft^3/hr$, ◇:F = 120 $ft^3/hr$ ]

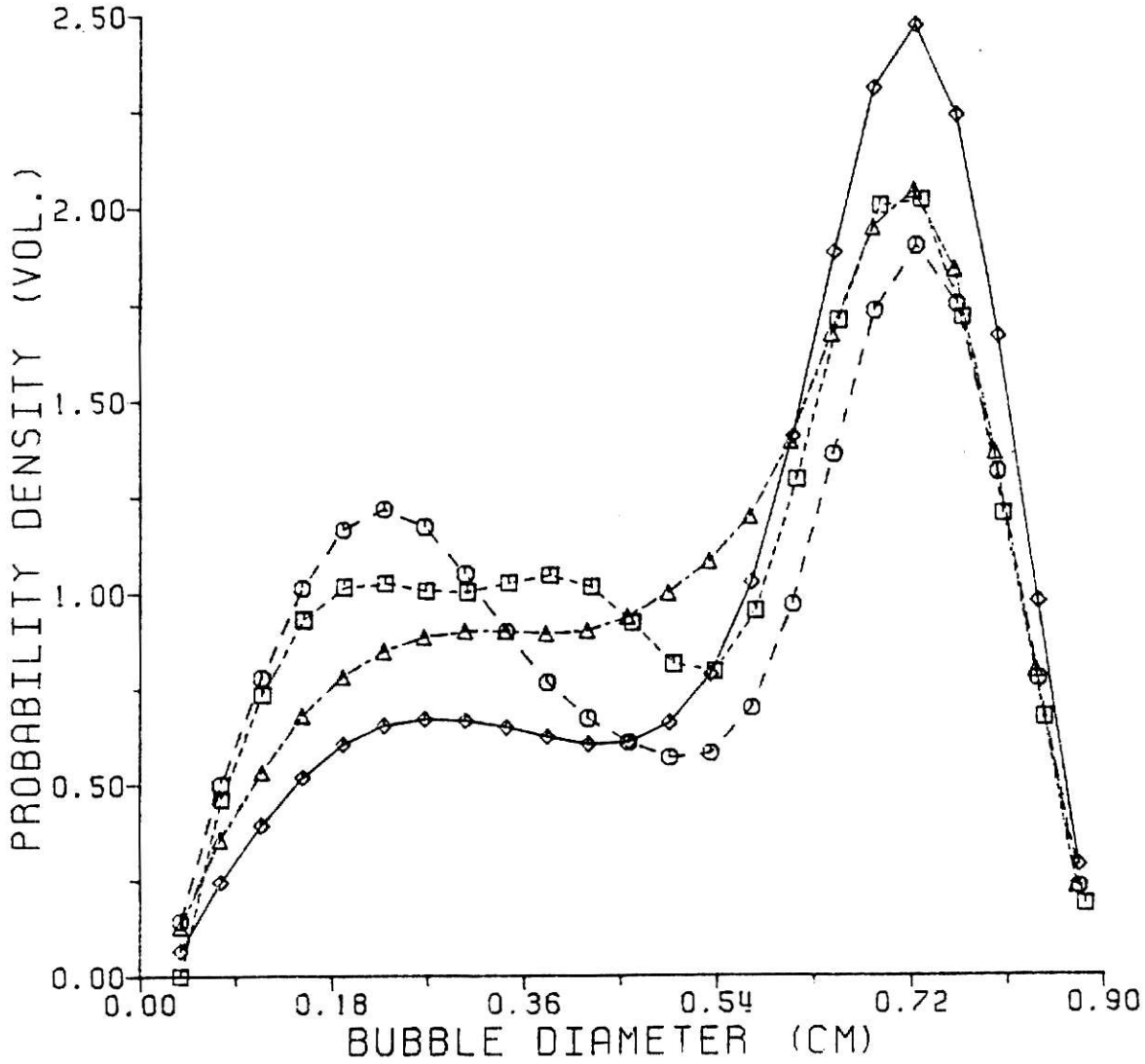



Figure 3.31 Bubble size distribution for air-CMC solution (0.8%) at window #2 for various air flow rates. [□:F = 30 $ft^3/hr$, ○:F = 60 $ft^3/hr$, △:F = 90 $ft^3/hr$, ◇:F = 120 $ft^3/hr$]

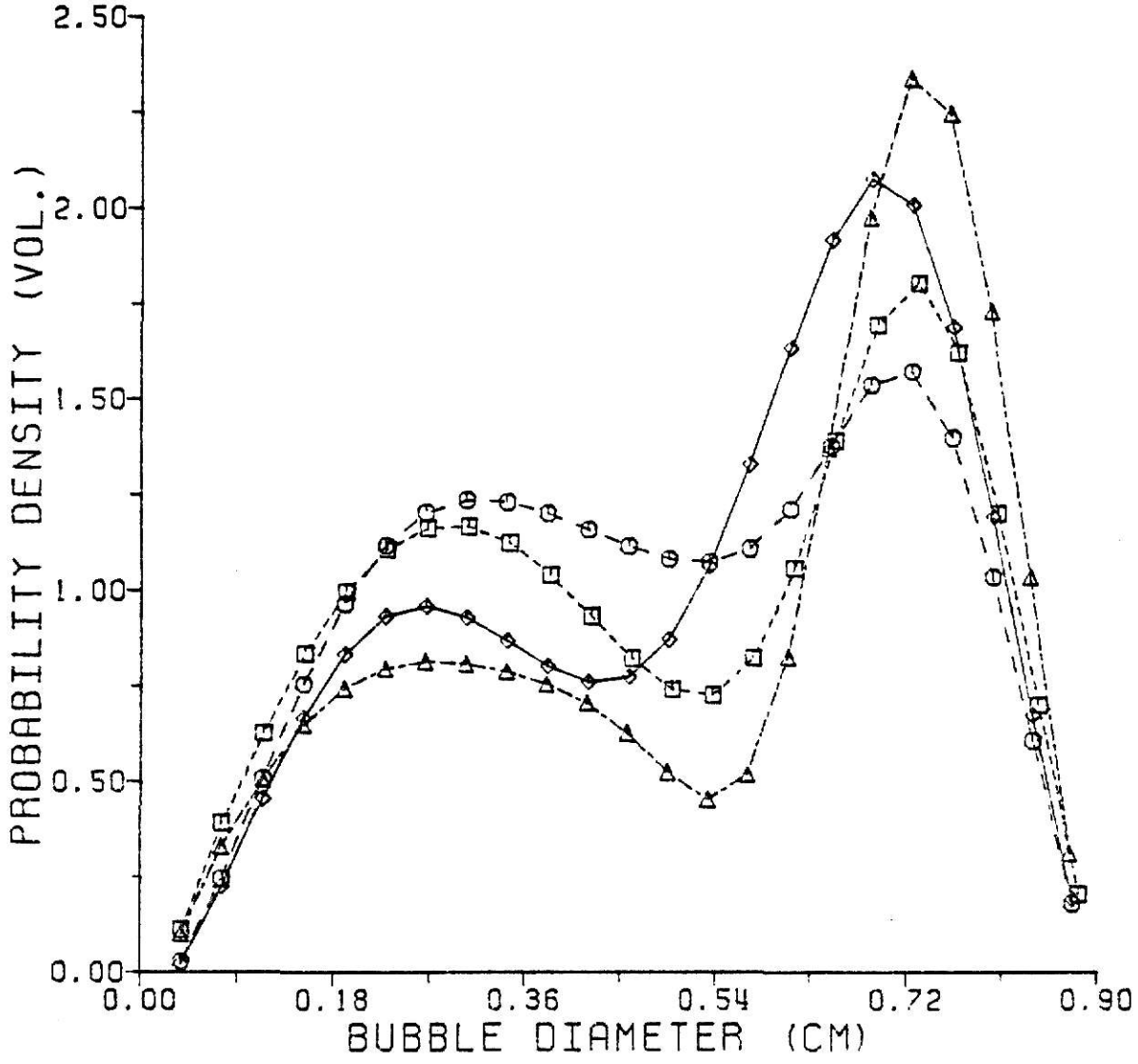



Figure 3.32 Bubble size distribution for air-CMC solution (0.8%) at window #3 for various air flow rates. [□:F = 30 $ft^3/hr$, ○:F = 60 $ft^3/hr$, △:F = 90 $ft^3/hr$, ◇:F = 120 $ft^3/hr$ ]

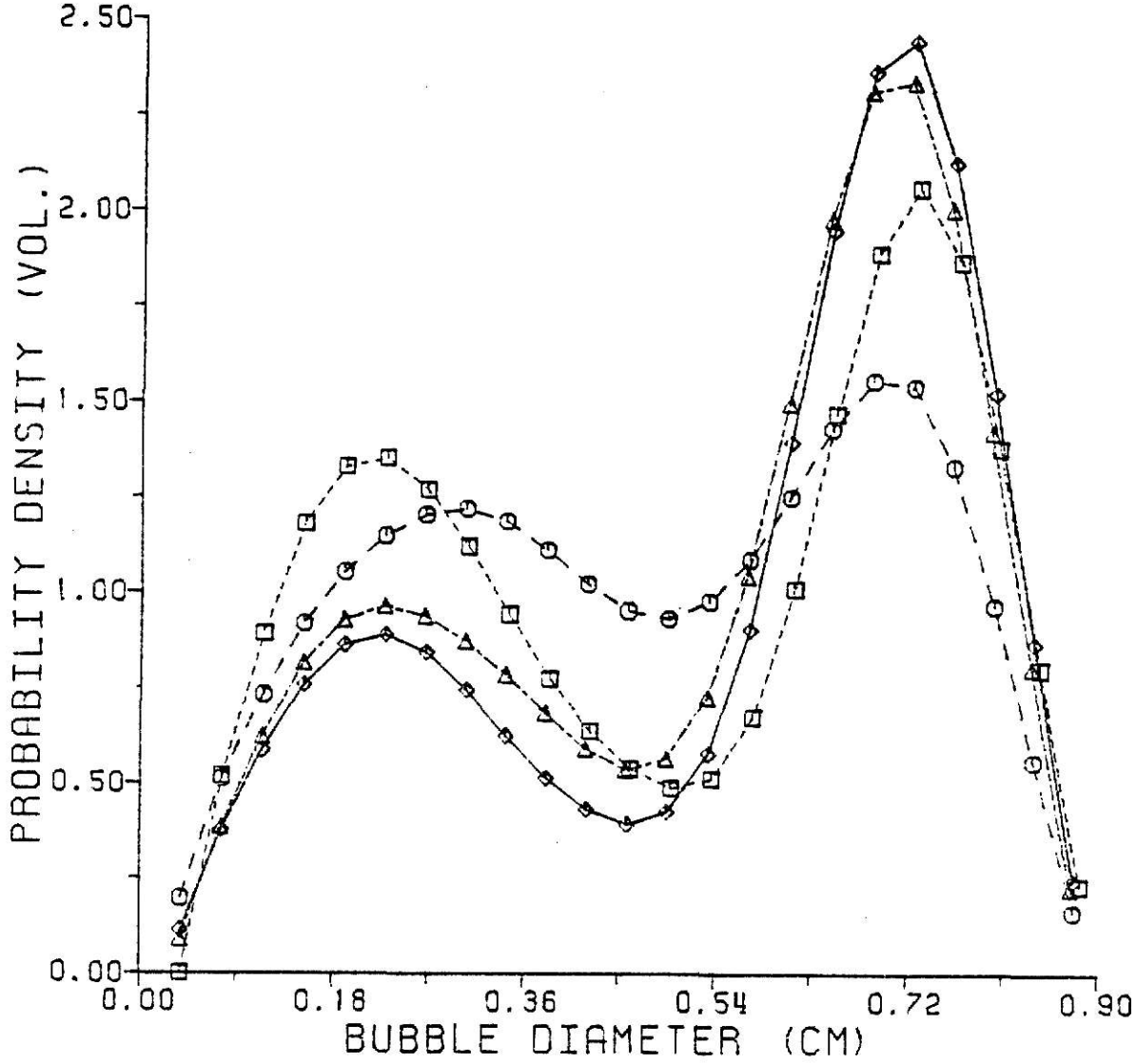



Figure 3.33 Bubble size distribution for air-CMC solution (0.8%) at window #4 for various air flow rates. [□:F = 30 $ft^3/hr$, ○:F = 60 $ft^3/hr$, △:F = 90 $ft^3/hr$, ◇:F = 120 $ft^3/hr$ ]

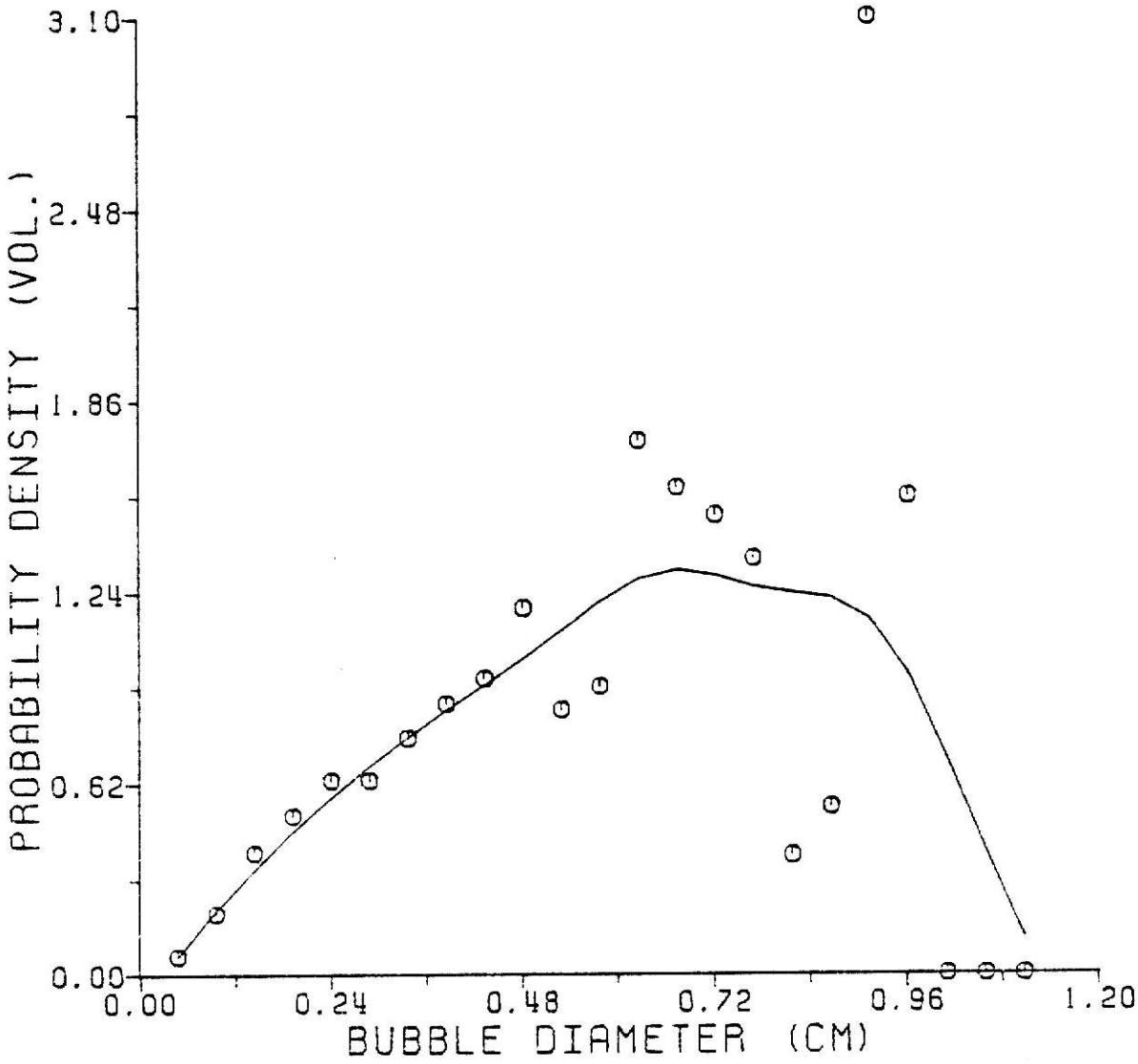



Figure 3.34 The effect of smoothing on bubble size distribution using a digital filter. (system : air-water @ 30 $ft^3$/hr of air /observed at window #4) [ ——— : data after smoothing, ○ : original data ]

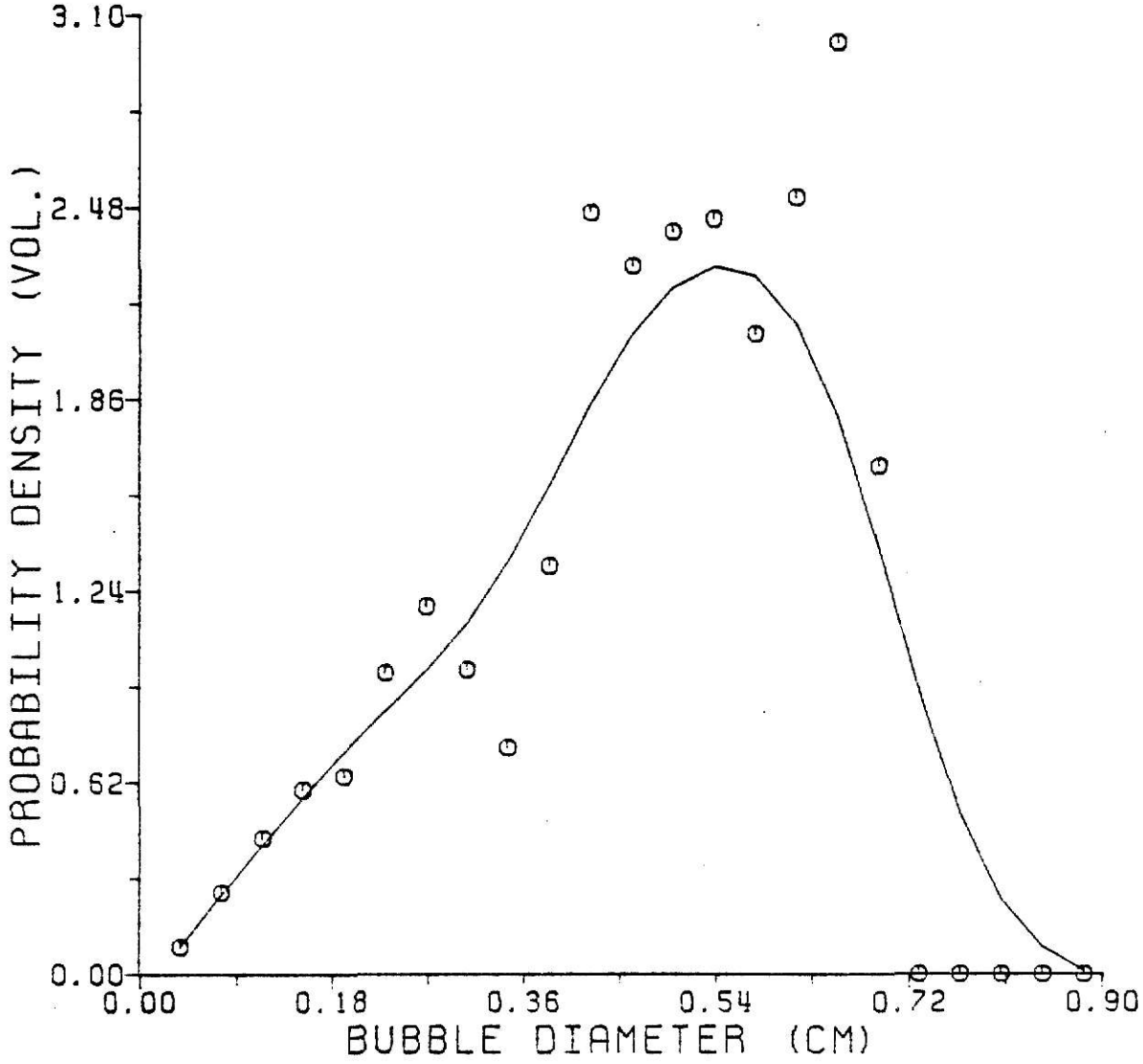



Figure 3.35 The effect of smoothing on bubble size distribution using a digital filter.(system : air-water @ 60 $ft^3$/hr of air /observed at window #4) [ ——— : data after smoothing, ⓘ : original data ]

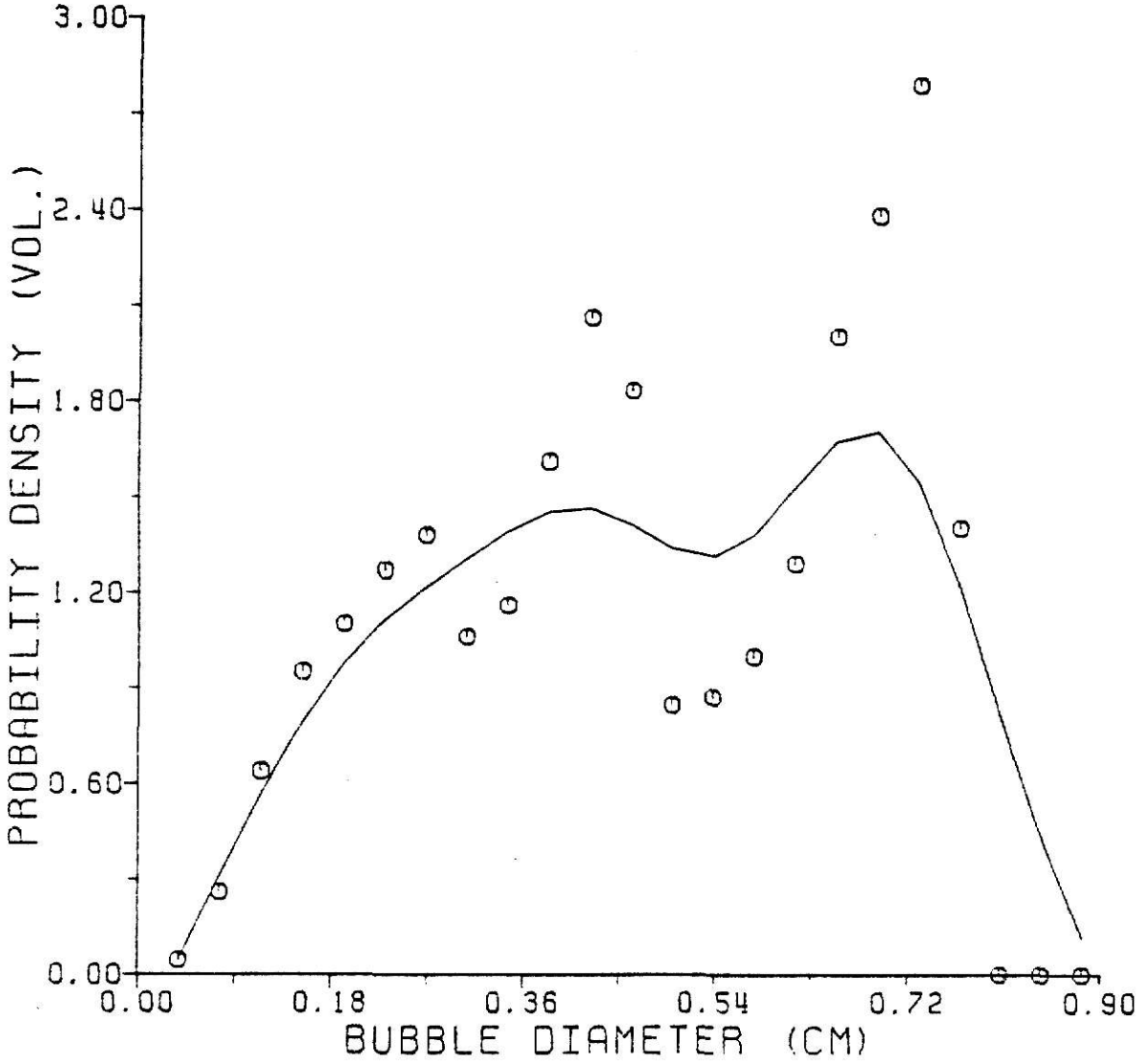



Figure 3.36 The effect of smoothing on bubble size distribution using a digital filter.(system : air-water @ 90 $ft^3$/hr of air /observed at window #4) [——— : data after smoothing, ○ : original data ]

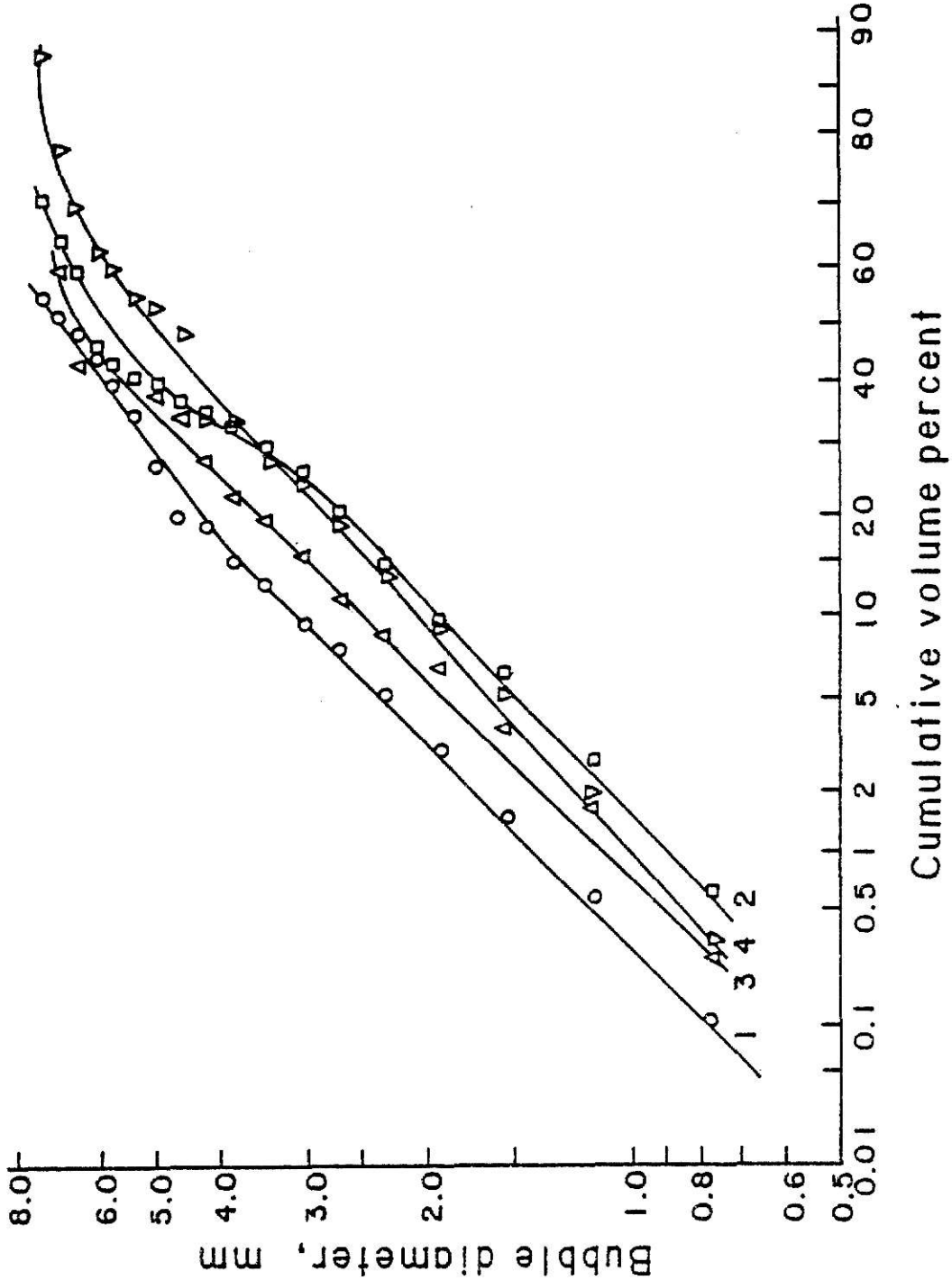



Figure 3.37 Cumulative volume distribution of bubbles for air-water system at air flow rate F=90 $ft^3/hr$; numbers refer to window locations shown in Fig. 3.1.

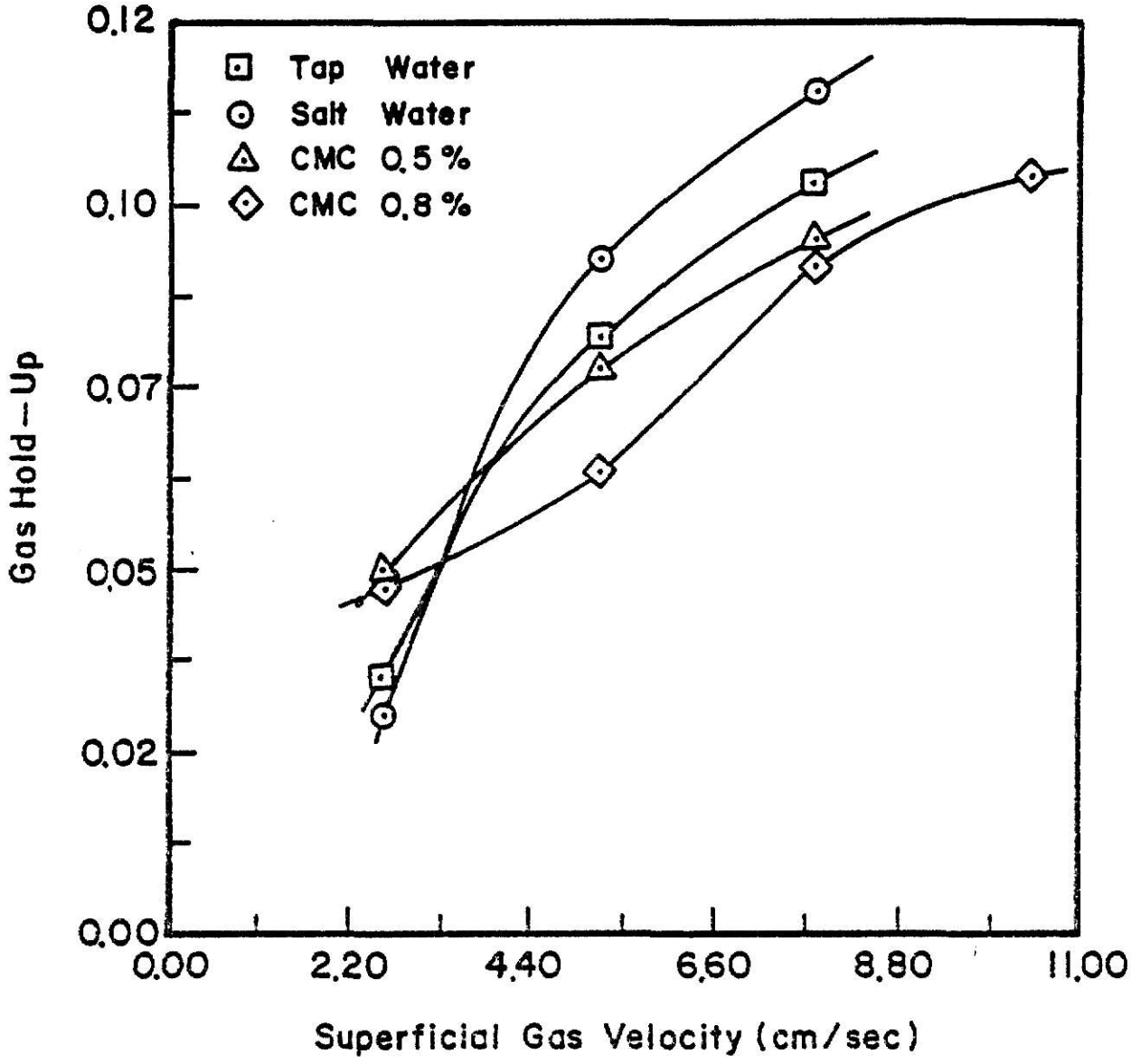



Figure 3.38 Influence of superficial gas velocity on gas hold-up.

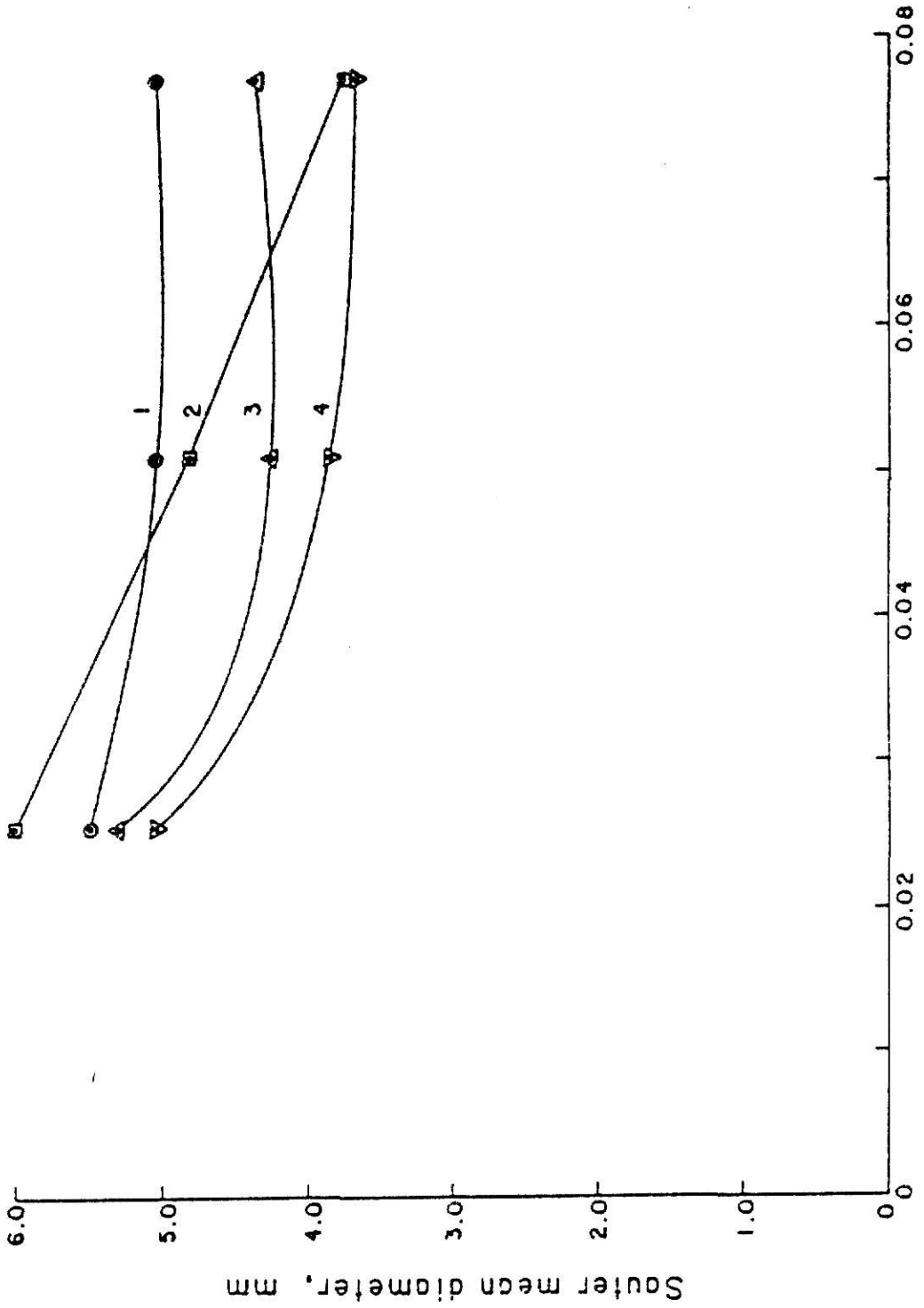



Figure 3.39 Influence of superficial gas velocity on Sauter mean diameter of bubbles for air-water system; numbers refer to window locations shown in Fig. 3.1.

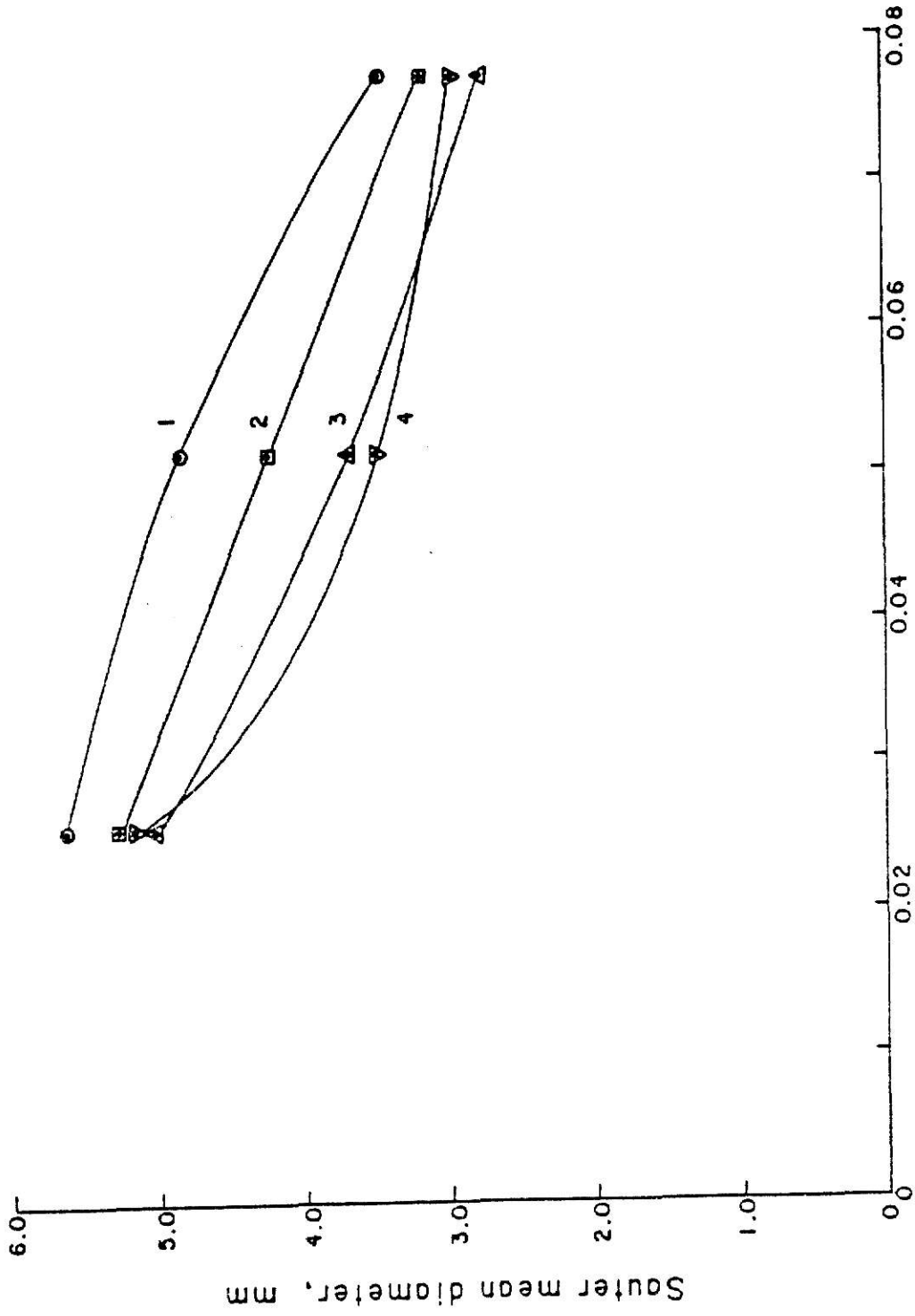



Figure 3.40 Influence of superficial gas velocity on Sauter mean diameter of bubbles for air-salt water system; numbers refer to window locations shown in Fig. 3.1.

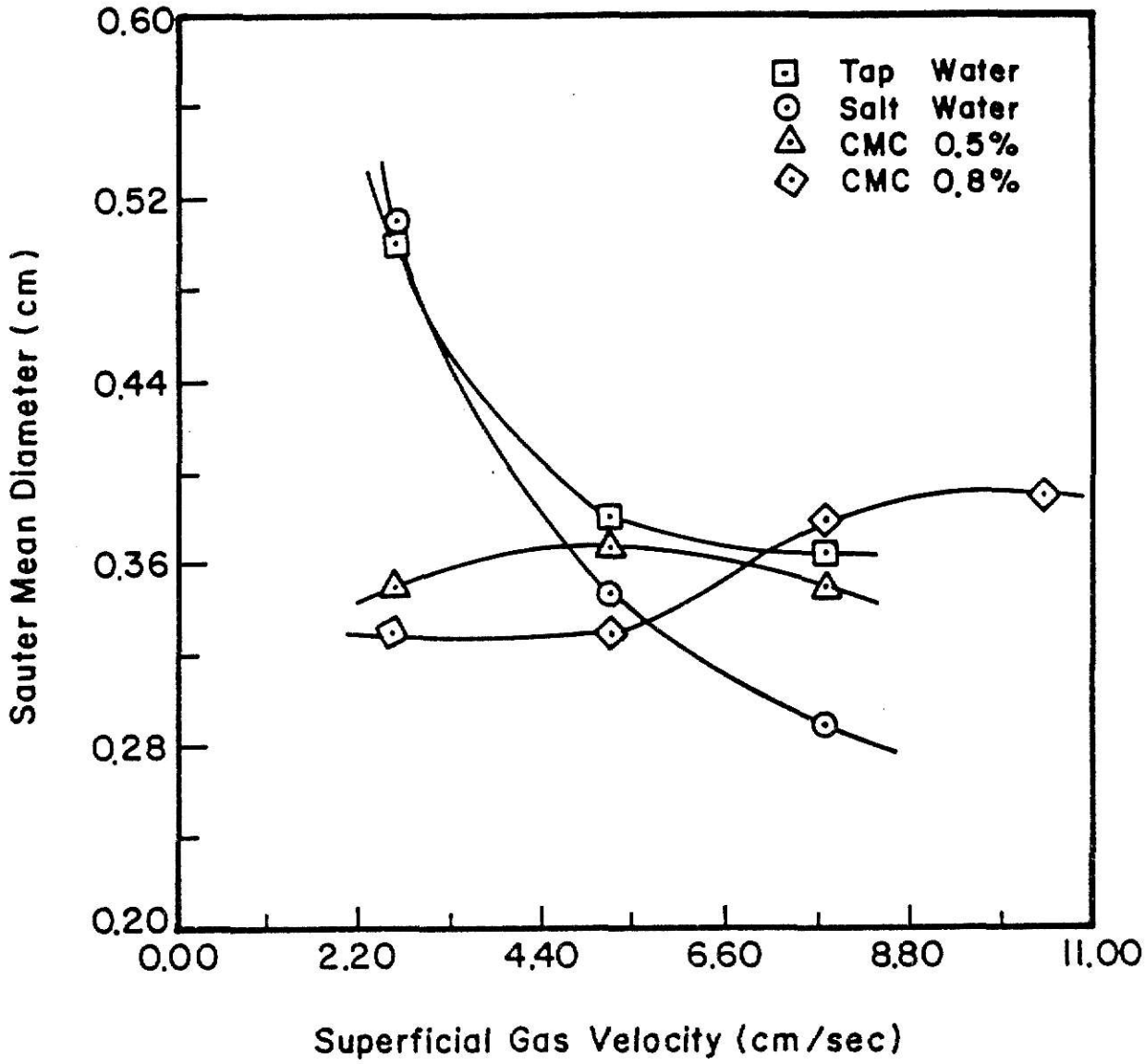



Figure 3.41 Influence of superficial gas velocity on Sauter mean diameter of bubbles at window #4.

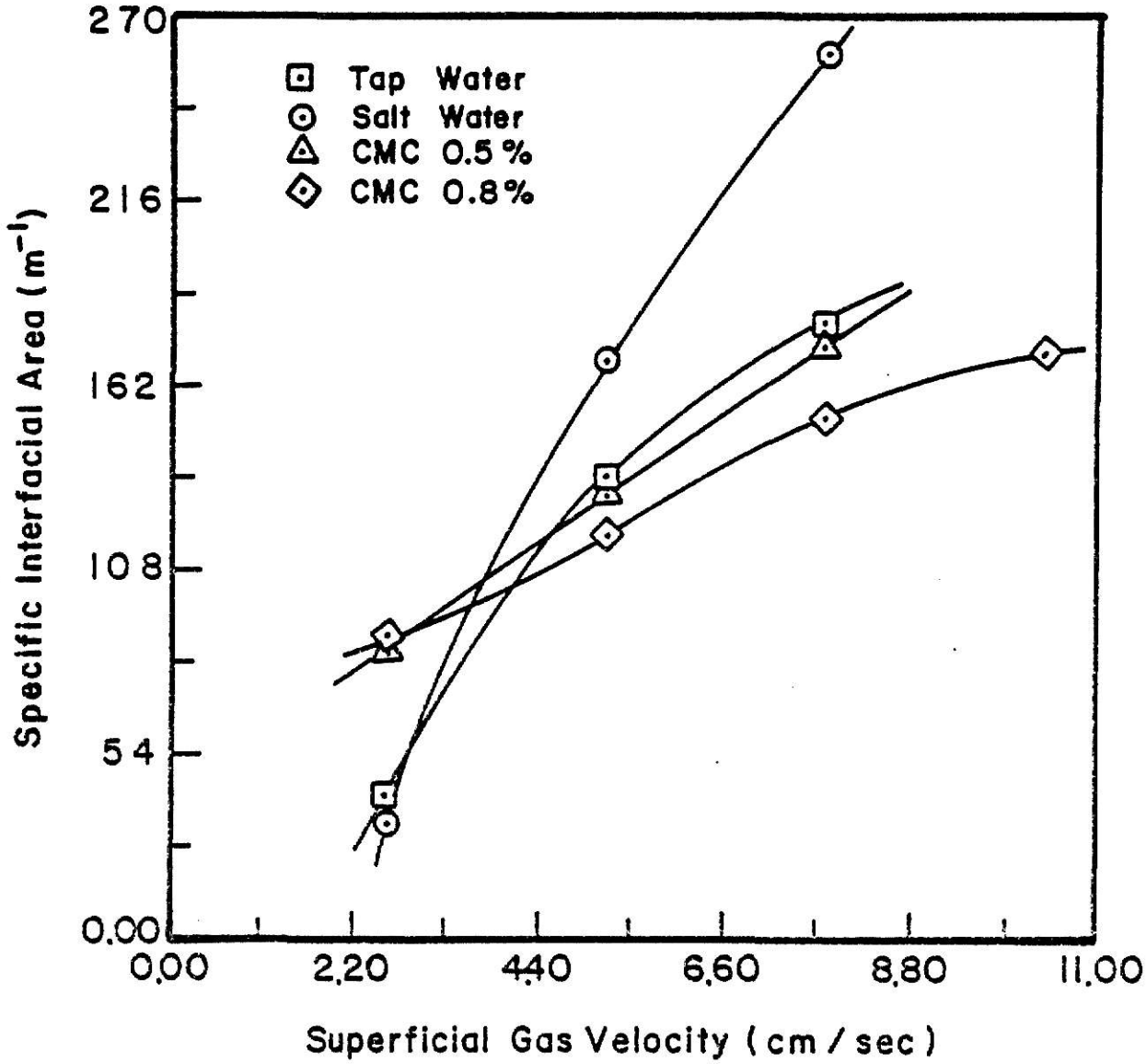



Figure 3.42 Influence of superficial gas velocity on specific interfacial area at window #4.

# CHAPTER IV

## WALL-PRESSURE FLUCTUATIONS IN TWO-PHASE SYSTEM

### 1. Introduction

The characterization of viscous fermentation media often requires measurement of system responses for which simple, direct procedures are not available. An indirect method that has seen little investigation involves measurement of the wall-pressure fluctuations associated with airlift fermentor operation. In particular, there is some indication that the spectra obtained by Fourier transformation of the pressure autocorrelation may be used to illuminate changes in the bubble size distribution occurring as the result of coalescence and/or breakup. The purpose of this chapter is to discuss the methods used for the analysis of the dynamic pressure fluctuations and the results. A review of previous work and underlying theory on this subject is also presented.

The measurement of mean total pressure or fluctuating total pressure in hydrodynamic investigations can be achieved with a properly designed Pitot tube; surface pressure fluctuations can be observed with a flush-mounted transducer. In either case, however, one must consider the spatial resolution of the instrument -- if the entire pressure-fluctuation spectrum is to be measured, then the Pitot tube diameter should be smaller than the Kolmogorov microscale, $\eta$ where

$$\eta = (\nu^3/\varepsilon)^{1/4} \tag{4.1}$$

$\nu$ is the kinematic viscosity and $\varepsilon$ is the dissipation rate per unit mass. Pressure transducers may respond to fluctuations generated within the boundary layer or beyond. The latter case is common with transducers connected to the wall surface by a tube; such installations also suffer from signal delay governed by the length of the tube and the

velocity of sound in the medium used. As Bradshaw (1971) has noted, the mean pressure recorded by small Pitot tubes corresponds to

$$P + \frac{1}{2}\rho \left(U^2 + \overline{u_1^2} + \overline{u_2^2} + \overline{u_3^2}\right) \tag{4.2}$$

where P is the static pressure, U is the mean velocity, and the $u_i$'s are the fluctuating velocity components. Bradshaw observes that it is very difficult to measure static pressure fluctuations in most laboratory flows. Assuming the hydrodynamic pressure fluctuations can be determined, even approximately, some further developments are possible. Following Tennekes (1977), we note that

$$p(\kappa) \approx \frac{1}{2}\rho u^2(\kappa) \tag{4.3}$$

where p is the fluctuating component of pressure and $\kappa$ is the wave number. In the inertial subrange, the three-dimensional wave-number spectrum is

$$E(\kappa) = \alpha \varepsilon^{2/3} \kappa^{-5/3} \tag{4.4}$$

Since the total eddy energy at wave number $\kappa$ is roughly proportional to $\kappa E(\kappa)$, we find

$$p(\kappa) \sim \rho \varepsilon^{2/3} \kappa^{-2/3} \tag{4.5}$$

Thus, the spectrum of pressure fluctuations, $S_p(\kappa)$, arising from fluid motions in the inertial subrange should be

$$S_p(\kappa) \sim \rho^2 \varepsilon^{4/3} \kappa^{-7/3} \tag{4.6}$$

In the case of the surface-mounted transducer the spatial resolution of the instrument has a decided effect upon frequency spectra. For example, Geib (1969) has found that for frequency spectra,

$$\frac{S_{measured}}{S_{actual}} = f(\frac{nd}{U_c}) \tag{4.7}$$

where d is the diameter of the transducer and $U_c$ is the phase or convection velocity and $n$ is the circular frequency. For vertical, two-phase flows, the passage of a buoyant bubble or particle can produce three distinct response characteristics in suitably sensitive flush-mounted transducers due to: sound or noise of approach, the pressure field around the object, and the wake or vortex-street behind the object. The first of these is not likely to be significant unless the velocity of approach is very high. The second can be approximately quantified by using results from potential flow theory; in the case of a sphere,

$$p - p_\infty = \frac{1}{2}\rho v^2(1 - \frac{9}{4}\sin^2\theta) \tag{4.8}$$

where v is the approach or relative velocity, and $\theta$ is the angle measured from the forward stagnation point. By virtue of the symmetry of ideal flow, the minimum local surface pressure will occur at $\theta = \pi/2$ radians. For spherical objects in water with a relative velocity of 5 cm/sec, $(p - p_\infty)$ varies from about 12.5 dynes/cm$^2$ to -15.6 at the location of maximum velocity. In real fluids at high velocities, of course, the pressure variation is not that extreme; see Fage (1937), for example.

In order to quantify wake-induced pressure fluctuations, it is necessary to know characteristic wake or vortex velocities. The characteristic frequency of such fluctuations can be determined from knowledge of the Strouhal number,

$$St = \frac{df}{v} \tag{4.9}$$

and the convection velocity. In Eq.(4.9), d is the object or cylinder diameter, f is the radian frequency of shedding and v is the

characteristic relative velocity. Roshko (1954) has measured St for flow past circular cylinders at Reynolds numbers ranging form 60 to about 7000; at Re = 200, for example, St ≃ 0.19. A cylindrical object in water with a diameter of 1 cm and a relative velocity such that Re = 200 would yield $f \simeq 0.38^{-1}$, or about 0.06 Hz. This is the shedding frequency for <u>one</u> side of the cylinder -- since this is an alternating phenomenon, the frequency encountered in the center of the vortex street (at a fixed position relative to the cylinder) would be roughly 0.12 Hz. A wall-mounted pressure transducer would record periodic pressure fluctuations in the wake at a different frequency, one determined by vortex spacing and the advection velocity; the signal, of course, should be one of decaying intensity since each vortex is attenuated with time as shown by Lamb (1945):

$$v_\theta = \frac{\Gamma}{2\pi r}\left(1 - e^{-r^2/4\nu t}\right) \qquad (4.10)$$

where $\Gamma$ is the vortex strength, r is the vortex radius and t is time. Roshko (1954) has noted that in a real vortex street, at large distances from the cylinder, the relative velocity between vortex structures and the fluid approach zero. He also reports that the ratio of vortex spacing to cylinder diameter, $\ell/d$, has a nearly constant value of 8. Thus, for the example cited above, the wall-mounted pressure transducer would record a vortex-derived signal at a frequency of about v/8 Hz.

In the vertical two-phase flows of interest here, the vortex-inducing bluff bodies are bubbles with characteristic shapes ranging from spherical to prolate, from symmetric to convolute. Furthermore, the high numerical density of bubbles and the interaction of vortex-streets makes interpretation of wall pressure fluctuations as distinct form

and wake phenomena impractically difficult. Hubbard and Dukler (1966) pioneered the use of wall pressure measurements for characterization of horizontal two-phase flow regimes. The observed dynamic pressure records are strikingly different for dispersed plug and slug flows; slug flows were found to produce large amplitude fluctuations of low (<1 Hz) frequency while plug flows gave more uniform fluctuations with frequencies on the order of 3 or 4 Hz. Hubbard and Dukler also Fourier-transformed the pressure autocovariance, $R(\tau)$, to obtain frequency spectra. By definition,

$$S_p(n) = \frac{1}{2\pi} \int_{-\infty}^{\infty} e^{-i\tau n} R(\tau)\, d\tau \qquad (4.11)$$

where

$$R(\tau) = \frac{\overline{p(t)\ p(t+\tau)}}{\overline{p^2}} \qquad (4.12)$$

Since $R(\tau)$ is an even function, the Fourier cosine transform is used and the resulting spectrum is one-sided. The measured spectra exhibited the following characteristics: in the annular flow regime, spectra were found to have isolated peaks at about 2.5 Hz; in the slug flow regime, major peaks were typically located around 1 Hz; one spectrum measured in the plug flow regime exhibited two principal peaks, located at about 2 and 4 Hz. Since it is evident that pressure fluctuations associated with wake phenomena can have frequencies greatly in excess of 10 Hz, we infer that either the instrumentation lacked the necessary sensitivity or the energy content of such signals was so low as to be insignificant.

Recent studies of liquid-phase turbulence in air-water flows include Schügerl (1982) and Lance and Bataille (1983); vertical, two-phase

flows have been discussed by Taitel et al., (1980). Schügerl (1982) has reported one-dimensional spectra in bubble column measured by hot-film anemometry at various superficial gas velocities ($V_G$'s). When the air was sparged through perforated plates, $V_G$ did not greatly affect the spectra; with a porous plate with 5 μm openings, however, the integral

$$\int_0^\infty F_{11}(\kappa_1)d\kappa_1 \tag{4.13}$$

where $F_{11}$ is the one-dimensional longitudinal spectrum, went through a maximum and then decreased with higher $V_G$. Schügerl attributes this behavior to the damping effect high numerical bubble densities have upon turbulence. It is interesting to note that the spectra reported by Schügerl contain an extensive region with a slope of -2 and virtually no part of the observed spectra follows the Kolmogorov, or -5/3, power-law. It has been suggested by von Weizsäcker (1948) that a spectral dependence of $\kappa_1^{-2}$ indicates substantial structural fluctuation.

Lance and Bataille (1983) used both hot-film and laser-Doppler anemometry in their study in which 5 mm bubbles were combined with grid-generated turbulence in a water tunnel. Void fractions (relative hold-ups) in their study were restricted to values $\leq$ 5%. They found two distinct regimes; at low hold-ups, grid-generated turbulence was dominant and at higher values, bubbles were found to transfer a significant amount of kinetic energy to the liquid phase. The transition hold-up value between the two regimes was also found to vary with relative intensity, but typical values were on the order of 1 to 2%. Spectra measured by Lance and Bataille indicate a range of wave numbers in which $F_{11}(\kappa_1) \simeq \kappa_1^{-8/3}$ for a void fraction of 2.56%.

Taitel et al. (1980) were primarily concerned with flow pattern transitions in vertical, two-phase flows; identified patterns (or

regimes) are bubble, slug, churn and annular. Flow pattern maps are presented and the regimes identified as functions of superficial gas and liquid velocities. Bubble flow does not occur in small diameter tubes except at very high liquid flow rates. The column diameter associated with bubble flow is given by

$$\left[\frac{\rho_L^2 \, g \, D^2}{(\rho_L - \rho_G)\sigma}\right]^{1/4} \leq 4.36 \qquad (4.14)$$

where bubble flow occurs at low liquid flow rates only when this criteria is violated. For a vertical air-water system in a 4 cm diameter pipe, the bracketed quantity is 3.87. Thus, only studies performed in relatively large columns or towers will generally violate Eq.(4.14). By their results, most studies in small tower reactors and columns will involve slug or churn-flow patterns.

2. Experimental Procedure

A cylindrical plexiglass airlift column has been constructed as shown in Figure 3.1 in the previous chapter. Five pairs of pressure taps distributed along the length of the column were used with Gould-Statham pressure transducers to measure wall pressure fluctuations; the smaller of the pressure transducers had a $\pm$ 0.15 psid pressure range while the larger one had a $\pm$ 0.7 psid range. The appropriate tap for each measurement was connected to the input port of the transducer while the reference port was maintained at a pressure equal to the static value.

The pressure signals were fed to an online correlation and probability analyzer (Honeywell Model SAI-43A) which calculated the autocorrelation functions of the fluctuating signals. An online Fourier transform analyzer (Honeywell Model SAI-470) performed a Fourier analysis on the functions calculated by the correlator. The outputs from the two analyzers could be sent to either an X-Y plotter or an oscilloscope. Figure 4.1 illustrates the instrumentation assembly described above. Air flow rates ranging from 30 scfh to 250 scfh were used and measured using Dwyer air-flow rotameters.

Three different air-liquid systems were studied; the liquid media were tap water, salt water, and CMC solution. Two different CMC concentrations, 0.5% and 0.8% by weight, were used in this study.

3. Discussion of Results

Experiments performed with single, large hemispherical bubbles rising through both CMC solution and water reveal four sharply distinct pressure phenomena recorded with the wall-mounted transducer. The first of these is a formation and adjustment phase in which the observed wall pressure increases dramatically while oscillating with a decaying amplitude and a characteristic frequency of about 20 Hz. These superimposed fluctuations probably result from damped interfacial disturbances and/or surges in the sparger following bubble detachment. The second phase is indicated by a precipitous drop in pressure observed as the bubble passes the transducer port; under the experimental conditions employed, this phenomenon occurred over a period of about 200 msec. The third phase was detected during pressure recovery immediately after the bubble passed the pressure port, when small fluctuations with typical frequencies on the order of 8 to 10 Hz were observed. These disturbances undoubtedly result from the wake (vortex structures) trailing the bubble. Finally, fairly large variations in column pressure were recorded after disengagement of the bubble at the top of the column due to the interfacial disturbance. These oscillations had a very low frequency, typically about 0.5 Hz, and slowly decay in amplitude. Phenomena observed for air bubbles rising in pure water were quantitatively similar. An illustration of these results is shown in Figure 4.2.

A typical autocorrelation curve and its Fourier transform, which were calculated on-line, of the wall pressure fluctuations measured at location $P_5$ (see Figure 3.1) for air flow rate of 60 $ft^3/hr$ in an air-tap water system is shown in Figure 4.3. This was done for each

system at locations $P_1$ through $P_5$ using air flow rates ranging from 30 $ft^3/hr$ to 250 $ft^3/hr$.

The magnitude of the pressure fluctuations was characterized using the standard deviation of the fluctuations about the mean, and the dominant frequencies present in a given signal were obtained from the corresponding spectra (or the Fourier transformation of the auto-correlation curve). The magnitude of the autocorrelation curve at zero time lag was used to estimate the standard deviation value. Equation (4.12) gives the normalized autocorrelation function which in the non-normalized form would be:

$$R(\tau)\ \overline{p^2} = \overline{p(t)p(t+\tau)} \qquad (4.15)$$

where the overbar indicates a time-average. Since p(t) represents pressure fluctuations, $\overline{p(t)} = 0$ for a statistically stationary process. Therefore with zero delay ($\tau = 0$) the right hand side of Eq.(4.15) gives the variance of the pressure fluctuations. The root mean square (RMS) of the pressure fluctuations is the square root of the average of the right hand side of Eq.(4.15) for $\tau = 0$.

Figures 4.4 and 4.5 show the measured values of the RMS of the pressure fluctuations for tap water and salt water as a function of superficial gas velocity at various positions of the column. The values appear to increase with the distance from the sparger with the results at the two highest pressure taps being very similar. The increase of the RMS of the pressure fluctuations with the height of the pressure tap may reflect an increase in dynamic energy content of the two-phase system associated with liquid turbulence, oscillating interfacial motion, and wakes associated with rising bubbles. The results suggest that there may be a dynamic energy transport process associated with airlift system that occurs as the gas and liquid flow cocurrently upward and some time is needed to reach a steady state condition.

Figures 4.6 to 4.9 show the comparisons of the RMS values for tap water and salt water as a function of superficial gas velocity from $P_1$ to $P_4$. As can be seen from these figures, the RMS values of the pressure fluctuations for salt water are larger than those for tap water except at the highest position $P_4$ in which both are essentially similar. This is probably due to the different resistance of the dynamic energy transport process for tap water and salt water systems in the transition region (the region close to the sparger). The dynamic energy transport process in the region close to the sparger may be in part due to the breakage of the primary bubbles which tend to transfer energy from the gas phase to liquid phase and gas-liquid interface. This is because vortices are generated and surface energy between the gas-liquid interface is increased during the bubble breakage process. And the surface tension force may play an important role in this energy transport process because it tends to prevent the bubbles from breaking up. This implies that the lower the surface tension force, the easier the energy transport process in the upward cocurrent two-phase system.

Figures 4.10 and 4.11 show the RMS values of the pressure fluctuations for tap water and 0.8% CMC solution as a function of superficial gas velocity. In Figures 4.12 to 4.14, results for tap water and 0.8% CMC are compared at positions $P_1$, $P_2$, and $P_4$, respectively. In all cases, the RMS of the pressure fluctuations is lower for the CMC solution than for tap water. This is an expected result because more energy is dissipated by viscous forces in CMC solution and the magnitude of the pressure fluctuations is also damped to a greater extent by fluids with higher viscosity.

The RMS of the pressure fluctuations presented in Figures 4.4 to 4.14 appear to increase linearly with the superficial gas velocity. This is probably due to the fact that the power input, $\overline{P}$, in Eq.(3.19) is directly

proportional to the volumetric gas flow rate, F, and the superficial gas velocity, $V_G$, is given by

$$V_G = \frac{F}{A} \tag{4.16}$$

where A is the cross sectional area in the upflow zone of the airlift column. So if the RMS of the pressure fluctuations is directly related to the dynamic energy content of the system, then it can be shown to increase in an approximately linear manner with superficial gas velocity.

Figures 4.15 to 4.29 show the spectra of pressure fluctuations at locations $P_1$ through $P_5$ with air flow rate ranging from 30 $ft^3/hr$ to 150 $ft^3/hr$ for tap water, 0.8 wt.% and 0.5 wt.% CMC solutions. Figures 4.15 to 4.19 indicate that the spectra of pressure fluctuations for tap water at locations $P_1$ and $P_2$ contain three distinct regions: the first is the peak with frequency between 4.5 and 5 Hz, the second is the region with frequency around 10 Hz, the third is the region with frequency between 15 and 20 Hz. There is no signal was detected with frequency beyond 35 Hz. This implies that the characteristic frequencies of the equilibrium range eddies cannot be detected by the existing instrumentation. The first peak with frequency around 4.5 to 5 Hz is probably due to the passage of the primary bubbles; this peak is less significant at $P_4$ and $P_5$ as compared with that at $P_1$ and $P_2$. This is because the primary bubbles break up when they leave the sparger and go up the column, so that at a lower position in the column ($P_1$ and $P_2$) the dynamic pressure fluctuations due to bubble passage are more significant than those at $P_4$ and $P_5$. The second region with frequency about 10 Hz is probably due to the vortex shedding (wake behind the bubble) according to the single bubble experiments. As can be seen from Figures 4.15 to 4.19, this peak is more significant at low air flow rate as compared with that at

higher air flow rate. This is because at higher air flow rate the vortices generated by different bubbles interact each other, so that this peak is less distinct and gradually loses its identity with increasing air flow rate. The third region with frequency between 15 and 20 Hz may be due to either energetic eddies (energy containing eddies) or the interfacial oscillation of the bubbles. There is reason to believe that interfacial oscillation may contribute substantially to pressure signals received in the 10 to 30 Hz range. Lamb (1932) has shown that for a spherical globule,

$$f_B^2 = \frac{12\,\sigma}{\rho_c\, r_B^3} \tag{4.17}$$

where $f_B$ is the radian frequency of the interfacial oscillation. For tap water with $\sigma$ = 70 dyne/cm and $\rho_c$ = 1 g/cm$^3$, the air bubble with $r_B$ = 0.4 cm will have the characteristic frequency about 18 Hz. On the other hand, the experiment performed by Lance and Bataille (1983) in order to study the turbulence in the liquid phase of a bubbly air-water flow has shown that the turbulent eddies in the system they investigated have a typical integral length scale $\ell$ = 2 cm, when the mean liquid velocity is about 30 cm/sec. Thus, these energetic turbulent eddies should have a characteristic frequency around 15 Hz. It appears that a separate experiment should be devised to differentiate between eddy-induced signals and interfacial oscillation.

If we only compare the spectra of the dynamic pressure fluctuations in the range of frequency between 15 and 30 Hz in Figures 4.15 to 4.19, the spectrum at $P_4$ is always the broadest and the peak frequency is the highest as it contains more energetic turbulent eddies with higher frequency and more bubbles with smaller size than the other three positions ($P_1$, $P_2$ and $P_5$). It suggests that the turbulence at $P_4$ is more intense than that at other three positions causing the RMS value of the pressure fluctuations at $P_4$ to

be larger than the others. As can be seen from Figures 4.15 to 4.19, there is one distinct peak with frequency between 0 and 5 Hz at $P_5$. This may be due to the static pressure fluctuations which are caused by the change of the liquid head.

Some striking differences can be seen if we compare the spectra of pressure fluctuations for CMC solutions (0.8% and 0.5%) as shown in Figures 4.20 to 4.29 with those for the tap water system. The spectra for 0.5% CMC solution at $P_1$ are similar to those for tap water except the magnitude of the pressure fluctuations due to the liquid turbulence and interfacial oscillation is decreased dramatically, and only the dynamic pressure fluctuations due to the bubble passage and vortex shedding are important. As we go to the higher viscosity with 0.8% CMC solution, the spectrum at $P_1$ is only significant at characteristic frequencies around 5 Hz. This is probably due to the more significant of the damping effect and the lower intensity of the liquid turbulence in high viscosity media as compared with those in the tap water system. Spectra of the pressure fluctuations at $P_1$ for 0.8% CMC solution are essentially due to the passage of the primary bubbles. Furthermore, the dynamic pressure fluctuations due to bubble passage are more significant at $P_2$ and $P_4$ for CMC solutions (0.8% and 0.5%) than those for tap water. This is because the metastable bubble size in high viscosity system is larger as compared with that in tap water system. Thus, the contribution of the signals due to bubble passage is larger for CMC solutions than that for tap water.

## 4. Conclusions

The results of the experiments described in this chapter lead to the following conclusions:

i) The RMS of the pressure fluctuations is shown to increase in an approximately linear manner with the power input and is closely related to the dynamic energy content of the two-phase system associated with liquid turbulence, oscillating interfacial motion, and wakes associated with rising bubbles. The higher the RMS value of pressure fluctuations, the larger the dynamic energy content in the system.

ii) High viscosity media in the upward cocurrent two-phase flow are less efficient for the energy transport process because more energy is dissipated by viscous forces.

iii) The RMS of pressure fluctuations is basically composed of two components: the first is the static pressure fluctuation which is caused by the change of the liquid head, the other is the dynamic pressure fluctuation which is due to the local pressure variation because of the bubble passage, the wake behind the bubble, the turbulent eddies, and the interfacial oscillation.

iv) The magnitude of the static pressure fluctuations is relatively small compared with the dynamic pressure fluctuations in low viscosity systems. This is because the gas hold-up is nearly constant. The variation of the liquid head above each pressure tap is small as compared with the local pressure fluctuations. The characteristic frequencies of the static pressure fluctuations are between 0 and 5 Hz.

v) The dynamic pressure fluctuations due to bubble passage are more significant in CMC solutions and their characteristic frequencies are about $4 \sim 5$ Hz which are roughly independent of air flow rate.

vi) The frequency associated with the vortex shedding (wake behind the bubble) is approximately on the order of 8 ~ 10 Hz; it is less significant at higher air flow rates because of the interaction of the vortices.

vii) The largest contribution to the spectrum of pressure fluctuations in tap-water system is the dynamic pressure fluctuations due to the interfacial oscillation and energetic turbulent eddies which have a characteristic frequency between 15 and 20 Hz.

NOMENCLATURE

| | | |
|---|---|---|
| $d$ | : | diameter of transducer or cylinder diameter |
| $D$ | : | column diameter |
| $E$ | : | three-dimensional power spectrum |
| $f$ | : | radian frequency of shedding |
| $F_{11}$ | : | one-dimensional longitudinal spectrum |
| $g$ | : | acceleration due to gravity |
| $\ell$ | : | vortex spacing |
| $n$ | : | circular frequency associated with turbulent eddy |
| $p$ | : | dynamic pressure fluctuation or pressure around a circular cylinder |
| $p_\infty$ | : | free stream pressure |
| $P$ | : | static pressure |
| $r$ | : | vortex radius |
| $R$ | : | autocorrelation function of pressure signals |
| Re | : | Reynolds number ( $= \frac{vd}{\nu}$ ) |
| $S$ | : | spectrum of pressure fluctuations |
| St | : | Strouhal number ( $= \frac{df}{v}$ ) |
| $t$ | : | time |
| $u$ | : | fluctuating velocity |
| $u_1$, $u_2$, $u_3$ | : | component of fluctuating velocity in 1, 2, 3 direction respectively |
| $U$ | : | main stream velocity |
| $U_c$ | : | convection velocity |
| $v$ | : | relative velocity |

Greek Letters:

| | | |
|---|---|---|
| $\alpha$ | : | proportionality constant |
| $\Gamma$ | : | vortex strength |
| $\varepsilon$ | : | energy dissipation rate per unit mass |

$\eta$ : Kolmogorov microscale of length

$\theta$ : angle measured from the forward stagnation point

$\kappa$ : wave number

$\nu$ : kinematic viscosity

$\rho$ : density of fluid

$\sigma$ : surface tension

$\tau$ : time delay

Subscripts:

c : convection

G : gas phase

L : liquid phase

p : pressure

$\theta$ : angular direction

1, 2, 3 : direction 1, 2, 3 respectively

REFERENCES

Bradshaw, P., "An Introduction to Turbulence and its Measurement," Pergamon Press (1971)

Fage, A. and V. M. Falkner, Brit. Aeronautical Res. Commission R & M, 1369 (1937)

Geib, F. E., Jr., "Measurements on the Effect of Transducer Size on the Resolution of Boundary-Layer Pressure Fluctuations," The Journal of the Acoustical Society of America, Vol. 46, No.1, 253 (1969)

Hubbard, M. G., and A. E. Dukler, "The Characterization of Flow Regimes for Horizontal Two-Phase Flow. I. Statistical Analysis of Wall Pressure Fluctuations," Heat Transfer and Fluid Mechanics Institute, Proc., p. 100 (1966)

Lamb, H., "Hydrodynamics," New York Dover Publications Ltd. (1945)

Lance, M., and J. Bataille, "Turbulence in the Liquid Phase of a Bubbly Air-Water Flow," NATO Specialist Meeting, West Germany, September 1983.

Ramkrishna, D., "Drop-Breakage in Agitated Liquid-Liquid Dispersions," Chem. Eng. Sci., 29, 987 (1974)

Roshko, A., NACA Report 1191 (1954)

Schügerl, K., "Characterization and Performance of Single and Multistage Tower Reactors with Outer Loop for Cell Mass Production," Advances in Biochemical Engineering, 22, 93 (1982)

Taitel, Y., D. Bornea, and A. E. Dukler, "Modelling Flow Pattern Transitions for Steady Upward Gas-Liquid Flow in Vertical Tubes," A.I.Ch.E. J., 26, 345 (1980)

Tennekes, H., "Turbulence: Diffusion, Statistics, Spectral Dynamics," Handbook of Turbulence, Vol. 1, Chapt. 5, Plenum Press (1977)

von Weizsäcker, G. F., Proc. Roy. Soc. London, 195A: 402 (1948)

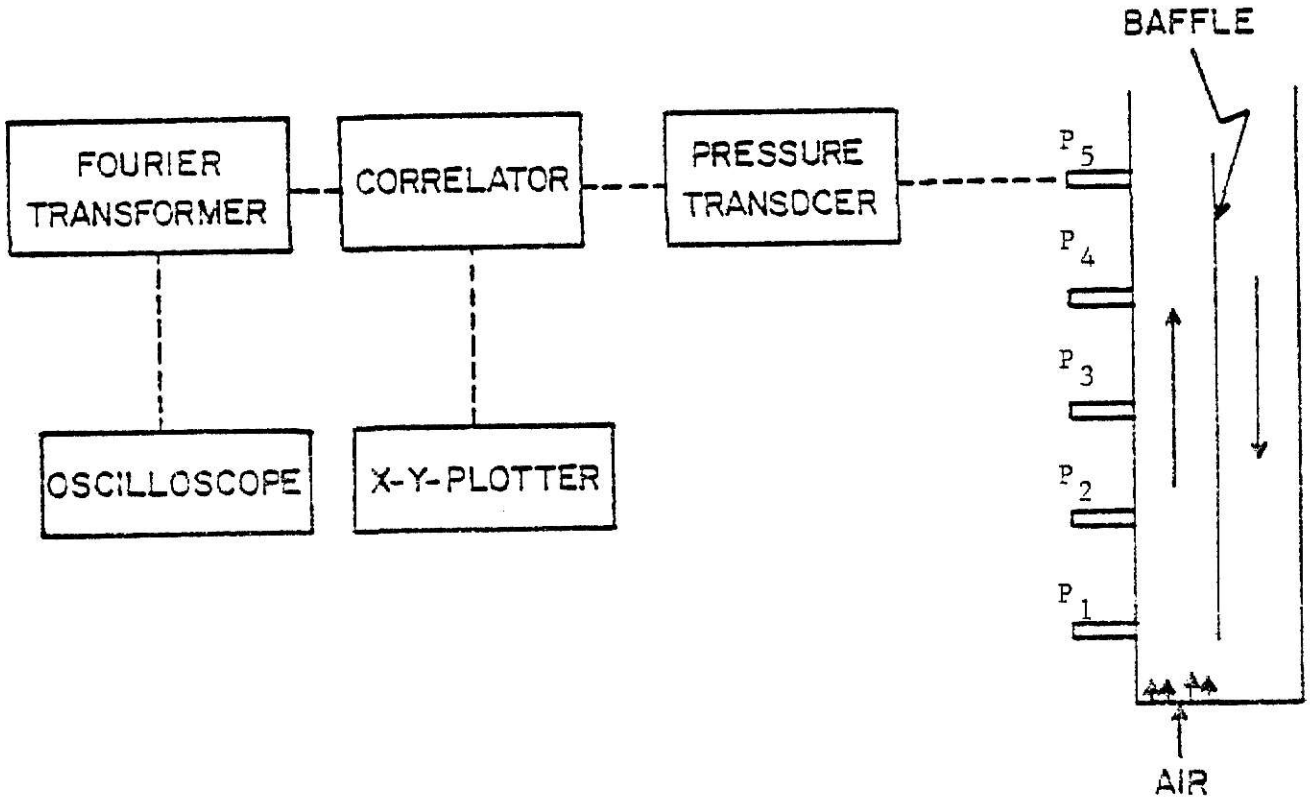



Figure 4.1 Experimental set-up for pressure fluctuation measurements.

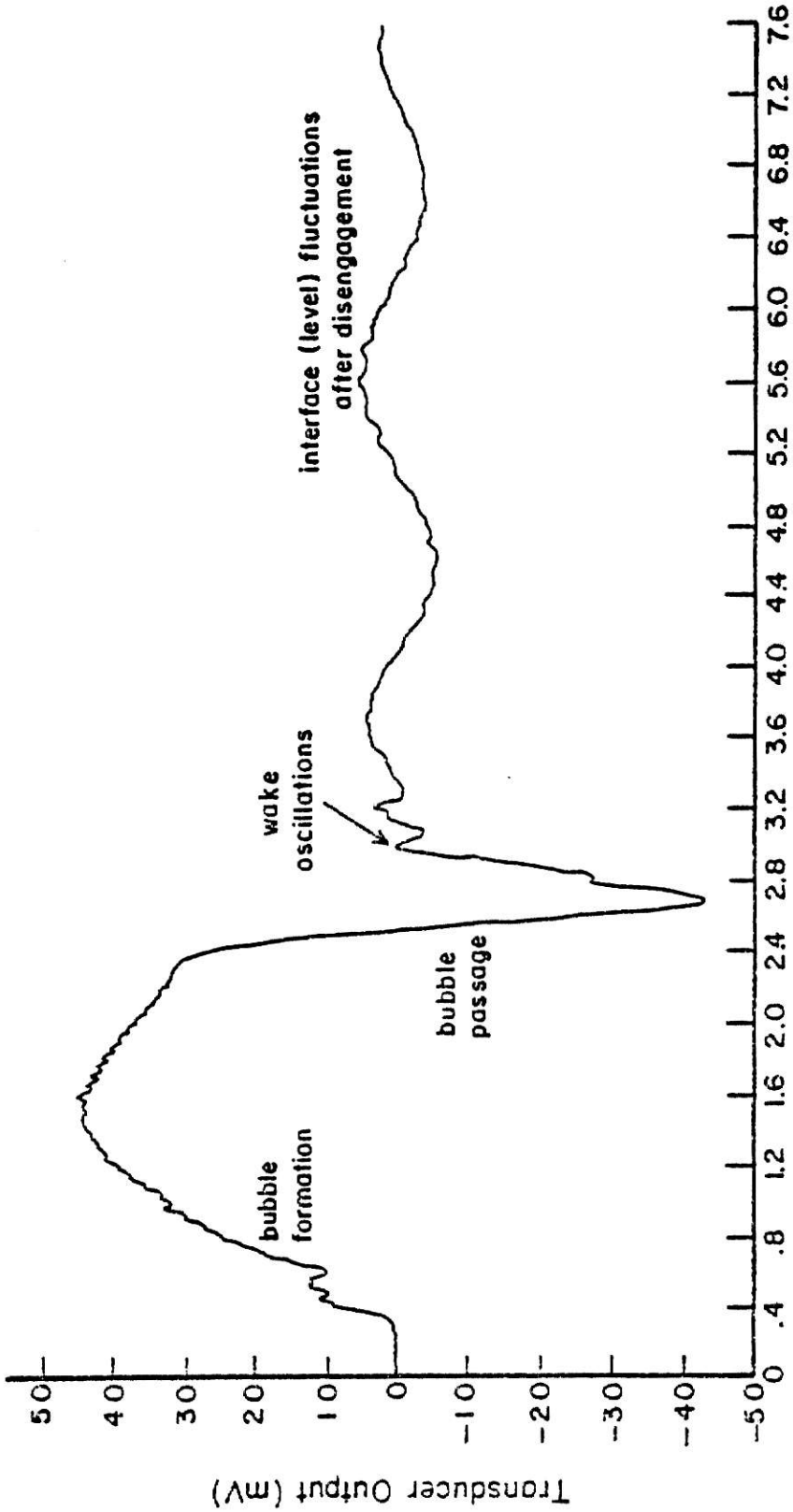



Figure 4.2 Pressure fluctuations associated with the passage of a single bubble in the airlift column as measured at pressure tap $P_4$.

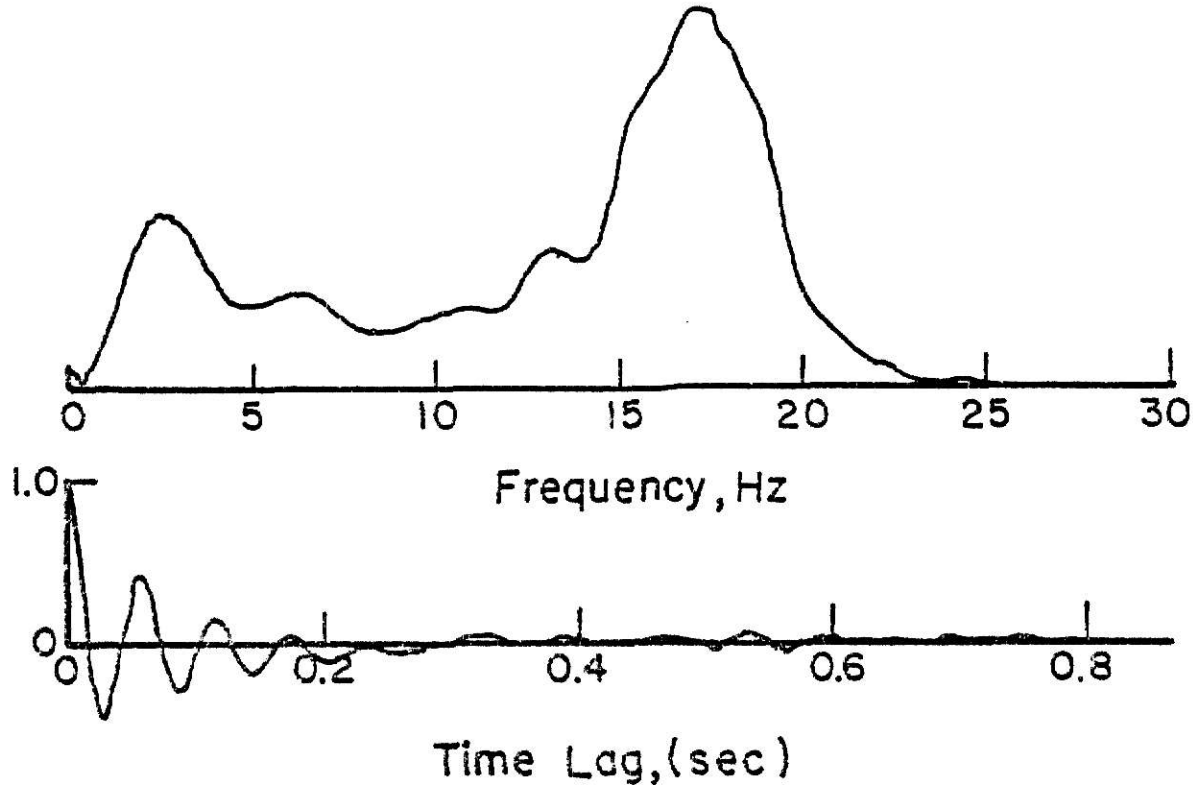



Figure 4.3 Autocorrelation (below) and Fourier transform of the autocorrelation (spectrum of pressure fluctuations) (above) for air-tap water system at location $P_5$ for air flow rate of 60 $ft^3/hr$.

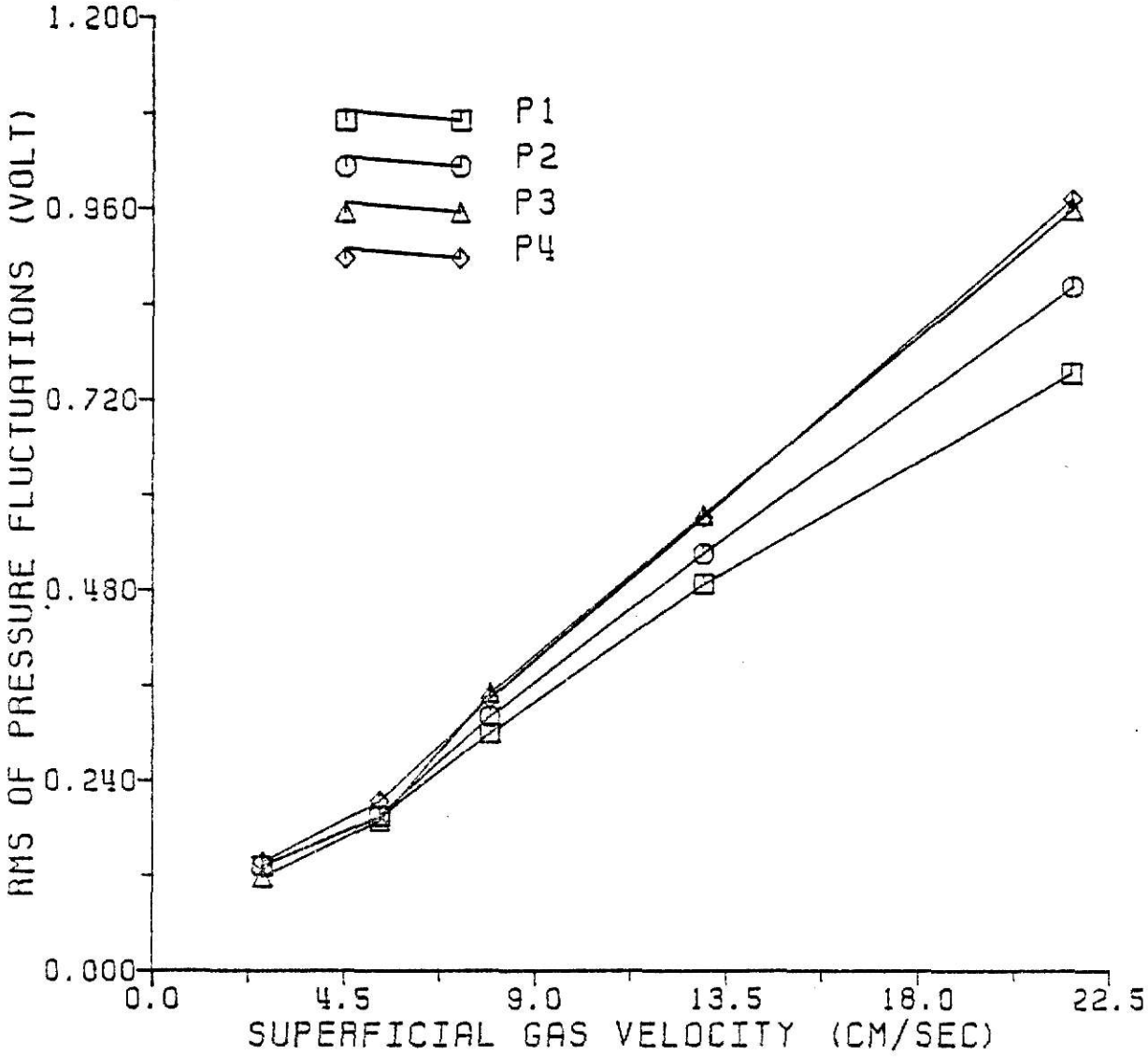



Figure 4.4 Root mean square of pressure fluctuations as a function of superficial gas velocity for air-tap water system ( see Fig. 3.1 for positions of pressure taps).

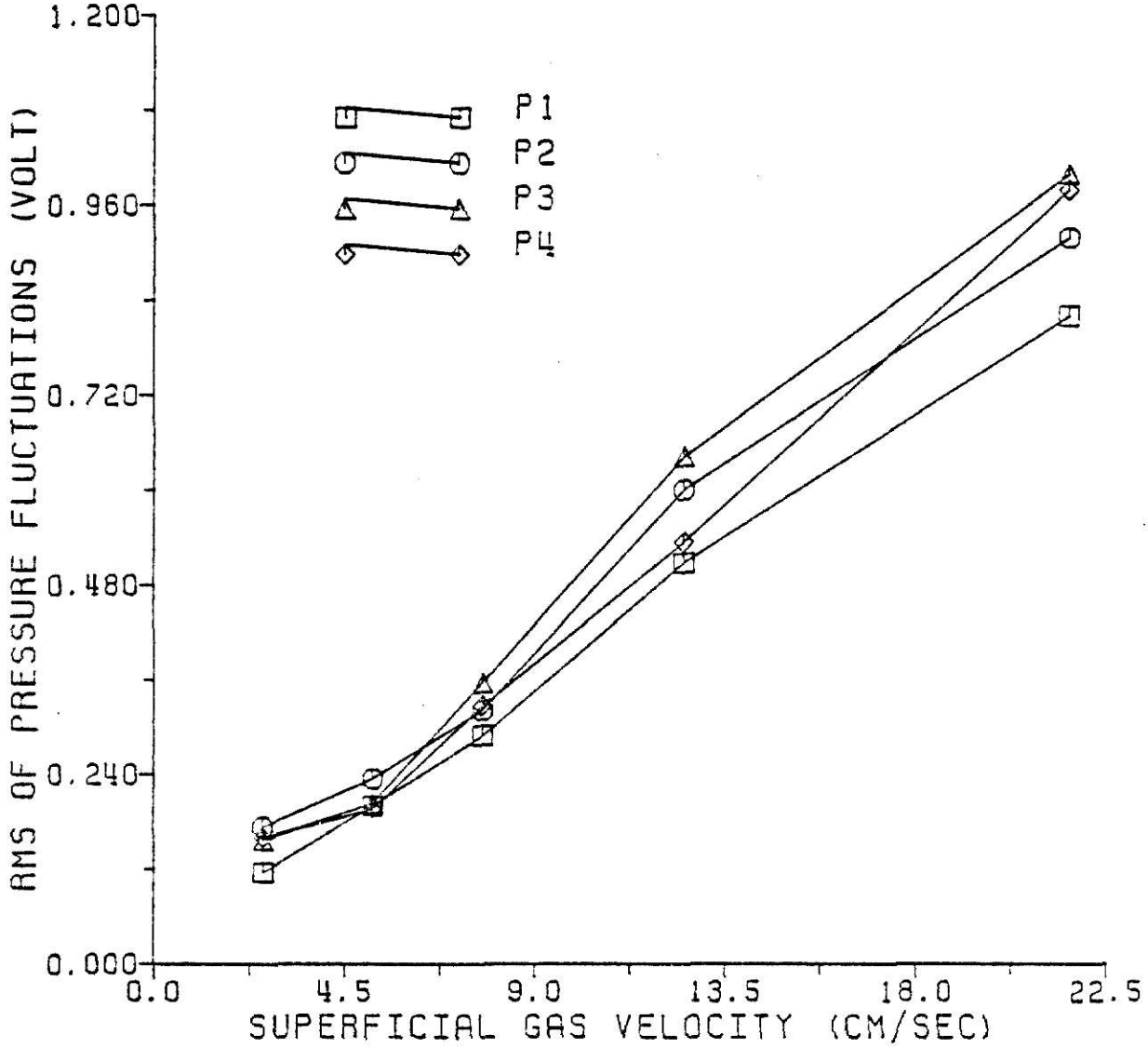



Figure 4.5 Root mean square of pressure fluctuations as a function of superficial gas velocity for air-salt water system ( see Fig 3.1 for positions of pressure taps).

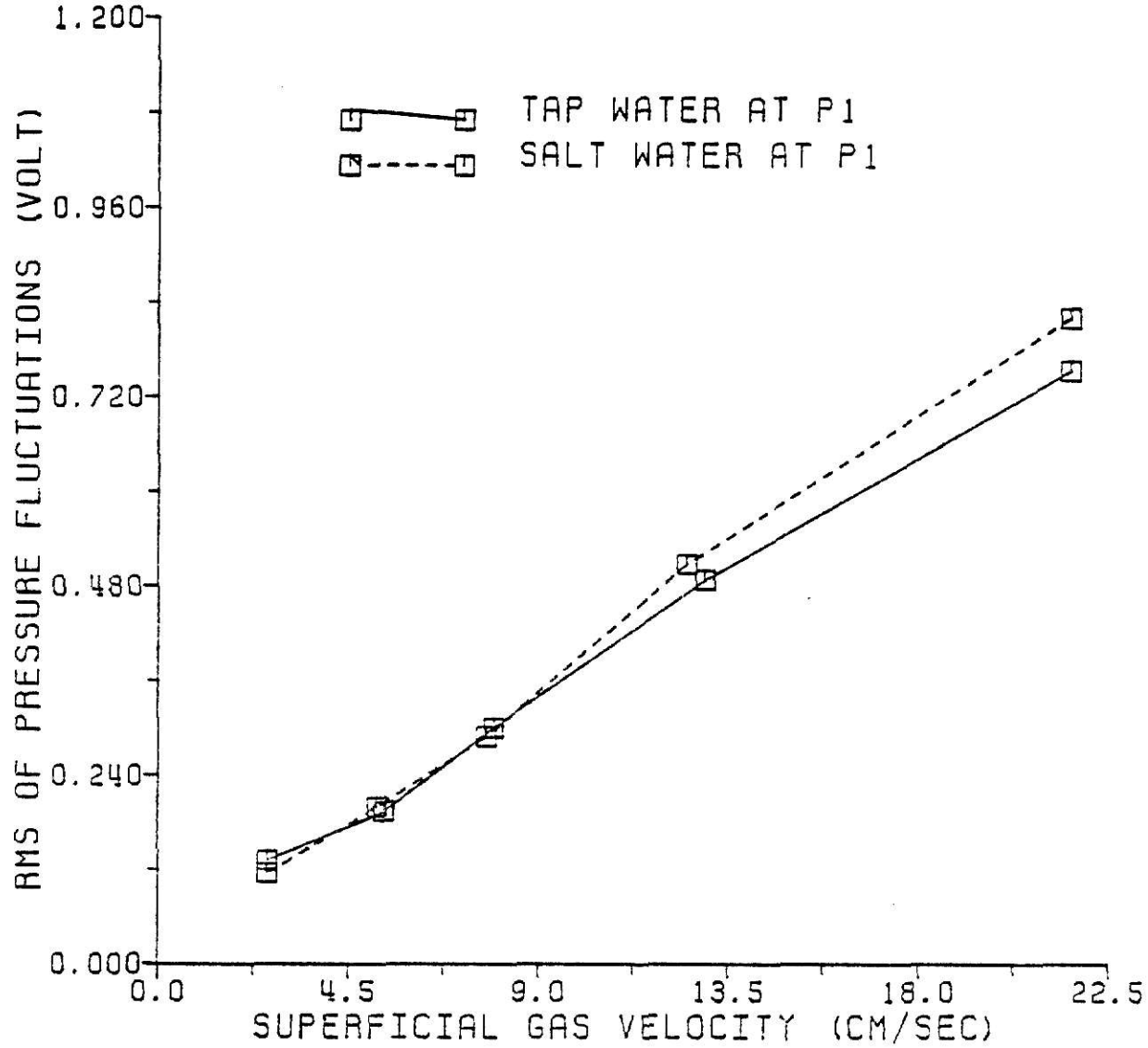



Figure 4.6 Comparison of root mean square of pressure fluctuations for tap water and salt water at pressure tap $P_1$.

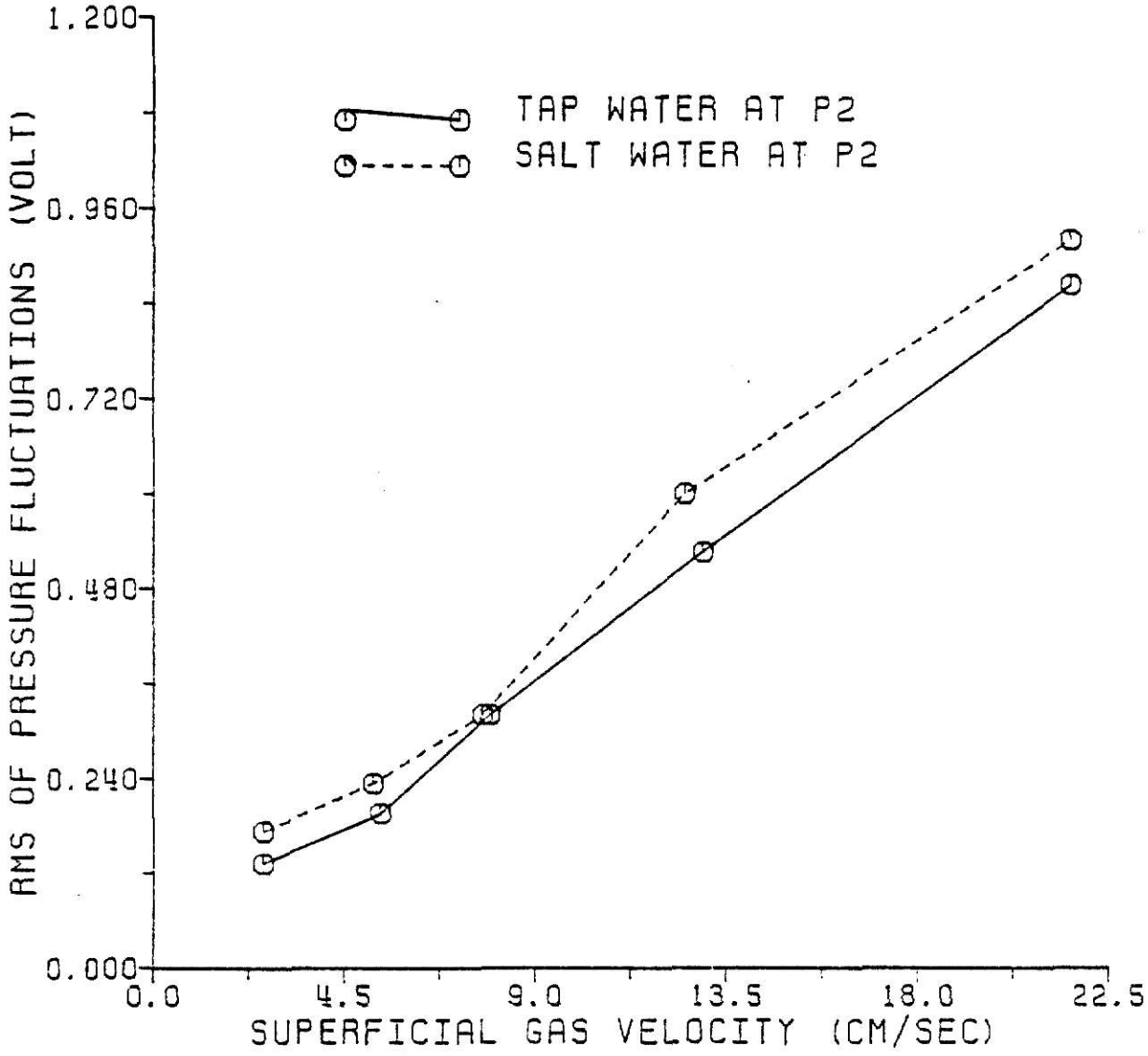



Figure 4.7 Comparison of root mean square of pressure fluctuations for tap water and salt water at pressure tap $P_2$.

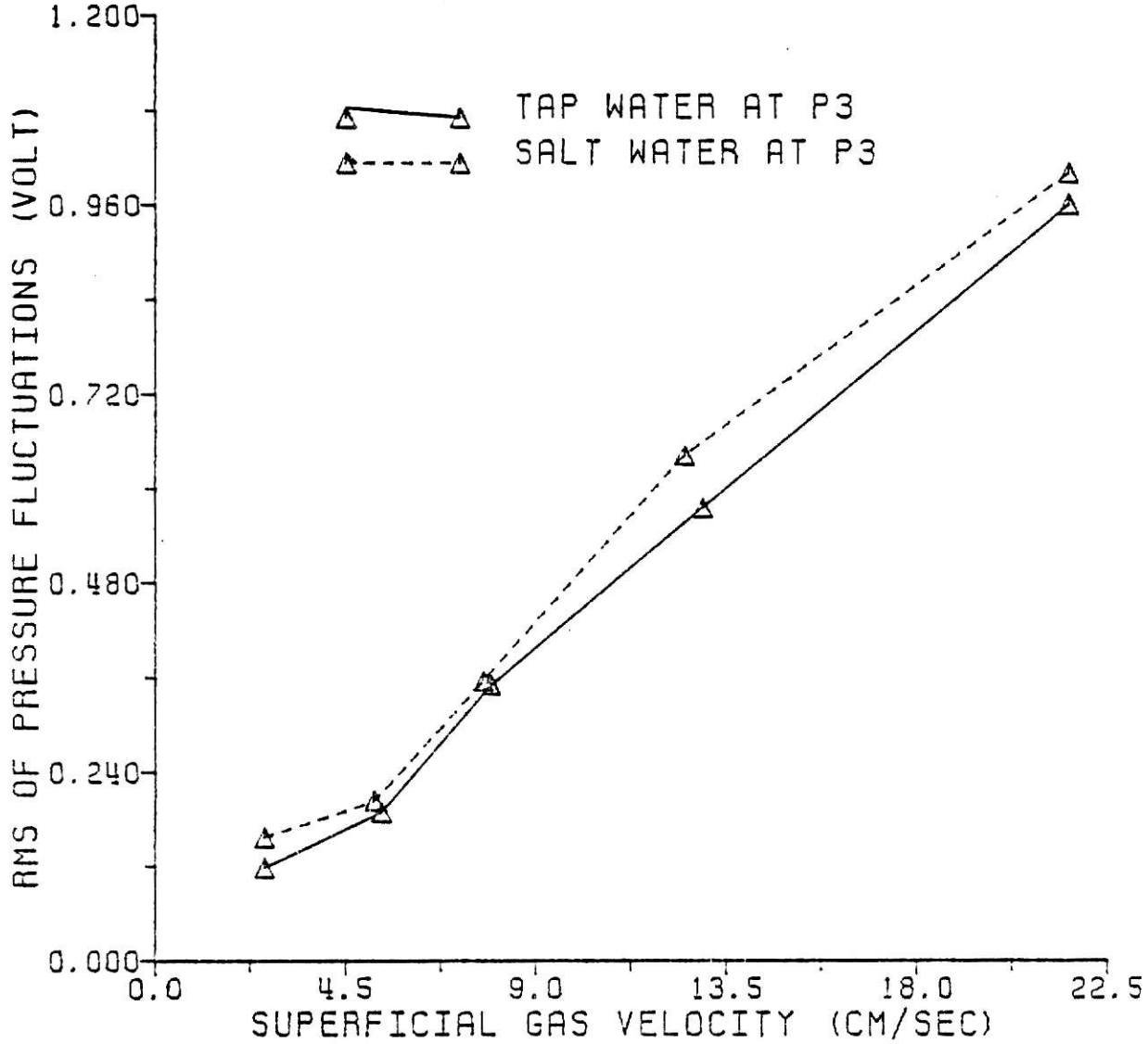



Figure 4.8 Comparison of root mean square of pressure fluctuations for tap water and salt water at pressure tap $P_3$.

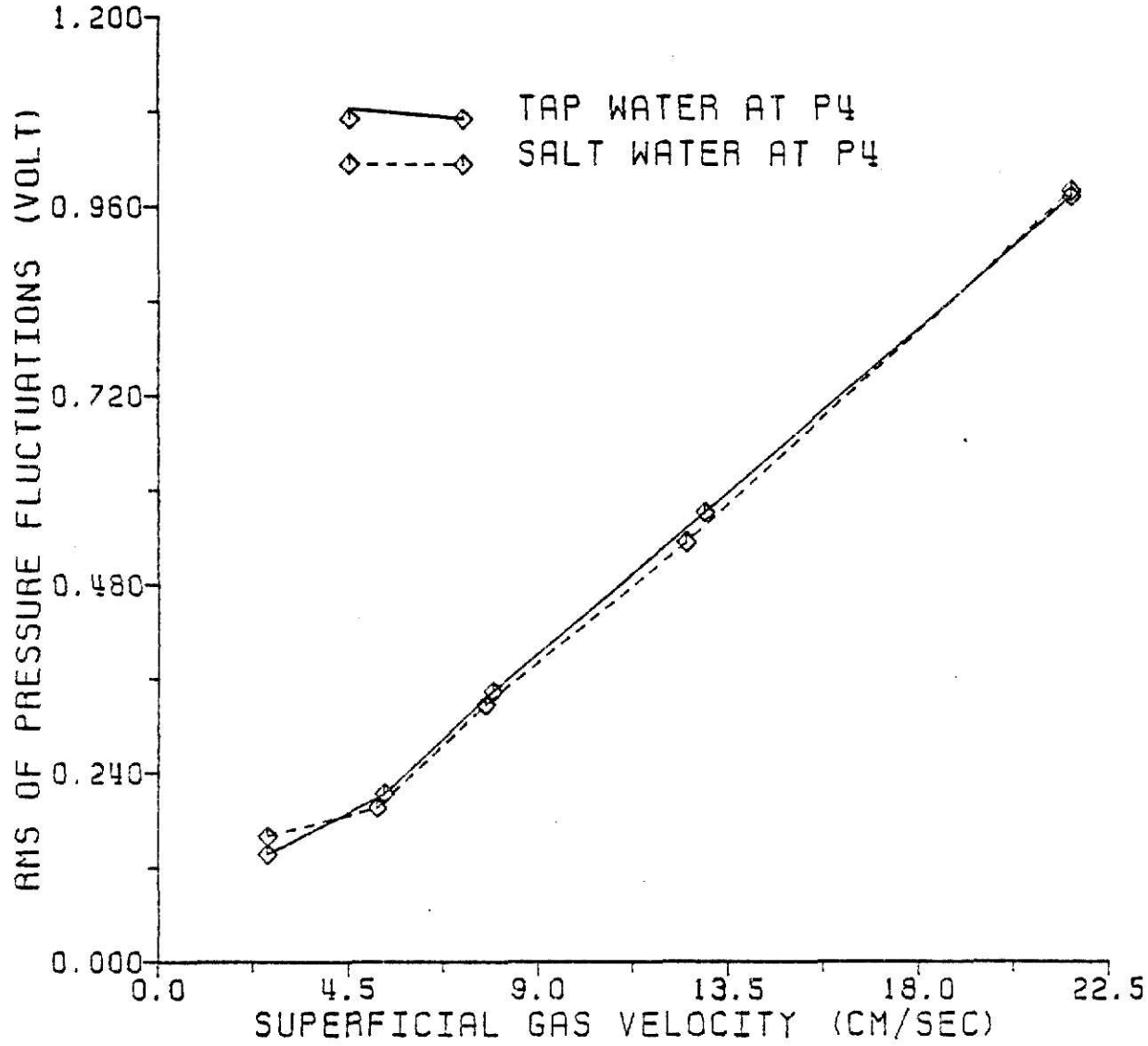



Figure 4.9 Comparison of root mean square of pressure fluctuations for tap water and salt water at pressure tap $P_4$.

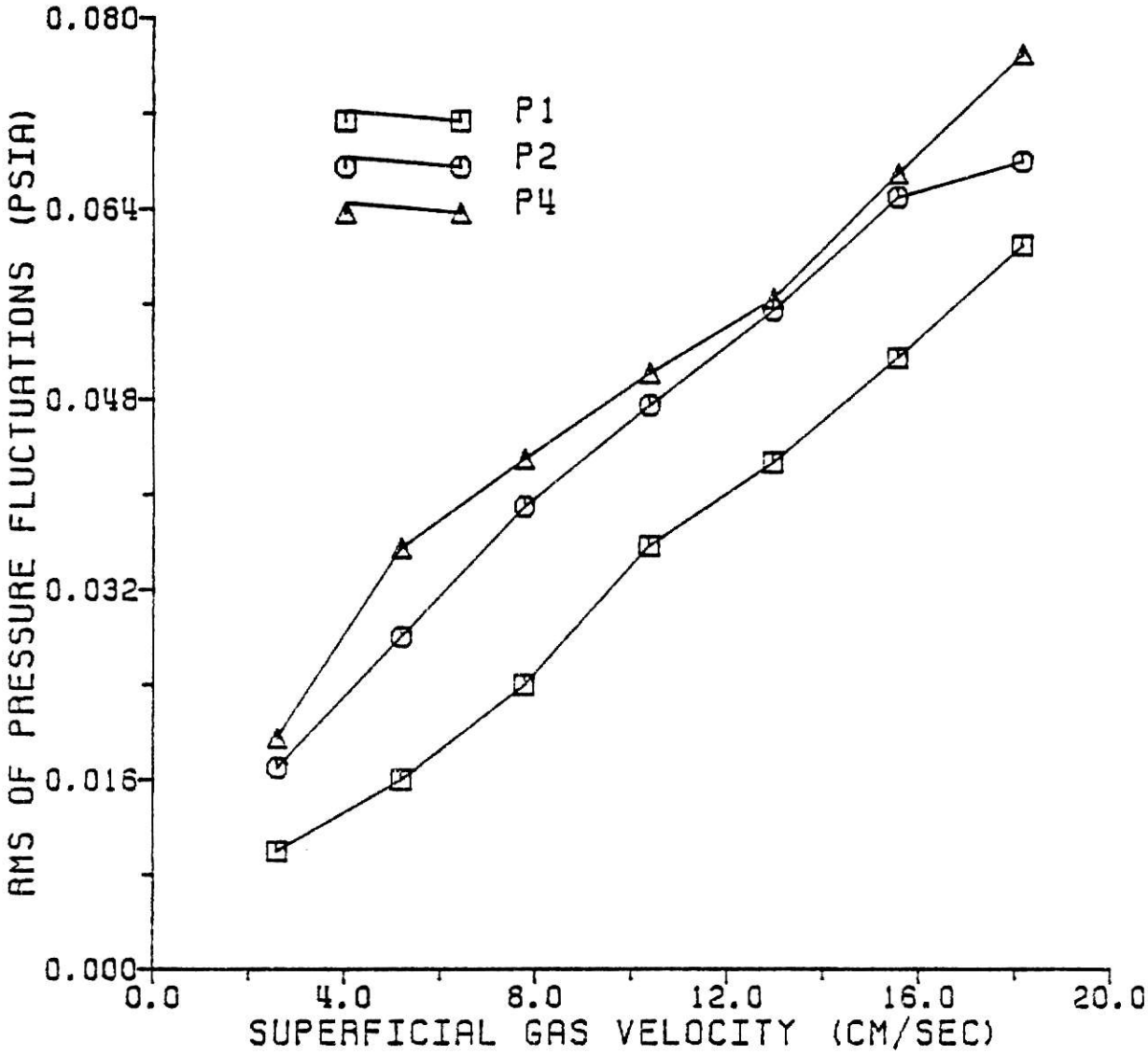



Figure 4.10 Root mean square of pressure fluctuations as a function of superficial gas velocity for air-tap water system ( see Fig. 3.1 for positions of pressure taps).

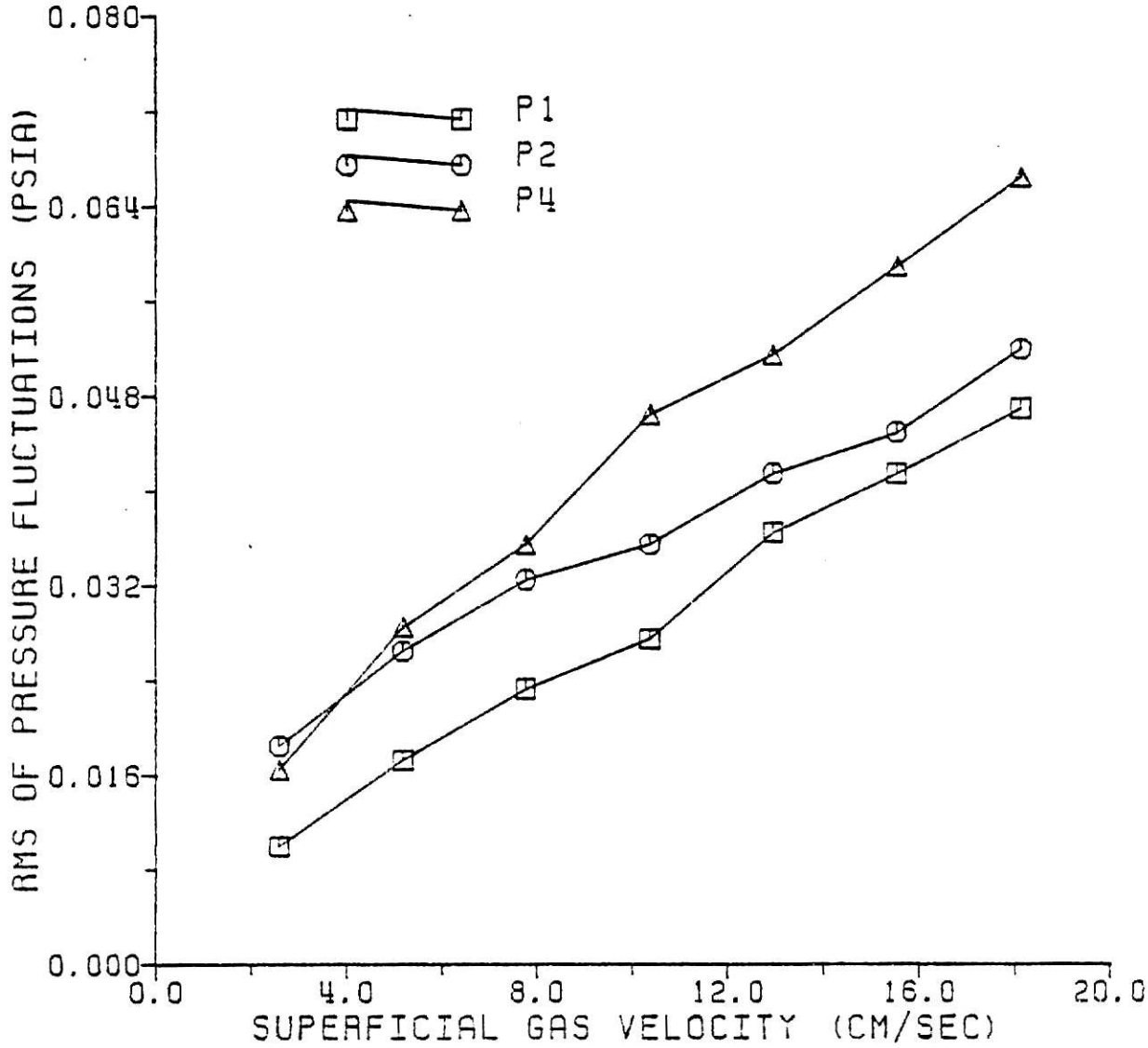



Figure 4.11 Root mean square of pressure fluctuations as a function of superficial gas velocity for 0.8 wt. % CMC solution (see Fig. 3.1 for positions of pressure taps).

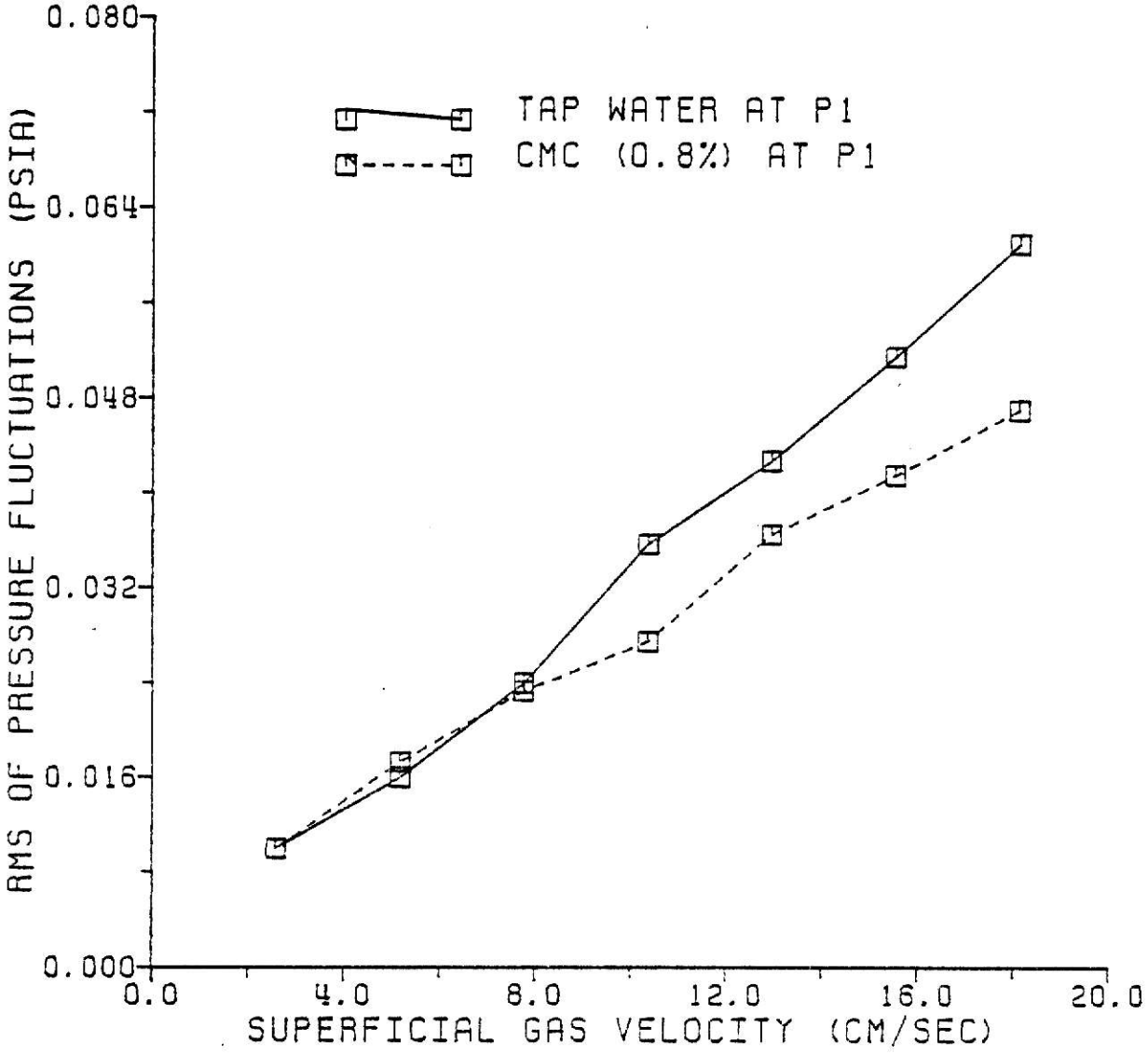



Figure 4.12 Comparison of root mean square of pressure fluctuations for tap water and 0.8 wt. % CMC solution at pressure tap $P_1$.

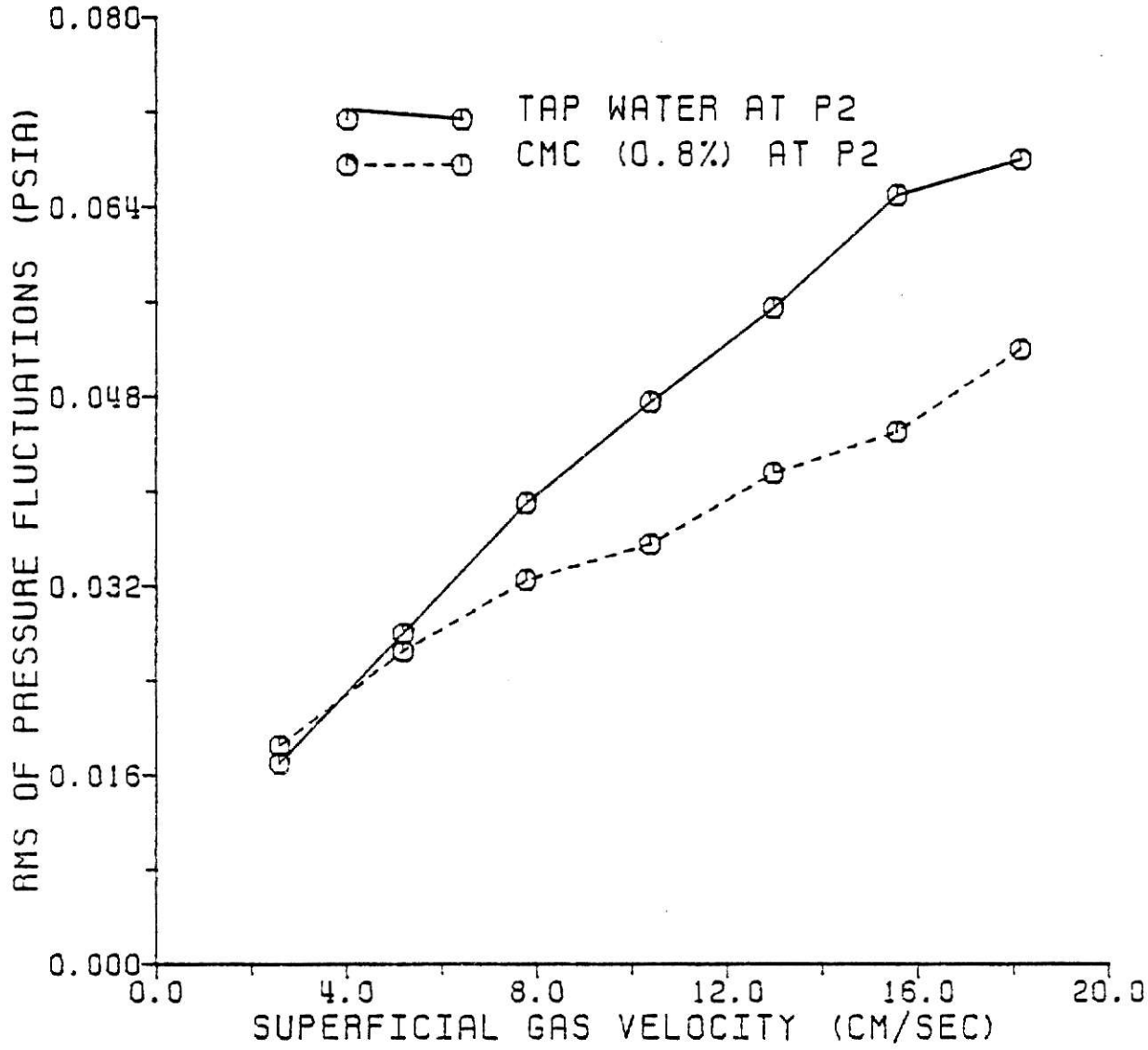



Figure 4.13 Comparison of root mean square of pressure fluctuations for tap water and 0.8 wt. % CMC solution at pressure tap $P_2$.

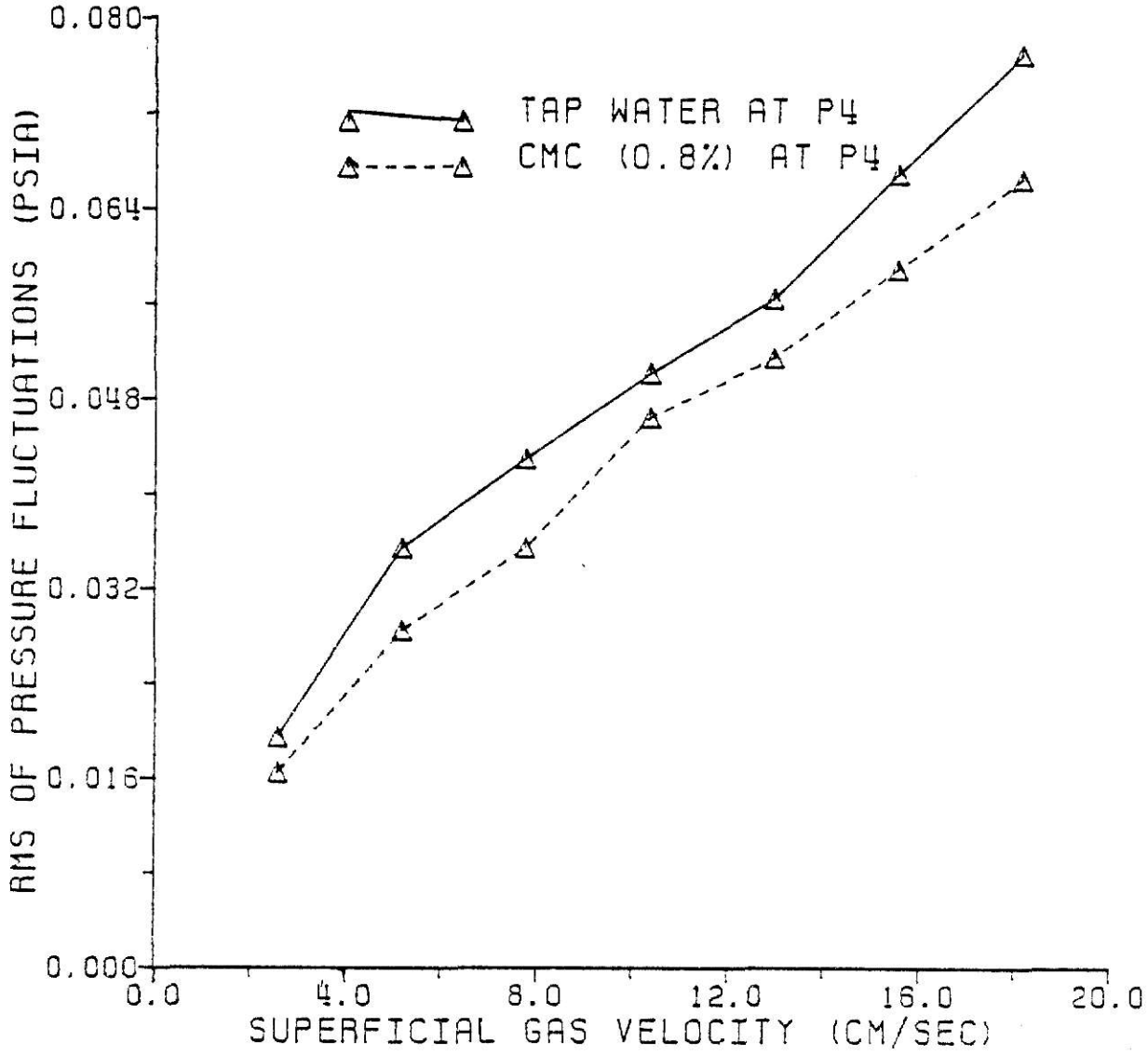



Figure 4.14 Comparison of root mean square of pressure fluctuations for tap water and 0.8 wt. % CMC solution at pressure tap $P_4$.

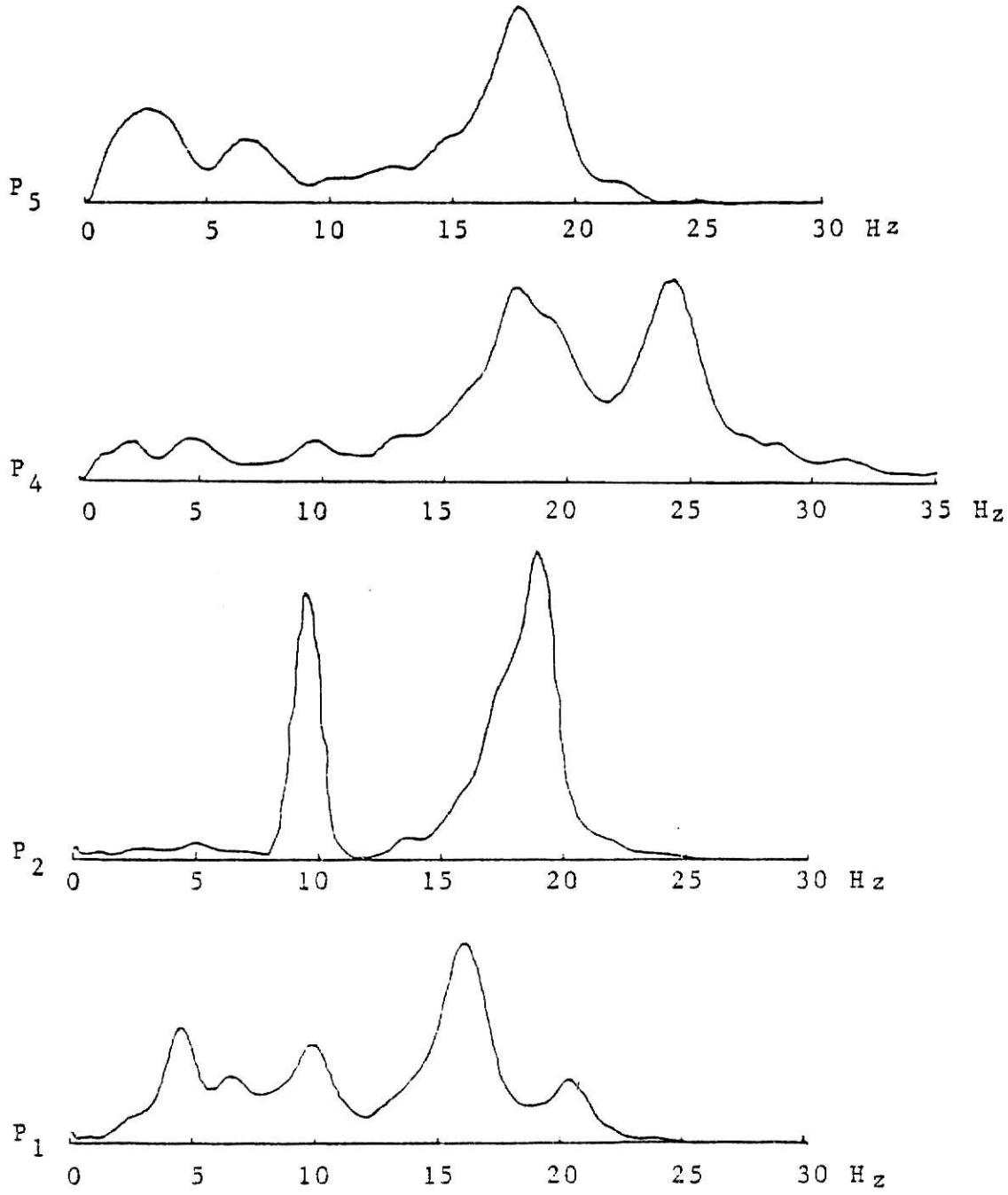



Figure 4.15 The spectra of pressure fluctuations for air-tap water at air flow rate of 30 $ft^3/hr$ at various distances from the sparger (see Fig. 3.1 for locations of pressure taps).

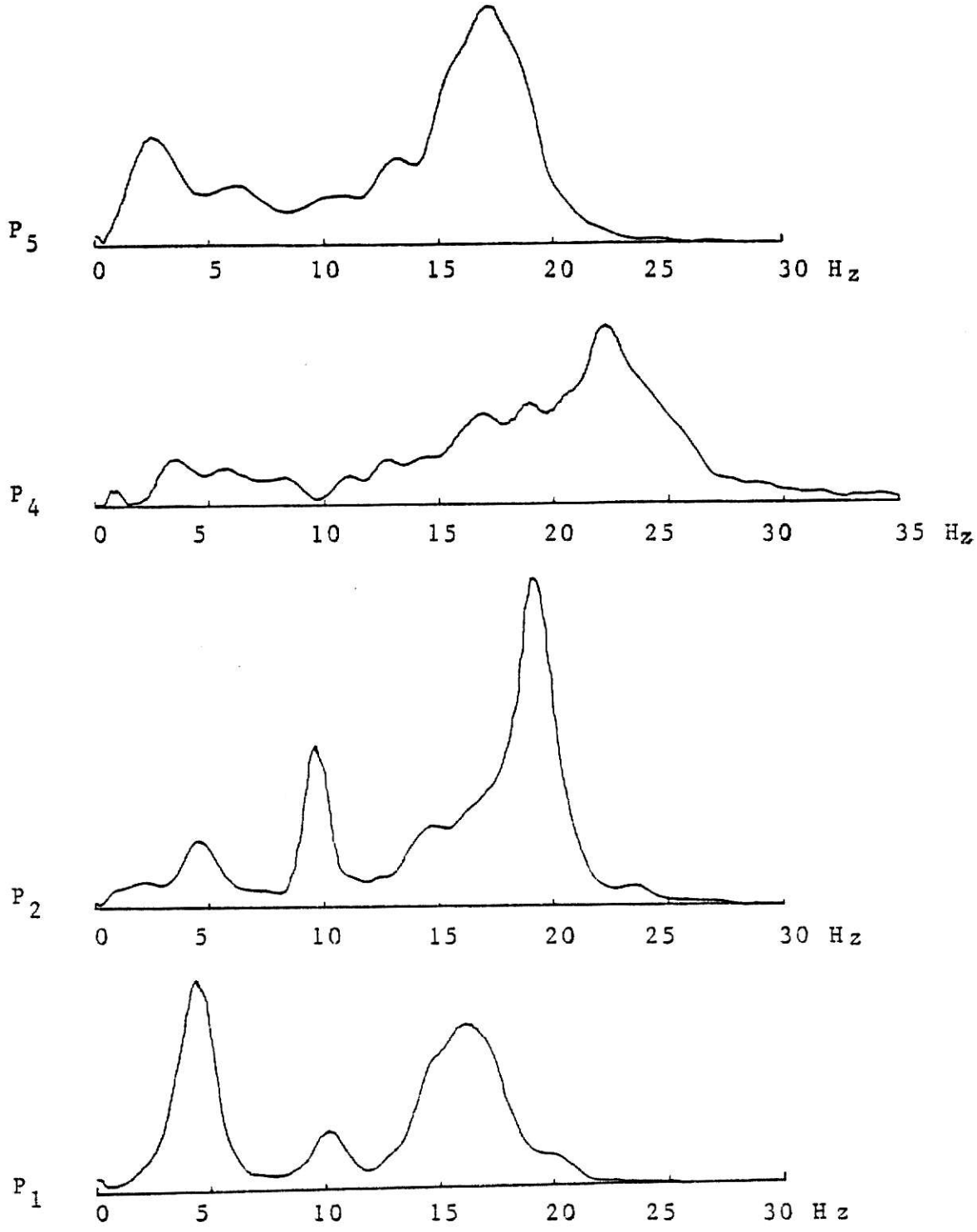



Figure 4.16 The spectra of pressure fluctuations for air-tap water system at air flow rate of 60 $ft^3/hr$ at various distances from the sparger (see Fig. 3.1 for locations of pressure taps).

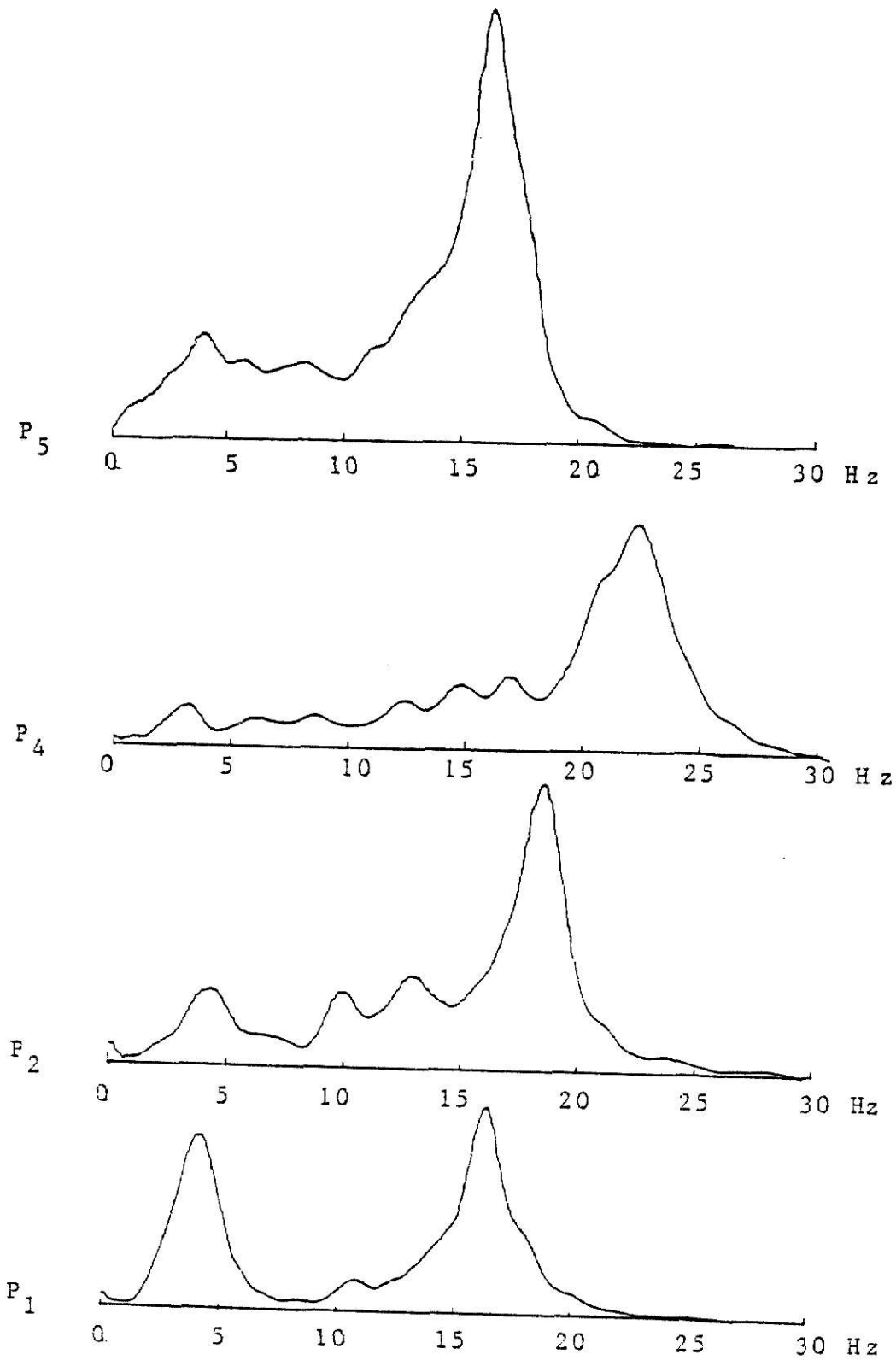



Figure 4.17 The spectra of pressure fluctuations for air-tap water at air flow rate of 90 $ft^3/hr$ at various distances from the sparger (see Fig. 3.1 for locations of pressure taps).

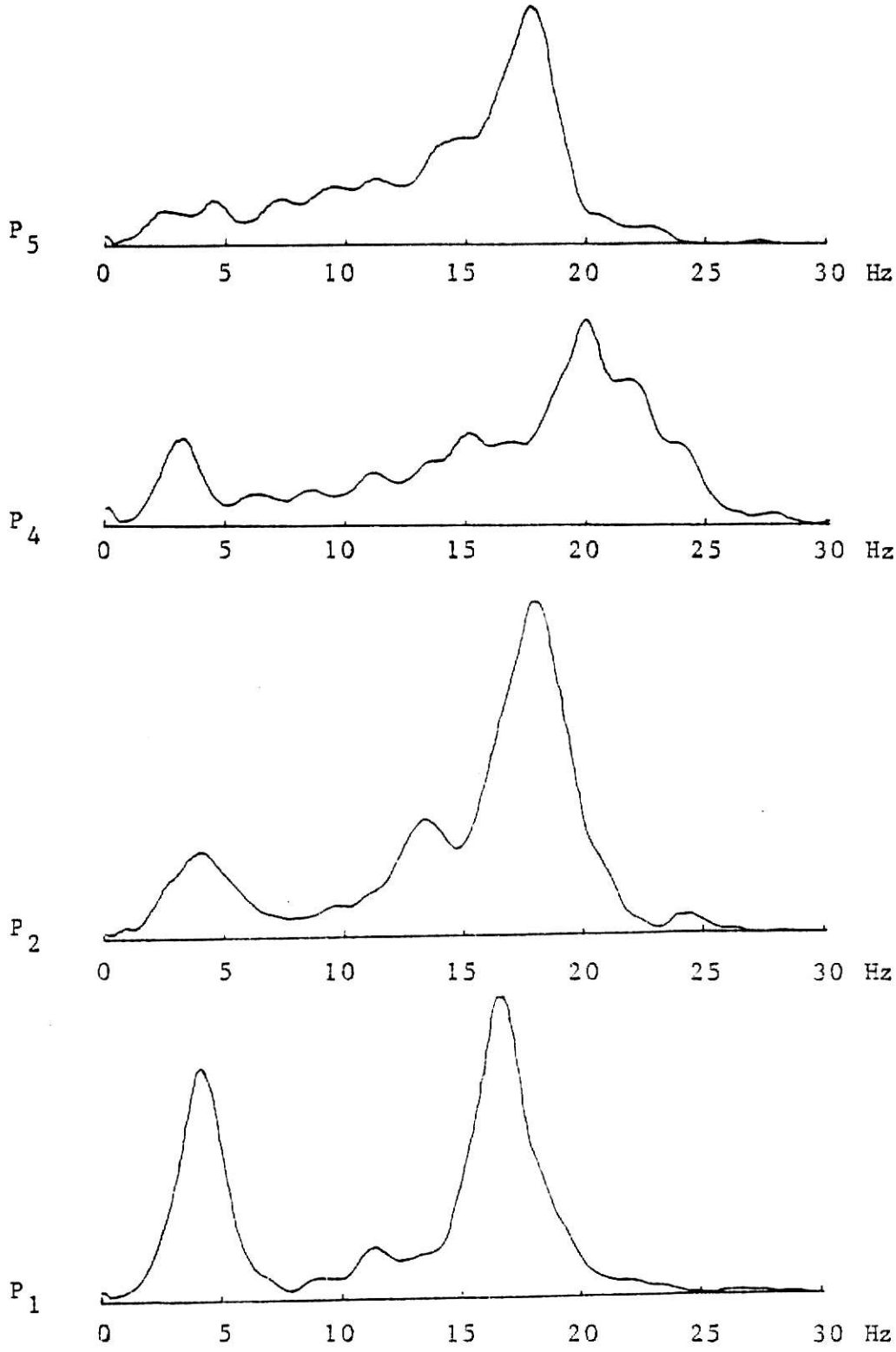



Figure 4.18 The spectra of pressure fluctuations for air-tap water at air flow rate of 120 $ft^3/hr$ at various distances from the sparger (see Fig. 3.1 for locations of pressure taps).

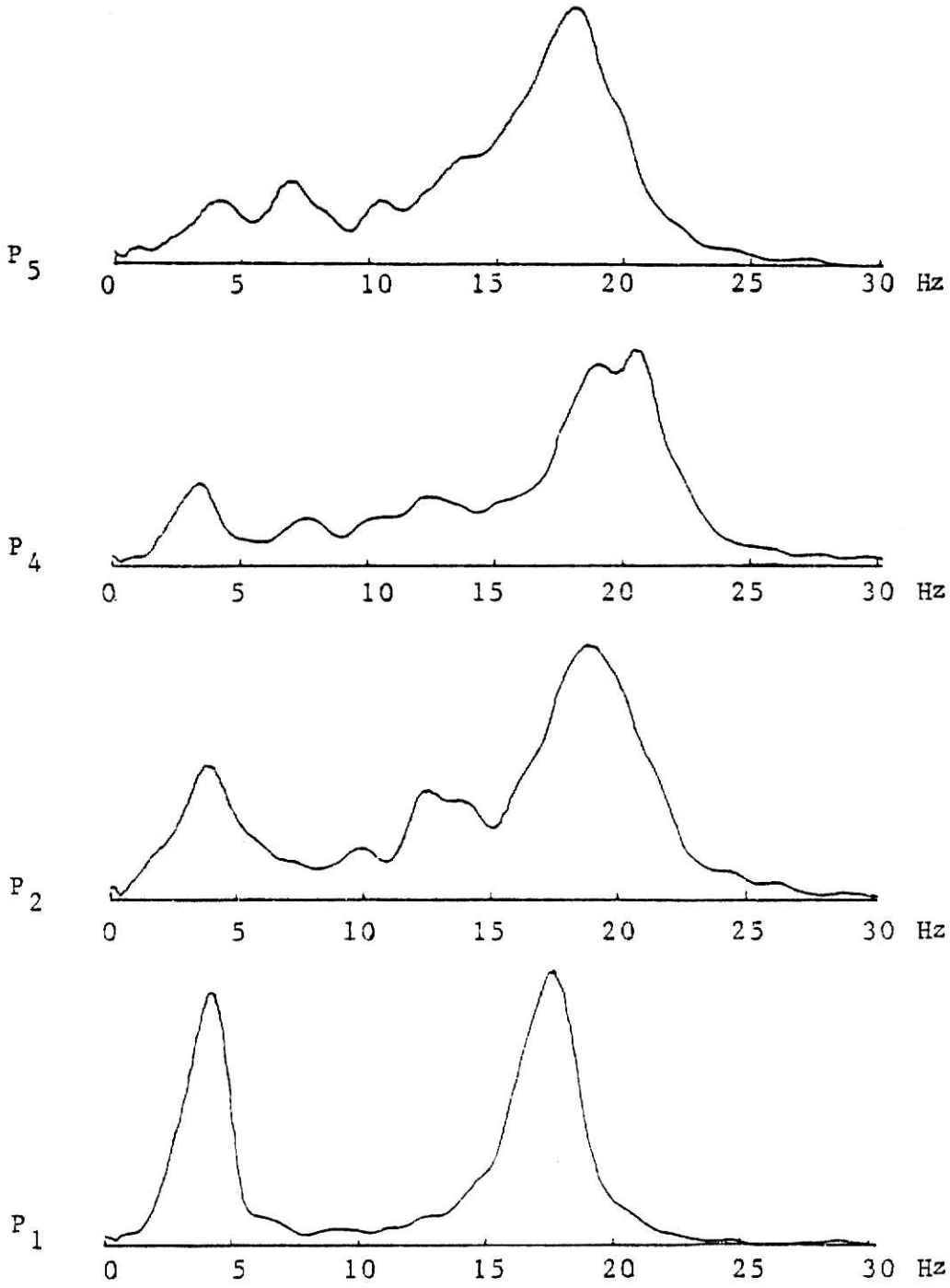



Figure 4.19 The spectra of pressure fluctuations for air-tap water at air flow rate of 150 $ft^3/hr$ at various distances from the sparger (see Fig. 3.1 for locations of pressure taps).

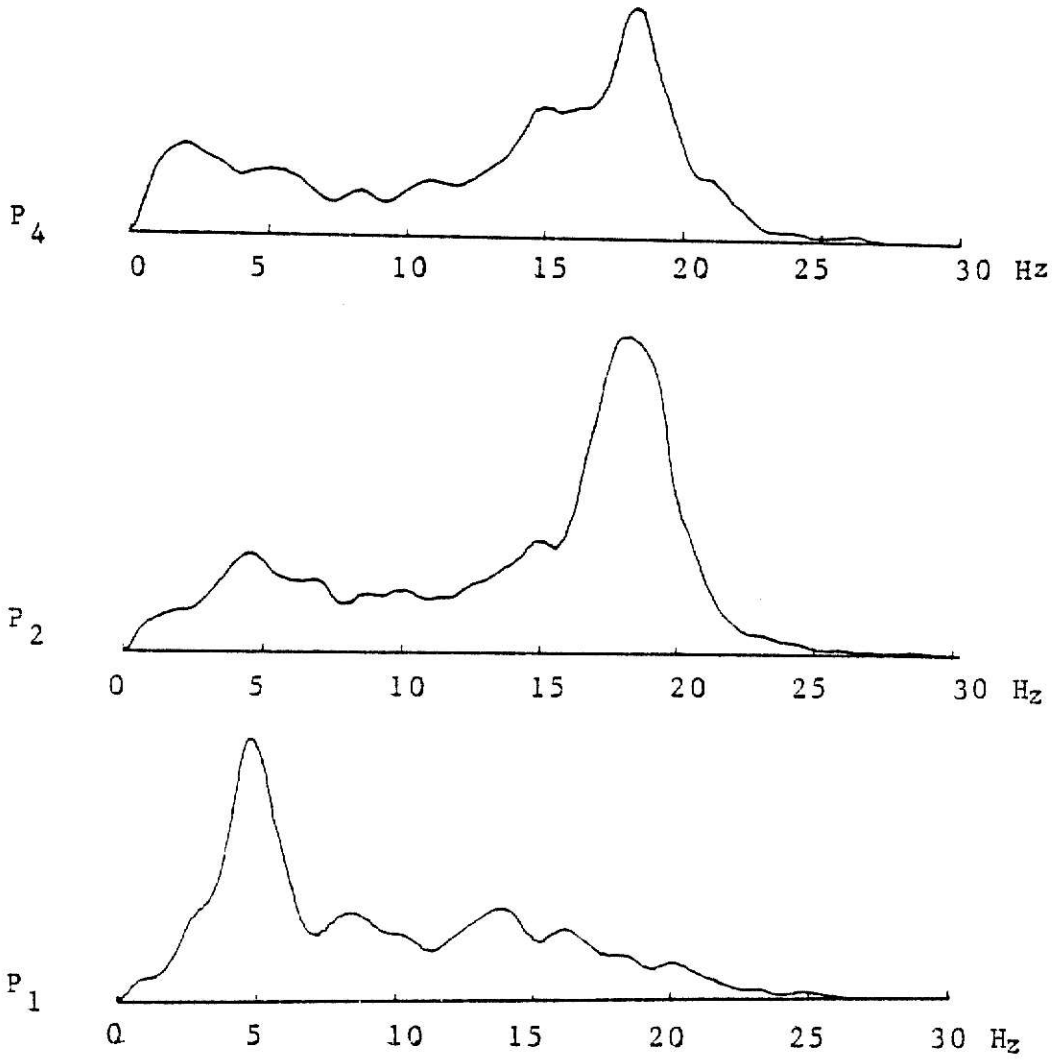



Figure 4.20 The spectra of pressure fluctuations for air-CMC (0.8 wt.%) solution at air flow rate of 30 $ft^3/hr$ at various distances from the sparger (see Fig. 3.1 for locations of pressure taps).

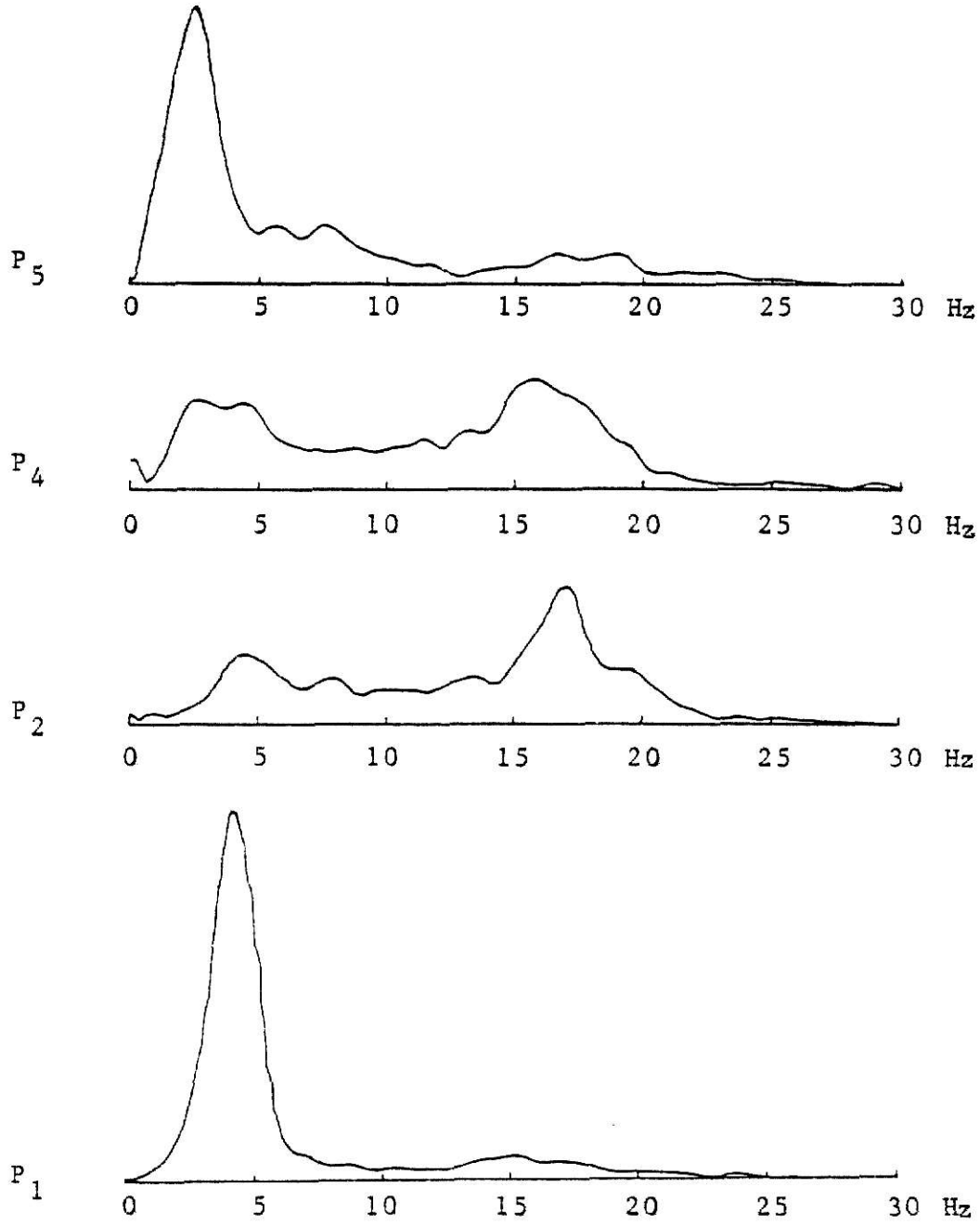



Figure 4.21 The spectra of pressure fluctuations for air-CMC (0.8 wt.%) solution at air flow rate of 60 $ft^3/hr$ at various distances from the sparger (see Fig. 3.1 for locations of pressure taps).

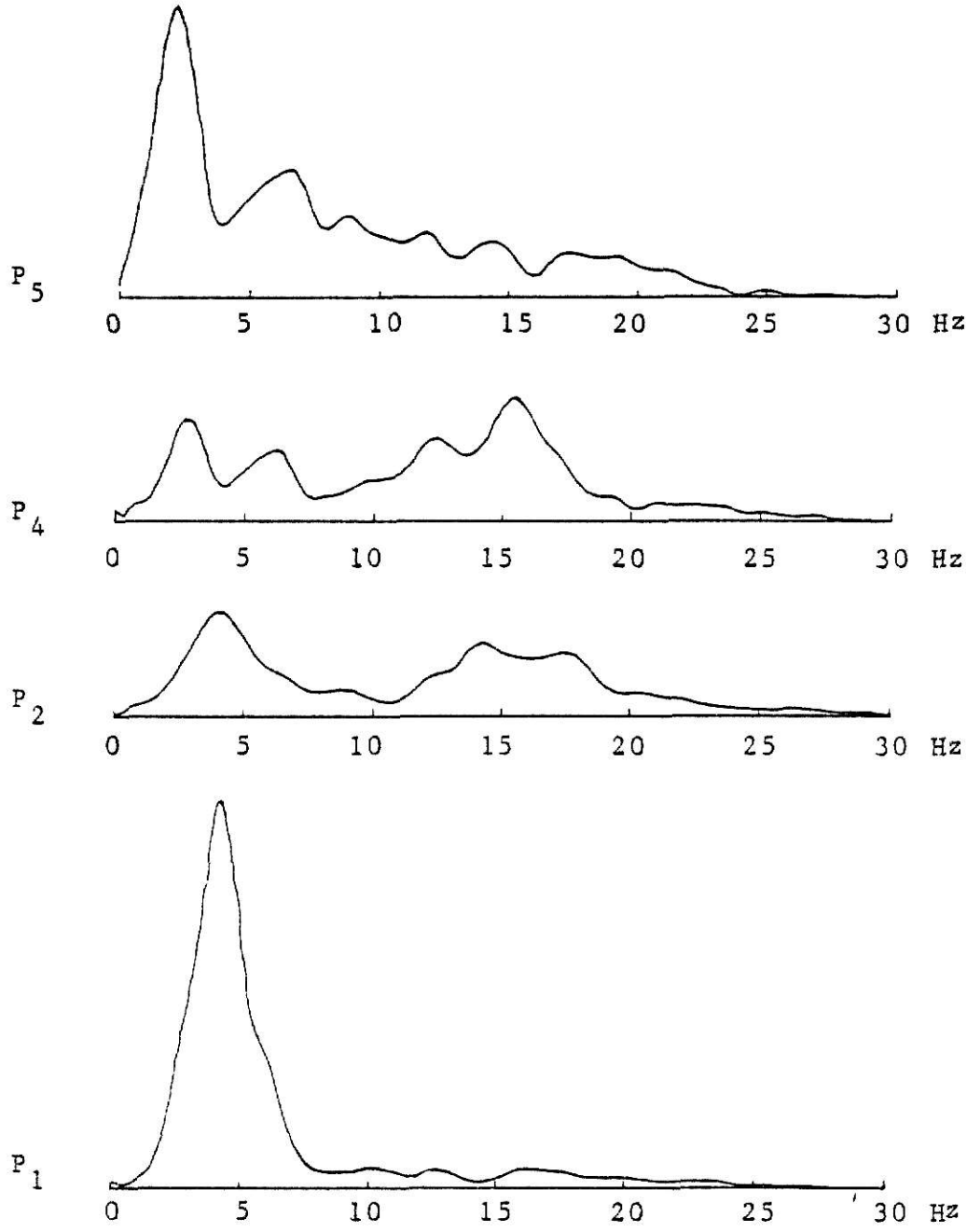



Figure 4.22 The spectra of pressure fluctuations for air-CMC (0.8 wt.%) solution at air flow rate of 90 $ft^3$/hr at various distances from the sparger (see Fig. 3.1 for locations of pressure taps).

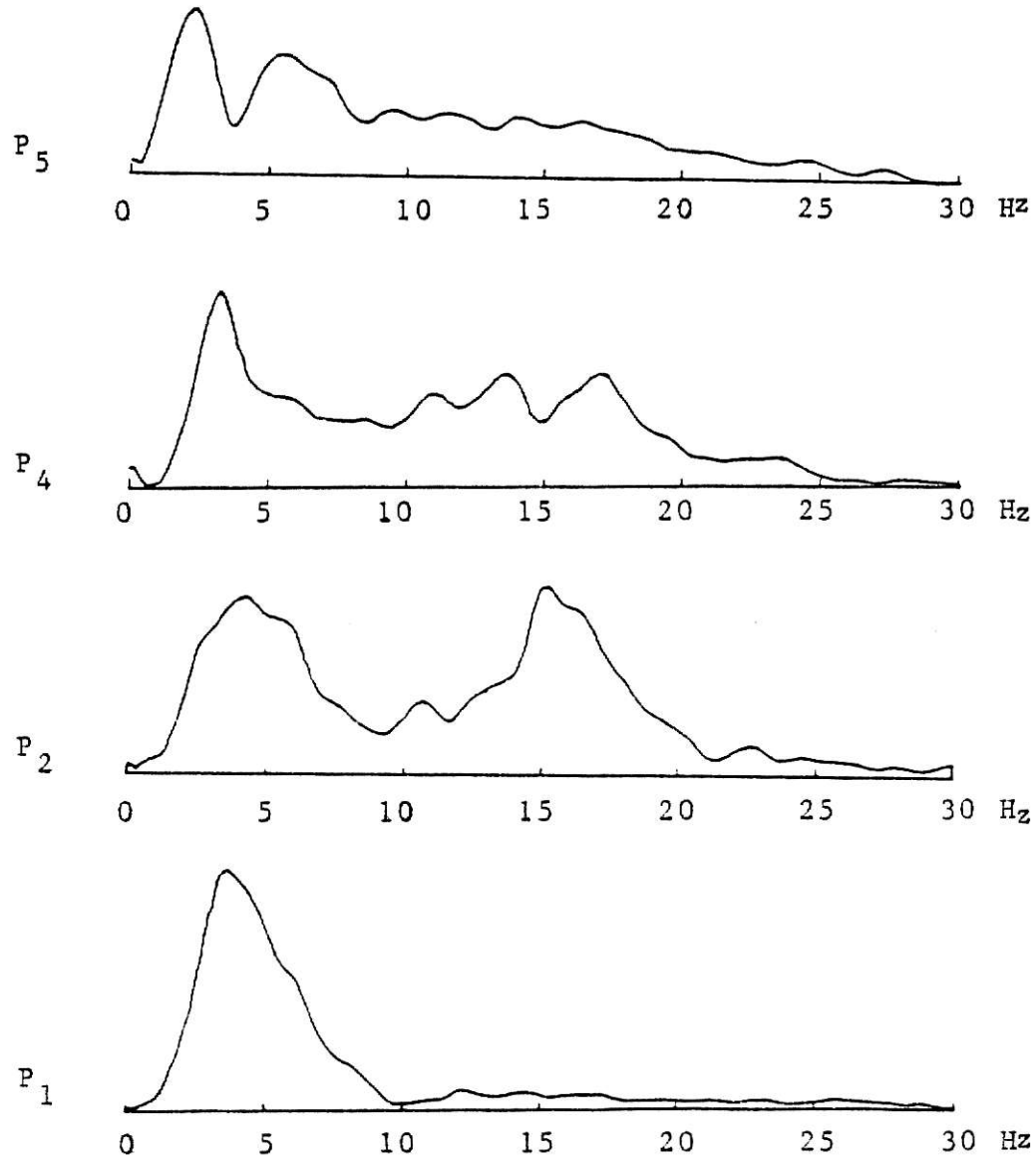



Figure 4.23 The spectra of pressure fluctuations for air-CMC (0.8 wt.%) solution at air flow rate of 120 $ft^3/hr$ at various distances from the sparger (see Fig. 3.1 for locations of pressure taps).

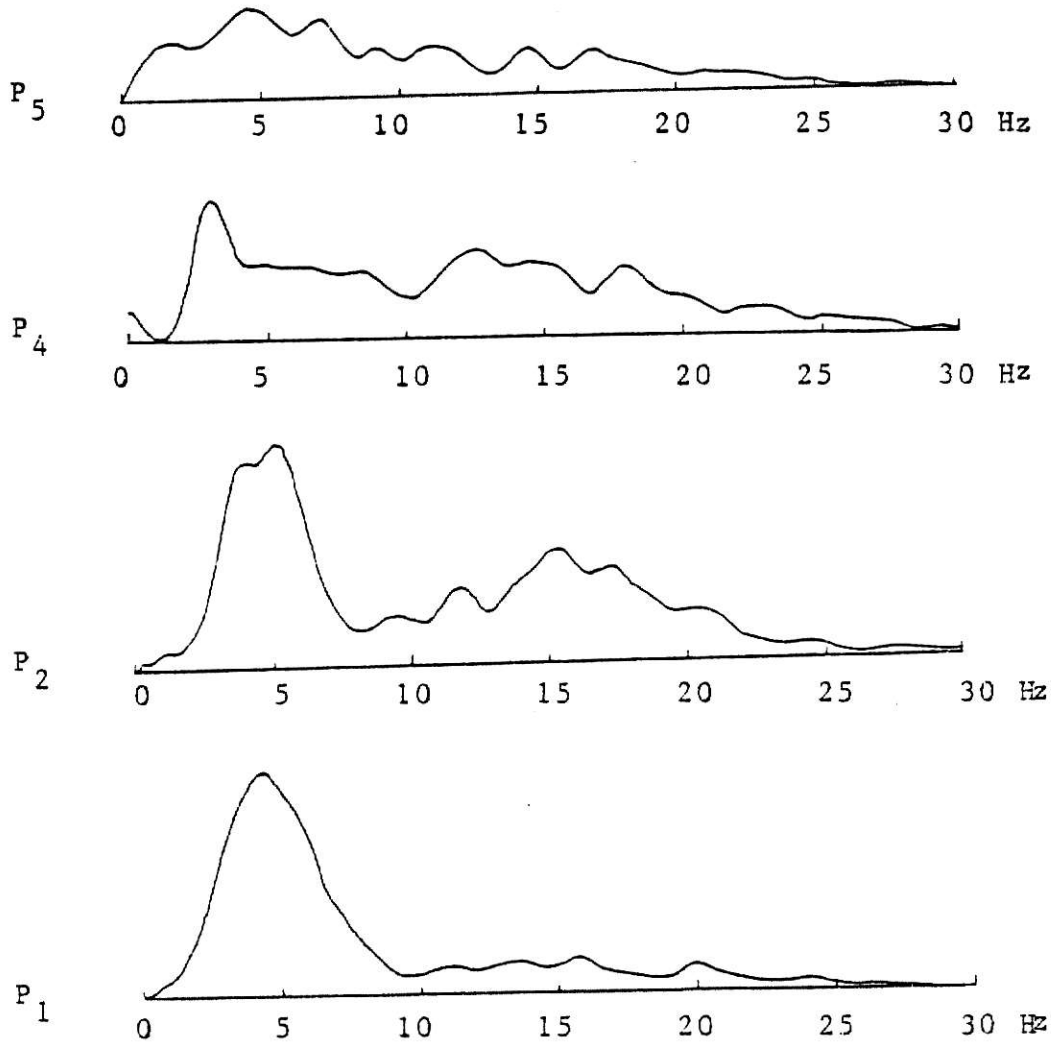



Figure 4.24 The spectra of pressure fluctuations for air-CMC (0.8 wt.%) solution at air flow rate of 150 $ft^3/hr$ at various distances from the sparger (see Fig. 3.1 for locations of pressure taps).

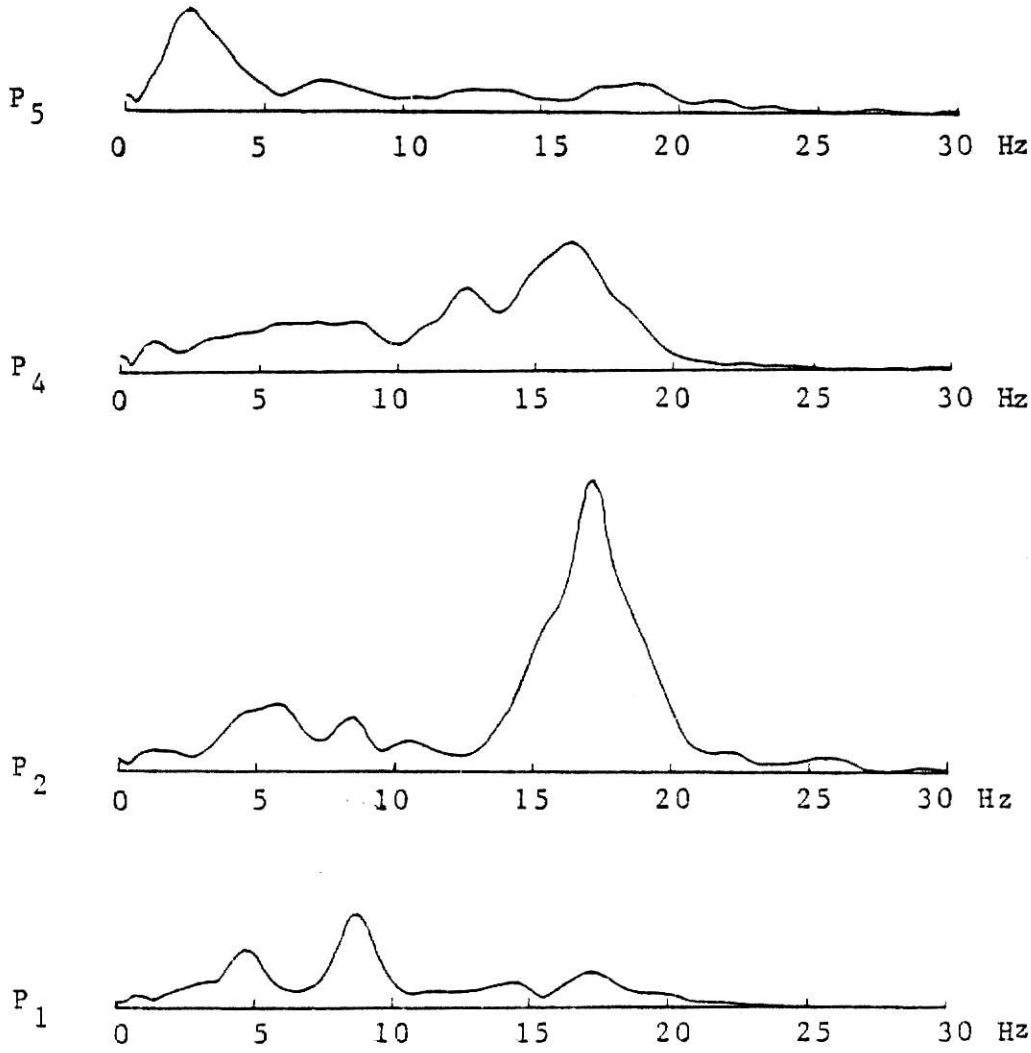



Figure 4.25 The spectra of pressure fluctuations for air-CMC (0.5 wt.%) solution at air flow rate of 30 $ft^3$/hr at various distances from the sparger (see Fig. 3.1 for locations of pressure taps).

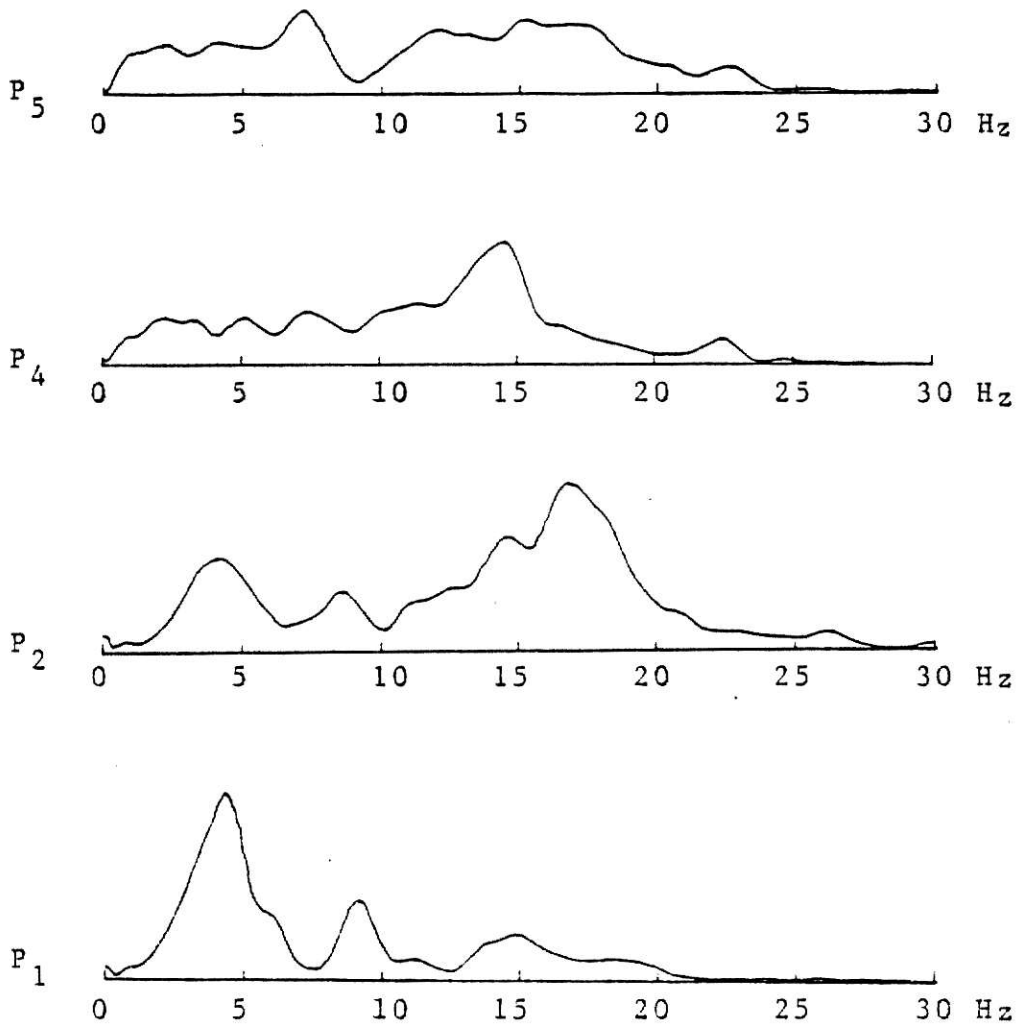



Figure 4.26 The spectra of pressure fluctuations for air-CMC (0.5 wt.%) solution at air flow rate of 60 $ft^3/hr$ at various distances from the sparger (see Fig. 3.1 for locations of pressure taps).

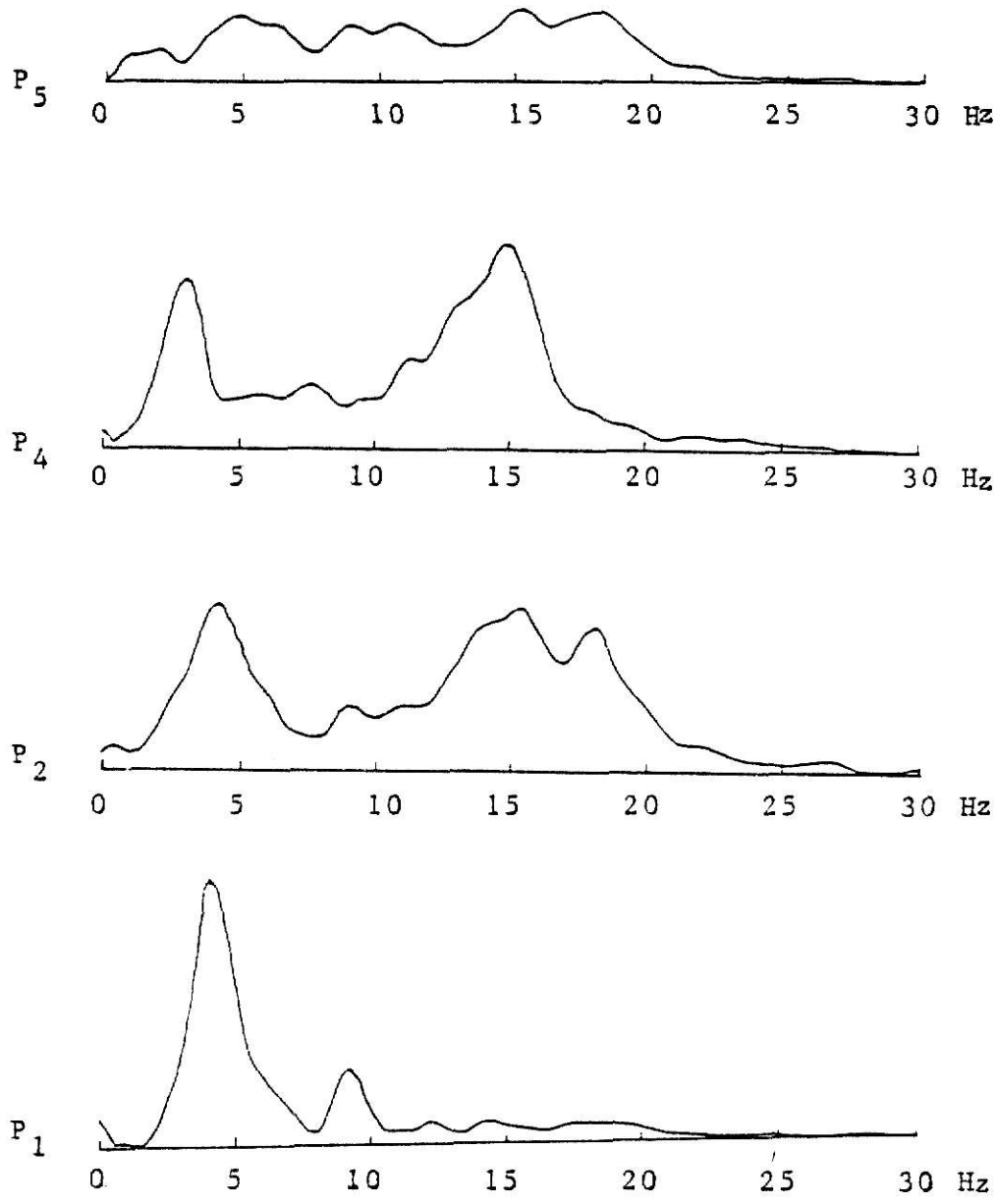



Figure 4.27 The spectra of pressure fluctuations for air-CMC (0.5 wt.%) solution at air flow rate of 90 $ft^3/hr$ at various distances from the sparger (see Fig. 3.1 for locations of pressure taps).

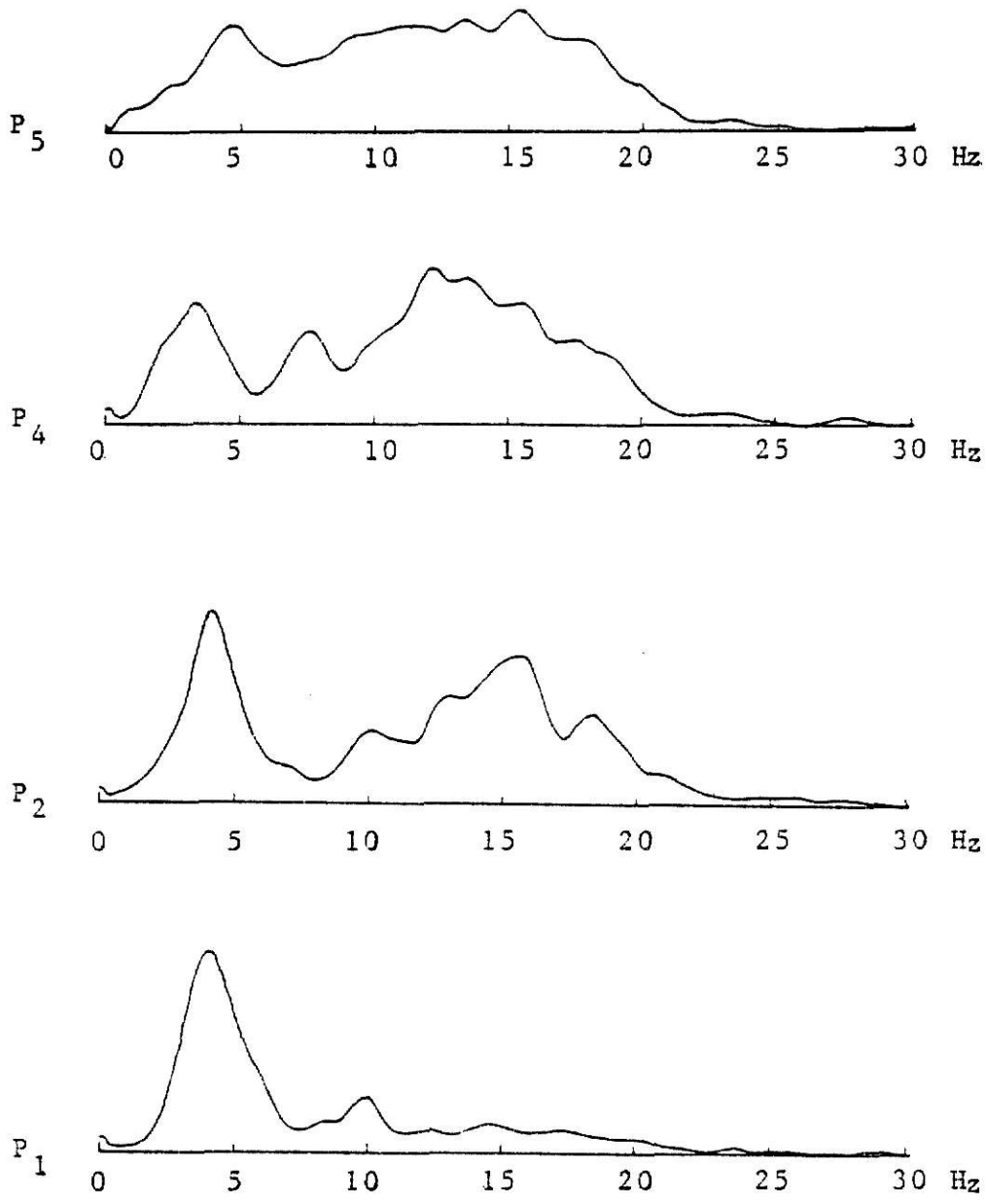



Figure 4.28 The spectra of pressure fluctuations for air-CMC (0.5 wt.%) solution at air flow rate of 120 $ft^3/hr$ at various distances from the sparger (see Fig. 3.1 for locations of pressure taps).

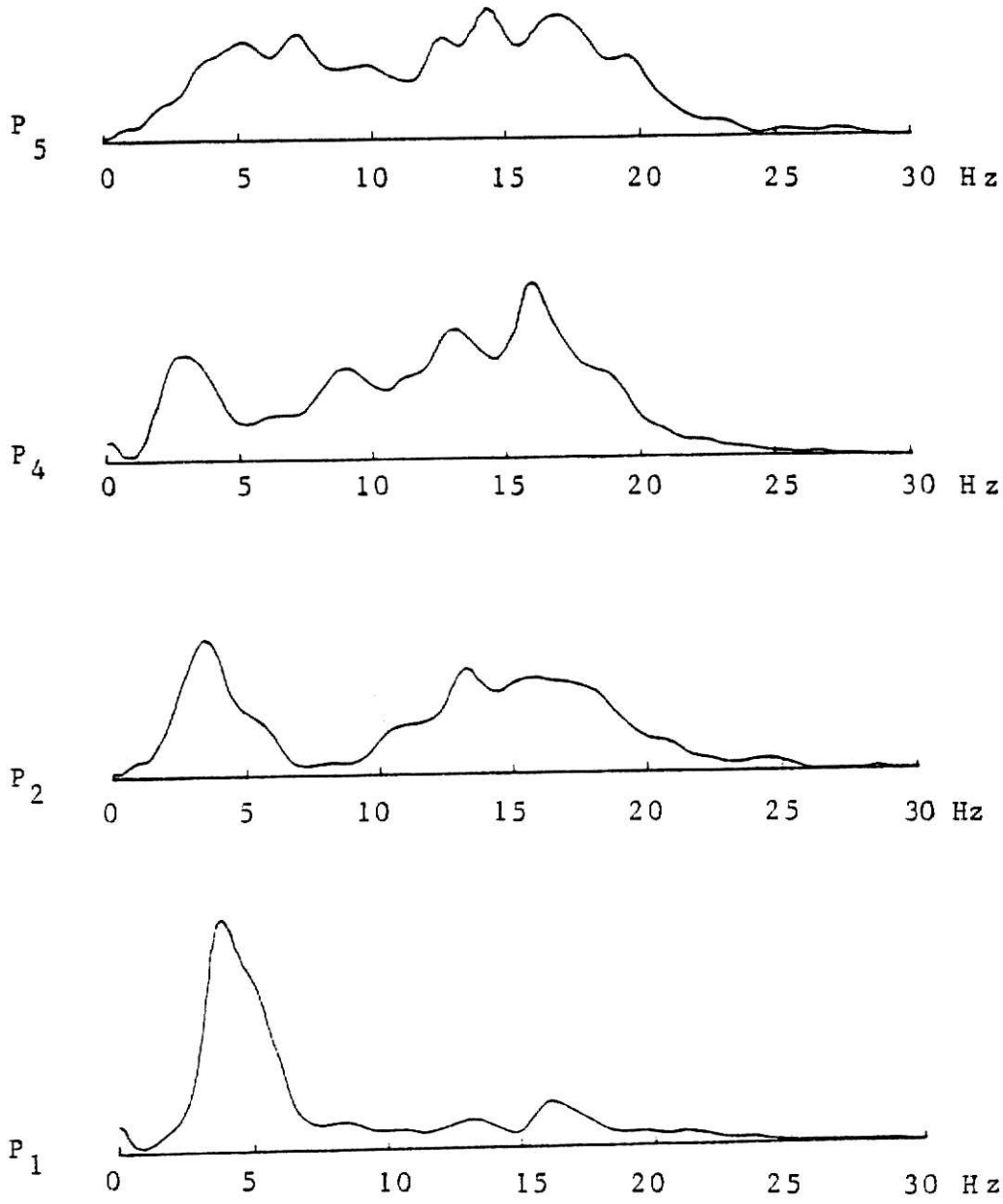



Figure 4.29 The spectra of pressure fluctuations for air-CMC (0.5 wt.%) solution at air flow rate of 150 $ft^3/hr$ at various distances from the sparger (see Fig. 3.1 for locations of pressure taps).

# CHAPTER V

## RECOMMENDATIONS FOR FUTURE WORK

1. The mechanism of bubble break-up appears to be mainly due to the dynamic pressure fluctuations in the vicinity of the bubble which are closely related to the kinetic energy of the turbulent eddies. It is therefore suggested that the influence of the turbulent energy spectrum on the gas dispersion be investigated directly.

2. The maximum stable bubble diameter can be predicted by applying isotropic turbulence theory, and it was found to be proportional to the -2/5 power of the energy dissipation rate, $\varepsilon$. Since $\varepsilon$ is a spatially variable quantity, it is recommended that the local energy dissipation rate in airlift fermentors be investigated.

3. Bubble coalescence was found to have a significant influence on the bubble size distribution under higher air flow rate conditions. In order to predict the dynamic behavior of bubble size distribution at higher energy input conditions the bubble coalescence frequency should be formulated in terms of the fluid properties and the operating conditions either by theory, dimensional reasoning or probabilistic model.

4. The bubble size was found to be a spatial variable in the airlift column. It is therefore suggested that Eq. (3.9) be improved by offering plausible formulations of $H_{11}$, $H_{12}$, $G_{12}$ and $G_{22}$ from either theoretical or dimensional arguments in order to simulate the dynamic behavior of the bubbles.

# APPENDIX

The experimental data of the bubble size distribution for different systems at various air flow rates and window positions are shown in the following tables. The first column of the table is the bubble diameter, the second column is the number of bubbles with diameters larger than the corresponding bubble diameter in the first column. The third column shows the cumulative volume distribution, the fourth column the probability density function and the fifth column gives the probability density function after smoothing.

TABLE A-1 BUBBLE SIZE DISTRIBUTION FOR TAP WATER SYSTEM AT WINDOW #1 AND F= 30 SCFH

| DIA.(CM) | NO. OF BUBBLES | CUMUL. VOL. | PROB. DEN. | PROB. DEN. AFTER SMOOTHING |
|---|---|---|---|---|
| 0.0 | 354. | 0.0 | 0.0 | 0.0 |
| 0.048 | 253. | 0.000 | 0.096 | 0.096 |
| 0.096 | 114. | 0.009 | 0.241 | 0.216 |
| 0.144 | 67. | 0.023 | 0.422 | 0.291 |
| 0.193 | 35. | 0.050 | 0.384 | 0.349 |
| 0.241 | 29. | 0.060 | 0.442 | 0.386 |
| 0.289 | 19. | 0.092 | 0.443 | 0.419 |
| 0.337 | 17. | 0.103 | 0.279 | 0.465 |
| 0.385 | 15. | 0.119 | 0.415 | 0.542 |
| 0.433 | 13. | 0.143 | 0.589 | 0.645 |
| 0.481 | 11. | 0.176 | 0.575 | 0.745 |
| 0.529 | 10. | 0.198 | 1.449 | 0.801 |
| 0.578 | 6. | 0.315 | 1.218 | 0.792 |
| 0.626 | 6. | 0.315 | 0.492 | 0.743 |
| 0.674 | 5. | 0.363 | 0.492 | 0.729 |
| 0.722 | 5. | 0.363 | 0.0 | 0.837 |
| 0.770 | 5. | 0.363 | 0.899 | 1.111 |
| 0.818 | 4. | 0.449 | 0.899 | 1.499 |
| 0.866 | 4. | 0.449 | 1.267 | 1.846 |
| 0.914 | 3. | 0.571 | 5.719 | 1.963 |
| 0.963 | 0. | 1.000 | 0.0 | 1.756 |

TABLE A-2 BUBBLE SIZE DISTRIBUTION FOR TAP WATER SYSTEM AT WINDOW #2 AND F= 30 SCFH

| DIA.(CM) | NO. OF BUBBLES | CUMUL. VOL. | PROB. DEN. | PROB. DEN. AFTER SMOOTHING |
|---|---|---|---|---|
| 0.0 | 458. | 0.0 | 0.0 | 0.0 |
| 0.048 | 357. | 0.000 | 0.049 | 0.049 |
| 0.096 | 205. | 0.005 | 0.169 | 0.156 |
| 0.144 | 122. | 0.016 | 0.293 | 0.238 |
| 0.193 | 79. | 0.033 | 0.367 | 0.309 |
| 0.241 | 56. | 0.052 | 0.428 | 0.367 |
| 0.289 | 41. | 0.074 | 0.386 | 0.418 |
| 0.337 | 35. | 0.089 | 0.350 | 0.467 |
| 0.385 | 30. | 0.108 | 0.540 | 0.513 |
| 0.433 | 24. | 0.141 | 0.663 | 0.546 |
| 0.481 | 20. | 0.172 | 0.751 | 0.557 |
| 0.529 | 16. | 0.213 | 0.574 | 0.555 |
| 0.578 | 15. | 0.227 | 0.324 | 0.560 |
| 0.626 | 14. | 0.244 | 0.412 | 0.596 |
| 0.674 | 13. | 0.267 | 0.514 | 0.682 |
| 0.722 | 12. | 0.294 | 0.979 | 0.837 |
| 0.770 | 10. | 0.361 | 1.113 | 1.084 |
| 0.818 | 9. | 0.401 | 0.419 | 1.413 |
| 0.866 | 9. | 0.401 | 0.0 | 1.730 |
| 0.914 | 9. | 0.401 | 6.222 | 1.871 |
| 0.963 | 0. | 1.000 | 0.0 | 1.717 |

TABLE A-3 BUBBLE SIZE DISTRIBUTION FOR TAP WATER SYSTEM AT WINDOW #3 AND F= 30 SCFH

| DIA.(CM) | NO. OF BUBBLES | CUMUL. VOL. | PROB. DEN. | PROB. DEN. AFTER SMOOTHING |
|---|---|---|---|---|
| 0.0 | 587. | 0.0 | 0.0 | 0.0 |
| 0.048 | 513. | 0.000 | 0.057 | 0.057 |
| 0.096 | 294. | 0.005 | 0.165 | 0.184 |
| 0.144 | 202. | 0.016 | 0.321 | 0.311 |
| 0.193 | 137. | 0.036 | 0.468 | 0.433 |
| 0.241 | 100. | 0.061 | 0.623 | 0.548 |
| 0.289 | 71. | 0.096 | 0.596 | 0.654 |
| 0.337 | 60. | 0.118 | 0.710 | 0.745 |
| 0.385 | 45. | 0.165 | 1.041 | 0.813 |
| 0.433 | 33. | 0.219 | 0.886 | 0.850 |
| 0.481 | 28. | 0.250 | 1.030 | 0.857 |
| 0.529 | 20. | 0.318 | 0.819 | 0.848 |
| 0.578 | 19. | 0.329 | 0.561 | 0.842 |
| 0.626 | 16. | 0.372 | 0.819 | 0.851 |
| 0.674 | 14. | 0.408 | 1.069 | 0.885 |
| 0.722 | 11. | 0.475 | 0.978 | 0.963 |
| 0.770 | 10. | 0.502 | 0.624 | 1.111 |
| 0.818 | 9. | 0.535 | 0.749 | 1.319 |
| 0.866 | 8. | 0.574 | 0.888 | 1.505 |
| 0.914 | 7. | 0.620 | 4.426 | 1.545 |
| 0.963 | 0. | 1.000 | 0.0 | 1.363 |

TABLE A-4 BUBBLE SIZE DISTRIBUTION FOR TAP WATER SYSTEM AT WINDOW #4 AND F= 30 SCFH

| DIA.(CM) | NO. OF BUBBLES | CUMUL. VOL. | PROB. DEN. | PROB. DEN. AFTER SMOOTHING |
|---|---|---|---|---|
| 0.0 | 601. | 0.0 | 0.0 | 0.0 |
| 0.048 | 508. | 0.000 | 0.061 | 0.061 |
| 0.096 | 301. | 0.006 | 0.200 | 0.209 |
| 0.144 | 197. | 0.019 | 0.398 | 0.342 |
| 0.193 | 127. | 0.044 | 0.518 | 0.466 |
| 0.241 | 94. | 0.069 | 0.632 | 0.577 |
| 0.289 | 68. | 0.105 | 0.633 | 0.677 |
| 0.337 | 57. | 0.130 | 0.769 | 0.771 |
| 0.385 | 43. | 0.179 | 0.879 | 0.858 |
| 0.433 | 36. | 0.215 | 0.961 | 0.941 |
| 0.481 | 28. | 0.272 | 1.189 | 1.025 |
| 0.529 | 22. | 0.329 | 0.860 | 1.116 |
| 0.578 | 20. | 0.354 | 0.935 | 1.210 |
| 0.626 | 16. | 0.419 | 1.732 | 1.284 |
| 0.674 | 11. | 0.521 | 1.585 | 1.313 |
| 0.722 | 9. | 0.572 | 1.487 | 1.294 |
| 0.770 | 6. | 0.664 | 1.349 | 1.257 |
| 0.818 | 5. | 0.702 | 0.387 | 1.237 |
| 0.866 | 5. | 0.702 | 0.545 | 1.221 |
| 0.914 | 4. | 0.754 | 3.100 | 1.151 |
| 0.963 | 0. | 1.000 | 0.0 | 0.974 |

TABLE A-5 BUBBLE SIZE DISTRIBUTION FOR TAP WATER SYSTEM AT WINDOW #1 AND F= 60 SCFH

| DIA.(CM) | NO. OF BUBBLES | CUMUL. VOL. | PROB. DEN. | PROB. DEN. AFTER SMOOTHING |
|---|---|---|---|---|
| 0.0 | 204. | 0.0 | 0.0 | 0.0 |
| 0.038 | 185. | 0.000 | 0.045 | 0.045 |
| 0.077 | 114. | 0.003 | 0.183 | 0.161 |
| 0.115 | 66. | 0.014 | 0.328 | 0.250 |
| 0.154 | 42. | 0.029 | 0.341 | 0.325 |
| 0.192 | 33. | 0.040 | 0.397 | 0.379 |
| 0.230 | 25. | 0.059 | 0.550 | 0.413 |
| 0.269 | 19. | 0.082 | 0.460 | 0.437 |
| 0.307 | 17. | 0.094 | 0.382 | 0.474 |
| 0.345 | 15. | 0.112 | 0.385 | 0.555 |
| 0.384 | 14. | 0.124 | 0.372 | 0.688 |
| 0.422 | 13. | 0.140 | 0.214 | 0.839 |
| 0.461 | 13. | 0.140 | 2.162 | 0.940 |
| 0.499 | 7. | 0.306 | 2.162 | 0.951 |
| 0.537 | 7. | 0.306 | 0.0 | 0.916 |
| 0.576 | 7. | 0.306 | 0.0 | 0.963 |
| 0.614 | 7. | 0.306 | 0.829 | 1.214 |
| 0.652 | 6. | 0.370 | 0.829 | 1.672 |
| 0.691 | 6. | 0.370 | 0.0 | 2.164 |
| 0.729 | 6. | 0.370 | 8.209 | 2.418 |
| 0.768 | 0. | 1.000 | 0.0 | 2.252 |

TABLE A-6 BUBBLE SIZE DISTRIBUTION FOR TAP WATER SYSTEM AT WINDOW #2 AND F= 60 SCFH

| DIA.(CM) | NO. OF BUBBLES | CUMUL. VOL. | PROB. DEN. | PROB. DEN. AFTER SMOOTHING |
|---|---|---|---|---|
| 0.0 | 428. | 0.0 | 0.0 | 0.0 |
| 0.038 | 385. | 0.000 | 0.049 | 0.049 |
| 0.077 | 222. | 0.004 | 0.156 | 0.152 |
| 0.115 | 145. | 0.012 | 0.248 | 0.250 |
| 0.154 | 108. | 0.023 | 0.376 | 0.346 |
| 0.192 | 79. | 0.041 | 0.472 | 0.438 |
| 0.230 | 63. | 0.059 | 0.481 | 0.529 |
| 0.269 | 53. | 0.078 | 0.619 | 0.624 |
| 0.307 | 43. | 0.107 | 0.648 | 0.723 |
| 0.345 | 38. | 0.128 | 0.883 | 0.820 |
| 0.384 | 30. | 0.174 | 1.022 | 0.907 |
| 0.422 | 26. | 0.206 | 0.953 | 0.978 |
| 0.461 | 22. | 0.247 | 1.062 | 1.028 |
| 0.499 | 19. | 0.287 | 1.177 | 1.068 |
| 0.537 | 16. | 0.338 | 1.199 | 1.136 |
| 0.576 | 14. | 0.379 | 0.873 | 1.293 |
| 0.614 | 13. | 0.405 | 0.731 | 1.585 |
| 0.652 | 12. | 0.436 | 1.353 | 1.974 |
| 0.691 | 10. | 0.509 | 2.079 | 2.301 |
| 0.729 | 8. | 0.595 | 6.401 | 2.367 |
| 0.768 | 0. | 1.000 | 0.0 | 2.071 |

TABLE A-7 BUBBLE SIZE DISTRIBUTION FOR TAP WATER SYSTEM AT WINDOW #3 AND F= 60 SCFH

| DIA.(CM) | NO. OF BUBBLES | CUMUL. VOL. | PROB. DEN. | PROB. DEN. AFTER SMOOTHING |
|---|---|---|---|---|
| 0.0 | 242. | 0.0 | 0.0 | 0.0 |
| 0.038 | 216. | 0.000 | 0.067 | 0.067 |
| 0.077 | 134. | 0.005 | 0.261 | 0.256 |
| 0.115 | 82. | 0.020 | 0.472 | 0.426 |
| 0.154 | 55. | 0.041 | 0.627 | 0.585 |
| 0.192 | 39. | 0.068 | 0.828 | 0.723 |
| 0.230 | 27. | 0.105 | 0.742 | 0.828 |
| 0.269 | 23. | 0.125 | 1.072 | 0.884 |
| 0.307 | 15. | 0.187 | 1.398 | 0.879 |
| 0.345 | 11. | 0.232 | 0.794 | 0.826 |
| 0.384 | 10. | 0.248 | 0.483 | 0.763 |
| 0.422 | 9. | 0.269 | 0.642 | 0.748 |
| 0.461 | 8. | 0.297 | 0.365 | 0.833 |
| 0.499 | 8. | 0.297 | 0.590 | 1.051 |
| 0.537 | 7. | 0.343 | 1.320 | 1.400 |
| 0.576 | 6. | 0.399 | 1.623 | 1.837 |
| 0.614 | 5. | 0.467 | 1.969 | 2.266 |
| 0.652 | 4. | 0.550 | 3.646 | 2.548 |
| 0.691 | 2. | 0.747 | 4.086 | 2.554 |
| 0.729 | 1. | 0.864 | 3.295 | 2.244 |
| 0.768 | 0. | 1.000 | 0.0 | 1.702 |

TABLE A-8 BUBBLE SIZE DISTRIBUTION FOR TAP WATER SYSTEM AT WINDOW #4 AND F= 60 SCFH

| DIA.(CM) | NO. OF BUBBLES | CUMUL. VOL. | PROB. DEN. | PROB. DEN. AFTER SMOOTHING |
|---|---|---|---|---|
| 0.0 | 428. | 0.0 | 0.0 | 0.0 |
| 0.038 | 377. | 0.000 | 0.088 | 0.088 |
| 0.077 | 208. | 0.007 | 0.264 | 0.256 |
| 0.115 | 134. | 0.020 | 0.439 | 0.417 |
| 0.154 | 94. | 0.040 | 0.597 | 0.573 |
| 0.192 | 70. | 0.066 | 0.640 | 0.718 |
| 0.230 | 58. | 0.090 | 0.977 | 0.852 |
| 0.269 | 42. | 0.141 | 1.188 | 0.983 |
| 0.307 | 34. | 0.181 | 0.986 | 1.135 |
| 0.345 | 29. | 0.217 | 0.732 | 1.335 |
| 0.384 | 27. | 0.237 | 1.324 | 1.583 |
| 0.422 | 21. | 0.318 | 2.457 | 1.845 |
| 0.461 | 15. | 0.426 | 2.291 | 2.070 |
| 0.499 | 12. | 0.494 | 2.401 | 2.221 |
| 0.537 | 8. | 0.610 | 2.437 | 2.287 |
| 0.576 | 6. | 0.681 | 2.071 | 2.256 |
| 0.614 | 4. | 0.769 | 2.513 | 2.101 |
| 0.652 | 2. | 0.874 | 3.013 | 1.801 |
| 0.691 | 0. | 1.000 | 1.639 | 1.378 |
| 0.729 | 0. | 1.000 | 0.0 | 0.916 |
| 0.768 | 0. | 1.000 | 0.0 | 0.515 |

TABLE A-9 BUBBLE SIZE DISTRIBUTION FOR TAP WATER SYSTEM AT WINDOW #1 AND F= 90 SCFH

| DIA.(CM) | NO. OF BUBBLES | CUMUL. VOL. | PROB. DEN. | PROB. DEN. AFTER SMOOTHING |
|---|---|---|---|---|
| 0.0 | 313. | 0.0 | 0.0 | 0.0 |
| 0.038 | 294. | 0.000 | 0.016 | 0.016 |
| 0.077 | 228. | 0.001 | 0.077 | 0.107 |
| 0.115 | 173. | 0.006 | 0.177 | 0.215 |
| 0.154 | 135. | 0.015 | 0.323 | 0.321 |
| 0.192 | 103. | 0.031 | 0.491 | 0.422 |
| 0.230 | 79. | 0.052 | 0.615 | 0.510 |
| 0.269 | 62. | 0.078 | 0.541 | 0.586 |
| 0.307 | 55. | 0.094 | 0.646 | 0.659 |
| 0.345 | 45. | 0.128 | 0.741 | 0.745 |
| 0.384 | 40. | 0.151 | 0.798 | 0.860 |
| 0.422 | 34. | 0.189 | 0.601 | 1.008 |
| 0.461 | 33. | 0.197 | 1.079 | 1.166 |
| 0.499 | 26. | 0.272 | 2.020 | 1.297 |
| 0.537 | 20. | 0.352 | 1.698 | 1.385 |
| 0.576 | 17. | 0.402 | 1.179 | 1.468 |
| 0.614 | 15. | 0.443 | 1.167 | 1.614 |
| 0.652 | 13. | 0.492 | 1.019 | 1.846 |
| 0.691 | 12. | 0.521 | 0.830 | 2.070 |
| 0.729 | 11. | 0.555 | 6.244 | 2.118 |
| 0.768 | 0. | 1.000 | 0.0 | 1.872 |

TABLE A-10 BUBBLE SIZE DISTRIBUTION FOR TAP WATER SYSTEM AT WINDOW #2 AND F= 90 SCFH

| DIA.(CM) | NO. OF BUBBLES | CUMUL. VOL. | PROB. DEN. | PROB. DEN. AFTER SMOOTHING |
|---|---|---|---|---|
| 0.0 | 590. | 0.0 | 0.0 | 0.0 |
| 0.038 | 553. | 0.000 | 0.082 | 0.082 |
| 0.077 | 361. | 0.006 | 0.367 | 0.367 |
| 0.115 | 215. | 0.028 | 0.716 | 0.620 |
| 0.154 | 135. | 0.061 | 0.910 | 0.847 |
| 0.192 | 93. | 0.098 | 1.127 | 1.018 |
| 0.230 | 62. | 0.148 | 1.439 | 1.114 |
| 0.269 | 39. | 0.209 | 1.480 | 1.123 |
| 0.307 | 26. | 0.261 | 1.150 | 1.056 |
| 0.345 | 20. | 0.297 | 0.785 | 0.945 |
| 0.384 | 17. | 0.322 | 0.758 | 0.829 |
| 0.422 | 14. | 0.355 | 0.626 | 0.744 |
| 0.461 | 13. | 0.370 | C.680 | 0.723 |
| 0.499 | 11. | 0.407 | C.490 | 0.797 |
| 0.537 | 11. | 0.407 | 0.382 | 0.986 |
| 0.576 | 10. | 0.437 | 0.849 | 1.281 |
| 0.614 | 9. | 0.472 | 2.157 | 1.626 |
| 0.652 | 6. | 0.602 | 2.362 | 1.923 |
| 0.691 | 5. | 0.654 | 1.466 | 2.061 |
| 0.729 | 4. | 0.715 | 4.513 | 1.956 |
| 0.768 | 0. | 1.000 | 0.0 | 1.611 |

TABLE A-11 BUBBLE SIZE DISTRIBUTION FOR TAP WATER SYSTEM AT WINDOW #3 AND F= 90 SCFH

| DIA.(CM) | NO. OF BUBBLES | CUMUL. VOL. | PROB. DEN. | PROB. DEN. AFTER SMOOTHING |
|---|---|---|---|---|
| 0.0 | 522. | 0.0 | 0.0 | 0.0 |
| 0.038 | 501. | 0.000 | 0.036 | 0.036 |
| 0.077 | 372. | 0.003 | 0.215 | 0.219 |
| 0.115 | 232. | 0.017 | 0.481 | 0.371 |
| 0.154 | 146. | 0.040 | 0.623 | 0.510 |
| 0.192 | 103. | 0.064 | 0.607 | 0.633 |
| 0.230 | 82. | 0.086 | 0.624 | 0.746 |
| 0.269 | 67. | 0.112 | 0.960 | 0.852 |
| 0.307 | 49. | 0.160 | 1.075 | 0.951 |
| 0.345 | 40. | 0.195 | 0.875 | 1.037 |
| 0.384 | 34. | 0.227 | 1.086 | 1.091 |
| 0.422 | 27. | 0.278 | 1.537 | 1.093 |
| 0.461 | 20. | 0.345 | 1.353 | 1.038 |
| 0.499 | 17. | 0.382 | 0.883 | 0.964 |
| 0.537 | 15. | 0.413 | 0.653 | 0.963 |
| 0.576 | 14. | 0.432 | 0.250 | 1.137 |
| 0.614 | 14. | 0.432 | 0.0 | 1.515 |
| 0.652 | 14. | 0.432 | 2.196 | 1.988 |
| 0.691 | 9. | 0.601 | 3.753 | 2.334 |
| 0.729 | 6. | 0.720 | 5.203 | 2.348 |
| 0.768 | 0. | 1.000 | 0.0 | 1.986 |

TABLE A-12 BUBBLE SIZE DISTRIBUTION FOR TAP WATER SYSTEM AT WINDOW #4 AND F= 90 SCFH

| DIA.(CM) | NO. OF BUBBLES | CUMUL. VOL. | PROB. DEN. | PROB. DEN. AFTER SMOOTHING |
|---|---|---|---|---|
| 0.0 | 568. | 0.0 | 0.0 | 0.0 |
| 0.038 | 539. | 0.000 | 0.045 | 0.045 |
| 0.077 | 410. | 0.003 | 0.260 | 0.312 |
| 0.115 | 274. | 0.020 | 0.639 | 0.565 |
| 0.154 | 177. | 0.052 | 0.951 | 0.793 |
| 0.192 | 120. | 0.093 | 1.103 | 0.978 |
| 0.230 | 86. | 0.137 | 1.273 | 1.115 |
| 0.269 | 61. | 0.191 | 1.384 | 1.218 |
| 0.307 | 45. | 0.243 | 1.060 | 1.307 |
| 0.345 | 39. | 0.272 | 1.159 | 1.391 |
| 0.384 | 30. | 0.332 | 1.608 | 1.453 |
| 0.422 | 23. | 0.395 | 2.060 | 1.462 |
| 0.461 | 15. | 0.490 | 1.832 | 1.411 |
| 0.499 | 12. | 0.536 | 0.846 | 1.338 |
| 0.537 | 11. | 0.555 | 0.870 | 1.311 |
| 0.576 | 9. | 0.603 | 0.998 | 1.379 |
| 0.614 | 8. | 0.632 | 1.291 | 1.527 |
| 0.652 | 6. | 0.702 | 2.002 | 1.672 |
| 0.691 | 4. | 0.786 | 2.376 | 1.702 |
| 0.729 | 2. | 0.884 | 2.794 | 1.546 |
| 0.768 | 0. | 1.000 | 0.0 | 1.219 |

TABLE A-13 BUBBLE SIZE DISTRIBUTION FOR SALT WATER SYSTEM AT WINDOW #1 AND F= 30 SCFH

| DIA.(CM) | NO. OF BUBBLES | CUMUL. VOL. | PROB. DEN. | PROB. DEN. AFTER SMOOTHING |
|---|---|---|---|---|
| 0.0 | 671. | 0.0 | 0.0 | 0.0 |
| 0.048 | 460. | 0.000 | 0.119 | 0.119 |
| 0.096 | 186. | 0.011 | 0.291 | 0.233 |
| 0.144 | 96. | 0.028 | 0.374 | 0.304 |
| 0.193 | 59. | 0.047 | 0.426 | 0.367 |
| 0.241 | 39. | 0.069 | 0.373 | 0.417 |
| 0.289 | 32. | 0.083 | 0.386 | 0.459 |
| 0.337 | 25. | 0.107 | 0.610 | 0.493 |
| 0.385 | 18. | 0.142 | 0.600 | 0.512 |
| 0.433 | 15. | 0.164 | 0.445 | 0.504 |
| 0.481 | 13. | 0.185 | 0.649 | 0.462 |
| 0.529 | 10. | 0.227 | 0.624 | 0.388 |
| 0.578 | 9. | 0.245 | 0.190 | 0.306 |
| 0.626 | 9. | 0.245 | 0.0 | 0.260 |
| 0.674 | 9. | 0.245 | 0.0 | 0.311 |
| 0.722 | 9. | 0.245 | 0.0 | 0.523 |
| 0.770 | 9. | 0.245 | 0.562 | 0.930 |
| 0.818 | 8. | 0.299 | 0.562 | 1.479 |
| 0.866 | 8. | 0.299 | 0.792 | 1.993 |
| 0.914 | 7. | 0.375 | 7.281 | 2.239 |
| 0.963 | 0. | 1.000 | 0.0 | 2.074 |

TABLE A- 14 BUBBLE SIZE DISTRIBUTION FOR SALT WATER SYSTEM AT WINDOW #2 AND F= 30 SCFH

| DIA.(CM) | NO. OF BUBBLES | CUMUL. VOL. | PROB. DEN. | PROB. DEN. AFTER SMOOTHING |
|---|---|---|---|---|
| 0.0 | 701. | 0.0 | 0.0 | 0.0 |
| 0.048 | 535. | 0.000 | 0.083 | 0.083 |
| 0.096 | 275. | 0.008 | 0.255 | 0.220 |
| 0.144 | 155. | 0.025 | 0.396 | 0.317 |
| 0.193 | 99. | 0.046 | 0.492 | 0.402 |
| 0.241 | 67. | 0.072 | 0.470 | 0.475 |
| 0.289 | 54. | 0.091 | 0.455 | 0.548 |
| 0.337 | 44. | 0.116 | 0.567 | 0.631 |
| 0.385 | 36. | 0.146 | 0.711 | 0.724 |
| 0.433 | 29. | 0.184 | 0.795 | 0.809 |
| 0.481 | 24. | 0.223 | 1.040 | 0.864 |
| 0.529 | 18. | 0.284 | 1.347 | 0.871 |
| 0.578 | 13. | 0.352 | 0.704 | 0.837 |
| 0.626 | 13. | 0.352 | 0.456 | 0.787 |
| 0.674 | 11. | 0.396 | 1.020 | 0.767 |
| 0.722 | 9. | 0.450 | 0.565 | 0.833 |
| 0.770 | 9. | 0.450 | 0.416 | 1.031 |
| 0.818 | 8. | 0.490 | 0.416 | 1.341 |
| 0.866 | 8. | 0.490 | 1.173 | 1.641 |
| 0.914 | 6. | 0.603 | 5.293 | 1.760 |
| 0.963 | 0. | 1.000 | 0.0 | 1.590 |

TABLE A-15 BUBBLE SIZE DISTRIBUTION FOR SALT WATER SYSTEM AT WINDOW #3 AND F= 30 SCFH

| DIA.(CM) | NO. OF BUBBLES | CUMUL. VOL. | PROB. DEN. | PROB. DEN. AFTER SMOOTHING |
|---|---|---|---|---|
| 0.0 | 522. | 0.0 | 0.0 | 0.0 |
| 0.048 | 462. | 0.000 | 0.063 | 0.063 |
| 0.096 | 279. | 0.006 | 0.251 | 0.223 |
| 0.144 | 160. | 0.024 | 0.428 | 0.353 |
| 0.193 | 105. | 0.047 | 0.470 | 0.473 |
| 0.241 | 80. | 0.070 | 0.619 | 0.580 |
| 0.289 | 57. | 0.107 | 0.695 | 0.679 |
| 0.337 | 46. | 0.136 | 0.777 | 0.775 |
| 0.385 | 35. | 0.182 | 0.782 | 0.868 |
| 0.433 | 30. | 0.212 | 0.920 | 0.952 |
| 0.481 | 23. | 0.270 | 1.313 | 1.012 |
| 0.529 | 17. | 0.338 | 1.167 | 1.039 |
| 0.578 | 14. | 0.383 | 1.057 | 1.035 |
| 0.626 | 11. | 0.440 | 0.844 | 1.018 |
| 0.674 | 10. | 0.464 | 0.868 | 1.013 |
| 0.722 | 8. | 0.523 | 1.374 | 1.045 |
| 0.770 | 6. | 0.596 | 0.756 | 1.136 |
| 0.818 | 6. | 0.596 | 0.544 | 1.272 |
| 0.866 | 5. | 0.649 | 1.186 | 1.386 |
| 0.914 | 4. | 0.710 | 3.651 | 1.377 |
| 0.963 | 0. | 1.000 | 0.0 | 1.187 |

TABLE A-16 BUBBLE SIZE DISTRIBUTION FOR SALT WATER SYSTEM AT WINDOW #4 AND F= 30 SCFH

| DIA.(CM) | NO. OF BUBBLES | CUMUL. VOL. | PROB. DEN. | PROB. DEN. AFTER SMOOTHING |
|---|---|---|---|---|
| 0.0 | 535. | 0.0 | 0.0 | 0.0 |
| 0.048 | 488. | 0.000 | 0.046 | 0.046 |
| 0.096 | 317. | 0.004 | 0.164 | 0.196 |
| 0.144 | 221. | 0.016 | 0.366 | 0.340 |
| 0.193 | 148. | 0.040 | 0.600 | 0.476 |
| 0.241 | 99. | 0.074 | 0.668 | 0.600 |
| 0.289 | 75. | 0.104 | 0.597 | 0.716 |
| 0.337 | 62. | 0.131 | 0.749 | 0.824 |
| 0.385 | 48. | 0.176 | 1.049 | 0.914 |
| 0.433 | 36. | 0.232 | 1.124 | 0.966 |
| 0.481 | 28. | 0.284 | 1.365 | 0.969 |
| 0.529 | 19. | 0.363 | 0.943 | 0.940 |
| 0.578 | 18. | 0.375 | 0.429 | 0.920 |
| 0.626 | 16. | 0.405 | 0.892 | 0.948 |
| 0.674 | 13. | 0.461 | 0.824 | 1.043 |
| 0.722 | 12. | 0.484 | 0.829 | 1.183 |
| 0.770 | 10. | 0.541 | 2.008 | 1.323 |
| 0.818 | 6. | 0.677 | 1.843 | 1.413 |
| 0.866 | 5. | 0.718 | 0.423 | 1.407 |
| 0.914 | 5. | 0.718 | 2.929 | 1.276 |
| 0.963 | 0. | 1.000 | 0.0 | 1.027 |

TABLE A-17 BUBBLE SIZE DISTRIBUTION FOR SALT WATER SYSTEM AT WINDOW #1 AND F= 60 SCFH

| DIA.(CM) | NO. OF BUBBLES | CUMUL. VOL. | PROB. DEN. | PROB. DEN. AFTER SMOOTHING |
|---|---|---|---|---|
| 0.0 | 252. | 0.0 | 0.0 | 0.0 |
| 0.039 | 223. | 0.000 | 0.046 | 0.046 |
| 0.077 | 147. | 0.004 | 0.228 | 0.200 |
| 0.116 | 81. | 0.018 | 0.409 | 0.310 |
| 0.155 | 51. | 0.035 | 0.485 | 0.398 |
| 0.193 | 35. | 0.055 | 0.552 | 0.453 |
| 0.232 | 25. | 0.078 | 0.537 | 0.483 |
| 0.270 | 20. | 0.097 | 0.466 | 0.503 |
| 0.309 | 17. | 0.114 | 0.441 | 0.526 |
| 0.348 | 15. | 0.131 | 0.368 | 0.555 |
| 0.386 | 14. | 0.142 | 0.765 | 0.577 |
| 0.425 | 11. | 0.190 | 0.882 | 0.582 |
| 0.464 | 10. | 0.210 | 0.614 | 0.584 |
| 0.502 | 9. | 0.237 | 0.345 | 0.636 |
| 0.541 | 9. | 0.237 | 0.0 | 0.819 |
| 0.579 | 9. | 0.237 | 0.658 | 1.195 |
| 0.618 | 8. | 0.288 | 1.452 | 1.757 |
| 0.657 | 7. | 0.349 | 1.741 | 2.385 |
| 0.695 | 6. | 0.422 | 3.184 | 2.851 |
| 0.734 | 4. | 0.595 | 7.477 | 2.925 |
| 0.773 | 0. | 1.000 | 0.0 | 2.534 |

TABLE A-18 BUBBLE SIZE DISTRIBUTION FOR SALT WATER SYSTEM AT WINDOW #2 AND F= 60 SCFH

| DIA.(CM) | NO. OF BUBBLES | CUMUL. VOL. | PROB. DEN. | PROB. DEN. AFTER SMOCTHING |
|---|---|---|---|---|
| 0.0 | 389. | 0.0 | 0.0 | 0.0 |
| 0.039 | 374. | 0.000 | 0.056 | 0.056 |
| 0.077 | 251. | 0.004 | 0.280 | 0.255 |
| 0.116 | 144. | 0.022 | 0.517 | 0.412 |
| 0.155 | 93. | 0.044 | 0.660 | 0.553 |
| 0.193 | 63. | 0.073 | 0.657 | 0.671 |
| 0.232 | 50. | 0.095 | 0.695 | 0.769 |
| 0.270 | 39. | 0.126 | 1.C84 | 0.850 |
| 0.309 | 27. | 0.179 | 0.844 | 0.913 |
| 0.348 | 25. | 0.191 | C.970 | 0.959 |
| 0.386 | 18. | 0.254 | 1.115 | 0.992 |
| 0.425 | 16. | 0.278 | 0.922 | 1.015 |
| 0.464 | 13. | 0.325 | 1.136 | 1.035 |
| 0.502 | 11. | 0.365 | 0.854 | 1.055 |
| 0.541 | 10. | 0.391 | 1.148 | 1.083 |
| 0.579 | 8. | 0.454 | 1.317 | 1.147 |
| 0.618 | 7. | 0.493 | 1.102 | 1.288 |
| 0.657 | 6. | 0.539 | C.602 | 1.516 |
| 0.695 | 6. | 0.539 | 0.0 | 1.753 |
| 0.734 | 6. | 0.539 | 5.966 | 1.844 |
| 0.773 | 0. | 1.000 | 0.0 | 1.670 |

TABLE A-19 BUBBLE SIZE DISTRIBUTION FOR SALT WATER SYSTEM AT WINDOW #3 AND F= 60 SCFH

| DIA.(CM) | NO. OF BUBBLES | CUMUL. VOL. | PROB. DEN. | PROB. DEN. AFTER SMOOTHING |
|---|---|---|---|---|
| 0.0 | 528. | 0.0 | 0.0 | 0.0 |
| 0.039 | 492. | 0.000 | 0.040 | 0.040 |
| 0.077 | 376. | 0.003 | 0.207 | 0.272 |
| 0.116 | 268. | 0.016 | 0.523 | 0.517 |
| 0.155 | 185. | 0.043 | 0.873 | 0.755 |
| 0.193 | 128. | 0.084 | 1.016 | 0.980 |
| 0.232 | 98. | 0.122 | 1.155 | 1.183 |
| 0.270 | 74. | 0.173 | 1.457 | 1.358 |
| 0.309 | 55. | 0.235 | 1.657 | 1.496 |
| 0.348 | 41. | 0.301 | 1.627 | 1.594 |
| 0.386 | 32. | 0.360 | 1.809 | 1.657 |
| 0.425 | 23. | 0.441 | 1.798 | 1.695 |
| 0.464 | 18. | 0.499 | 1.343 | 1.715 |
| 0.502 | 15. | 0.544 | 1.812 | 1.709 |
| 0.541 | 10. | 0.639 | 2.139 | 1.657 |
| 0.579 | 7. | 0.710 | 2.027 | 1.552 |
| 0.618 | 4. | 0.796 | 1.114 | 1.419 |
| 0.657 | 4. | 0.796 | 0.535 | 1.290 |
| 0.695 | 3. | 0.837 | 1.166 | 1.165 |
| 0.734 | 2. | 0.886 | 2.111 | 1.011 |
| 0.773 | 0. | 1.000 | 0.0 | 0.799 |

TABLE A-20 BUBBLE SIZE DISTRIBUTION FOR SALT WATER SYSTEM AT WINDOW #4 AND F= 60 SCFH

| DIA.(CM) | NO. OF BUBBLES | CUMUL. VOL. | PROB. DEN. | PROB. DEN. AFTER SMOOTHING |
|---|---|---|---|---|
| 0.0 | 542. | 0.0 | 0.0 | 0.0 |
| 0.039 | 517. | 0.000 | 0.064 | 0.063 |
| 0.077 | 374. | 0.005 | 0.365 | 0.373 |
| 0.116 | 226. | 0.028 | 0.801 | 0.628 |
| 0.155 | 137. | 0.067 | 0.964 | 0.846 |
| 0.193 | 98. | 0.103 | 1.204 | 1.004 |
| 0.232 | 64. | 0.160 | 1.350 | 1.104 |
| 0.270 | 47. | 0.207 | 1.162 | 1.169 |
| 0.309 | 37. | 0.250 | 0.953 | 1.234 |
| 0.348 | 32. | 0.281 | 1.186 | 1.333 |
| 0.386 | 25. | 0.341 | 1.390 | 1.483 |
| 0.425 | 21. | 0.388 | 1.600 | 1.670 |
| 0.464 | 16. | 0.465 | 1.760 | 1.853 |
| 0.502 | 13. | 0.524 | 2.374 | 1.969 |
| 0.541 | 8. | 0.648 | 2.804 | 1.962 |
| 0.579 | 5. | 0.741 | 2.169 | 1.823 |
| 0.618 | 3. | 0.816 | 1.561 | 1.597 |
| 0.657 | 2. | 0.861 | 0.587 | 1.353 |
| 0.695 | 2. | 0.861 | 0.828 | 1.129 |
| 0.734 | 1. | 0.925 | 1.797 | 0.917 |
| 0.773 | 0. | 1.000 | 0.0 | 0.696 |

TABLE A-21 BUBBLE SIZE DISTRIBUTION FOR SALT WATER SYSTEM AT WINDOW #1 AND F= 90 SCFH

| DIA.(CM) | NO. OF BUBBLES | CUMUL. VOL. | PROB. DEN. | PROB. DEN. AFTER SMOOTHING |
|---|---|---|---|---|
| 0.0 | 310. | 0.0 | 0.0 | 0.0 |
| 0.029 | 303. | 0.000 | 0.012 | 0.012 |
| 0.058 | 272. | 0.001 | 0.105 | 0.202 |
| 0.087 | 217. | 0.006 | 0.338 | 0.427 |
| 0.116 | 165. | 0.020 | 0.792 | 0.638 |
| 0.145 | 110. | 0.052 | 1.075 | 0.820 |
| 0.174 | 81. | 0.083 | 1.068 | 0.965 |
| 0.203 | 63. | 0.114 | 1.002 | 1.086 |
| 0.233 | 53. | 0.141 | 1.065 | 1.207 |
| 0.262 | 44. | 0.176 | 1.354 | 1.352 |
| 0.291 | 36. | 0.220 | 1.256 | 1.524 |
| 0.320 | 32. | 0.249 | 1.670 | 1.698 |
| 0.349 | 25. | 0.317 | 2.445 | 1.839 |
| 0.378 | 19. | 0.391 | 2.088 | 1.918 |
| 0.407 | 16. | 0.438 | 1.807 | 1.941 |
| 0.436 | 13. | 0.496 | 2.221 | 1.961 |
| 0.465 | 10. | 0.567 | 1.712 | 2.042 |
| 0.494 | 9. | 0.596 | 1.077 | 2.199 |
| 0.523 | 8. | 0.630 | 1.278 | 2.342 |
| 0.552 | 7. | 0.670 | 6.366 | 2.310 |
| 0.581 | 0. | 1.000 | 0.0 | 1.995 |

TABLE A-22 BUBBLE SIZE DISTRIBUTION FOR SALT WATER SYSTEM AT WINDOW #2 AND F= 90 SCFH

| DIA.(CM) | NO. OF BUBBLES | CUMUL. VOL. | PROB. DEN. | PROB. DEN. AFTER SMOOTHING |
|---|---|---|---|---|
| 0.0 | 497. | 0.0 | 0.0 | 0.0 |
| 0.029 | 493. | 0.000 | 0.025 | 0.025 |
| 0.058 | 420. | 0.001 | 0.223 | 0.301 |
| 0.087 | 295. | 0.013 | 0.611 | 0.589 |
| 0.116 | 200. | 0.037 | 0.921 | 0.859 |
| 0.145 | 145. | 0.067 | 1.301 | 1.091 |
| 0.174 | 98. | 0.113 | 1.489 | 1.265 |
| 0.203 | 73. | 0.153 | 1.466 | 1.376 |
| 0.233 | 55. | 0.198 | 1.580 | 1.438 |
| 0.262 | 42. | 0.245 | 1.418 | 1.473 |
| 0.291 | 35. | 0.280 | 1.196 | 1.500 |
| 0.320 | 30. | 0.314 | 1.821 | 1.528 |
| 0.349 | 22. | 0.386 | 1.630 | 1.553 |
| 0.378 | 20. | 0.409 | 1.145 | 1.575 |
| 0.407 | 17. | 0.453 | 2.294 | 1.622 |
| 0.436 | 12. | 0.543 | 1.546 | 1.755 |
| 0.465 | 12. | 0.543 | 0.456 | 2.024 |
| 0.494 | 11. | 0.569 | 1.542 | 2.386 |
| 0.523 | 9. | 0.632 | 3.655 | 2.666 |
| 0.552 | 5. | 0.781 | 6.328 | 2.653 |
| 0.581 | 0. | 1.000 | 0.0 | 2.261 |

TABLE A-23 BUBBLE SIZE DISTRIBUTION FOR SALT WATER SYSTEM AT WINDOW #3 AND F= 90 SCFH

| DIA.(CM) | NO. OF BUBBLES | CUMUL. VOL. | PROB. DEN. | PROB. DEN. AFTER SMOOTHING |
|---|---|---|---|---|
| 0.0 | 461. | 0.0 | 0.0 | 0.0 |
| 0.029 | 442. | 0.000 | 0.019 | 0.019 |
| 0.058 | 398. | 0.001 | 0.213 | 0.336 |
| 0.087 | 297. | 0.012 | 0.618 | 0.722 |
| 0.116 | 217. | 0.037 | 1.076 | 1.105 |
| 0.145 | 159. | 0.075 | 1.577 | 1.466 |
| 0.174 | 114. | 0.129 | 2.246 | 1.764 |
| 0.203 | 75. | 0.206 | 2.312 | 1.979 |
| 0.233 | 56. | 0.263 | 1.899 | 2.111 |
| 0.262 | 44. | 0.316 | 2.391 | 2.177 |
| 0.291 | 30. | 0.402 | 2.339 | 2.197 |
| 0.320 | 24. | 0.452 | 2.172 | 2.178 |
| 0.349 | 17. | 0.528 | 2.037 | 2.111 |
| 0.378 | 14. | 0.570 | 2.242 | 1.986 |
| 0.407 | 9. | 0.659 | 2.648 | 1.815 |
| 0.436 | 6. | 0.724 | 1.129 | 1.647 |
| 0.465 | 6. | 0.724 | 0.555 | 1.550 |
| 0.494 | 5. | 0.756 | 1.216 | 1.541 |
| 0.523 | 4. | 0.795 | 1.443 | 1.552 |
| 0.552 | 3. | 0.840 | 3.528 | 1.470 |
| 0.581 | 0. | 1.000 | 0.0 | 1.229 |

TABLE A-24 BUBBLE SIZE DISTRIBUTION FOR SALT WATER SYSTEM AT WINDOW #4 AND F= 90 SCFH

| DIA.(CM) | NO. OF BUBBLES | CUMUL. VOL. | PROB. DEN. | PROB. DEN. AFTER SMOOTHING |
|---|---|---|---|---|
| 0.0 | 540. | 0.0 | 0.0 | 0.0 |
| 0.029 | 504. | 0.000 | 0.021 | 0.021 |
| 0.058 | 440. | 0.001 | 0.175 | 0.270 |
| 0.087 | 334. | 0.010 | 0.483 | 0.592 |
| 0.116 | 252. | 0.029 | 0.848 | 0.928 |
| 0.145 | 191. | 0.059 | 1.219 | 1.269 |
| 0.174 | 146. | 0.100 | 1.828 | 1.567 |
| 0.203 | 102. | 0.166 | 2.153 | 1.778 |
| 0.233 | 76. | 0.225 | 2.516 | 1.885 |
| 0.262 | 50. | 0.312 | 2.052 | 1.929 |
| 0.291 | 43. | 0.345 | 1.209 | 1.988 |
| 0.320 | 37. | 0.382 | 1.217 | 2.122 |
| 0.349 | 33. | 0.415 | 2.575 | 2.318 |
| 0.378 | 22. | 0.532 | 3.386 | 2.487 |
| 0.407 | 16. | 0.612 | 2.803 | 2.529 |
| 0.436 | 11. | 0.695 | 3.163 | 2.400 |
| 0.465 | 6. | 0.796 | 2.579 | 2.139 |
| 0.494 | 4. | 0.845 | 0.839 | 1.829 |
| 0.523 | 4. | 0.845 | 0.591 | 1.533 |
| 0.552 | 3. | 0.879 | 2.669 | 1.252 |
| 0.581 | 0. | 1.000 | 0.0 | 0.957 |

TABLE A-25 BUBBLE SIZE DISTRIBUTION FOR 0.5% CMC SYSTEM AT WINDOW #1 AND F= 30 SCFH

| DIA.(CM) | NO. OF BUBBLES | CUMUL. VOL. | PROB. DEN. | PROB. DEN. AFTER SMOOTHING |
|---|---|---|---|---|
| 0.0 | 365. | 0.0 | 0.0 | 0.0 |
| 0.048 | 365. | 0.0 | 0.0 | 0.0 |
| 0.096 | 365. | 0.0 | 0.373 | 0.247 |
| 0.144 | 142. | 0.036 | 0.649 | 0.374 |
| 0.192 | 82. | 0.062 | 0.569 | 0.468 |
| 0.240 | 52. | 0.090 | 0.471 | 0.515 |
| 0.288 | 42. | 0.108 | 0.532 | 0.535 |
| 0.336 | 30. | 0.141 | 0.670 | 0.541 |
| 0.384 | 23. | 0.172 | 0.448 | 0.545 |
| 0.432 | 21. | 0.184 | 0.499 | 0.556 |
| 0.480 | 17. | 0.220 | 0.616 | 0.577 |
| 0.528 | 15. | 0.243 | 0.411 | 0.604 |
| 0.576 | 14. | 0.259 | 0.791 | 0.629 |
| 0.624 | 11. | 0.319 | 0.892 | 0.653 |
| 0.672 | 10. | 0.345 | 0.591 | 0.705 |
| 0.720 | 9. | 0.376 | 0.327 | 0.841 |
| 0.768 | 9. | 0.376 | 0.482 | 1.105 |
| 0.816 | 8. | 0.422 | 1.056 | 1.465 |
| 0.863 | 7. | 0.477 | 1.253 | 1.785 |
| 0.911 | 6. | 0.542 | 5.447 | 1.889 |
| 0.959 | 0. | 1.000 | 0.0 | 1.685 |

TABLE A-26 BUBBLE SIZE DISTRIBUTION FOR 0.5% CMC SYSTEM AT WINDOW #2 AND F= 30 SCFH

| DIA.(CM) | NO. OF BUBBLES | CUMUL. VOL. | PROB. DEN. | PROB. DEN. AFTER SMOOTHING |
|---|---|---|---|---|
| 0.0 | 522. | 0.0 | 0.0 | 0.0 |
| 0.038 | 522. | 0.0 | 0.0 | 0.0 |
| 0.077 | 522. | 0.0 | 0.540 | 0.370 |
| 0.115 | 201. | 0.041 | 1.012 | 0.543 |
| 0.154 | 99. | 0.078 | 0.844 | 0.650 |
| 0.192 | 61. | 0.106 | 0.821 | 0.661 |
| 0.230 | 36. | 0.141 | 0.655 | 0.610 |
| 0.269 | 29. | 0.157 | 0.434 | 0.537 |
| 0.307 | 24. | 0.174 | 0.426 | 0.482 |
| 0.345 | 21. | 0.189 | 0.199 | 0.469 |
| 0.384 | 21. | 0.189 | 0.249 | 0.501 |
| 0.422 | 19. | 0.208 | 0.741 | 0.555 |
| 0.461 | 16. | 0.246 | 0.913 | 0.602 |
| 0.499 | 14. | 0.278 | 0.686 | 0.644 |
| 0.537 | 13. | 0.299 | 0.594 | 0.736 |
| 0.576 | 12. | 0.324 | 0.329 | 0.970 |
| 0.614 | 12. | 0.324 | 0.0 | 1.399 |
| 0.652 | 12. | 0.324 | 1.733 | 1.957 |
| 0.691 | 9. | 0.457 | 2.415 | 2.432 |
| 0.729 | 8. | 0.509 | 7.074 | 2.578 |
| 0.768 | 0. | 1.000 | 0.0 | 2.285 |

TABLE A-27 BUBBLE SIZE DISTRIBUTION FOR 0.5% CMC SYSTEM AT WINDOW #3 AND F= 30 SCFH

| DIA.(CM) | NO. OF BUBBLES | CUMUL. VOL. | PROB. DEN. | PROB. DEN. AFTER SMOOTHING |
|---|---|---|---|---|
| 0.0 | 499. | 0.0 | 0.0 | 0.0 |
| 0.038 | 499. | 0.0 | 0.0 | 0.0 |
| 0.077 | 499. | 0.0 | 0.650 | 0.447 |
| 0.115 | 200. | 0.050 | 1.158 | 0.690 |
| 0.154 | 115. | 0.089 | 1.015 | 0.873 |
| 0.192 | 75. | 0.128 | 1.110 | 0.971 |
| 0.230 | 49. | 0.174 | 0.946 | 1.023 |
| 0.269 | 40. | 0.200 | 0.931 | 1.059 |
| 0.307 | 30. | 0.246 | 1.186 | 1.096 |
| 0.345 | 23. | 0.291 | 1.076 | 1.139 |
| 0.384 | 19. | 0.328 | 1.283 | 1.180 |
| 0.422 | 14. | 0.390 | 1.017 | 1.206 |
| 0.461 | 13. | 0.406 | 1.571 | 1.200 |
| 0.499 | 8. | 0.511 | 1.359 | 1.156 |
| 0.537 | 8. | 0.511 | 0.849 | 1.090 |
| 0.576 | 6. | 0.576 | 1.367 | 1.057 |
| 0.614 | 5. | 0.615 | 0.518 | 1.124 |
| 0.652 | 5. | 0.615 | 0.0 | 1.309 |
| 0.691 | 5. | 0.615 | 0.881 | 1.526 |
| 0.729 | 4. | 0.683 | 5.010 | 1.616 |
| 0.768 | 0. | 1.000 | 0.0 | 1.464 |

TABLE A-28 BUBBLE SIZE DISTRIBUTION FOR 0.5% CMC SYSTEM AT WINDOW #4 AND F= 30 SCFH

| DIA.(CM) | NO. OF BUBBLES | CUMUL. VOL. | PROB. DEN. | PROB. DEN. AFTER SMOOTHING |
|---|---|---|---|---|
| 0.0 | 381. | 0.0 | 0.0 | 0.0 |
| 0.038 | 381. | 0.0 | 0.0 | 0.0 |
| 0.077 | 381. | 0.0 | 0.606 | 0.456 |
| 0.115 | 167. | 0.046 | 1.242 | 0.701 |
| 0.154 | 85. | 0.095 | 1.264 | 0.878 |
| 0.192 | 47. | 0.143 | 0.898 | 0.958 |
| 0.230 | 38. | 0.164 | 0.818 | 0.979 |
| 0.269 | 27. | 0.206 | 1.158 | 0.970 |
| 0.307 | 19. | 0.253 | 0.945 | 0.947 |
| 0.345 | 16. | 0.279 | 0.955 | 0.919 |
| 0.384 | 12. | 0.326 | 0.831 | 0.896 |
| 0.422 | 11. | 0.343 | 0.761 | 0.891 |
| 0.461 | 9. | 0.385 | 0.905 | 0.914 |
| 0.499 | 8. | 0.412 | 0.799 | 0.972 |
| 0.537 | 7. | 0.446 | 0.998 | 1.070 |
| 0.576 | 6. | 0.489 | 1.226 | 1.217 |
| 0.614 | 5. | 0.540 | 1.488 | 1.424 |
| 0.652 | 4. | 0.603 | 0.814 | 1.668 |
| 0.691 | 4. | 0.603 | 1.147 | 1.859 |
| 0.729 | 3. | 0.691 | 5.175 | 1.869 |
| 0.768 | 0. | 1.000 | 0.0 | 1.625 |

TABLE A-29 BUBBLE SIZE DISTRIBUTION FOR 0.5% CMC SYSTEM AT WINDOW #1 AND F= 60 SCFH

| DIA.(CM) | NO. OF BUBBLES | CUMUL. VOL. | PROB. DEN. | PROB. DEN. AFTER SMOOTHING |
|---|---|---|---|---|
| 0.0 | 422. | 0.0 | 0.0 | 0.0 |
| 0.072 | 422. | 0.0 | 0.122 | 0.122 |
| 0.144 | 124. | 0.018 | 0.232 | 0.184 |
| 0.216 | 66. | 0.033 | 0.235 | 0.216 |
| 0.288 | 42. | 0.051 | 0.291 | 0.238 |
| 0.360 | 27. | 0.075 | C.307 | 0.248 |
| 0.432 | 20. | 0.096 | 0.208 | 0.254 |
| 0.504 | 18. | 0.105 | 0.169 | 0.265 |
| 0.576 | 16. | 0.120 | 0.326 | 0.288 |
| 0.648 | 13. | 0.152 | 0.224 | 0.327 |
| 0.720 | 13. | 0.152 | 0.422 | 0.389 |
| 0.792 | 10. | 0.213 | 0.422 | 0.477 |
| 0.863 | 10. | 0.213 | 0.237 | 0.584 |
| 0.935 | 9. | 0.247 | 0.834 | 0.697 |
| 1.007 | 7. | 0.333 | 1.337 | 0.797 |
| 1.079 | 5. | 0.439 | 0.740 | 0.885 |
| 1.151 | 5. | 0.439 | 0.545 | 0.974 |
| 1.223 | 4. | 0.518 | 1.196 | 1.065 |
| 1.295 | 3. | 0.611 | 0.650 | 1.118 |
| 1.367 | 3. | 0.611 | 2.700 | 1.074 |
| 1.439 | 0. | 1.000 | 0.0 | 0.903 |

TABLE A-30 BUBBLE SIZE DISTRIBUTION FOR 0.5% CMC SYSTEM AT WINDOW #2 AND F= 60 SCFH

| DIA.(CM) | NO. OF BUBBLES | CUMUL. VOL. | PROB. DEN. | PROB. DEN. AFTER SMOOTHING |
|---|---|---|---|---|
| 0.0 | 708. | 0.0 | 0.0 | 0.0 |
| 0.048 | 708. | 0.0 | 0.356 | 0.356 |
| 0.096 | 211. | 0.034 | 0.731 | 0.550 |
| 0.144 | 98. | 0.070 | 0.748 | 0.646 |
| 0.192 | 57. | 0.106 | 0.702 | 0.719 |
| 0.240 | 40. | 0.137 | 0.894 | 0.755 |
| 0.288 | 24. | 0.192 | 0.740 | 0.768 |
| 0.336 | 21. | 0.208 | 0.802 | 0.769 |
| 0.384 | 14. | 0.269 | 0.887 | 0.777 |
| 0.432 | 12. | 0.294 | 0.443 | 0.814 |
| 0.480 | 11. | 0.311 | 0.673 | 0.894 |
| 0.528 | 9. | 0.358 | 1.137 | 1.009 |
| 0.576 | 7. | 0.420 | 1.060 | 1.124 |
| 0.624 | 6. | 0.460 | 1.459 | 1.193 |
| 0.672 | 4. | 0.560 | 1.691 | 1.182 |
| 0.720 | 3. | 0.622 | 1.437 | 1.103 |
| 0.768 | 2. | 0.698 | 0.790 | 1.015 |
| 0.816 | 2. | 0.698 | 0.0 | 0.979 |
| 0.863 | 2. | 0.698 | 0.0 | 0.994 |
| 0.911 | 2. | 0.698 | 3.148 | 0.986 |
| 0.959 | 0. | 1.000 | 0.0 | 0.877 |

TABLE A-31 BUBBLE SIZE DISTRIBUTION FOR 0.5% CMC SYSTEM AT WINDOW #3 AND F= 60 SCFH

| DIA.(CM) | NO. OF BUBBLES | CUMUL. VOL. | PROB. DEN. | PROB. DEN. AFTER SMOOTHING |
|---|---|---|---|---|
| 0.0 | 667. | 0.0 | 0.0 | 0.0 |
| 0.038 | 667. | 0.0 | 0.0 | 0.0 |
| 0.077 | 667. | 0.0 | 0.492 | 0.396 |
| 0.115 | 312. | 0.038 | 1.036 | 0.634 |
| 0.154 | 169. | 0.080 | 1.070 | 0.809 |
| 0.192 | 104. | 0.120 | 1.028 | 0.889 |
| 0.230 | 70. | 0.158 | 0.989 | 0.899 |
| 0.269 | 50. | 0.196 | 0.862 | 0.872 |
| 0.307 | 40. | 0.225 | 0.756 | 0.842 |
| 0.345 | 33. | 0.254 | 0.686 | 0.839 |
| 0.384 | 29. | 0.277 | 0.715 | 0.877 |
| 0.422 | 25. | 0.309 | 0.816 | 0.954 |
| 0.461 | 22. | 0.340 | 1.271 | 1.060 |
| 0.499 | 17. | 0.406 | 1.303 | 1.187 |
| 0.537 | 15. | 0.440 | 0.707 | 1.328 |
| 0.576 | 14. | 0.461 | 1.592 | 1.478 |
| 0.614 | 10. | 0.562 | 2.518 | 1.628 |
| 0.652 | 7. | 0.654 | 1.196 | 1.755 |
| 0.691 | 7. | 0.654 | 0.562 | 1.807 |
| 0.729 | 6. | 0.697 | 4.510 | 1.715 |
| 0.768 | 0. | 1.000 | 0.0 | 1.440 |

TABLE A-32 BUBBLE SIZE DISTRIBUTION FOR 0.5% CMC SYSTEM AT WINDOW #4 AND F= 60 SCFH

| DIA.(CM) | NO. OF BUBBLES | CUMUL. VOL. | PROB. DEN. | PROB. DEN. AFTER SMOOTHING |
|---|---|---|---|---|
| 0.0 | 954. | 0.0 | 0.0 | 0.0 |
| 0.038 | 954. | 0.0 | 0.156 | 0.156 |
| 0.077 | 492. | 0.012 | 0.534 | 0.445 |
| 0.115 | 250. | 0.041 | 0.811 | 0.637 |
| 0.154 | 149. | 0.074 | 0.934 | 0.785 |
| 0.192 | 94. | 0.113 | 1.084 | 0.864 |
| 0.230 | 59. | 0.157 | 1.077 | 0.886 |
| 0.269 | 41. | 0.195 | 0.790 | 0.874 |
| 0.307 | 34. | 0.218 | 0.602 | 0.852 |
| 0.345 | 29. | 0.242 | 0.907 | 0.834 |
| 0.384 | 22. | 0.288 | 0.948 | 0.818 |
| 0.422 | 19. | 0.314 | 0.804 | 0.801 |
| 0.461 | 16. | 0.349 | 0.847 | 0.797 |
| 0.499 | 14. | 0.379 | 0.637 | 0.834 |
| 0.537 | 13. | 0.398 | 0.246 | 0.941 |
| 0.576 | 13. | 0.398 | 1.117 | 1.134 |
| 0.614 | 10. | 0.484 | 2.016 | 1.408 |
| 0.652 | 8. | 0.553 | 0.899 | 1.715 |
| 0.691 | 8. | 0.553 | 0.633 | 1.955 |
| 0.729 | 7. | 0.602 | 5.824 | 1.993 |
| 0.768 | 0. | 1.000 | 0.0 | 1.751 |

TABLE A-33 BUBBLE SIZE DISTRIBUTION FOR 0.5% CMC SYSTEM AT WINDOW #1 AND F= 90 SCFH

| DIA.(CM) | NO. OF BUBBLES | CUMUL. VOL. | PROB. DEN. | PROB. DEN. AFTER SMOOTHING |
|---|---|---|---|---|
| 0.0 | 1836. | 0.0 | 0.0 | 0.0 |
| 0.073 | 456. | 0.004 | 0.228 | 0.228 |
| 0.145 | 124. | 0.033 | 0.384 | 0.292 |
| 0.218 | 56. | 0.060 | 0.353 | 0.307 |
| 0.291 | 34. | 0.084 | 0.359 | 0.316 |
| 0.363 | 22. | 0.112 | 0.280 | 0.323 |
| 0.436 | 19. | 0.125 | 0.233 | 0.349 |
| 0.509 | 16. | 0.146 | 0.294 | 0.411 |
| 0.581 | 14. | 0.168 | 0.365 | 0.513 |
| 0.654 | 12. | 0.199 | 0.367 | 0.630 |
| 0.727 | 11. | 0.221 | 1.170 | 0.719 |
| 0.799 | 6. | 0.369 | 1.555 | 0.747 |
| 0.872 | 4. | 0.447 | 0.536 | 0.717 |
| 0.945 | 4. | 0.447 | 0.0 | 0.666 |
| 1.017 | 4. | 0.447 | 0.537 | 0.628 |
| 1.090 | 3. | 0.525 | 1.192 | 0.621 |
| 1.163 | 2. | 0.620 | 0.656 | 0.649 |
| 1.235 | 2. | 0.620 | 0.0 | 0.712 |
| 1.308 | 2. | 0.620 | 0.0 | 0.783 |
| 1.381 | 2. | 0.620 | 2.611 | 0.805 |
| 1.453 | 0. | 1.000 | 0.0 | 0.724 |

TABLE A-34 BUBBLE SIZE DISTRIBUTION FOR 0.5% CMC SYSTEM AT WINDOW #2 AND F= 90 SCFH

| DIA.(CM) | NO. OF BUBBLES | CUMUL. VOL. | PROB. DEN. | PROB. DEN. AFTER SMOOTHING |
|---|---|---|---|---|
| 0.0 | 1109. | 0.0 | 0.0 | 0.0 |
| 0.048 | 680. | 0.002 | 0.521 | 0.521 |
| 0.097 | 203. | 0.051 | 1.127 | 0.797 |
| 0.145 | 76. | 0.111 | 1.213 | 0.839 |
| 0.194 | 32. | 0.168 | 1.048 | 0.823 |
| 0.242 | 16. | 0.212 | 0.718 | 0.729 |
| 0.291 | 11. | 0.238 | 0.433 | 0.604 |
| 0.339 | 9. | 0.254 | 0.437 | 0.479 |
| 0.388 | 7. | 0.280 | 0.457 | 0.383 |
| 0.436 | 6. | 0.299 | 0.192 | 0.344 |
| 0.484 | 6. | 0.299 | 0.0 | 0.396 |
| 0.533 | 6. | 0.299 | 0.0 | 0.564 |
| 0.581 | 6. | 0.299 | 0.612 | 0.837 |
| 0.630 | 5. | 0.358 | 1.383 | 1.158 |
| 0.678 | 4. | 0.433 | 1.727 | 1.439 |
| 0.727 | 3. | 0.525 | 2.123 | 1.600 |
| 0.775 | 2. | 0.638 | 2.575 | 1.610 |
| 0.824 | 1. | 0.775 | 1.408 | 1.495 |
| 0.872 | 1. | 0.775 | 0.0 | 1.305 |
| 0.921 | 1. | 0.775 | 2.324 | 1.074 |
| 0.969 | 0. | 1.000 | 0.0 | 0.817 |

TABLE A-35 BUBBLE SIZE DISTRIBUTION FOR 0.5% CMC SYSTEM AT WINDOW #3 AND F= 90 SCFH

| DIA.(CM) | NO. OF BUBBLES | CUMUL. VOL. | PROB. DEN. | PROB. DEN. AFTER SMOOTHING |
|---|---|---|---|---|
| 0.0 | 2015. | 0.0 | 0.0 | 0.0 |
| 0.039 | 1592. | 0.001 | 0.643 | 0.643 |
| 0.078 | 598. | 0.050 | 1.651 | 1.224 |
| 0.116 | 253. | 0.129 | 1.972 | 1.504 |
| 0.155 | 135. | 0.203 | 2.004 | 1.700 |
| 0.194 | 74. | 0.284 | 1.834 | 1.769 |
| 0.233 | 49. | 0.345 | 1.718 | 1.746 |
| 0.271 | 31. | 0.417 | 1.888 | 1.647 |
| 0.310 | 19. | 0.491 | 1.999 | 1.492 |
| 0.349 | 10. | 0.572 | 1.043 | 1.315 |
| 0.388 | 10. | 0.572 | 0.655 | 1.159 |
| 0.426 | 7. | 0.623 | 0.943 | 1.046 |
| 0.465 | 6. | 0.645 | 1.024 | 0.964 |
| 0.504 | 4. | 0.702 | 1.202 | 0.874 |
| 0.543 | 3. | 0.738 | 1.040 | 0.758 |
| 0.581 | 2. | 0.783 | 0.575 | 0.643 |
| 0.620 | 2. | 0.783 | 0.0 | 0.588 |
| 0.659 | 2. | 0.783 | 0.0 | 0.630 |
| 0.698 | 2. | 0.783 | 0.0 | 0.733 |
| 0.736 | 2. | 0.783 | 2.799 | 0.800 |
| 0.775 | 0. | 1.000 | 0.0 | 0.748 |

TABLE A-36 BUBBLE SIZE DISTRIBUTION FOR 0.5% CMC SYSTEM AT WINDOW #4 AND F= 90 SCFH

| DIA.(CM) | NO. OF BUBBLES | CUMUL. VOL. | PROB. DEN. | PROB. DEN. AFTER SMOOTHING |
|---|---|---|---|---|
| 0.0 | 1115. | 0.0 | 0.0 | 0.0 |
| 0.039 | 964. | 0.000 | 0.194 | 0.194 |
| 0.078 | 493. | 0.015 | 0.604 | 0.551 |
| 0.116 | 274. | 0.047 | 1.001 | 0.814 |
| 0.155 | 160. | 0.093 | 1.302 | 1.027 |
| 0.194 | 95. | 0.148 | 1.334 | 1.156 |
| 0.233 | 64. | 0.196 | 1.415 | 1.204 |
| 0.271 | 40. | 0.258 | 1.353 | 1.187 |
| 0.310 | 29. | 0.301 | 1.003 | 1.134 |
| 0.349 | 23. | 0.335 | 0.960 | 1.067 |
| 0.388 | 18. | 0.375 | 1.074 | 0.997 |
| 0.426 | 14. | 0.419 | 0.924 | 0.924 |
| 0.465 | 12. | 0.447 | 1.072 | 0.853 |
| 0.504 | 9. | 0.502 | 0.706 | 0.809 |
| 0.543 | 9. | 0.502 | 0.367 | 0.838 |
| 0.581 | 8. | 0.530 | 0.367 | 0.983 |
| 0.620 | 8. | 0.530 | 1.082 | 1.239 |
| 0.659 | 6. | 0.614 | 1.727 | 1.534 |
| 0.698 | 5. | 0.664 | 1.408 | 1.739 |
| 0.736 | 4. | 0.723 | 4.334 | 1.731 |
| 0.775 | 0. | 1.000 | 0.0 | 1.474 |

TABLE A-37 BUBBLE SIZE DISTRIBUTION FOR 0.8% CMC SYSTEM AT WINDOW #1 AND F= 30 SCFH

| DIA.(CM) | NO. OF BUBBLES | CUMUL. VOL. | PROB. DEN. | PROB. DEN. AFTER SMOOTHING |
|---|---|---|---|---|
| 0.0 | 938. | 0.0 | 0.0 | 0.0 |
| 0.048 | 938. | 0.0 | 0.115 | 0.115 |
| 0.096 | 424. | 0.011 | 0.343 | 0.268 |
| 0.144 | 205. | 0.033 | 0.461 | 0.364 |
| 0.192 | 123. | 0.055 | 0.470 | 0.440 |
| 0.240 | 84. | 0.078 | 0.546 | 0.484 |
| 0.288 | 56. | 0.108 | 0.584 | 0.495 |
| 0.336 | 41. | 0.134 | 0.555 | 0.476 |
| 0.384 | 31. | 0.161 | 0.567 | 0.434 |
| 0.432 | 24. | 0.188 | 0.286 | 0.389 |
| 0.480 | 24. | 0.188 | 0.077 | 0.356 |
| 0.528 | 23. | 0.196 | 0.380 | 0.341 |
| 0.576 | 20. | 0.225 | 0.433 | 0.343 |
| 0.624 | 19. | 0.237 | 0.457 | 0.374 |
| 0.672 | 17. | 0.269 | 0.327 | 0.481 |
| 0.720 | 17. | 0.269 | 0.0 | 0.739 |
| 0.768 | 17. | 0.269 | 0.0 | 1.185 |
| 0.816 | 17. | 0.269 | 1.426 | 1.739 |
| 0.863 | 13. | 0.406 | 2.689 | 2.198 |
| 0.911 | 10. | 0.527 | 6.195 | 2.336 |
| 0.959 | 0. | 1.000 | 0.0 | 2.064 |

TABLE A-38 BUBBLE SIZE DISTRIBUTION FOR 0.8% CMC SYSTEM AT WINDOW #2 AND F= 30 SCFH

| DIA.(CM) | NO. OF BUBBLES | CUMUL. VOL. | PROB. DEN. | PROB. DEN. AFTER SMOOTHING |
|---|---|---|---|---|
| 0.0 | 731. | 0.0 | 0.0 | 0.0 |
| 0.038 | 731. | 0.0 | 0.0 | 0.0 |
| 0.077 | 731. | 0.0 | 0.583 | 0.463 |
| 0.115 | 334. | 0.045 | 1.196 | 0.736 |
| 0.154 | 182. | 0.092 | 1.272 | 0.932 |
| 0.192 | 105. | 0.142 | 1.238 | 1.017 |
| 0.230 | 68. | 0.187 | 1.043 | 1.025 |
| 0.269 | 50. | 0.222 | 0.941 | 1.006 |
| 0.307 | 38. | 0.259 | 0.822 | 1.003 |
| 0.345 | 32. | 0.286 | 0.669 | 1.026 |
| 0.384 | 28. | 0.310 | 1.084 | 1.045 |
| 0.422 | 21. | 0.369 | 1.906 | 1.015 |
| 0.461 | 13. | 0.457 | 1.327 | 0.921 |
| 0.499 | 12. | 0.471 | 0.184 | 0.814 |
| 0.537 | 12. | 0.471 | 0.287 | 0.795 |
| 0.576 | 11. | 0.493 | 0.287 | 0.953 |
| 0.614 | 11. | 0.493 | 0.422 | 1.294 |
| 0.652 | 10. | 0.525 | 1.934 | 1.707 |
| 0.691 | 7. | 0.641 | 2.702 | 2.005 |
| 0.729 | 5. | 0.732 | 4.676 | 2.019 |
| 0.768 | 0. | 1.000 | 0.0 | 1.714 |

TABLE A-39 BUBBLE SIZE DISTRIBUTION FOR 0.8% CMC SYSTEM AT WINDOW #3 AND F= 30 SCFH

| DIA.(CM) | NO. OF BUBBLES | CUMUL. VOL. | PROB. DEN. | PROB. DEN. AFTER SMOOTHING |
|---|---|---|---|---|
| 0.0 | 956. | 0.0 | 0.0 | 0.0 |
| 0.038 | 956. | 0.0 | 0.111 | 0.111 |
| 0.077 | 557. | 0.009 | 0.412 | 0.391 |
| 0.115 | 325. | 0.032 | 0.733 | 0.626 |
| 0.154 | 203. | 0.065 | 0.916 | 0.834 |
| 0.192 | 139. | 0.102 | 1.130 | 0.996 |
| 0.230 | 92. | 0.152 | 1.307 | 1.106 |
| 0.269 | 63. | 0.202 | 1.218 | 1.162 |
| 0.307 | 47. | 0.245 | 1.169 | 1.166 |
| 0.345 | 35. | 0.292 | 1.320 | 1.123 |
| 0.384 | 25. | 0.346 | 1.285 | 1.040 |
| 0.422 | 19. | 0.391 | 0.701 | 0.932 |
| 0.461 | 18. | 0.400 | 0.773 | 0.822 |
| 0.499 | 14. | 0.450 | 0.850 | 0.740 |
| 0.537 | 13. | 0.465 | 0.456 | 0.725 |
| 0.576 | 12. | 0.485 | 0.252 | 0.823 |
| 0.614 | 12. | 0.485 | 0.744 | 1.057 |
| 0.652 | 10. | 0.542 | 1.187 | 1.389 |
| 0.691 | 9. | 0.576 | 0.444 | 1.692 |
| 0.729 | 9. | 0.576 | 5.525 | 1.801 |
| 0.768 | 0. | 1.000 | 0.0 | 1.621 |

TABLE A-40 BUBBLE SIZE DISTRIBUTION FOR 0.8% CMC SYSTEM AT WINDOW #4 AND F= 30 SCFH

| DIA.(CM) | NO. OF BUBBLES | CUMUL. VOL. | PROB. DEN. | PROB. DEN. AFTER SMOOTHING |
|---|---|---|---|---|
| 0.0 | 579. | 0.0 | 0.0 | 0.0 |
| 0.038 | 579. | 0.0 | 0.0 | 0.0 |
| 0.077 | 579. | 0.0 | 0.447 | 0.519 |
| 0.115 | 347. | 0.034 | 1.409 | 0.892 |
| 0.154 | 165. | 0.108 | 1.760 | 1.179 |
| 0.192 | 94. | 0.169 | 1.496 | 1.328 |
| 0.230 | 60. | 0.223 | 1.443 | 1.350 |
| 0.269 | 38. | 0.280 | 1.526 | 1.268 |
| 0.307 | 23. | 0.340 | 1.311 | 1.119 |
| 0.345 | 16. | 0.381 | 0.847 | 0.942 |
| 0.384 | 13. | 0.405 | 0.460 | 0.774 |
| 0.422 | 12. | 0.416 | 0.518 | 0.637 |
| 0.461 | 10. | 0.445 | 0.616 | 0.539 |
| 0.499 | 9. | 0.463 | 0.544 | 0.488 |
| 0.537 | 8. | 0.487 | 0.303 | 0.514 |
| 0.576 | 8. | 0.487 | 0.0 | 0.675 |
| 0.614 | 8. | 0.487 | 0.554 | 1.009 |
| 0.652 | 7. | 0.529 | 0.554 | 1.469 |
| 0.691 | 7. | 0.529 | 1.562 | 1.888 |
| 0.729 | 5. | 0.649 | 6.134 | 2.058 |
| 0.768 | 0. | 1.000 | 0.0 | 1.865 |

TABLE A-41 BUBBLE SIZE DISTRIBUTION FOR 0.8% CMC SYSTEM AT WINDOW #1 AND F= 60 SCFH

| DIA.(CM) | NO. OF BUBBLES | CUMUL. VOL. | PROB. DEN. | PROB. DEN. AFTER SMOOTHING |
|---|---|---|---|---|
| 0.0 | 366. | 0.0 | 0.0 | 0.0 |
| 0.071 | 366. | 0.0 | 0.106 | 0.106 |
| 0.143 | 80. | 0.015 | 0.174 | 0.129 |
| 0.214 | 40. | 0.025 | 0.144 | 0.134 |
| 0.286 | 24. | 0.036 | 0.145 | 0.137 |
| 0.357 | 17. | 0.046 | 0.106 | 0.136 |
| 0.429 | 15. | 0.051 | 0.097 | 0.135 |
| 0.500 | 13. | 0.060 | 0.199 | 0.128 |
| 0.572 | 10. | 0.079 | 0.206 | 0.114 |
| 0.643 | 9. | 0.089 | 0.067 | 0.096 |
| 0.715 | 9. | 0.089 | 0.0 | 0.087 |
| 0.786 | 9. | 0.089 | 0.0 | 0.099 |
| 0.858 | 9. | 0.089 | 0.0 | 0.136 |
| 0.929 | 9. | 0.089 | 0.270 | 0.196 |
| 1.001 | 8. | 0.128 | 0.270 | 0.285 |
| 1.072 | 8. | 0.128 | 0.409 | 0.432 |
| 1.144 | 7. | 0.186 | 0.409 | 0.681 |
| 1.215 | 7. | 0.186 | 0.0 | 1.036 |
| 1.287 | 7. | 0.186 | 0.0 | 1.402 |
| 1.358 | 7. | 0.186 | 5.694 | 1.606 |
| 1.430 | 0. | 1.000 | 0.0 | 1.520 |

TABLE A-42 BUBBLE SIZE DISTRIBUTION FOR 0.8% CMC SYSTEM AT WINDOW #2 AND F= 60 SCFH

| DIA.(CM) | NO. OF BUBBLES | CUMUL. VOL. | PROB. DEN. | PROB. DEN. AFTER SMOOTHING |
|---|---|---|---|---|
| 0.0 | 516. | 0.0 | 0.0 | 0.0 |
| 0.038 | 473. | 0.000 | 0.144 | 0.144 |
| 0.076 | 273. | 0.011 | 0.561 | 0.501 |
| 0.114 | 146. | 0.043 | 0.917 | 0.780 |
| 0.152 | 91. | 0.081 | 1.190 | 1.014 |
| 0.191 | 55. | 0.134 | 1.395 | 1.166 |
| 0.229 | 35. | 0.187 | 1.456 | 1.219 |
| 0.267 | 22. | 0.245 | 1.555 | 1.172 |
| 0.305 | 13. | 0.306 | 1.190 | 1.050 |
| 0.343 | 10. | 0.335 | 0.751 | 0.900 |
| 0.381 | 8. | 0.363 | 0.362 | 0.767 |
| 0.419 | 8. | 0.363 | 0.321 | 0.672 |
| 0.457 | 7. | 0.387 | 1.146 | 0.608 |
| 0.496 | 5. | 0.450 | 0.825 | 0.569 |
| 0.534 | 5. | 0.450 | 0.0 | 0.580 |
| 0.572 | 5. | 0.450 | 0.0 | 0.699 |
| 0.610 | 5. | 0.450 | 0.948 | 0.969 |
| 0.648 | 4. | 0.523 | C.948 | 1.358 |
| 0.686 | 4. | 0.523 | 0.0 | 1.732 |
| 0.724 | 4. | 0.523 | 6.261 | 1.901 |
| 0.762 | 0. | 1.000 | 0.0 | 1.748 |

TABLE A-43 BUBBLE SIZE DISTRIBUTION FOR 0.8% CMC SYSTEM AT WINDOW #3 AND F= 60 SCFH

| DIA.(CM) | NO. OF BUBBLES | CUMUL. VOL. | PROB. DEN. | PROB. DEN. AFTER SMOOTHING |
|---|---|---|---|---|
| 0.0 | 485. | 0.0 | 0.0 | 0.0 |
| 0.038 | 429. | 0.000 | 0.026 | 0.026 |
| 0.076 | 348. | 0.002 | 0.137 | 0.245 |
| 0.114 | 272. | 0.010 | 0.409 | 0.508 |
| 0.152 | 198. | 0.033 | 0.879 | 0.754 |
| 0.191 | 130. | 0.078 | 1.252 | 0.965 |
| 0.229 | 87. | 0.129 | 1.341 | 1.116 |
| 0.267 | 61. | 0.180 | 1.264 | 1.202 |
| 0.305 | 46. | 0.225 | 1.227 | 1.235 |
| 0.343 | 35. | 0.273 | 1.358 | 1.229 |
| 0.381 | 26. | 0.329 | 1.267 | 1.200 |
| 0.419 | 21. | 0.370 | 0.971 | 1.158 |
| 0.457 | 18. | 0.403 | 1.344 | 1.114 |
| 0.496 | 13. | 0.472 | 0.916 | 1.081 |
| 0.534 | 13. | 0.472 | 0.858 | 1.072 |
| 0.572 | 10. | 0.538 | 1.207 | 1.108 |
| 0.610 | 9. | 0.564 | 1.192 | 1.211 |
| 0.648 | 7. | 0.629 | 0.843 | 1.376 |
| 0.686 | 7. | 0.629 | 0.0 | 1.535 |
| 0.724 | 7. | 0.629 | 4.869 | 1.571 |
| 0.762 | 0. | 1.000 | 0.0 | 1.397 |

TABLE A-44 BUBBLE SIZE DISTRIBUTION FOR 0.8% CMC SYSTEM AT WINDOW #4 AND F= 60 SCFH

| DIA.(CM) | NO. OF BUBBLES | CUMUL. VOL. | PROB. DEN. | PROB. DEN. AFTER SMOOTHING |
|---|---|---|---|---|
| 0.0 | 937. | 0.0 | 0.0 | 0.0 |
| 0.038 | 751. | 0.000 | 0.196 | 0.196 |
| 0.076 | 368. | 0.015 | 0.589 | 0.510 |
| 0.114 | 198. | 0.045 | 0.908 | 0.731 |
| 0.152 | 118. | 0.084 | 1.097 | 0.917 |
| 0.191 | 75. | 0.129 | 1.205 | 1.052 |
| 0.229 | 50. | 0.176 | 1.031 | 1.146 |
| 0.267 | 40. | 0.207 | 1.102 | 1.203 |
| 0.305 | 29. | 0.260 | 1.701 | 1.218 |
| 0.343 | 18. | 0.337 | 1.264 | 1.185 |
| 0.381 | 16. | 0.357 | 1.120 | 1.111 |
| 0.419 | 11. | 0.422 | 1.091 | 1.021 |
| 0.457 | 10. | 0.440 | 0.518 | 0.952 |
| 0.496 | 9. | 0.462 | 1.026 | 0.931 |
| 0.534 | 7. | 0.518 | 0.734 | 0.976 |
| 0.572 | 7. | 0.518 | 0.556 | 1.087 |
| 0.610 | 6. | 0.560 | 1.896 | 1.249 |
| 0.648 | 4. | 0.663 | 1.341 | 1.429 |
| 0.686 | 4. | 0.663 | 0.0 | 1.555 |
| 0.724 | 4. | 0.663 | 4.426 | 1.539 |
| 0.762 | 0. | 1.000 | 0.0 | 1.330 |

TABLE A-45 BUBBLE SIZE DISTRIBUTION FOR 0.8% CMC SYSTEM AT WINDOW #1 AND F= 90 SCFH

| DIA.(CM) | NO. OF BUBBLES | CUMUL. VOL. | PROB. DEN. | PROB. DEN. AFTER SMOOTHING |
|---|---|---|---|---|
| 0.0 | 395. | 0.0 | 0.0 | 0.0 |
| 0.038 | 356. | 0.000 | 0.029 | 0.029 |
| 0.076 | 258. | 0.002 | 0.165 | 0.166 |
| 0.114 | 157. | 0.013 | 0.330 | 0.283 |
| 0.152 | 105. | 0.027 | 0.454 | 0.383 |
| 0.190 | 72. | 0.047 | 0.549 | 0.454 |
| 0.228 | 52. | 0.069 | 0.598 | 0.492 |
| 0.266 | 39. | 0.093 | 0.565 | 0.502 |
| 0.304 | 32. | 0.112 | 0.522 | 0.497 |
| 0.342 | 27. | 0.132 | 0.340 | 0.495 |
| 0.380 | 26. | 0.138 | 0.375 | 0.505 |
| 0.418 | 23. | 0.161 | 0.565 | 0.525 |
| 0.456 | 21. | 0.181 | 0.771 | 0.547 |
| 0.494 | 18. | 0.219 | 0.508 | 0.576 |
| 0.532 | 18. | 0.219 | 0.528 | 0.661 |
| 0.570 | 16. | 0.259 | 0.528 | 0.894 |
| 0.608 | 16. | 0.259 | 0.389 | 1.354 |
| 0.646 | 15. | 0.289 | 0.389 | 2.010 |
| 0.684 | 15. | 0.289 | 1.646 | 2.645 |
| 0.722 | 12. | 0.414 | 9.356 | 2.945 |
| 0.760 | 0. | 1.000 | 0.0 | 2.717 |

TABLE A-46 BUBBLE SIZE DISTRIBUTION FOR 0.8% CMC SYSTEM AT WINDOW #2 AND F= 90 SCFH

| DIA.(CM) | NO. OF BUBBLES | CUMUL. VOL. | PROB. DEN. | PROB. DEN. AFTER SMOOTHING |
|---|---|---|---|---|
| 0.0 | 554. | 0.0 | 0.0 | 0.0 |
| 0.038 | 442. | 0.000 | 0.131 | 0.131 |
| 0.076 | 223. | 0.010 | 0.361 | 0.357 |
| 0.114 | 137. | 0.028 | 0.642 | 0.533 |
| 0.152 | 82. | 0.059 | 0.898 | 0.680 |
| 0.190 | 51. | 0.096 | 0.922 | 0.784 |
| 0.228 | 36. | 0.129 | 0.766 | 0.849 |
| 0.266 | 29. | 0.154 | 0.918 | 0.886 |
| 0.304 | 21. | 0.199 | 1.011 | 0.901 |
| 0.342 | 17. | 0.231 | 0.872 | 0.900 |
| 0.380 | 14. | 0.265 | 1.048 | 0.894 |
| 0.418 | 11. | 0.311 | 0.866 | 0.901 |
| 0.456 | 10. | 0.331 | 0.264 | 0.936 |
| 0.494 | 10. | 0.331 | 1.279 | 0.999 |
| 0.532 | 7. | 0.428 | 1.279 | 1.080 |
| 0.570 | 7. | 0.428 | 1.291 | 1.197 |
| 0.608 | 5. | 0.526 | 1.291 | 1.391 |
| 0.646 | 5. | 0.526 | 0.0 | 1.672 |
| 0.684 | 5. | 0.526 | 1.098 | 1.948 |
| 0.722 | 4. | 0.609 | 6.239 | 2.045 |
| 0.760 | 0. | 1.000 | 0.0 | 1.838 |

TABLE A-47 BUBBLE SIZE DISTRIBUTION FOR 0.8% CMC SYSTEM AT WINDOW #3 AND F= 90 SCFH

| DIA.(CM) | NO. OF BUBBLES | CUMUL. VOL. | PROB. DEN. | PROB. DEN. AFTER SMOOTHING |
|---|---|---|---|---|
| 0.0 | 528. | 0.0 | 0.0 | 0.0 |
| 0.038 | 407. | 0.000 | 0.100 | 0.100 |
| 0.076 | 230. | 0.008 | 0.338 | 0.329 |
| 0.114 | 136. | 0.026 | 0.634 | 0.504 |
| 0.152 | 80. | 0.056 | 0.841 | 0.647 |
| 0.190 | 50. | 0.090 | 0.883 | 0.743 |
| 0.228 | 34. | 0.123 | 0.795 | 0.796 |
| 0.266 | 26. | 0.150 | 0.774 | 0.814 |
| 0.304 | 20. | 0.182 | 1.018 | 0.808 |
| 0.342 | 14. | 0.228 | 0.744 | 0.787 |
| 0.380 | 13. | 0.238 | 0.709 | 0.755 |
| 0.418 | 10. | 0.281 | 0.569 | 0.704 |
| 0.456 | 10. | 0.281 | 0.959 | 0.625 |
| 0.494 | 7. | 0.354 | 0.959 | 0.523 |
| 0.532 | 7. | 0.354 | 0.0 | 0.452 |
| 0.570 | 7. | 0.354 | 0.0 | 0.518 |
| 0.608 | 7. | 0.354 | 0.0 | 0.825 |
| 0.646 | 7. | 0.354 | 0.0 | 1.371 |
| 0.684 | 7. | 0.354 | 0.0 | 1.973 |
| 0.722 | 7. | 0.354 | 8.497 | 2.334 |
| 0.760 | 0. | 1.000 | 0.0 | 2.244 |

TABLE A-48 BUBBLE SIZE DISTRIBUTION FOR 0.8% CMC SYSTEM AT WINDOW #4 AND F= 90 SCFH

| DIA.(CM) | NO. OF BUBBLES | CUMUL. VOL. | PROB. DEN. | PROB. DEN. AFTER SMOOTHING |
|---|---|---|---|---|
| 0.0 | 619. | 0.0 | 0.0 | 0.0 |
| 0.038 | 525. | 0.000 | 0.088 | 0.088 |
| 0.076 | 334. | 0.007 | 0.354 | 0.384 |
| 0.114 | 207. | 0.027 | 0.763 | 0.623 |
| 0.152 | 121. | 0.065 | 1.085 | 0.815 |
| 0.190 | 73. | 0.109 | 1.260 | 0.928 |
| 0.228 | 43. | 0.160 | 1.152 | 0.963 |
| 0.266 | 30. | 0.197 | 0.764 | 0.937 |
| 0.304 | 25. | 0.219 | 0.945 | 0.872 |
| 0.342 | 17. | 0.269 | 0.892 | 0.785 |
| 0.380 | 15. | 0.286 | 0.698 | 0.685 |
| 0.418 | 12. | 0.322 | 0.672 | 0.591 |
| 0.456 | 11. | 0.337 | 0.205 | 0.536 |
| 0.494 | 11. | 0.337 | 0.331 | 0.566 |
| 0.532 | 10. | 0.363 | 0.331 | 0.726 |
| 0.570 | 10. | 0.363 | 0.501 | 1.044 |
| 0.608 | 9. | 0.401 | 1.106 | 1.496 |
| 0.646 | 8. | 0.447 | 2.047 | 1.977 |
| 0.684 | 6. | 0.556 | 2.294 | 2.313 |
| 0.722 | 5. | 0.621 | 5.841 | 2.337 |
| 0.760 | 0. | 1.000 | 0.0 | 2.003 |

TABLE A-49 BUBBLE SIZE DISTRIBUTION FOR 0.8% CMC SYSTEM AT WINDOW #1 AND F=120 SCFH

| DIA.(CM) | NO. OF BUBBLES | CUMUL. VOL. | PROB. DEN. | PROB. DEN. AFTER SMOOTHING |
|---|---|---|---|---|
| 0.0 | 414. | 0.0 | 0.0 | 0.0 |
| 0.071 | 219. | 0.001 | 0.072 | 0.072 |
| 0.143 | 84. | 0.010 | 0.179 | 0.127 |
| 0.214 | 37. | 0.026 | 0.207 | 0.149 |
| 0.286 | 22. | 0.040 | 0.165 | 0.165 |
| 0.357 | 17. | 0.050 | 0.169 | 0.171 |
| 0.429 | 13. | 0.064 | 0.141 | 0.174 |
| 0.500 | 12. | 0.070 | 0.232 | 0.177 |
| 0.572 | 9. | 0.097 | 0.190 | 0.185 |
| 0.643 | 9. | 0.097 | 0.0 | 0.201 |
| 0.715 | 9. | 0.097 | 0.348 | 0.229 |
| 0.786 | 7. | 0.147 | 0.348 | 0.273 |
| 0.858 | 7. | 0.147 | 0.0 | 0.336 |
| 0.929 | 7. | 0.147 | 0.370 | 0.416 |
| 1.001 | 6. | 0.200 | 0.829 | 0.515 |
| 1.072 | 5. | 0.265 | 0.459 | 0.646 |
| 1.144 | 5. | 0.265 | 0.676 | 0.830 |
| 1.215 | 4. | 0.362 | 0.676 | 1.066 |
| 1.287 | 4. | 0.362 | 0.0 | 1.287 |
| 1.358 | 4. | 0.362 | 4.462 | 1.376 |
| 1.430 | 0. | 1.000 | 0.0 | 1.252 |

TABLE A-50 BUBBLE SIZE DISTRIBUTION FOR 0.8% CMC SYSTEM AT WINDOW #2 AND F=120 SCFH

| DIA.(CM) | NO. OF BUBBLES | CUMUL. VOL. | PROB. DEN. | PROB. DEN. AFTER SMOOTHING |
|---|---|---|---|---|
| 0.0 | 541. | 0.0 | 0.0 | 0.0 |
| 0.038 | 455. | 0.000 | 0.066 | 0.066 |
| 0.076 | 273. | 0.005 | 0.217 | 0.246 |
| 0.114 | 181. | 0.017 | 0.507 | 0.394 |
| 0.152 | 103. | 0.044 | 0.663 | 0.520 |
| 0.191 | 71. | 0.067 | 0.697 | 0.606 |
| 0.229 | 49. | 0.097 | 0.766 | 0.655 |
| 0.267 | 36. | 0.126 | 0.646 | 0.672 |
| 0.305 | 30. | 0.146 | 0.659 | 0.667 |
| 0.343 | 24. | 0.176 | 0.754 | 0.649 |
| 0.381 | 20. | 0.204 | 0.609 | 0.624 |
| 0.419 | 18. | 0.222 | 0.568 | 0.605 |
| 0.457 | 16. | 0.247 | 0.529 | 0.610 |
| 0.496 | 15. | 0.263 | 0.468 | 0.660 |
| 0.534 | 14. | 0.282 | 0.584 | 0.787 |
| 0.572 | 13. | 0.307 | 0.718 | 1.027 |
| 0.610 | 12. | 0.337 | 1.346 | 1.405 |
| 0.648 | 10. | 0.410 | 0.952 | 1.883 |
| 0.686 | 10. | 0.410 | 0.671 | 2.312 |
| 0.724 | 9. | 0.461 | 7.741 | 2.476 |
| 0.762 | 0. | 1.000 | 0.0 | 2.241 |

TABLE A-51 BUBBLE SIZE DISTRIBUTION FOR 0.8% CMC SYSTEM AT WINDOW #3 AND F=120 SCFH

| DIA.(CM) | NO. OF BUBBLES | CUMUL. VOL. | PROB. DEN. | PROB. DEN. AFTER SMOOTHING |
|---|---|---|---|---|
| 0.0 | 355. | 0.0 | 0.0 | 0.0 |
| 0.038 | 319. | 0.000 | 0.021 | 0.021 |
| 0.076 | 264. | 0.002 | 0.132 | 0.224 |
| 0.114 | 201. | 0.010 | 0.415 | 0.455 |
| 0.152 | 138. | 0.033 | 0.746 | 0.665 |
| 0.191 | 95. | 0.067 | 1.098 | 0.833 |
| 0.229 | 60. | 0.117 | 1.244 | 0.932 |
| 0.267 | 41. | 0.162 | 1.111 | 0.959 |
| 0.305 | 30. | 0.202 | 0.869 | 0.929 |
| 0.343 | 25. | 0.228 | 0.829 | 0.868 |
| 0.381 | 20. | 0.265 | 0.875 | 0.801 |
| 0.419 | 17. | 0.295 | 0.734 | 0.759 |
| 0.457 | 15. | 0.321 | 0.563 | 0.774 |
| 0.496 | 14. | 0.338 | 0.220 | 0.871 |
| 0.534 | 14. | 0.338 | 1.031 | 1.061 |
| 0.572 | 11. | 0.416 | 1.451 | 1.328 |
| 0.610 | 10. | 0.448 | 1.432 | 1.635 |
| 0.648 | 8. | 0.526 | 2.221 | 1.915 |
| 0.686 | 6. | 0.618 | 1.208 | 2.073 |
| 0.724 | 6. | 0.618 | 5.015 | 2.006 |
| 0.762 | 0. | 1.000 | 0.0 | 1.687 |

TABLE A-52 BUBBLE SIZE DISTRIBUTION FOR 0.8% CMC SYSTEM AT WINDOW #4 AND F=120 SCFH

| DIA.(CM) | NO. OF BUBBLES | CUMUL. VOL. | PROB. DEN. | PROB. DEN. AFTER SMOOTHING |
|---|---|---|---|---|
| 0.0 | 708. | 0.0 | 0.0 | 0.0 |
| 0.038 | 610. | 0.000 | 0.113 | 0.113 |
| 0.076 | 343. | 0.009 | 0.387 | 0.377 |
| 0.114 | 200. | 0.030 | 0.725 | 0.586 |
| 0.152 | 115. | 0.064 | 0.887 | 0.757 |
| 0.191 | 76. | 0.097 | 1.053 | 0.861 |
| 0.229 | 46. | 0.144 | 1.191 | 0.888 |
| 0.267 | 29. | 0.188 | 0.992 | 0.842 |
| 0.305 | 21. | 0.220 | 0.719 | 0.744 |
| 0.343 | 17. | 0.243 | 0.620 | 0.625 |
| 0.381 | 14. | 0.267 | 0.317 | 0.514 |
| 0.419 | 14. | 0.267 | 0.375 | 0.431 |
| 0.457 | 12. | 0.296 | 0.375 | 0.393 |
| 0.496 | 12. | 0.296 | 0.303 | 0.426 |
| 0.534 | 11. | 0.319 | 0.303 | 0.579 |
| 0.572 | 11. | 0.319 | 0.0 | 0.903 |
| 0.610 | 11. | 0.319 | 0.554 | 1.394 |
| 0.648 | 10. | 0.361 | 2.536 | 1.948 |
| 0.686 | 7. | 0.512 | 1.982 | 2.363 |
| 0.724 | 7. | 0.512 | 6.399 | 2.443 |
| 0.762 | 0. | 1.000 | 0.0 | 2.124 |

# DYNAMICS OF BUBBLE SIZE DISTRIBUTION AND WALL PRESSURE FLUCTUATIONS IN AIRLIFT FERMENTORS

by

CHUNG-HUR LEE

B. S., National Taiwan University, 1979

---

AN ABSTRACT OF A MASTER'S THESIS

submitted in partial fulfillment of the

requirements for the degree

MASTER OF SCIENCE

Department of Chemical Engineering

KANSAS STATE UNIVERSITY
Manhattan, Kansas

1983

The dynamic behavior of the bubble size distribution and the wall pressure fluctuations in a vertival, buoyancy-driven, turbulent gas-liquid flow was investigated. The objectives included the advancement of knowledge of vertical two-phase flow, the characterization of the turbulent structures and the bubble behavior in airlift fermentors and the effect of liquid viscosity upon fermentation processes.

Three different air-liquid systems were studied; the liquid media were tap water, salt water and CMC solutions with concentrations 0.5 wt.% and 0.8 wt.%. The gas bubbles were photographed in the upflow zone of the 6.0 in. I. D. airlift column at various distances from the sparger. The negatives were then analyzed using a Bausch & Lomb Omnicon Image Analysis System which converted the photographic data into a histographic tabulation of bubble size. An on-line statistical study of the pressure fluctuations in airlift fermentors was also conducted by using pressure transducers, a correlation and probability analyzer and a Fourier transform analyzer.

The mechanism of bubble break-up appeared to be mainly due to the dynamic pressure fluctuations in the vicinity of the bubble at column positions remote from the sparger. The maximum stable bubble diameter was found to be proportional to the -2/5 power of the energy input and to increase with liquid viscosity and surface tension. The standard deviation of the pressure fluctuations was found to increase in an approximately linear manner with the power input and was closely related to the dynamic energy content of the two-phase system. Furthermore, the nature and origin of the pressure fluctuations were identified by experiments performed with single bubbles.